

# Observations of pre- and proto-brown dwarfs in nearby clouds: paving the way to further constraining theories of brown dwarf formation

Aina Palau<sup>a</sup>, Nuria Huéramo<sup>b</sup>, David Barrado<sup>b</sup>, Michael M. Dunham<sup>c,d</sup>, Chang Won Lee<sup>e,f</sup>

<sup>a</sup>*Instituto de Radioastronomía y Astrofísica, Universidad Nacional Autónoma de México, Antigua Carretera a Patzcuaro 8701, Ex-Hda. San José de la Huerta, Morelia, 58089, Michoacán, México*

<sup>b</sup>*Centro de Astrobiología (CAB), CSIC-INTA, Camino Bajo del Castillo s/n, Villanueva de la Canada, 28692, Madrid, Spain*

<sup>c</sup>*Department of Physics, Middlebury College, Middlebury, 05753, VT, USA*

<sup>d</sup>*Department of Physics, State University of New York at Fredonia, 280 Central Avenue, Fredonia, 14063, NY, USA*

<sup>e</sup>*Korea Astronomy and Space Science Institute (KASI), 776 Daedeokdae-ro, Yuseong-gu, 34055, Daejeon, Republic of Korea*

<sup>f</sup>*University of Science and Technology, Korea (UST), 217 Gajeong-ro, Yuseong-gu, 34113, Daejeon, Republic of Korea*

## Abstract

Brown Dwarfs (BDs) are crucial objects in our understanding of both star and planet formation, as well as in our understanding of what mechanisms shape the lower end of the Initial Mass Function (IMF). However, since the discovery of the first BD in 1995, there is still an unconcluded debate about which is the dominant formation mechanism of these objects. For this, it is mandatory to study BDs in their earliest evolutionary stages (what we call pre- and proto-BDs), comparable to the ‘pre-stellar’ and ‘Class 0/I’ stages well characterized for the formation of low-mass stars. In this review, the recent efforts aimed at searching, identifying and characterising pre- and proto-BD candidates in nearby star-forming regions are presented, and revised requirements for an object to be a promising proto-BD or pre-BD candidate are provided, based on a new, unexplored so far, relation between the internal luminosity and the accreted mass. By applying these requirements, a list of 68 promising proto-BD candidates is presented, along with a compilation of possible pre-BDs from the literature. In addition, updated correlations of protostellar properties such as mass infall rate or outflow momentum rate with bolometric luminosity are provided down to the low-mass BD regime, where no significant deviations are apparent. Furthermore, the number proto-BD candidates in different clouds of the Solar Neighborhood seem to follow the known relations of number of protostars with cloud properties. In addition, proto(star-to-BD) ratios for the different clouds are also explored, unveiling a particular underproduction of low-mass proto-BD candidates in Ophiuchus compared to Lupus and Taurus. Possible explanations for this behavior are discussed, including heating of the Ophiuchus cloud by the nearby OB stars. The overall results of this work, along with the possibility that the planetary-mass regime of the IMF is subtly shaped by stellar feedback, tend to favor a Jeans-fragmentation process and therefore a star-like formation scenario down to the planetary boundary, of  $\sim 0.01 M_{\odot}$ , below which other mechanisms might be at work. Future observational constraints, such as those provided by upcoming facilities like the next-generation Very Large Array, or the use of isotopologues ( $^{13}\text{CO}$ ,  $^{15}\text{NH}_3$ , etc.) based on James Webb Space Telescope data, will provide definite clues to disentangle the origin of BDs in the planetary-mass regime.

**Keywords:** brown dwarf, substellar, formation

## 1. Why to worry about how brown dwarfs form: their relation to planet formation

Nowadays it is well established that brown dwarfs (BDs) are fundamentally different from low-mass stars because their mass,  $< 0.075 M_{\odot}$  for solar metallicity (e.g., Chabrier et al., 2023), is too low to sustain prolonged hydrogen fusion reactions. These objects were first predicted by Kumar (1963) and Hayashi and Nakano (1963) and subsequent works such as Staller and de Jong (1981) predicted some of their observational properties. They were finally discovered by Nakajima et al. (1995), Oppenheimer et al. (1995) and Rebolo et al. (1995). The lack of an internal source of energy in these substellar objects (a part from gravitational contraction) completely determines their fate and makes them, in some sense, objects much closer to planets than to stars. In fact, high-quality spectroscopy of BDs can be collected and used as reference for atmospheric

studies in exoplanets (see, for instance Barrado et al. 2023). It is commonly assumed that the border line between planets and BDs is at  $0.012 M_{\odot}$  or  $13 M_{\text{Jup}}$  (e.g., Lecavelier des Etangs and Lissauer, 2022), because this is the mass limit for deuterium burning. However, there is probably a more essential process that could set a fundamental difference between BDs and giant planets: their formation mechanism, and several authors have proposed to use a formation-based definition (e.g., Chabrier et al., 2014; Kirkpatrick et al., 2024), which is given below and is adopted in this work.

Initially it was thought that BDs could not be formed as a scaled-down version of low-mass stars because typical Jeans masses of molecular clouds were thought to be well above the substellar limit. However, since the beginning of the XXI century, an important number of theoretical and numerical works in the literature proposed that BDs do form in a similar manner as low-mass stars: from fragmentation of (turbulent) molecular

clouds (e.g., Padoan and Nordlund, 2002, 2004; Hennebelle and Chabrier, 2008; Chabrier and Hennebelle, 2010; Chabrier et al., 2014; Haugbølle et al., 2018; Vázquez-Semadeni et al., 2019; Dhandha et al., 2023). In most of these works, the Jeans mass decreases significantly because turbulence allows the formation of extremely dense density fluctuations, but high densities can also be achieved as a natural outcome of gravitational collapse<sup>1</sup>. If BDs form like stars, BDs and giant planets should have a different internal structure. Furthermore, several authors proposed that BDs are indeed a scaled-down version of low-mass stars but forming in a very low mass and compact core with the *particular property* of having an unusually poor accretion history. Such a particularly poor accretion history could be related to competition with other protostars that prevent them from gaining further mass (e.g., Bonnell and Bate, 2006), to tidal shear and high velocity dispersion within a nascent stellar cluster (e.g., Bonnell et al., 2008), to ejection from their natal environments (e.g., Reipurth and Clarke, 2001; Bate et al., 2002; Bate, 2019; Basu and Vorobyov, 2012; Reipurth and Mikkola, 2015), to extreme outflows that can remove the material from the cloud that is available for star formation (e.g., Kratter and Lodato, 2016; Machida et al., 2009), or to the strong effects of radiative feedback in the surroundings of OB stars (e.g., Whitworth and Zinnecker, 2004; Whitworth et al., 2007; Whitworth, 2018).

From an observational point of view, works studying the complete (typically down to  $\sim 0.01 M_{\odot}$ ) Initial Mass Function (IMF) in the central bulge of the Galaxy or in other complexes such as the Pleiades, 25 Ori, W3 or NGC 1333 seem to find results consistent with a lognormal IMF (e.g., Moraux et al., 2003; Scholz et al., 2012; Kirkpatrick et al., 2019; Suárez et al., 2019; Huston and Luhman, 2021; Chabrier and Lenoble, 2023)<sup>2</sup>. The lognormal IMF is the expected outcome of turbulence-driven star formation (e.g., Zinnecker, 1984; Chabrier, 2005), and the finding of a lognormal IMF down to  $\sim 0.01 M_{\odot}$  suggests that BD formation is a continuation of the star formation process. Other authors fit the low-mass regime of the IMF, down to substellar masses, using one single power-law, which also suggests that the formation of BDs is a continuation of the star-formation process (e.g., Barrado y Navascués et al., 2002, 2004; Moraux et al., 2007; Lodieu et al., 2007; Bayo et al., 2011; Damian et al., 2023). This has been recently found using *Euclid* down to  $4 M_{\text{Jup}}$  in the  $\sigma$  Ori cluster (Martín et al., 2024), and is supported by other recent works. Parker and Alves de Oliveira (2023) find that the spatial distribution of planetary-mass objects down to  $\sim 0.005 M_{\odot}$  in NGC 1333

is indistinguishable from that of low-mass stars, and that this distribution should be different if it stemmed from ejected objects formed in circumstellar discs. In the same line, Scholz et al. (2023) find that the disc fraction in the same region does not decline towards smaller masses, suggesting that planetary-mass objects seem to form like stars at least down to  $\sim 0.01 M_{\odot}$ . This limit was pushed down to  $\sim 0.004 M_{\odot}$  by Langeveld et al. (2024), using the James Webb Space Telescope (JWST) also in NGC 1333. The formation of BDs as a scaled-down version of low-mass stars is additionally favored by the recent study of the BD desert with Gaia DR3 (Stevenson et al., 2023) (with some hints of two different parent distributions) and by JWST measurements of the  $^{14}\text{N}/^{15}\text{N}$  ratio in the atmosphere of a BD (Barrado et al., 2023).

However, other works report that the very low-mass end of the IMF (from 0.01 to  $0.3 M_{\odot}$ ) is bimodal, in regions such as NGC 1333, M35, the Pleiades or the Orion Nebula Cloud (Barrado y Navascués et al., 2001; Oasa et al., 2008; Bouy et al., 2015; Drass et al., 2016), and also a clear excess of planetary-mass objects, also known as Free-Floating Planets (FFPs, with masses  $\lesssim 0.01 M_{\odot}$ ) has been recently found in Ophiuchus and Upper Sco (e.g., Miret-Roig et al., 2022; Miret-Roig, 2023), suggesting that additional mechanisms other than the standard star-formation pathways must be at work, at least in certain environments of the Galaxy or for a certain range of masses. Additional searches of even lower mass objects (DeRocco et al., 2024 about sub-terrestrial FFPs; Pearson and McCaughrean 2023 for alleged binary FFPs in the Trapezium) support this view.

To explain this excess, ‘planet-like’ formation mechanisms such as disc fragmentation and subsequent ejection are invoked, along with stellar encounters or dynamical interactions between the members of multiple systems (e.g., Stamatellos et al., 2007; Stamatellos and Whitworth, 2009; Basu and Vorobyov, 2012; Reipurth and Mikkola, 2015; Thies et al., 2015; Vorobyov et al., 2017c; Wang et al., 2023; Chen et al., 2023; Yu and Lai, 2024; Coleman and DeRocco, 2024)<sup>3</sup>. Moreover, the theoretical predictions of binary separation distributions of BDs and stars (Thies et al., 2015) do not agree with the numerous observations in the field and in stellar associations (Bouy et al., 2003; Burgasser et al., 2003; Martín et al., 2003; Close et al., 2003), which are more consistent with the predictions of a dynamical origin of BD binaries being ejected from multiple systems (e.g., Reipurth and Mikkola, 2015). Additionally, there are evidences of very-low mass stars ejected by dynamical decay of multiple systems, such as the case of HH24 (Reipurth et al., 2023). In this case, a border-limit star moves at  $25 \text{ km s}^{-1}$  and was ejected about 5800 yr ago. All these evidences point to a possible non-negligible role of alternate scenarios to the star-like scenario for BD formation.

As a summary, there are two main scenarios for BD for-

<sup>1</sup>There are a number of problems with the turbulent fragmentation scenario, as summarized in Lomax et al. (2016) and Whitworth (2018). Alternatively, in scenarios where turbulence does not have such a dominant role (e.g., Bate, 2019; Vázquez-Semadeni et al., 2019), fragmentation proceeds isothermally as the cloud undergoes hierarchical collapse, increasing its density, and the fragmentation is only stopped by the change in the fragmentation regime, from isothermal to adiabatic. This transition takes place when the gas is so dense that it becomes optically thick and does not allow the radiation to escape, and can occur for masses as low as  $\sim 0.005 M_{\odot}$  (e.g., Larson, 1969; Young, 2023).

<sup>2</sup>Among the works reporting no deviations of the IMF with respect to a lognormal distribution, some of them, such as Suárez et al. (2019) or Huston and Luhman (2021) do not reach the planetary regime.

<sup>3</sup>Alternatively, Dhandha et al. (2023) and Kuruwita et al. (2024) suggest that solenoidal turbulence would naturally produce a BD excess. This would allow to explain the BD excess found in some regions again from fragmentation of molecular clouds.

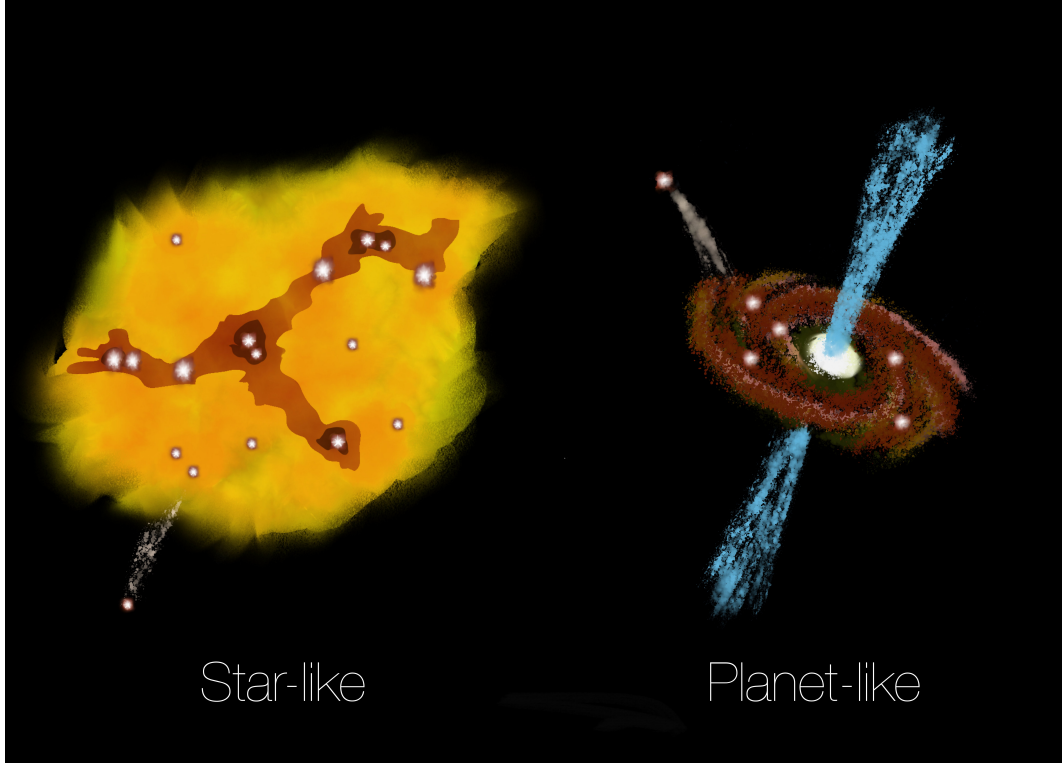


Figure 1: Sketch of the two main scenarios proposed for the formation of isolated BDs. Left: Star-like scenario, which might involve, in some cases, ejection from the cloud. Right: Planet-like scenario, which always requires ejection from a protostellar disc.

mation: the star-like scenario (fragmentation of a molecular cloud + possible ejection) or the planet-like scenario (disc fragmentation + ejection), both sketched in Fig. 1. It is important to note that in both scenarios the objects might be ejected at some point from their natal places, either a molecular core, a filament, a multiple system or a protostellar disc. But the decisive question to understand is how the original seed of the young BD was formed. The current view of BD formation is that BDs form as low-mass stars in most/some star-forming regions of the Galaxy and probably down to a certain mass, below which they would form like planets. A possible lower-limit for the formation of objects like stars is suggested to be around  $10\text{--}15 M_{\text{Jup}}$  (e.g., [Schlaufman, 2018](#); [Miret-Roig et al., 2022](#); [Kirkpatrick et al., 2024](#); [Scholz et al., 2023](#)), and we will adopt here a tentative upper limit for the planetary regime of  $\sim 10 M_{\text{Jup}}$ . In turn, there are already evidences (based on the trend of companions around metal-rich hosts, on the ratio of C/O values, and on radial velocity distributions) consistently indicating that objects with mass  $< 4 M_{\text{Jup}}$  do always form like planets (e.g., [Schlaufman, 2018](#); [Kirkpatrick et al., 2024](#)). In any case, there must be some overlapping in the mass range, where both formation mechanisms could co-exist. In addition, specific regions of the Galaxy might be more prone to the star-like or the planet-like mode of formation due to several factors unexplored so far. Thus, the study of BDs (and FFPs) in their *earliest* stages of formation is essential to constrain the different formation theories of these mysterious objects and to better understand their siblings: both very low-mass stars and

planets.

A direct method to further constrain theories of BD formation is to study these objects in their earliest evolutionary stages. For example, if BDs form indeed as a scaled-down version of low-mass stars, they should have properties that are a scaled-down version of the properties of the most embedded protostars, the Class 0 and Class I protostars (e.g., following the classification by [Adams et al., 1987](#); [Lada, 1987](#); [Andre et al., 1993](#)). Class 0 and I protostars are known to follow several trends, such as the mass infall rate vs the internal luminosity, the centimeter luminosity vs bolometric luminosity, or the outflow momentum rate vs the bolometric luminosity or envelope mass (e.g., [Bontemps et al., 1996](#); [Kim et al., 2021](#); [Anglada et al., 2018](#)). Thus, proto-BDs should fall in the corresponding low-end of these relations if their formation path was star-like. What is more, in the star-like scenario, the equivalent to pre-stellar cores should be found in the substellar regime, the so-called ‘pre-BDs’. Pre-stellar cores are gravitationally-bound compact objects at the verge of collapse to form a star, but with no signs of stellar activity yet, such as infrared emission or outflow signatures (e.g., [Pagani et al., 2010](#); [Simpson et al., 2011](#); [Maret et al., 2013](#)). Throughout this work, we will use the term ‘proto-BD’ to refer to deeply embedded BDs whose properties are comparable to the properties of Class 0/I protostars. In this work we aim at compiling the observational evidence reported so far in the literature about proto-BDs and pre-BDs, so that constraints on the different BD formation scenarios can be explored. Therefore,

this review will not include Class II BDs, or young FFPs.

Although it is clear that observations of pre- and proto-BDs are required to constrain theories of BD formation, there is nowadays a rather confusing knowledge on which kind of objects can actually qualify as robust pre- and proto-BD candidates, and there is a lack of consensus in the literature about the precise meaning of these terms. The advent of ‘last-generation’ telescopes, such as ALMA upgrades or the JWST, and the next-generation VLA and SKA in the future, is progressively unveiling fainter objects in star-forming regions which might well be excellent pre- and proto-BD candidates (e.g., Kawabe et al., 2018; Lee et al., 2018a). Thus, there is the need and it is the proper time of clearly defining what these terms refer to, where we are, and where we should address our future efforts.

This review is organized as follows. In Sec. 2 we provide several definitions essential to this work. In Sec. 3 we present the main efforts of searching (pre-) and proto-BDs in the literature. In Sec. 4 we mention the main challenges to properly identify these objects. In Sec. 5 we describe the necessary conditions that a candidate must fulfill to be a robust proto-BD candidate, and apply these criteria to the SUCANES database (Pérez-García et al., 2025) to extract the first statistically significant sample of robust proto-BD candidates. In Sec. 6 we present a similar procedure for pre-BDs. In Sec. 7 we compare the proto-BD candidate content in different clouds of the solar neighborhood. In Sec. 8 we discuss possible constraints from the compiled information. Finally, in Sec. 9 we outline future research lines in view of the recent and upcoming exciting last-generation telescopes.

## 2. Definitions

Before summarizing the main strategies to search for proto-BDs reported so far in the literature, we define here the most important parameters that are used to characterize these objects.

*Effective radius,  $r_{\text{eff}}$ .* Given the area  $A$  of the millimetre/sub-millimetre source, taken at the  $3\sigma$  contour or as the full-width at half maximum,  $r_{\text{eff}}$  is the radius corresponding to  $A$  assuming that the emission is circular (e.g., Kauffmann et al., 2008):

$$r_{\text{eff}} = \sqrt{A/\pi}. \quad (1)$$

*Bolometric luminosity,  $L_{\text{bol}}$ .* The bolometric luminosity results from integrating the Spectral Energy Distribution (SED) for all frequencies:

$$L_{\text{bol}} = 4\pi D^2 \int_0^\infty F_\nu d\nu, \quad (2)$$

where  $F_\nu$  is the flux density of the source at frequency  $\nu$ . It is important that the targets have a relatively complete and well-sampled SED covering from the infrared to the sub-millimetre regime to have an accurate estimate of  $L_{\text{bol}}$ .

*Luminosity in the sub-millimetre range,  $L_{\text{submm}}$ .* The sub-millimetre luminosity is the result from integrating the SED from the lowest frequency available up to the frequency corresponding to  $350 \mu\text{m}$ :

$$L_{\text{submm}} = 4\pi D^2 \int_0^{c/350\mu\text{m}} F_\nu d\nu, \quad (3)$$

where  $c$  is the speed of light. The  $L_{\text{submm}}/L_{\text{bol}}$  parameter is considered an evolutionary indicator so that higher values correspond to more embedded (younger) objects (e.g., Andre et al., 1993; Kauffmann et al., 2008).

*Bolometric temperature,  $T_{\text{bol}}$ .* The bolometric temperature is the temperature of a blackbody having the same mean frequency as the observed SED (Myers and Ladd, 1993). It can be calculated as (e.g., Chen et al., 1995; Dunham et al., 2008):

$$T_{\text{bol}} = 1.25 \times 10^{-11} \frac{\int_0^\infty \nu F_\nu d\nu}{\int_0^\infty F_\nu d\nu} \text{ K}, \quad (4)$$

and is considered an evolutionary indicator, with  $T_{\text{bol}} < 70 \text{ K}$  corresponding to Class 0 objects,  $70 < T_{\text{bol}} < 650 \text{ K}$  corresponding to Class I objects,  $650 < T_{\text{bol}} < 2800 \text{ K}$  corresponding to Class II, and  $T_{\text{bol}} > 2800 \text{ K}$  corresponding to Class III (Chen et al., 1995; Evans et al., 2009). The  $T_{\text{bol}}$  evolutionary indicator anticorrelates with other indicators such as the slope of the SED from 2 to  $20 \mu\text{m}$  (e.g., Evans et al., 2009), and correlates with the  $L_{\text{submm}}/L_{\text{bol}}$  indicator (Fig. 10 of Kauffmann et al., 2008).

*Internal luminosity,  $L_{\text{int}}$ .* The internal luminosity is the luminosity coming from both the central protostar and a circumstellar disc/envelope, excluding the external luminosity  $L_{\text{ext}}$ , which is the luminosity arising from heating of the disc/envelope by the interstellar radiation field (ISRF). Thus,  $L_{\text{bol}} = L_{\text{int}} + L_{\text{ext}}$ . To estimate  $L_{\text{int}}$ , radiative transfer modeling of the SED is required. Therefore,  $L_{\text{int}} = L_{\text{star}} + L_{\text{disc}}$  (Keplerian disc) and usually  $L_{\text{int}}$  is around 70% of  $L_{\text{bol}}$ . Consequently,  $L_{\text{int}}$  includes accretion and luminosity from the photosphere but does not include luminosity from external heating by the interstellar radiation field (Vorobyov et al., 2017b). Dunham et al. (2008) explore the relation of  $L_{\text{int}}$  vs the flux at different wavelengths and find that the flux at  $70 \mu\text{m}$  correlates very well with  $L_{\text{int}}$  calculated using radiative transfer models.  $L_{\text{int}}$  can be calculated using the following equation (Pérez-García et al., 2025):

$$L_{\text{int}} = 3.3 \times 10^8 [F_{70\text{cgs}} (D/140)^2]^{0.94}, \quad (5)$$

where  $L_{\text{int}}$  is given in  $L_\odot$ ,  $D$  is the distance (in pc), and  $F_{70\text{cgs}}$  corresponds to  $\nu F_\nu$  at  $70 \mu\text{m}$  given in cgs units, i.e.,  $\text{erg cm}^{-2} \text{ s}^{-1}$ . In practical units:

$$L_{\text{int}} = 8.96 \times 10^{-5} [F_{70\text{mJy}} (D/140)^2]^{0.94}, \quad (6)$$

where  $F_{70\text{mJy}}$  corresponds to the flux density at  $70 \mu\text{m}$  in mJy.



*Envelope mass,  $M_{\text{env}}$ .* The envelope mass is the mass of the core surrounding the protostar (or hydrostatic core).  $M_{\text{env}}$  is usually inferred from observations in the millimetre/sub-millimetre range, which allow to measure the flux at the corresponding wavelength,  $F_\nu$ . Adopting a dust temperature  $T_d$  and a dust opacity  $\kappa_\nu$ ,  $M_{\text{env}}$  can be estimated as:

$$M_{\text{env}} = \frac{F_\nu D^2}{B_\nu(T_d) \kappa_\nu}. \quad (7)$$

*Dynamical or accreted mass,  $M_{\text{acc}}$  or  $M_{\text{dyn}}$ .* The dynamical or accreted mass is the mass of the hydrostatic core or protostar, and, for the most embedded objects, is typically estimated from the velocity pattern tracing Keplerian motions of the gas in the disc (see Sec. 4.3). If the Keplerian motion is not fully resolved and only a velocity gradient is detected, the accreted mass can be estimated from:

$$M_{\text{acc}} = M_{\text{dyn}} = \frac{R v_{\text{tot}}^2}{G}, \quad (8)$$

where  $R$  is the distance from the central object, of mass  $M_{\text{dyn}}$ , to the position where the observed velocity  $v_{\text{tot}}$  is measured. If this method is used to estimate the accreted mass, the term ‘dynamical mass’ is typically used, to emphasize that it has been obtained from the observed gas kinematics. If other methods are used (as outlined in Sec. 4.3), the term ‘accreted mass’ ( $M_{\text{acc}}$ ) is used.

*Accretion luminosity,  $L_{\text{acc}}$ .* The accretion luminosity corresponds to the energy per unit time radiated as heat by the matter infalling towards the hydrostatic core.  $L_{\text{acc}}$  is directly proportional to the mass accretion rate:

$$L_{\text{acc}} = \eta_L \frac{G M_{\text{acc}} \dot{M}_{\text{acc}}}{R_*}, \quad (9)$$

where  $\eta_L$  is the accretion luminosity efficiency with respect to steady spherical infall (for steady accretion through an optically thick disc,  $\eta_L \sim 1/2$ , Hartmann 1998), and  $R_*$  is the radius of the central hydrostatic object.

*Virial mass,  $M_{\text{vir}}$ .* The virial mass is the mass that an object needs to have to be gravitationally bound, assuming the virial theorem applies, i.e., that  $2E_k = |E_g|$ . For the most simple case of the virial theorem, and assuming a uniform-density sphere of radius  $R$ ,  $E_g = -3GM^2/5R$  and  $E_k = 3M\sigma_{\text{tot}}^2/2$  (e.g., André et al., 2012; Camacho et al., 2023):

$$M_{\text{vir}} = \frac{3 R \sigma_{\text{tot}}^2}{G}, \quad (10)$$

where  $\sigma_{\text{tot}}$  is the total 1D velocity dispersion including thermal and non-thermal contributions<sup>4</sup>. The virial parameter is then  $\alpha_{\text{vir}} \equiv M_{\text{vir}}/M_{\text{obs}} = 2E_k/E_g$  and it has the following meaning:

if  $\alpha_{\text{vir}} \lesssim 1$ , the object is strongly self-gravitating; if  $\alpha_{\text{vir}} \sim 1$ , the object is gravitationally bound; if  $\alpha_{\text{vir}} \gg 2$ , self-gravity is not dominant.

*Gravitational mass,  $M_{\text{grav}}$ .* The gravitational mass is the mass required to have equipartition between gravitational energy and kinetic energy, i.e.,  $E_k = |E_g|$ , or, equivalently,  $\alpha_{\text{vir}} \sim 2$ . This is a criterion less severe than the constraint arising from the virial parameter, and has also been used as a measure of the gravitational boundness of a core, for example, by Pound and Blitz (1993, 1995) and Palau et al. (2012):

$$M_{\text{grav}} = \frac{3 R \sigma_{\text{tot}}^2}{2 G}. \quad (11)$$

*Bonnor-Ebert mass,  $M_{\text{BE}}$ .* The Bonnor-Ebert mass is the maximum possible mass of an isothermal sphere in hydrostatic equilibrium embedded in a medium exerting an external pressure  $p_0$  on it.  $M_{\text{BE}}$  can be estimated as (e.g., Bonnor, 1956; Ebert, 1957; Draine, 2011):

$$M_{\text{BE}} = 0.26 \left( \frac{T}{10 \text{ K}} \right)^2 \left( \frac{10^6 \text{ cm}^{-3} \text{ K}}{p_0/k} \right)^{1/2} \quad (12)$$

in  $M_\odot$ , and with  $k$  being the Boltzmann’s constant and  $T$  the temperature of the sphere. A pressure-bounded isothermal sphere with mass equal to  $M_{\text{BE}}$  has a density at the center of  $\sim 14$  times the density at the surface,  $\rho_0$ . Taking into account that  $\rho_0 = p_0/c_s^2$  (with  $c_s$  being the sound speed) and using the number density at the surface of the sphere,  $n_0$ , equation 12 can be re-written as

$$M_{\text{BE}} = 2.6 \left( \frac{T}{10 \text{ K}} \right)^{3/2} \left( \frac{n_0}{10^3 \text{ cm}^{-3}} \right)^{-1/2}, \quad (13)$$

comparable to equation (1) of Padoan and Nordlund (2004).

*Jeans mass,  $M_{\text{Jeans}}$ .* The Jeans mass is the minimum mass that a perturbation, occurring within a uniform, stationary, non-rotating and unmagnetized gas, needs to have to become gravitationally unstable.  $M_{\text{Jeans}}$  can be estimated as (e.g., Jeans, 1928; Draine, 2011; Palau et al., 2015):

$$M_{\text{Jeans}} = 0.6285 \left( \frac{T}{10 \text{ K}} \right)^{3/2} \left( \frac{n_{\text{H}_2}}{10^5 \text{ cm}^{-3}} \right)^{-1/2}, \quad (14)$$

where  $n_{\text{H}_2}$  is the density of  $\text{H}_2$  molecules, typically used when considering the dense parts of molecular clouds.  $M_{\text{Jeans}}$  is of the order of  $M_{\text{BE}}$ , with  $M_{\text{BE}} \sim 1.2 M_{\text{Jeans}}$  (e.g., Draine, 2011). Thus, for higher temperatures of the gas,  $M_{\text{Jeans}}$  is larger, making more difficult to fragment a cloud down to very small masses.

<sup>4</sup>It is important to note that the total 1D velocity dispersion includes both thermal,  $\sigma_{\text{th}}$ , and non-thermal,  $\sigma_{\text{nth}}$ , contributions, i.e.,  $\sigma_{\text{tot}} = \sqrt{\sigma_{\text{th}}^2 + \sigma_{\text{nth}}^2}$ . However, for pre-BDs the non-thermal contribution is small, and care must be taken to properly measure the thermal contribution, by calculating it using

the mean molecular weight per particle of molecular gas,  $\mu$ , typically taken as 2.3, instead of using the molecular weight of the observed molecular tracer:  $\sigma_{\text{th}} = \sqrt{kT/(\mu m_{\text{H}})}$ , with  $k$  being the Boltzmann constant,  $m_{\text{H}}$  the mass of the hydrogen atom and  $T$  the temperature.

### 3. Systematic searches and serendipitous discoveries

Up to now, a number of systematic searches have been carried out to search for proto-BDs and pre-BDs. But also an important number of these discoveries have been serendipitous. Here we briefly summarize each one of these main discoveries, in order to learn from the crucial criteria and characteristics of the proto-BD and pre-BD candidates discovered so far.

#### 3.1. Systematic searches

Systematic searches of pre- and proto-BDs have been based on two main strategies. On one hand, an important number of works started from a selection criteria based on the identification of deeply embedded infrared sources, and then carried out a follow-up in the millimetre/sub-millimetre bands, where a number of criteria were applied to identify the reddest and least massive objects, typically with additional indicators to reject background contaminants. On the other hand, searches based on millimetre/sub-millimetre imaging have also been carried out. We present below the main works based on each strategy.

##### 3.1.1. Searches of infrared sources and follow-ups

In this section, a list of the searches of very low-luminosity infrared sources is presented. It has been usual in the literature to refer to embedded objects with  $L_{\text{int}} \lesssim 0.1\text{--}0.2 L_{\odot}$  as Very Low Luminosity Objects (VeLLOs) (e.g., [Kauffmann et al., 2005](#); [di Francesco et al., 2007](#); [Dunham et al., 2008](#); [Kim et al., 2016](#)), and they certainly constitute an excellent base to look for proto-BDs. We exclude from this review the works searching for millimetre/sub-millimetre emission towards samples of Class II/III BDs (with ages  $\gtrsim 1$  Myr; e.g., [Klein et al., 2003](#); [Scholz et al., 2006](#); [Spezzi et al., 2013](#); [Harvey et al., 2012b,a](#)), and the works searching for embedded protostars in entire clouds, regardless of luminosity (e.g., [Kirk et al., 2007](#); [Jørgensen et al., 2007, 2008](#); [Enoch et al., 2007, 2008](#); [Hsieh and Lai, 2013](#); [Harvey et al., 2013](#)). The most relevant studies based on searches of very low-luminosity infrared sources are presented below, listing first the work and then the main telescopes/surveys used for the searches:

**White and Hillenbrand (2004), Keck I:** A spectroscopic optical study with the Keck I telescope is presented for 15 Class I and Class II sources driving HH objects, selected from the IRAS catalog in the Taurus-Auriga cloud. All stars in the cloud with Class I-like SED (based on either their mid-infrared spectral index, [Myers et al. 1987](#)) or their  $T_{\text{bol}}$  ([Myers and Ladd 1993](#)) were selected and masses were inferred based on the spectral type classification and the [Siess et al. \(2000\)](#) isochrones at 1 Myr. They found 3 objects that qualify as Class I proto-BD candidates (IRAS 04158+2805, IRAS 04248+2612, IRAS 04489+3042), given their  $T_{\text{bol}} < 650$  K, spectral types later than M5.5 and substellar masses (see Sec. 3.2 and Fig. 11 of [White and Hillenbrand, 2004](#)). The sub-millimetre emission was studied in [Motte and André \(2001\)](#) with the IRAM 30m radiotelescope. Follow-up sub-millimetre Array (SMA)

observations of IRAS 04158+2805 were presented in [Andrews et al. \(2008\)](#). However, the model fitting the CO (3–2) velocity gradient of this source yields  $M_{\text{acc}} \sim 0.15\text{--}0.45 M_{\odot}$ , challenging the substellar nature (see also [Luhman et al. 2010](#)).

**Dunham et al. (2008), Spitzer IRAC+MIPS (c2d):** After the works of [Young et al. \(2004\)](#) and [Di Francesco et al. \(2008\)](#), [Dunham et al. \(2008\)](#) base their selection criteria on detections in MIPS bands, IRAC colors characteristic of rising SEDs, infrared luminosity smaller than  $0.5 L_{\odot}$ , and not classifying as a galaxy candidate according to [Harvey et al. \(2007\)](#). A value of  $L_{\text{int}} \lesssim 0.1 L_{\odot}$  and association with a dense core were established as the criteria to consider an object a Very Low Luminosity Object, and [Kauffmann et al. \(2005\)](#) and [Dunham et al. \(2008\)](#) identify 15 VeLLOs, being L1014, IRAM 04191, L673-7, L1148-IRS, IRAS 16253–2429, L328-IRS, IRAS 16253–2429 among them.

**Sicilia-Aguilar et al. (2008), VLT/FLAMES + Spitzer/IRS:**

A sample of 62 very low-mass stars and BDs, previously detected in X-rays, was observed in the optical and infrared with the VLT/FLAMES and *Spitzer*/IRS in the Coronet cluster. The optical spectra reveal spectral types between M1 and M7.5, confirm the Class I nature for 11 of the sources (2 classified as ‘flared’), and show the presence of accretion and shocks. The IRS spectra, together with infrared photometry from the IRAC/MIPS instruments on *Spitzer* and 2MASS, confirm the presence of infrared excesses characteristic of discs around  $\sim 70\%$  of the objects. The Class I sources are: G-6, G-17, G-28 (flare source), G-36, G-43, G-45, G-64 (late M spectral type, shocks), G-101, G-108 (flare source, late M spectral type), G-112, and G-122. This study was followed-up in [Sicilia-Aguilar et al. \(2011\)](#) where APEX observations were presented. This later study reveals sub-millimetre emission associated with source G-17, whose integrated flux corresponds to a mass of  $0.18 M_{\odot}$  (assuming a dust temperature of 20 K and a dust+gas opacity of  $0.0175 \text{ cm}^2 \text{ g}^{-1}$ , [Ossenkopf and Henning 1994](#)).

**Barrado et al. (2009), Spitzer IRAC:** The Taurus cloud was surveyed to identify all sources with detections in the four IRAC bands, whose location in color-color diagrams corresponds to Class 0/I sources and whose IRAC1 magnitude was below 11 mag, corresponding to the expected value for a substellar photosphere at the Taurus distance, according to the models of [Baraffe et al. \(2003\)](#). Further criteria to reject extragalactic contamination were applied. This resulted in 12 proto-BD candidates. Follow-ups were carried out by [Palau et al. \(2012\)](#) and [Morata et al. \(2015\)](#), where millimetre/sub-millimetre emission was studied along with a search for thermal radiojets.

**Bulger et al. (2014), Herschel for M4–L0 members:** A sample of Taurus members with spectral type M4–L0 was built by requiring that they have been observed with *Herschel*,

yielding a total of 150 objects. Among the 150 members, 7 are Class I or earlier (Sec. 6.7 of [Bulger et al. 2014](#)), and 3 are VeLLOs: [GKH94]41, IRAS 04191+1523 B, and L1521F-IRS. IRAS 04191+1523B is the secondary component of a binary system in which the primary is of stellar nature. A follow-up work by [Dang-Duc et al. \(2016\)](#) with CARMA at 2.9 mm reveal that [GKH94]41 and IRAS 04191+1523B have  $M_{\text{acc}} \lesssim 0.057 M_{\odot}$ , but subsequent ALMA observations yield  $M_{\text{acc}} \lesssim 0.120 M_{\odot}$ , twice the estimate from CARMA ([Lee et al., 2017](#)). This gives an idea of the uncertainty in the estimate of  $M_{\text{acc}}$ .

**Riaz et al. (2015), UKIDSS+WISE:** A systematic search for proto-BDs in the UKIDSS+WISE data of the  $\sigma$ -Orionis region was carried out, finding that the sources Mayrit1701117 and Mayrit1082188 are good Class I/Flat proto-BD candidates. Further optical spectroscopic and sub-millimetre observations were used to complement the characterization of these two sources, for which  $L_{\text{bol}}$  in the range 0.16–0.18  $L_{\odot}$ , and  $M_{\text{env}} \sim 0.022\text{--}0.036 M_{\odot}$  were inferred. Mayrit1701117 was further studied in [Riaz et al. \(2017, 2019a\)](#) and [Riaz and Bally \(2021\)](#), who report that the source is driving a Herbig-Haro object and that has an associated pseudo-disc seen with ALMA. This strategy was later applied to the Ophiuchus, Perseus, Taurus and Serpens-Aquila clouds ([Riaz and Thi, 2022b,a,c](#); [Riaz et al., 2023](#)), and several studies of the chemistry in these objects were also carried out ([Riaz et al., 2018, 2019b](#); [Riaz and Bally, 2021](#); [Riaz and Thi, 2022b,a,c](#); [Riaz et al., 2023](#)).

**Kim et al. (2016): Spitzer c2d IRAC + MIPS + Herschel:**

The work of [Kim et al. \(2016\)](#) includes five c2d clouds at distances  $< 350$  pc, and eleven nearby molecular clouds from the Gould Belt survey<sup>5</sup>, along with the Orion and Taurus molecular clouds. For these 16 clouds, about 100000 point-sources were detected by *Spitzer* and *Herschel*, and the criteria of [Dunham et al. \(2008\)](#) were applied along with the additional criteria:  $L_{\text{int}} < 0.2 L_{\odot}$ <sup>6</sup>, detection at 70  $\mu\text{m}$ ,  $F_{1.65\mu\text{m}}/F_{70\mu\text{m}} < 2.8$ , and  $[8] - [24] > 2.2$ , to assure that the sources are embedded. Furthermore, the criteria of [Harvey et al. \(2007\)](#) to reject extragalactic contaminants were also applied. This resulted in 320 sources, of which 95 present evidences of having a dusty envelope associated from *Herschel*/SPIRE or James Clerk Maxwell Telescope (JCMT/SCUBA) data. In addition, firm evidence of dense ( $\text{N}_2\text{H}^+$ ) gas was found in 44 of the 95 objects, being these objects classified as confirmed VeLLOs. The remaining 51 objects with no dense gas associated were classified

as VeLLO candidates (detected only in the sub-millimetre continuum). It is important to note that the [Kim et al. \(2016\)](#) strategy recovers the bona-fide IC348-SMM2E proto-BD in the confirmed VeLLOs group. This study was followed-up in [Kim et al. \(2019\)](#) and [Kim et al. \(2021\)](#) to look for outflow and inflow motions, making it the most complete and uniform sample of VeLLOs up to date from 16 nearby molecular clouds.

**Riaz et al. (2016): Spitzer c2d IRAC:** The Serpens Main and Serp/G3–G6 clusters were studied using the c2d *Spitzer* catalog. The selection criteria were a Class 0/I/Flat SED and  $L_{\text{bol}} \leq 0.3 L_{\odot}$ . These criteria resulted in 28 very low-mass stars or proto-BD candidates, 13 of which were classified as Class 0/I and 15 as Flat sources, according to the *Spitzer* c2d catalog. Most targets listed in this analysis are associated with bright 250  $\mu\text{m}$  *Herschel* emission and JCMT 450 and 850  $\mu\text{m}$  emission. These data were complemented with spectroscopy in the near- and mid-infrared, as well as with  $\text{HCO}^+$  observations with the Caltech Submillimeter Observatory (CSO). From this study, one proto-BD candidate with a significant (non-tenuous) envelope was discovered, J182902. This object is a Class I/Flat source with  $L_{\text{int}} \sim 0.03 L_{\odot}$ , for which  $M_{\text{acc}} \lesssim 0.04 M_{\odot}$ . The detection with the JCMT at 450 and 850  $\mu\text{m}$  corresponds to  $M_{\text{env}}$  in the range 0.01–0.03  $M_{\odot}$ . However, after the work of [Riaz et al. \(2016\)](#), where a distance of 260 pc was adopted, [Ortiz-León et al. \(2023\)](#) report an updated distance to the Serpens cluster from  $\text{H}_2\text{O}$  maser parallax of  $440.7 \pm 3.5$  pc. In the following, the parameters of the Serpens sources for which a distance of 260 pc had been adopted in previous works, have been recalculated to the new distance of 440 pc, implying that some of the candidates of [Riaz et al. \(2016\)](#) and [Kim et al. \(2016\)](#), initially classified as VeLLOs, are re-classified now as likely protostars. Follow-up studies combined this strategy with the strategy carried out by [Riaz et al. \(2015\)](#) and performed a chemical study of the resulting combined sample ([Riaz et al., 2018, 2019b](#); [Riaz and Bally, 2021](#)).

### 3.1.2. Sub-millimetre/millimetre imaging and follow-ups

A second approach to search for pre- and proto-BDs consisted on performing large-scale imaging surveys in the sub-millimetre/millimetre bands of specific regions of molecular clouds. This has the advantage of including pre-BDs and objects more deeply embedded because the detection of an infrared source is not required. We list here a number of this kind of searches in the literature:

**Pound and Blitz (1993), AT&T Bell Labs and NRAO 12m:**

A sample of 400 clumps in 7 nearby High-Latitude clouds (from [Magnani et al., 1985](#)) was observed with AT&T Bell Labs 7m Telescope. The 7 clouds were imaged in CO (1–0) and  $^{13}\text{CO}$  (1–0) with a beam of  $\sim 100''$ . Seventy clumps with moderate bright integrated intensity and size  $< 3'$  were selected and imaged at higher angular resolution with the NRAO 12m Kitt Peak radiotelescope

<sup>5</sup>The five clouds from c2d are Perseus, Serpens, Chamaeleon II, Lupus, and Ophiuchus; and the 11 clouds from the Gould Belt survey are California, Chamaeleon I, Chamaeleon III, Musca, Lupus V, Lupus VI, Ophiuchus North, Aquila, Corona Australis, Cepheus, and IC 5146.

<sup>6</sup>Although the original definition of VeLLOs requires that  $L_{\text{int}} \leq 0.1 L_{\odot}$ , [Kim et al. \(2016\)](#) adopted  $L_{\text{int}} \leq 0.2 L_{\odot}$  to take into account the dispersion in the  $F_{70\mu\text{m}}$  vs  $L_{\text{int}}$  relation found by [Dunham et al. \(2008\)](#).



in CO,  $^{13}\text{CO}$ , and CS, allowing to estimate masses from  $^{13}\text{CO}$ . The estimated masses were compared to the gravitational mass, but all objects had estimated masses smaller than the gravitational mass  $M_{\text{grav}}$ , with only two objects being nearly gravitationally bound, although they were not substellar. This was followed-up by [Pound and Blitz \(1995\)](#) by applying the same strategy to the Ophiuchus (Oph B) and Taurus (B18) molecular clouds. Imaging in  $\text{C}^{34}\text{S}$  (2–1),  $\text{DCO}^+$  (1–0) and  $\text{DCO}^+$  (3–2) was performed using the AT&T and NRAO antennas, and the CSO telescope was used to image the continuum emission at 800  $\mu\text{m}$ . From this work, 4 objects were found close to the substellar limit and to be gravitationally bound, being Oph-B11 one of the most promising proto-BD candidates. Follow-ups of this work are presented in [Greaves et al. \(2003\)](#), where the JCMT was used to image part of the  $\rho$ -OphB region, finding 11 compact cores with  $M_{\text{env}} < 15 M_{\text{Jup}}$ . Among these 11 compact cores, CO (3–2) wings were detected in the Oph-B11 source. This object was later found to be a pre-BD core ([André et al., 2012](#)).

**Tachihara et al. (1996), Nagoya University telescope :** The proto-BD candidate IRAS 15398–3359 was discovered as the driving source of a  $^{13}\text{CO}$  outflow in a survey carried out using the Nagoya University telescope towards the Lupus clouds. Later [Oya et al. \(2014\)](#) report ALMA observations of the outflow and the driving source, finding that it is a Class 0 source with molecular gas detections in  $\text{H}_2\text{CO}$  and  $\text{C}_2\text{H}$ . The position-velocity diagrams of some transitions of these molecules suggest a central mass 0.02–0.09  $M_{\odot}$ . However, [Jørgensen et al. \(2013\)](#) study the chemistry in this object and report  $M_{\text{env}} \sim 1.2 M_{\odot}$ , and  $L_{\text{bol}} \sim 1.8 L_{\odot}$ , possibly due to an accretion burst. Later [Yen et al. \(2017\)](#) and [Okoda et al. \(2018\)](#) present ALMA observations of  $\text{C}^{18}\text{O}$ ,  $\text{C}_2\text{H}$  and SO, from where  $M_{\text{acc}}$  was estimated to be in the range 0.007–0.01  $M_{\odot}$ . [Tabatabaei et al. \(2023\)](#) and [Thieme et al. \(2023\)](#) further study the kinematics and magnetic field of the region.

**Motte et al. (1998), IRAM 30m:** The central region of  $\rho$ -Ophiuchi was imaged at 1.3 mm with the IRAM 30m telescope, revealing about 68 clumps, out of which 26 have  $M_{\text{env}} < 0.15 M_{\odot}$ , and 18 of these 26 have  $M_{\text{env}} > M_{\text{BE}}$ , suggesting that they are gravitationally unstable. A follow-up of these 18 least massive gravitationally bound objects of this sample would be very useful.

**Kauffmann et al. (2008), IRAM30m:** A sample of 38 cores selected from the initial target list of the c2d *Spitzer* survey and having sizes  $\lesssim 0.5 \text{ pc}$  ( $\lesssim 5'$  at distances  $\lesssim 400 \text{ pc}$ ) was observed at 1.3 mm with the MAMBO bolometer array at the IRAM 30m telescope. The combination of these deep millimetre maps with archival infrared data enabled the derivation of  $L_{\text{bol}}$  and  $T_{\text{bol}}$ , as well as  $M_{\text{env}}$ , and to identify a number of VeLLOs, which were found to have density profiles steeper and with larger central densities than

starless cores. This suggests that VeLLO cores are structurally different from starless cores.

**Nakamura et al. (2012), JCMT+SMA:** Two prestellar cores (SM1 and B2-N5) in  $\rho$ -Ophiuchi were studied using sub-millimetre single-dish emission and the SMA, revealing that each prestellar core splits up into 3–4 subcondensations of 0.01–0.1  $M_{\odot}$ , and sizes of a few hundred AU. Since the mean densities are higher than  $10^8 \text{ cm}^{-3}$ , their masses are larger than  $M_{\text{BE}}$  (eq. 12), suggesting that the subcondensations are gravitationally unstable and are, consequently, good pre-BD candidates.

**Liu et al. (2016), Planck:** Dedicated observations towards Planck Galactic Cold Clumps in the  $\lambda$ -Orionis complex reveal an extremely young Class 0 protostellar object and a proto-BD candidate in the bright-rimmed clump G192.32-11.88, which seems to be externally heated and compressed, reducing the star formation efficiency and core formation efficiency.

**Gahm et al. (2013), Onsala+APEX:** The Onsala and APEX telescopes were used to study the molecular gas in the Rosette Nebula, detecting CO (3–2), CO (2–1),  $^{13}\text{CO}$  (3–2), and  $^{13}\text{CO}$  (2–1) in narrow lines of about  $1 \text{ km s}^{-1}$ . About 7 globulettes were found with  $M_{\text{env}} < 0.075 M_{\odot}$ . The study was complemented with broad JHK filters, narrow Paschen $\beta$ , and  $\text{H}_2$  imaging. The dynamical state of these 7 globulettes should be assessed by studying the gas kinematics.

**de Gregorio-Monsalvo et al. (2016), APEX:** The Chamaleon II cloud was studied using LABOCA at 850  $\mu\text{m}$  on APEX, and 5 pre-BD candidates and 1 proto-BD candidate, Cha-APEX-L, were found. Regarding the pre-BDs, their masses range from 0.016 to 0.021  $M_{\odot}$ , and have no counterpart in MPG, VLT, 2MASS, WISE, *Spitzer*, AKARI, *Herschel*/PACS. Since they were unresolved, their radius must be  $< 2500 \text{ au}$  at the distance of the Chamaleon clouds. It was tentatively estimated that these objects could be gravitationally bound by comparing their masses to  $M_{\text{BE}}$ . Kinematic information on molecular gas would help define their stability. Regarding the proto-BD candidate, Cha-APEX-L, it has  $L_{\text{bol}} \sim 0.08 L_{\odot}$ , and  $M_{\text{env}} \sim 0.050 M_{\odot}$ , and its infrared and sub-millimetre fluxes are comparable to those of other Class 0/I proto-BD candidates, with a clear counterpart at 3.6 and 4.5  $\mu\text{m}$ .

**Barrado et al. (2018), APEX:** The star-forming region B30, at the border of the bubble in the  $\lambda$  Ori cluster, was studied using LABOCA on APEX at 850  $\mu\text{m}$ , resulting in 8 proto-BD candidates, with  $L_{\text{bol}} < 0.16 L_{\odot}$ , and  $M_{\text{env}} \lesssim 0.012 M_{\odot}$ . However, a follow-up study by [Huélamo et al. \(2017\)](#) with ALMA at 880  $\mu\text{m}$  (with a rms noise of  $0.2 \text{ Jy beam}^{-1}$ , corresponding to a  $5\sigma$  mass sensitivity of  $\sim 0.001 M_{\odot}$  for a dust temperature of 15 K) reveal no detections towards these objects, making its nature unclear. In the [Barrado et al. \(2018\)](#) study, six sub-millimetre cores, with  $M_{\text{env}}$  in the range 0.082–0.106  $M_{\odot}$ , have no



optical/infrared counterparts. [Huélamo et al. \(2017\)](#) find that 3 out of the 6 starless cores (cores LB8, LB10, LB31) have an ALMA compact millimetre source associated, being these three objects potential pre-BDs. Further observations of dense gas would help constrain the nature of these objects.

**Tokuda et al. (2019), IRAM 30m + ACA:** A survey at 1.2 mm was carried out using the IRAM 30m telescope and the ACA array in the L1495 region of the Taurus cloud. A condensation was identified to be dense and connected to a narrow filament of the L1495 region. This condensation, called MC5-N, was proposed to be a pre-BD candidate. The mass of the core is  $0.2\text{--}0.4 M_{\odot}$ , and observations of  $\text{N}_2\text{H}^+$  and  $\text{N}_2\text{D}^+$  reveal a high deuterium fractionation.

**Santamaría-Miranda et al. (2021), ASTE+ALMA:** The AzTEC 1.1 mm array camera at the Atacama sub-millimetre Telescope Experiment (ASTE) was used to image the Lupus I and Lupus III clouds, followed by ALMA observations. The measured  $M_{\text{env}}$  are below  $0.124 M_{\odot}$ , and among the 15 detections, 2 are new Class I/0 proto-BD candidates, and 12 are new possible pre-BDs. In particular, the Class 0/I source ALMA J154229–334241 could potentially be a promising proto-BD candidate.

### 3.2. Serendipitous discoveries

A number of (isolated) proto-BD candidates were discovered serendipitously, that is, without following a well-defined strategy specifically designed to find these kind of objects. We list here some relevant cases (excluding proto-BD candidates which are clearly part of a (close) multiple system where the primary is a young stellar object, e.g., [Apai et al. 2005](#)):

**Palau et al. (2014), IC348-SMM2E:** About 10 arcsec to the (north)east of the Class 0 source driving the HH 797 object (also known as IC348-MMS, with  $L_{\text{bol}} \sim 1.9 L_{\odot}$ , and  $M_{\text{env}} \sim 10 M_{\odot}$ , [Hatchell et al. 2007](#)), a faint compact core with  $M_{\text{env}} \sim 0.03\text{--}0.05 M_{\odot}$  also driving a compact outflow and a thermal radiojet was discovered ([Palau et al., 2014; Forbrich et al., 2015](#)). The SED of the compact object is typical of Class 0 sources, and has  $L_{\text{int}} \sim 0.1 L_{\odot}$ . A velocity gradient perpendicular to the outflow was identified in  $\text{C}^{18}\text{O}(2\text{--}1)$  with the SMA, which suggests  $M_{\text{acc}}$  in the range  $0.036\text{--}0.110 M_{\odot}$  for a disc inclination with respect to the plane of the sky of  $30\text{--}60^\circ$  and at the revised distance to IC348 of 320 pc ([Ortiz-León et al., 2018](#)). Since the distance from the proto-BD candidate to the stellar-mass Class 0 source is  $\sim 3000$  au, it is not likely that this object was formed in the disc of the nearby protostar and rather suggests that it was formed by gravitational fragmentation of the parental structure.

**Whelan et al. (2018), ISO Oph 200:** ISO Oph 200 is a Class I source with  $L_{\text{bol}} \sim 0.09 L_{\odot}$ , and its  $850 \mu\text{m}$  emission detected with the JCMT indicates  $M_{\text{env}} \sim 0.060 M_{\odot}$ . [Whelan et al. \(2018\)](#) report  $\text{H}_2$  and  $[\text{FeII}]$  emission with

VLT/SINFONI indicative of outflow activity. This object was also studied by [Riaz and Machida \(2021\)](#) with ALMA in CO and their isotopologues, who conducted a physical and chemical modelling of the internal structure. The model includes an extended outflow, envelope/pseudo-disc, and an inner pseudo-disc, and indicates that the object could have been misclassified due to its line-of-sight outflow orientation.

### **Kawabe et al. (2018), SM1-A and Source-X in Oph-A:**

Two proto-BD candidates were identified about 15 arcsec (or 2000 au) to the north-east of the VLA1623 source, named SM1-A and Source-X ([Di Francesco et al., 2004; Kawabe et al., 2018](#)). Both sources drive compact molecular outflows, have continuum millimetre emission associated an also X-ray emission detected with Chandra. Their  $L_{\text{bol}}$  are very low, of  $0.035$  and  $0.01 L_{\odot}$ , respectively, but their  $M_{\text{env}}$  cannot be easily estimated because both objects are embedded within the brightest sub-millimetre clump of Oph-A.

**Phan-Bao (2022), SMA1627–2441:** A proto-BD candidate was serendipitously discovered with the SMA about  $\sim 20$  arcsec ( $\sim 3000$  au) to the west of the Class II BD, ISO-Oph102 (e.g., [Greene and Young, 1992; Natta et al., 2002; Phan-Bao et al., 2008](#)). The source seems to be driving a small-scale bipolar outflow detected in CO(2–1).

It is important to note that a significant number of these serendipitous discoveries (at least IC348-SMM2E, SM1-A, Source-X and SMA1627–2441) were found in the surroundings ( $\lesssim 5000$  au) of well-known Class 0 protostars or BDs (IC348-MMS, VLA1623, and ISO-Oph102, respectively). At least another candidate has been discovered this way ([Palau et al., 2022](#)). If proto-BDs were typically found in the surroundings of protostars, this would imply that systematic offsets between the proto-BD positions and column density peaks should be found, as discussed also in [Kauffmann et al. \(2008\)](#). This suggests that a promising strategy to search for proto-BDs is to carry out deep interferometric observations in the immediate surroundings of Class 0–II protostars or BDs.

As a final note, a possibility worth exploring coming from the aforementioned studies is whether there are pre- and/or proto-BDs (preferentially) associated with shells or bubbles. [Kim et al. \(2016\)](#) report about 10 VeLLOs which are not associated with active star-forming regions and are classified as ‘small cores’, isolated and located in different clouds (Table 1 of [Kim et al. 2016](#)), and one of them, L328, is not associated with a large molecular cloud complex and lies within a shell-like structure, similar to OphB-11 (pre-BD of [André et al. 2012](#)) and the pre-BDs of B30 ([Huélamo et al., 2017; Barrado et al., 2018](#)). Thus, a non-negligible fraction of pre- or proto-BDs could potentially reside at the border of bubbles.

#### 4. Challenges and difficulties to identify promising pre- and proto-BD candidates

Given the searches and discoveries presented in the previous section, a number of challenges and difficulties can be identified in the pre- and proto-BD search. We enumerate these challenges and briefly describe them in the following subsections.

##### 4.1. Not all VeLLOs or FHCs are good proto-BD candidates

Proto-BDs can be confused with VeLLOs and First Hydrostatic Cores (FHCs). While VeLLOs are objects whose  $L_{\text{int}} \lesssim 0.1 L_{\odot}$  (Sec. 3.1.1), FHCs are compact objects in quasi-hydrostatic equilibrium, resulting from a change in the gravitational collapse regime, from isothermal to adiabatic, which occurs when the gas becomes optically thick, preventing the gravitational energy to be released and thus increasing the thermal pressure (e.g., Larson, 1969). With a lifetime of around 10 000 yr (e.g., Bate et al., 2014; Maureira et al., 2020), FHCs continuously accrete, increasing their temperature up to 2000 K, when collisional dissociation of  $\text{H}_2$  consumes energy triggering a second collapse. Observationally, FHCs are objects whose internal luminosity is still very low (emission at  $70 \mu\text{m}$  is marginal or undetected), have a clear millimetre source associated, drive small outflows, and have a very low  $T_{\text{bol}}$ , typically below 20 K (e.g., Commerçon et al., 2012; Palau et al., 2014; Maureira et al., 2020; Young, 2023). A summary of the FHC properties is presented in the wrap-up last figure of this work, along with the pre-stellar, pre-BD, protostellar and proto-BD cases. The FHC stage of the low-mass star-formation process, and the proto-BD phase of the substellar regime share similar properties and can be easily confused, but there are clues that allow us to distinguish between them. In the criteria used to select both VeLLOs or FHCs there is no restriction about the mass of the parental core, which can reach values up to  $\sim 10 M_{\odot}$  in some cases (e.g., Kauffmann et al., 2011; Palau et al., 2014; Maureira et al., 2020). With such a large  $M_{\text{env}}$ , the object could accrete enough mass in the future and become stellar. Thus, a low value of  $M_{\text{env}}$  is a crucial property of proto-BDs that VeLLOs or FHCs might not necessarily fulfill.

##### 4.2. Difficulty to find infrared/optical counterparts of submm cores and to constrain their evolutionary stage

If the strategy to search for proto-BDs is based on submillimetre continuum surveys of clouds (Sec. 3.1.2), then the identification of the infrared/optical counterpart might be very complicated because proto-BDs are intrinsically very faint, and this problem worsens if the object is deeply embedded and highly extincted (e.g., de Gregorio-Monsalvo et al., 2016; Barado et al., 2018; Santamaría-Miranda et al., 2021). This in turn implies that no estimate of  $L_{\text{bol}}$  and  $T_{\text{bol}}$  can be made because of poorly sampled SEDs, leaving the nature of the candidates uncertain (e.g., Huélamo et al., 2017; Phan-Bao, 2022).

##### 4.3. Uncertain accreted mass $M_{\text{acc}}$

In order to assess whether a proto-BD candidate is robust, it is vital to estimate its current accreted mass  $M_{\text{acc}}$ . There are

several methods in the literature used to estimate  $M_{\text{acc}}$ , that we outline below:

**Evolutionary models:** Isochrones and mass tracks from theoretical evolutionary models (such as Chabrier et al. 2000; Baraffe et al. 2017) can be used to estimate accreted masses (Dang-Duc et al., 2016; Riaz et al., 2019a). However, these models are typically calculated for too evolved stages (ages  $\sim 1$  Myr) with little accretion, and this is not consistent with the proto-BD nature. One exception is the work of Vorobyov et al. (2017a), who provide  $L_{\text{int}}-T_{\text{eff}}$  tracks for Class 0 objects, but this method should be more explored. In the cases where both this method and also a rough estimate from the method presented below (disc kinematics) have been applied, the results are not fully consistent. For example, Riaz and Machida (2021) apply this method to ISO Oph200 and find that  $M_{\text{acc}}$  is in the range 0.01–0.02  $M_{\odot}$  while, if the velocity gradient reported in their Fig. 5 is assumed to trace a Keplerian motion, then  $M_{\text{acc}} \sim 0.23 M_{\odot}$ , an order of magnitude larger, probably due to the contribution from infall.

**Mass-accretion rate:** If both the mass-accretion rate onto the proto-BD and the time during which the object has been accreting can be determined, then an estimate of  $M_{\text{acc}}$  can be made (e.g., Dunham et al., 2010; Lee et al., 2013; Kim et al., 2019). However, the determination of the mass-accretion rate, usually inferred from the mass-loss rate of the detected outflow, is a quantity highly uncertain. Mass-loss rates from molecular outflows are affected by the sensitivity of the telescope (the extension of the outflow can vary depending on the sensitivity), assumption of CO abundance, beam dilution (particularly important for proto-BDs with very small and compact outflows), inclination and opacity effects (see discussion by, e.g., Kim et al. 2019). Similarly, the time of accretion is also uncertain. Thus, this method, although useful to make first and preliminary estimates of  $M_{\text{acc}}$ , needs to be complemented with another method, as indicated in Schwarz et al. (2012). We compared the result of this method and the result of the disc-kinematics method (described in the next paragraph) for the particular case of IC348-SMM2E, and find that this method yields  $M_{\text{acc}} \sim 5 \times 10^{-5} M_{\odot}$  (Kim et al., 2019), while  $M_{\text{acc}}$  is 0.038–0.115  $M_{\odot}$  from the disc-kinematics method (Palau et al., 2014, and this work), thus differing by more than two orders of magnitude.

**Disc kinematics:** If a velocity gradient perpendicular to the outflow is identified, it is reasonable to assume that this is tracing a Keplerian motion associated with a disc structure. In this case,  $M_{\text{acc}}$ , usually referred to as ‘dynamical mass’ or  $M_{\text{dyn}}$ , can be estimated following eq. 8, or fitting the Keplerian curve for well resolved cases. This is routinely done for protostars in all the range of masses (e.g., Tobin et al., 2012; Guilloteau et al., 2014; Maret et al., 2020; Thieme et al., 2023). However, the typical uncertainties of this method can be large, at least of 50% (e.g., Andrews et al., 2008; Maret et al., 2020), and in Class 0 objects

infall needs to be taken into account. For more evolved objects, a good match between dynamical masses inferred from disc kinematics and masses from evolutionary models has been reported (Guilloteau et al., 2014). Thus, to properly obtain accurate  $M_{\text{dyn}}$  using this method, it is imperative the use of sensitive interferometric observations, to detect the Keplerian motion with detail and constrain the model. If the Keplerian motion is properly resolved, this method can be considered the most reliable to constrain the accreted mass in proto-BDs.

#### 4.4. Need to determine the mass that will be accreted in the future

Assuming that  $M_{\text{acc}}$  could be determined reasonably well, this is not enough yet to definitely confirm that the object is a bona-fide proto-BD. Since proto-BDs are still undergoing an active accretion phase, it is required to somehow estimate the total amount of mass that the object will accrete in the future. A first approach is based on  $M_{\text{env}}$ , which in principle constitutes the mass reservoir of the object. Thus, a good estimate of  $M_{\text{env}}$  is vital to assess whether the object will remain substellar or not after the main accretion phase. For this, it is essential to measure  $M_{\text{env}}$  using a single-dish, because masses inferred using interferometric measurements suffer from filtered flux. In addition, it is required to adopt a certain Star Formation Efficiency (SFE). However, which value to adopt is not well defined yet and probably depends on the large-scale environment. For example, Alves et al. (2007) and André et al. (2010) suggest  $\text{SFE} \sim 30\%$ , but in early stages it has been shown that the core formation efficiency depends on the density of the environment (Motte et al., 1998; Bontemps et al., 2010; Palau et al., 2013; Pandian et al., 2024). It is also important to keep in mind that the material accreted could eventually come from scales larger than the dense core associated with the proto-BD (e.g., Valdivia-Mena et al., 2023). Another approach to estimate the mass that will be accreted in the future is to determine the mass-accretion rate and to estimate the remaining time of accretion. Once the mass that will be accreted in the future is determined, it must be added to the current mass,  $M_{\text{acc}}$ , and if the total mass remains  $< 0.075 M_{\odot}$ , the object can be considered a robust proto-BD.

#### 4.5. Episodic accretion and variability complicate the estimate of luminosity

Episodic mass accretion complicates the classification of proto-BDs because proto-BDs could also be protostars that are in a quiescent state (e.g., Lee, 2007; Schwarz et al., 2012). Dunham and Vorobyov (2012) show that accretion bursts are required to solve the so-called ‘luminosity problem’, which refers to the fact that the luminosities measured for embedded protostars are about factors 10–100 smaller than expected given the predicted mass accretion rates in the ‘standard model’ of star formation (assuming that, in the embedded phase, the luminosity mainly comes from accretion as in eq. 9). Thus, when detecting a very-low luminosity object, it could be either a very low mass object or a more massive object in a quiescent stage,

and it has been proposed that chemistry could be a useful tool to distinguish between both possibilities (e.g., Lee, 2007).

One of the first cases where chemistry was shown to trace a recent accretion burst in a low-mass protostar is IRAS 15398–3359 (Jørgensen et al., 2013, see Sec. 5.3 for further details on the chemistry). The burst was supposed to have occurred about 100–1000 years ago, increasing the luminosity by two orders of magnitude. This would naturally explain the high luminosity measured for this source ( $L_{\text{bol}} \sim 1.8 L_{\odot}$ ) and the low  $M_{\text{acc}}$ , of around  $0.01\text{--}0.09 M_{\odot}$  (e.g., Oya et al., 2014; Yen et al., 2017; Okoda et al., 2018).

Another case where chemistry reveals a possible accretion burst is IRAM 04191+1522 (hereafter IRAM 04191). Anderl et al. (2020) find, using the Plateau de Bure Interferometer (PdBI), that the morphology of the  $\text{N}_2\text{H}^+$  and  $\text{C}^{18}\text{O}$  lines is not consistent with a constant luminosity model using the present-day internal luminosity, and that the  $\text{N}_2\text{H}^+$  peaks are rather consistent with an accretion burst corresponding to a luminosity 150 times higher than the current luminosity, that should have taken place about 150 years ago. Taking into account the accretion rate in the bursts and an accretion rate in the quiescent phase and a number of additional assumptions, a final mass in the Class 0 stage of  $0.2\text{--}0.25 M_{\odot}$  is estimated for this object. However the authors assume an infinite mass reservoir, while IRAM 04191 is located in an isolated environment (see Fig. C.2-top) and the largest  $M_{\text{env}}$  reported is of  $\sim 0.5 M_{\odot}$  (André et al., 1999)<sup>7</sup>. This would require a SFE of 50%, which seems too high. Additionally, the mass loss rate should be taken into account also in the calculation of the final mass. Thus, although the precise final mass of IRAM 04191 is still open, chemistry has already been shown to be able to trace accretion bursts in several cases, including larger samples of VeLLOs (e.g., Hsieh et al., 2018). In a very recent work, the NO molecule has been proposed as a potential outburst tracer in the VeLLO DC3272+18 by Kulterer et al. (2024).

Episodic accretion can also be characterized by studying the molecular outflows or jets. For example, Okoda et al. (2021) and Guzmán Ccolque et al. (2024) find signs of episodic ejection in IRAS 15398–3359, consistent with the chemical results of Jørgensen et al. (2013). Similarly, Dutta et al. (2024) report episodic accretion based on a study of molecular jets in the Orion Nebula Cloud. They report that mass-loss rates, mass-accretion rates, and periods of accretion events are dependent on  $L_{\text{bol}}$  and  $M_{\text{env}}$ , indicating that a large envelope favors the accretion-ejection processes. They determine mean periods of ejection events of 20–175 years in their sample (high-accretion rates may trigger more frequent ejection events), consistent with the assumptions done in Hsieh et al. (2018), who adopt about 100–200 years for the duration of the bursts, an a time interval between bursts of 10 000–20 000 yr.

All these studies demonstrate the presence of accretion bursts in protostellar and proto-BD objects, illustrate the complexity of dealing with episodic accretion, and show that chemistry is a powerful tool to distinguish between very low-mass objects

<sup>7</sup>  $M_{\text{env}}$  for IRAM 04191 has been estimated in different ways, being the value reported by Kim et al. (2016) among the lowest,  $M_{\text{env}} \sim 0.05 M_{\odot}$ .



and quiescent protostars. Further details on the chemistry of accretion bursts are provided in Sec. 5.3.

#### 4.6. Multiplicity could hinder proto-BD selection

In addition to the aforementioned difficulties to identify proto-BDs, it must be kept in mind that the proto-BD candidates could actually be multiple systems, implying that  $L_{\text{int}}$  is an upper limit. This would be expected, given the high multiplicity fraction found for deeply embedded protostars (e.g., [Chen et al., 2012a, 2013](#); [Tobin et al., 2018](#)). On the other hand, it is well known that the stellar binary fraction increases with the mass of the primary (e.g., [Offner et al., 2023](#)). Thus, it is of decisive importance to study multiplicity among proto-BDs, and to take this into account when defining upper limits to  $L_{\text{int}}$  for proto-BD selection. Studies of large samples of proto-BDs with high angular resolution would be key to shed light on this topic.

#### 4.7. Extragalactic contamination

Finally, if no molecular gas is detected towards the proto-BD candidates, it is necessary to consider the possibility that the object is a background object. There are several tests applied in the literature to assess this possibility, mainly focused on color-color diagrams (e.g., [Harvey et al., 2007](#); [Barrado et al., 2009](#)). In addition to this, the study of proper motions ([Huélamo et al., in prep.](#)) or centimeter emission (e.g., [Morata et al., 2015](#); [Rodríguez et al., 2017, 2024](#)) are very useful tools to assess the extragalactic nature.

Given the aforementioned list of challenges to properly identify pre- and proto-BDs, it can be easily understood that there are no large samples of pre- and proto-BDs in the literature. Thus, it becomes mandatory to focus our efforts on defining criteria that help to efficiently select bona-fide pre- and proto-BD candidates. In addition, very high angular resolution observations as provided by new-generation telescopes will be crucial to refine or re-define the criteria.

## 5. Main properties of proto-BD candidates known so far

### 5.1. Requirements for bona-fide proto-BD candidates

The observational efforts to identify proto-BDs presented in the previous sections constitute a very good starting point, but they contain very different approaches and criteria. In this section we synthesize what we consider as the backbones to select promising candidates. These backbones are intended to serve as a guide to build reasonable samples of proto-BD candidates from big data surveys and catalogs. By no means these requirements are enough conditions for an object to be a confirmed proto-BD. The confirmation of the candidates will have to be done using interferometers in follow-up deep, dedicated studies. Taking into account the criteria applied in the aforementioned strategies, along with the lessons learned from these works, we propose the following four requirements for an object to be a promising proto-BD candidate:

### Requirement 1. Substellar central object, $L_{\text{int}} \leq 0.13 L_{\odot}$ :

Ideally, it would be desirable to have good measurements of  $M_{\text{acc}}$  and to use this parameter for proto-BD identification and searches. However, as stated in Sec. 4.3, the determination of  $M_{\text{acc}}$  is highly uncertain or difficult to obtain because it would require sensitive interferometric observations of the gaseous disc, or very accurate mass-accretion rates and accretion timescales. This prompts to search for alternate parameters that could be related to  $M_{\text{acc}}$ . In principle, the luminosity should be a proxy to the accreted mass  $M_{\text{acc}}$ . For Class 0/I objects, where an important amount of the luminosity comes from accretion,  $M_{\text{acc}} \sim L_{\text{acc}}$  (see eq. 9). In turn,  $M_{\text{acc}} \sim L_{\text{acc}} \sim L_{\text{int}}$  because  $L_{\text{int}}$  corresponds to the luminosity contribution due to only star+disc, without taking into account the external contribution of the ISRF. Since  $L_{\text{int}}$  is easily calculated from observations at  $70 \mu\text{m}$  (eq. 6), establishing a relation between  $M_{\text{acc}}$  and  $L_{\text{int}}$  would be of great help in the proto-BD search. In the literature, the criterion of  $L_{\text{int}} \leq 0.2 L_{\odot}$  is used to assess the substellar nature for the most embedded cases (common to almost all the strategies mentioned in Sec. 3, [Young et al. 2004](#); [Dunham et al. 2008](#); [Kim et al. 2016](#)), which takes into account the uncertainty in the relation between the flux at  $70 \mu\text{m}$  and  $L_{\text{int}}$  of [Dunham et al. \(2008\)](#). In the case that  $70 \mu\text{m}$  fluxes were not available, it is required in some cases that  $L_{\text{bol}} < 0.3 L_{\odot}$  (e.g., [Riaz et al., 2016](#)), which is used as an upper limit for  $L_{\text{int}}$ . However, the criterion of  $L_{\text{int}} \leq 0.2 L_{\odot}$  is probably too relaxed to select promising proto-BDs for the following reason. We have compiled a list of protostars and VeLLOs for which  $L_{\text{int}}$  has been estimated following eq. 6, and for which  $M_{\text{acc}}$  has been derived from the ‘disc-kinematics’ method outlined in Sec. 4.3, i.e.,  $M_{\text{acc}} = M_{\text{dyn}}$ . In this compilation, we have restricted  $L_{\text{int}}$  to be  $< 10 L_{\odot}$ , because the relation between flux at  $70 \mu\text{m}$  and  $L_{\text{int}}$  was explored only for  $< 10 L_{\odot}$  ([Dunham et al., 2008](#)). This compilation is presented in Table 1 and the  $L_{\text{int}}-M_{\text{dyn}}$  relation is presented in Fig. 2. A few objects from Table 1 have not been plotted in Fig. 2 for several reasons. The cases of known multiple systems for which  $L_{\text{int}}$  is obtained including all components while  $M_{\text{dyn}}$  was obtained for only one of the components, yielding an obvious mismatch, have not been plotted in the figure. Other causes of exclusion are evidences in the literature that the source is outbursting, or  $T_{\text{bol}} < 20 \text{ K}$ <sup>8</sup>. The objects of Table 1 that have not been included in the figure, along with the reason for this exclusion, are indicated in column 5 of the table. As can be seen from the figure, there is a strong correlation with a Spearman’s rank correlation coefficient  $\rho = 0.902$ , and  $p$  value (the probability that the null hypothesis is true, that is, that the relation arises from a random process)  $< 0.001$ <sup>9</sup>. A fit

<sup>8</sup>Sources with  $T_{\text{bol}} < 20 \text{ K}$  are not included because for these very early evolutionary stages (considered as FHCs in some papers) the emission at  $70 \mu\text{m}$  could still be increasing (e.g., see Fig. 2 of [Young, 2023](#)) and very low  $T_{\text{bol}}$  has been associated also with pre-stellar cores (e.g., [Young and Evans, 2005](#)).

<sup>9</sup>We note that a certain dispersion in this relation is expected due to possible



was performed using the Orthogonal Distance Regression (ODR) package of Python, taking into account errors in both axes. The resulting fit is:

$$\log(L_{\text{int}}) = (0.41 \pm 0.11) + (1.62 \pm 0.14) \log(M_{\text{dyn}}), \quad (15)$$

where  $L_{\text{int}}$  is given in  $L_{\odot}$ , and  $M_{\text{dyn}}$  is given in  $M_{\odot}$ . It is interesting to note that this relation resembles as a first approximation the relation between photospheric luminosity and accreted mass from the models of D’Antona and Mazzitelli (1994) (Tables 1 and 5 of this paper), for a time step of  $5 \times 10^5$  yr (red thin solid line in Fig. 2). This timescale is the typical timescale estimated for the Class 0+I phases (e.g., Evans et al., 2009; Dunham et al., 2015; Heiderman and Evans, 2015). The empirical relation is also similar to the  $L_{\text{int}}$  vs  $M_{\text{acc}}$  relation for the hybrid models of Vorobyov et al. (2017b) for the same time step (blue thin solid line in Fig. 2). These last set of models take into account the accretion luminosity. The fact that the empirical relation is very close to the theoretical relations suggests that this relation is real. Once we have found a reasonable relation between  $L_{\text{int}}$  and  $M_{\text{dyn}}$ , it is possible to set a  $L_{\text{int}}$  criterion for proto-BDs. In order to select promising proto-BD candidates, we are interested in  $L_{\text{int}}$  corresponding to  $M_{\text{dyn}} < 0.12 M_{\odot}$ . We have chosen  $M_{\text{dyn}} < 0.12 M_{\odot}$  instead of  $M_{\text{dyn}} < 0.075 M_{\odot}$  because the typical uncertainty in  $M_{\text{dyn}}$  from the ‘disc-kinematics’ method is around 50% (Sec. 4.3), implying that an object with  $M_{\text{dyn}} = 0.075 M_{\odot}$  might have an error associated of  $\sim 0.04 M_{\odot}$ , giving an upper limit of  $M_{\text{dyn}} \sim 0.12 M_{\odot}$ . In addition, adopting  $M_{\text{acc}} < 0.12 M_{\odot}$  allows to take into account possible binary BD-BD systems, something which cannot be ignored (Sec. 4.6). From the fit to the data of Fig. 2,  $M_{\text{dyn}} = 0.12 M_{\odot}$  corresponds to  $L_{\text{int}} = 0.13 L_{\odot}$  (taking into account two times the uncertainty of the fit, whose corresponding shaded area includes  $\sim 70\%$  of the points used to infer the correlation). In the figure, the dashed vertical green line indicates  $M_{\text{dyn}} = 0.12 M_{\odot}$ , and the dashed blue horizontal line indicates  $L_{\text{int}} = 0.2 L_{\odot}$ . As can be seen in the figure, if we took  $L_{\text{int}} \leq 0.2 L_{\odot}$  as the criterion to select proto-BD candidates (as in previous searches, e.g., Kim et al. 2016), we would be including a significant number of objects with  $M_{\text{dyn}} > 0.2 M_{\odot}$ , making our criterion too relaxed. Furthermore, our proposed criterion of  $L_{\text{int}} \leq 0.13 L_{\odot}$  is also consistent with Young et al. (2004) and Kauffmann et al. (2011), who show that the restriction of  $L_{\text{int}} \lesssim 0.1 L_{\odot}$  limits the current mass to  $M_{\text{acc}} \lesssim 0.1 M_{\odot}$ . It is important to note that Fig. 2 also shows a number of objects with  $M_{\text{dyn}} \sim 0.2$ – $0.3 M_{\odot}$  but  $L_{\text{int}} \lesssim 0.1$ . According to Tokuda et al. (2017), these protostars could be explained if they are undergoing cold accretion (no significant increase of entropy due

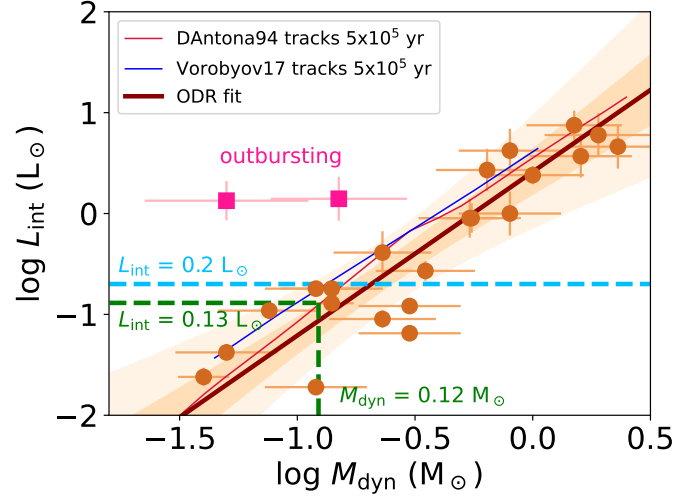


Figure 2:  $L_{\text{int}}$  vs  $M_{\text{dyn}}$  for the protostars, VeLLOs and proto-BD candidates for which the accreted mass has been measured from the ‘disc-kinematics’ method using interferometers, and  $L_{\text{int}}$  has been estimated from the  $70 \mu\text{m}$  flux (see Sec. 4.3). The correlation is strong, with a Spearman’s rank correlation coefficient  $\rho = 0.902$ , and  $p$  value  $< 0.001$ . The dashed vertical green line indicates  $M_{\text{dyn}} = 0.12 M_{\odot}$ , the dashed horizontal green line indicates  $L_{\text{int}} = 0.13 L_{\odot}$ , and the dashed horizontal blue line indicates  $L_{\text{int}} = 0.2 L_{\odot}$ . The linear fit, done with the ODR package of Python and weighting by both x and y errors, is:  $\log(L_{\text{int}}) = (0.41 \pm 0.11) + (1.62 \pm 0.14) \log(M_{\text{dyn}})$ . The shaded area corresponds to 2 times (dark) and 5 times (light) the uncertainty of the fit. The red thin solid line corresponds to the relation between photospheric luminosity and accreted mass from the models of D’Antona and Mazzitelli (1994) (Tables 1 and 5 of this paper), for a time of  $5 \times 10^5$  yr. The blue thin solid line corresponds to the  $L_{\text{int}}$  vs  $M_{\text{acc}}$  relation for the hybrid models of Vorobyov et al. (2017b) for the same time.

to their low mass-accretion rate). Thus, if we used the criterion of  $L_{\text{int}} \leq 0.2 L_{\odot}$ , the number of protostars (not proto-BDs) picked up undergoing cold accretion would probably be too high, while using  $L_{\text{int}} \leq 0.13 L_{\odot}$  allows to minimize this effect. Finally, our proposed criterion is slightly less strict than the criterion adopted by Burrows et al. (2001) and Riaz et al. (2018), who suggest that a proto-BD must have  $L_{\text{bol}} \lesssim 0.09 L_{\odot}$ . Thus, our criterion of  $L_{\text{int}} \leq 0.13 L_{\odot}$  is also a compromise between the different criteria adopted in the literature<sup>10</sup>.

**Requirement 2. Class 0/I SED,  $T_{\text{bol}} < 650$  K:** To consider a proto-BD as such, its SED must necessarily be equivalent to Class 0 or Class I of protostars SEDs. Having a complete well-sampled SED allows to establish the evolutionary stage of the object. A robust proto-BD candidate should show a peak at the far-IR, consistent with a Class-0/I stage. This was quantified by Chen et al. (1995), who proposed to use the  $T_{\text{bol}}$  parameter as an evolutionary indicator (see Sec. 2), with Class 0 objects having  $T_{\text{bol}} < 70$  K, and Class I or flat sources having  $T_{\text{bol}} < 650$  K.

**Requirement 3. Envelope mass low enough,  $M_{\text{env}} \lesssim 0.3 M_{\odot}$ :**

episodic accretion or variable mass accretion rate. For example, if the source is passing an accretion burst, its luminosity might be higher (by about two orders of magnitude, as recognized for the outbursting case of I15398, e.g., Jørgensen et al. 2013; Anderl et al. 2020) than expected from the typical accretion rate.

<sup>10</sup>We do not consider the use of  $L_{\text{bol}}$  to select proto-BD candidates because this measurement could be highly affected by the ISRF (see Sec. 5.2).

To warrant that the accreting object will not achieve a stellar mass in the future, the mass reservoir in its surroundings must be low enough (see Sec. 4.4). This mass reservoir is typically considered as the mass of the envelope around the object,  $M_{\text{env}}$ , and should be measured using single-dish observations in the millimetre/sub-millimetre range so that the bulk of the emission is not filtered out. The masses estimated from this kind of observations can be used to estimate the final mass that would be accreted onto the substellar candidates and then decide if they will end up as BDs or very low-mass stars. To do so, one can assume a core formation efficiency or CFE in low-mass dense cores. This quantity has been found to span a wide range of values and to increase with the density of the core (e.g., Motte et al., 1998; Bontemps et al., 2010; Palau et al., 2013; Pandian et al., 2024). From these works and taking into account typical densities of proto/pre-BDs cores of  $10^4$ – $10^5$  cm $^{-3}$  (e.g., de Gregorio-Monsalvo et al., 2016; Huélamo et al., 2017), a value of CFE  $\sim 10\%$  is obtained. This is close to the SFE value of  $30 \pm 10\%$  found by Alves et al. (2007), the value used in the eDisk program (e.g., Thieme et al., 2023), or previous works studying proto-BD candidates (e.g., Riaz and Bally, 2021, adopt 30–50% for the jet efficiency). The most delicate case is that of Class 0 proto-BDs because these still have to accrete half of their mass. And among the Class 0 proto-BDs, the most critical cases are those with  $M_{\text{acc}}$  already of about  $0.030$ – $0.035 M_{\odot}$ . Assuming CFE of 10%, the maximum mass measured with single-dish should be  $0.3 M_{\odot}$ , and the mass that should be added to  $M_{\text{acc}}$  would be  $\leq 0.03 M_{\odot}$ . We note that this is an orientative value and that each individual case should be studied in detail to carefully assess if the proto-BD candidate will remain substellar or not, given the current accreted mass, the mass-accretion rate, the mass reservoir in the envelope, and the extension of accretion, that in some cases can take place from further out of the envelope (Valdivia-Mena et al., 2023).

#### Requirement 4. Tests rejecting a background nature:

Given the intrinsic faint nature of proto-BD candidates, it is mandatory to apply as much tests as possible to rule a background nature out. These tests could consist of i) looking for line emission associated with the known cloud velocity or molecular outflows; ii) proper motion study in case there is infrared data available; iii) searching for extragalactic catalogues, e.g., in the NASA Extragalactic Database, or testing diagnostic color-color diagrams (e.g., Harvey et al., 2007; Barrado et al., 2009; Bouy et al., 2009); iv) looking for centimetre thermal emission, very unusual in extragalactic objects (e.g., Morata et al., 2015).

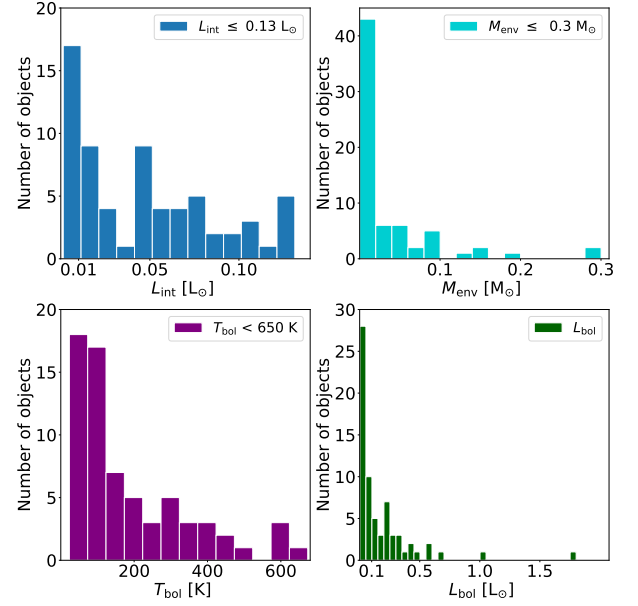


Figure 3: Histograms of best proto-BD candidates from SUCANES database following the criteria outlined in Sec. 5.1. Top-left:  $L_{\text{int}}$  histogram. Top-right:  $M_{\text{env}}$  histogram. Bottom-left:  $T_{\text{bol}}$  histogram. Bottom-right:  $L_{\text{bol}}$  histogram.

We would like to highlight at this point that the four criteria mentioned above are designed to conduct efficient searches of proto-BDs. However, to definitely confirm the most promising candidates as bona-fide proto-BDs, dedicated interferometric studies are required to shed light on the definite nature of the objects. These dedicated studies should be focused on identifying clues of mass ejection and disc-like structures. The interferometric detection of molecular outflows or thermal radiojets clearly associated with the candidate provides a very important indication of an accreting core (e.g., Bourke et al., 2005a; Lee et al., 2013; Morata et al., 2015). In addition, the detection of rotating disc-like structures with a substellar dynamical mass is probably one of the most reliable proves of the nature of the object (e.g., Palau et al., 2014; Lee et al., 2018b; Riaz and Machida, 2021), but this can only be done with interferometers.

#### 5.2. A large sample of proto-BD candidates

As explained in Sec. 3, the searches of pre- and proto-BDs have been performed using different observational approaches. As a result, there are hundreds of objects classified as VeLLOs, proto-BD and pre-BD candidates. All these objects have been gathered in a database that contains all the objects classified as SUBstellar Candidates at the Earliest Stages (SUCANES) and published until the year 2020 (included). All the details about how the database has been built and its contents are described in Pérez-García et al. (2025).

In brief, the database<sup>11</sup> contains a total of 174 objects that have been compiled from the literature. The identification and characterization of each object is described in the corresponding paper, and is based on different criteria based on the performed observations. This results in an inhomogeneous sample

<sup>11</sup><https://sucanes.cab.inta-csic.es/>

in terms of properties and observables. In any case, the database reflects the advances in the field of low luminosity Class 0/I objects.

All the data gathered in the database come from publications (including all the works mentioned in Sec. 3). The photometry has been complemented with data from public archives and covers from the optical to centimeter wavelengths. The only physical parameters that have been derived by the database developers are  $L_{\text{int}}$ ,  $T_{\text{bol}}$  and  $L_{\text{bol}}$ . They have also updated the distance values for different regions (e.g., Aquila, Perseus, IC348, Ophiuchus, Serpens,  $\sigma$  Ori, IC 5146, Chamaeleon, Cepheus and GF9), providing revised values for  $L_{\text{int}}$ ,  $L_{\text{bol}}$ , and  $M_{\text{env}}$  (see distances and references for each cloud in Table 1 of Pérez-García et al. 2025).

As shown in Pérez-García et al. (2025), the very young substellar candidates lie in the regions surveyed mainly by *Spitzer* and *Herschel*, with most of the candidates being identified in the regions of Taurus and Aquila. However, it is worth mentioning that the number of candidates has been substantially reduced when considering the revised distances in the case of Aquila (from 27 to 13), or IC 5146 (from 8 to 4).

The criteria outlined in Sec. 5.1 were applied to the SUCANES database with the goal of selecting the best proto-BD candidates. First, we took the subsample of SUCANES with measured  $L_{\text{int}}$  and excluding pre-BD candidates, which results in 135 objects<sup>12</sup>. Then, we used the following filters:

1.  $L_{\text{int}} < 0.13 L_{\odot}$ : We adopted the criterion that  $L_{\text{int}} - \text{err}L_{\text{int}} < 0.13 L_{\odot}$ , and  $\text{err}L_{\text{int}}/L_{\text{int}} < 20\%$  for objects with  $L_{\text{int}}$  around  $0.13 L_{\odot}$ . This yields 90 objects out of 135 with reported values of  $L_{\text{int}}$  (both detections and upper limits) in SUCANES.
2.  $T_{\text{bol}} < 650 \text{ K}$ <sup>13</sup>. This leaves six objects out in total: for five objects (L1448-IRS2E from Chen et al. 2010, SSTB213 J041913.10+274726.0 and SSTB213 J041726.38+273920.0 from Palau et al. 2012, ALMAJ153914.996-332907.62 from Santamaría-Miranda et al. 2021, and Source-X from Kawabe et al. 2018) the SED was not properly sampled, making the determination of  $T_{\text{bol}}$  uncertain, and were excluded. One object with  $T_{\text{bol}} > 650 \text{ K}$  (J190418.6-373556 from Kim et al. 2016) was excluded as well, so we ended up with 84 objects after requiring this criterion.
3.  $M_{\text{env}} \leq 0.3 M_{\odot}$ . We did not consider here any uncertainty and took a strict  $0.3 M_{\odot}$  value because this criterion is the most uncertain (see Sec. 5.1 point 3) and the masses were not computed as consistently as  $L_{\text{int}}$ , but were just taken from the literature, with each value having its own  $T_{\text{dust}}$

<sup>12</sup>Note that one object fulfilling this criteria, J041847 (Palau et al., 2012), was removed from the subsample, since recent *Euclid* data has spatially resolved it into a galaxy (Bouy et al., in prep).

<sup>13</sup>While the SUCANES database only includes  $T_{\text{bol}}$  and  $L_{\text{bol}}$  values if the objects have detections in at least three photometric tables (Pérez-García et al., 2025), in this review we have relaxed this condition to two photometric tables. The objects for which  $T_{\text{bol}}$  and  $L_{\text{bol}}$  have been obtained using only two photometric tables are marked in Table 3.

and dust opacity, etc. It is worth noting however that 78% of the sample have  $M_{\text{env}}$  calculated from *Herschel*/SPIRE at  $250 \mu\text{m}$ , and  $M_{\text{env}}$  has been obtained uniformly for all these objects. This 78% corresponds to the objects from Kim et al. (2016), and to the objects of SUCANES that have no  $M_{\text{env}}$  reported in the literature but have a flux at  $250 \mu\text{m}$  (from *Herschel*/SPIRE) in the database. In these cases,  $M_{\text{env}}$  is calculated in this work adopting  $T_{\text{dust}} = 15 \text{ K}$  and the same dust opacity at  $250 \mu\text{m}$  as Kim et al. (2016), to make the estimate of  $M_{\text{env}}$  as uniform as possible<sup>14</sup>. After adopting this criterion, we have 68 objects out of 84<sup>15</sup>. We note that all the 68 objects have  $M_{\text{env}}$  estimated from single dish data.

Table 2 lists the 22 objects that have been excluded from the 90 initial objects that fulfilled the first criterion of  $L_{\text{int}} < 0.13 L_{\odot}$ .

Table 3 presents the list of the 68 proto-BD candidates with their main properties, which are summarized in Fig. 3. The figure shows the histograms for the final sample of 68 proto-BD candidates for  $L_{\text{int}}$ , which have peaks around  $0.005$  and  $0.05 L_{\odot}$ ;  $M_{\text{env}}$  has a very well defined peak around  $0.01 M_{\odot}$ ;  $T_{\text{bol}}$  is  $\lesssim 100 \text{ K}$  in most of the cases; and  $L_{\text{bol}}$  also has the peak very well defined below  $0.1 L_{\odot}$ , with very few exceptions of objects that belong to the Orion Nebula Cluster and lie close to the Trapezium, being thus their  $L_{\text{bol}}$  highly affected by the ISRF of the nearby high-mass stars. The most extreme case of these objects is J053504, for which  $L_{\text{bol}} \sim 1.8 L_{\odot}$ , while  $L_{\text{int}} = 0.10 \pm 0.01 L_{\odot}$ , being the one closest to the Trapezium. This illustrates very well why it is recommended to use  $L_{\text{int}}$  to identify proto-BD candidates rather than  $L_{\text{bol}}$ .

In order to have a wide view of the spatial distribution of the proto-BD candidates of Table 3, in Figs. C.1–C.7 of Appendix Appendix C, the positions of the SUCANES objects (with the subsample of Kim et al. 2016 highlighted), along with the proto-BD candidates of Table 3 are indicated on the top of the *Herschel*/SPIRE image at  $250 \mu\text{m}$  for each molecular cloud. Although a deep study of the spatial distribution of proto-BD candidates is beyond the scope of this review, this initial visualization is useful for future studies.

The ALMA archive was searched for the 68 proto-BD candidates of Table 3 and ALMA data were available in 34 cases,

<sup>14</sup>The uncertainty in  $M_{\text{env}}$  due to dust opacity can be of a factor of 2 or more. For example, Kim et al. (2016) adopted  $\kappa_{250\mu\text{m}} = 0.19 \text{ cm}^2 \text{ g}^{-1}$  by interpolating the Ossenkopf and Henning (1994) dust opacities for dust with thin ice mantles at  $10^6 \text{ cm}^{-3}$ , while a recent estimate of the dust optical depth at  $250 \mu\text{m}$  by Li et al. (2024) yields  $\kappa_{250\mu\text{m}} = 0.09 \text{ cm}^2 \text{ g}^{-1}$ , a factor of 2 smaller, translating into a factor of 2 larger  $M_{\text{env}}$ . In other cases, the dust opacity is a factor of 2.5 larger than the thin ice mantle models at  $10^6 \text{ cm}^{-3}$  of Ossenkopf and Henning (1994) (e.g., Lin et al., 2021). It is currently not clear which dust opacities are most appropriate for protostellar, VeLLO or proto-BD envelopes and this constitutes an important source of uncertainty.

<sup>15</sup>The 16 objects rejected by this criterion are comprised by: 2 objects (J182912.1–014845, J182958.3–015740) from Kim et al. 2016, for which there are no  $M_{\text{env}}$  in the literature, and 14 objects (see Table 2) for which  $M_{\text{env}} > 0.3 M_{\odot}$ . Among these 14 rejected objects there is L328-IRS, an object that was considered as a promising proto-BD during many years, but has  $M_{\text{env}} \sim 0.9 M_{\odot}$  from *Herschel*/SPIRE flux at  $250 \mu\text{m}$ . Additionally, the mass for the central object of L328-IRS has been estimated to be  $\sim 0.3 M_{\odot}$  from disc kinematics (Lee et al., 2018b), too high for a proto-BD.

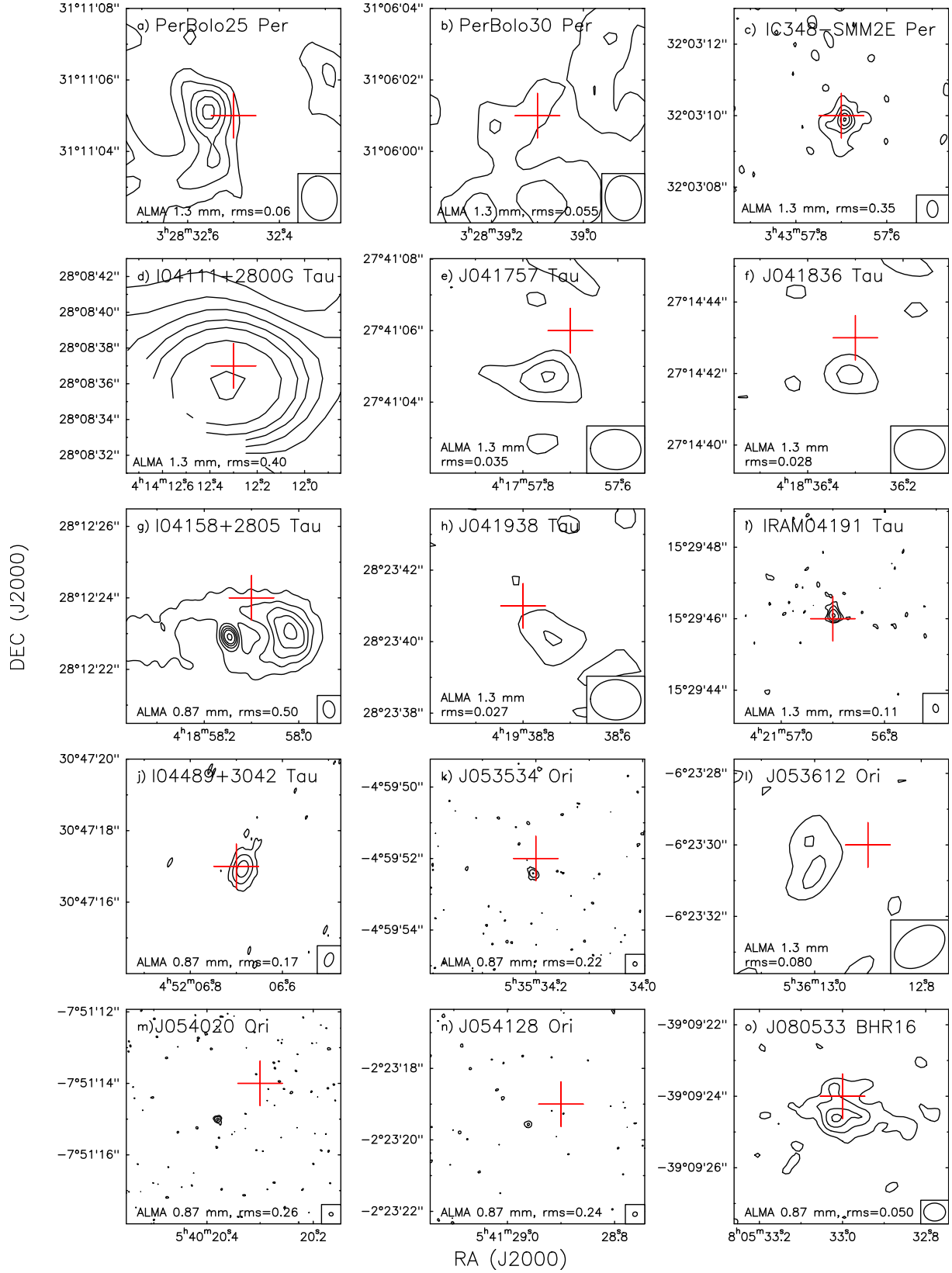


Figure 4: Archive ALMA emission of the proto-BD candidates of Table 3. In all the panels, the field of view is  $6'' \times 6''$  (except for panel 'd', for which the field of view is  $12'' \times 12''$ ), the beam is shown in the bottom-right corner, and the contours correspond to the 1.3 mm or 0.87 mm continuum emission (and are  $-3, 3, 6, 9, 12, 15, 20$ , and  $30$  times the rms noise, except for IRAM04191 and J054020, which are  $-3, 3, 6, 12, 24$  times the rms noise, and for I04489+3042, J053534 and J054128, which are  $-3, 3, 12, 48$  times the rms noise). The rms noise of each image is indicated at the bottom of each panel and is given in mJy beam<sup>-1</sup>. In all the panels, the red plus sign corresponds to the coordinates of the proto-BD candidate as provided in the SUCANES database (Pérez-García et al., 2025). The ALMA project codes along with the corresponding references are listed in Table 3.



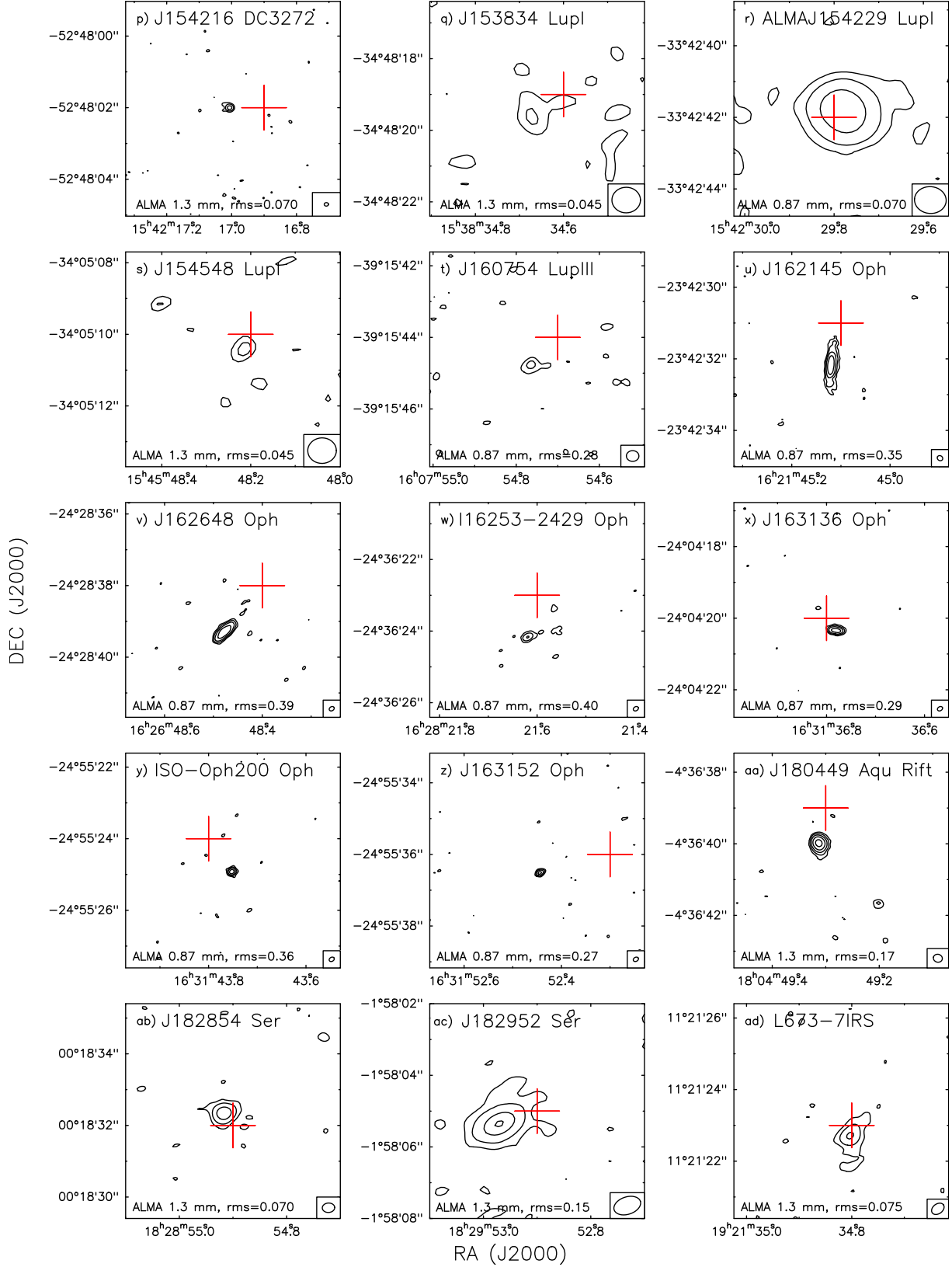


Figure 4: (cont.) Archive ALMA emission of the proto-BD candidates of Table 3. In all the panels, the field of view is  $6'' \times 6''$ , the beam is shown in the bottom-right corner, and the contours correspond to the 1.3 mm or 0.87 mm continuum emission (and are  $-3, 3, 6, 9, 12, 15, 20$ , and  $30$  times the rms noise, except for J154548, which are  $-3, 3, 4$  times the rms noise, for J162145, J162648, J163136, ISO-Oph200, J163152 and J180449, which are  $-3, 3, 6, 12, 24$  times the rms noise, and for J154216, ALMA-J154229, J16253-2429, J182854, J182952, and L673-7-IRS, which are  $-3, 3, 12, 48, 96$  times the rms noise). The rms noise of each image is indicated at the bottom of each panel and is given in  $\text{mJy beam}^{-1}$ . In all the panels, the red plus sign corresponds to the coordinates of the proto-BD candidate as provided in the SUCANES database (Pérez-García et al., 2025). The ALMA project codes along with the corresponding references are listed in Table 3.

with only 4 (out of the 34) being non-detections. The continuum detections are shown in Fig. 4, and the non-detections are shown in Fig. A.9. Although the images shown in Fig. 4 are very inhomogeneous, with a large range of angular resolutions and sensitivities, in an important number of cases the continuum emission is well resolved, and in some Class 0 candidates it is elongated along the outflow direction (e.g., IC348-SMM2E or IRAM 04191, Palau et al. 2014, André et al. 1999) while in other Class I/Flat candidates it is tracing a disc structure (e.g., I04158+2805, J162145, J162648, J163136, Ragusa et al. 2021, Cox et al. 2017, Encalada et al. 2021), both properties also seen in protostars.

### 5.3. Properties of proto-BD candidates and VeLLOs obtained from deep interferometric observations that can be compared to the properties of protostars

In Sec. 5.1, four criteria were proposed to select proto-BD candidates. These criteria are orientative requirements to build large samples of proto-BD candidates. However, additional deep and sensitive interferometric observations are required to definitely assess the nature of each object. We outline below the main properties that can be studied with dedicated interferometric observations, and the main results obtained so far in the very low-luminosity regime.

#### 5.3.1. Molecular outflows

In some specific cases, deep interferometric observations have already been carried out in VeLLOs of the literature. For example, Lee et al. (2018b) show ALMA data for the VeLLO candidate L328-IRS (excluded here as a proto-BD candidate because of its high reported  $M_{\text{env}}$ , see Table 2) and report the detection of an outflow. Similarly, Palau et al. (2014) report outflow emission from CO (3–2) and  $^{13}\text{CO}$ (2–1) with the SMA from the IC348-SMM2E proto-BD candidate. In addition, a PdBI interferometric study of a sample including two VeLLOs (IRAM 04191+1522 and L1521-F) and Class 0 protostars reveal, through observations of CO, SO and SiO, that the detection rate of jets in SiO and SO was found to increase with  $L_{\text{int}}$  and thus only very few jets of SiO and SO would be expected to be associated with proto-BDs (e.g., Podio et al., 2021). Thus, detection of SiO/SO outflows in the deep interferometric studies is challenging.

#### 5.3.2. Accretion discs and streamers

There are proto-BD candidates or VeLLOs for which putative discs have been studied using sensitive interferometric observations, which reveal velocity gradients perpendicular to the outflow (e.g., Palau et al., 2014; Lee et al., 2018b). The most reliable cases were gathered and presented in Table 1, for which  $M_{\text{acc}}$  was inferred using the ‘disc-kinematics’ method outlined in Sec. 4.3. Very recently, also accretion streamers and spiral structures (traced by  $\text{HCO}^+$  and c-HCCCH) near a possible proto-BD were reported (Riaz et al., 2024a), along with hints of molecules (such as HCN) tracing its inner disc (Riaz et al., 2024b).

#### 5.3.3. Chemistry and presence of Complex Organic Molecules

The first studies aimed at characterizing the chemistry in VeLLOs were carried out using single-dishes. Takakuwa et al. (2011) used the Nobeyama 45m telescope to observe carbon-chain and organic molecular lines towards L1521F-IRS (Table 2) and IRAM 04191 (Table 3). These authors report a much stronger detection of  $\text{CH}_3\text{CCH}$ ,  $\text{C}_4\text{H}$ , and  $\text{C}_3\text{H}_2$  towards L1521F-IRS compared to IRAM 04191, and non-detection of  $\text{CH}_3\text{OH}$  and  $\text{CH}_3\text{CN}$  in any of the two VeLLOs. They attribute the chemical differentiation identified among the two objects to different evolutionary stages. Another single-dish study focused on VeLLOs/proto-BD candidates is presented in Riaz et al. (2018), who observed N-bearing molecules in a sample of 10 objects with the IRAM 30m telescope. This work revealed that the chemistry related to CN, HCN and HNC could have a particular behavior in VeLLOs compared to protostars, with the HNC molecule proposed as a tracer of deeply embedded substellar objects. In a subsequent study, Riaz et al. (2019b) focused on the CO isotopologues,  $\text{H}_2\text{CO}$ ,  $\text{HCO}^+$ , and CS in a sample of 7 proto-BD candidates, also using the IRAM 30m telescope. These authors found evidences of CO depletion from the gas-phase, and that proto-BD candidates show a factor of 2 higher ortho-to-para  $\text{H}_2\text{CO}$  ratio than protostars. In addition, marginal signs of lower abundances of  $\text{HCO}^+$  and  $\text{H}_2\text{CO}$  for lower  $L_{\text{bol}}$  are reported. Follow-up works find evidences of cold and warm  $\text{CH}_3\text{OH}$  (Riaz et al., 2023), deuteration (Riaz and Thi, 2022b),  $\text{H}_2\text{CO}$  and methane in a sample of proto-BD candidates (Riaz and Thi, 2022a,c).

Regarding interferometric chemical studies, these have been mainly focused on single sources. The most studied objects using interferometers are IRAS 15398–3359 (not included in Tables 2 or 3 because of its high luminosity, see Sec. 3.1), L1521F (Table 2), and IRAM 04191 (Table 3), and in all of them hints of accretion shocks and/or bursts were identified<sup>16</sup> (e.g., Jørgensen et al., 2013; Favre et al., 2020; Anderl et al., 2020), along with complex chemistry in IRAS 15398–3359 unveiled both by ALMA (Okoda et al., 2023) and the JWST (Yang et al., 2022). These hints of burst-induced chemistry, initially found in individual objects, were also found in a sample of 8 VeLLOs studied with ALMA by Hsieh et al. (2018). The authors also suggest that the interval between accretion episodes in proto-BD or VeLLO candidates is shorter than that in Class 0/I protostars.

Chemistry can also provide clues on the formation scenario of BDs by studying isotope ratios. For example, Barrado et al. (2023) measure with the JWST the  $^{14}\text{N}/^{15}\text{N}$  ratio in a cool equal mass BD-BD binary of 15  $M_{\text{Jup}}$  each component, and find a value consistent with star-like formation by gravitational collapse, being the  $^{14}\text{N}/^{15}\text{N}$  ratio a very promising tool to distinguish among scenarios. This isotope ratio can be comple-

<sup>16</sup>The following features are considered signs of accretion bursts: absence of  $\text{HCO}^+$  where there is CO; extended  $\text{CH}_3\text{OH}$  given its current luminosity; warm carbon-chain chemistry on large scales; no massive dust continuum component on small scales (e.g., Jørgensen et al., 2013); morphology of the  $\text{N}_2\text{H}^+$ , CO and  $\text{C}^{18}\text{O}$  lines inconsistent with a constant luminosity model using the present-day internal luminosity (Hsieh et al., 2018; Anderl et al., 2020).

mented by others, such as  $^{13}\text{C}/^{12}\text{C}$  (e.g., Zhang et al., 2021b,a; González Picos et al., 2024).

In summary, chemistry can potentially help identify proto-BDs (e.g., Riaz et al., 2018) and trace their formation mechanism (Barrado et al., 2023). In addition, chemistry typical of warm-carbon chain objects, hot corinos and accretion bursts has been identified in VeLLOs and proto-BD candidates (e.g., Jørgensen et al., 2013; Okoda et al., 2023), indicating that these phenomena must be taken into account when identifying, modeling and interpreting these objects.

#### 5.3.4. Maser emission

Maser emission is a good tracer of energetic processes such as mass-loss and/or accretion and could potentially be a useful tool to study these processes with very high angular resolution in proto-BDs. A first search of water maser emission towards the L1014 VeLLO was conducted by Shirley et al. (2007), who report a non-detection. Later, a survey for water maser emission towards a sample of 44 VeLLOs, including proto-BD candidates, FHCs, and other protostars with  $L_{\text{bol}} \lesssim 0.4 L_{\odot}$ , was carried out by Gómez et al. (2017) using the Effelsberg telescope. The survey only detected maser emission towards the position of L1448 IRS 2E, which has been classified as a possible FHC or a dense blob interacting with a nearby outflow (Maureira et al., 2020). However, follow-up VLA observations showed that the maser emission is associated with the nearby object L1448 IRS2, a Class 0 protostar of  $L_{\text{bol}} \sim 4 L_{\odot}$ . The upper limits for water maser emission determined by Gómez et al. (2017) are one order of magnitude lower than expected from the correlation between water maser luminosities and  $L_{\text{bol}}$  found for protostars (Furuya et al., 2003; Shirley et al., 2007). This suggests that this correlation does not hold at the lower end of the (sub)stellar mass spectrum and calls for further studies to understand this behavior.

#### 5.3.5. Magnetic fields

A few works have studied the magnetic fields in cores harboring proto-BD candidates or VeLLOs. Both Soam et al. (2015a) and Soam et al. (2015b) perform optical and near-infrared polarization observations toward VeLLOs. Soam et al. (2015b) study five VeLLOs (IRAM 04191, L1521F, L328, L673-7, and L1014), two of which are classified in this work as proto-BD candidates (IRAM 04191 and L673-7, Table 3). The authors find that in 3 out of the 5 sources, the outflows tend to align with the envelope magnetic field, and if the inner magnetic field is taken into account (IRAM 04191) the alignment improves.

Soam et al. (2015a) focus on L328-IRS, known to be driving a sub-parsec-scale molecular outflow (Lee et al., 2013, 2018b). The magnetic field, with a strength of  $\sim 20 \mu\text{G}$ , is found to be ordered from 0.02 to 0.2 pc, and parallel to the outflow axis.

In a subsequent work, Soam et al. (2019) undergo the first sub-parsec-scale mapping of magnetic fields in the vicinity of the VeLLO L1521F-IRS, using sub-millimetre polarization measurements at  $850 \mu\text{m}$  with the JCMT. The magnetic fields are found to be ordered on multiple scales. At core scales, the magnetic field strength is  $330 \pm 100 \mu\text{G}$ , an order of magnitude larger than at clump/envelope scales. This strength implies

that the magnetic energies are larger than non-thermal kinetic energies, and corresponds to a mass-to-magnetic flux ratio of  $2.3 \pm 0.7$ , indicative of the core being magnetically supercritical.

All these results suggest that, even though the magnetic field does not seem to be strong enough to stop the collapse, it must play an important role in launching and collimating the molecular outflows driven by VeLLOs and proto-BDs. Further studies in other proto-BD candidates and VeLLOs need to be carried out to establish this on a more robust base.

Another technique used in the literature to measure the magnetic field strengths in BDs is based on the detection of electron cyclotron emission at radio wavelengths. The first detection of radio emission in a confirmed BD was done by Berger et al. (2001). Initially, it was interpreted as due to gyrosynchrotron emission from which the authors inferred a very weak  $\sim 5 \text{ G}$  magnetic field. Subsequent works showed that some BDs and their higher-mass ultracool dwarf stellar cousins can emit radio emission from the electron cyclotron maser instability (Hallinan et al., 2007; Kao et al., 2016), a mechanism also responsible for radio aurorae produced by Solar System planets (Zarka, 2007). Unlike gyrosynchrotron emission, electron cyclotron maser emission occurs at very near the fundamental cyclotron frequency (Treumann, 2006), providing a means to directly measure rather than infer magnetic field strengths. At GHz frequencies, such emission indicates kilogauss magnetic fields (e.g., Kao et al., 2016, 2018), probably related to the electron cyclotron maser instability (e.g., Pineda et al., 2017; Kao et al., 2019). This technique is very promising, especially for next-generation radio interferometers such as the ngVLA or the SKA (Sec. 9), which will enable detections of statistically significant samples of BDs associated with electron cyclotron emission and robustly constrain their magnetic field. However, at present, all the objects for which electron cyclotron emission has been detected have ages  $> 100 \text{ Myr}$  (e.g., Berger et al., 2001; Kao et al., 2016, 2018, 2019, 2023), older than the deeply embedded phases studied in this work ( $\lesssim 1 \text{ Myr}$ ), where the radio emission is supposed to be dominated by thermal radiojets (Forbrich et al., 2015; Morata et al., 2015; Rodríguez et al., 2017). It remains an open question whether electron cyclotron emission could be detected at earlier stages.

#### 5.3.6. Multiplicity

It is important to note that multiplicity could be crucial to determine the final mass of an object and therefore its final (sub)stellar nature. Multiplicity could also be of pivotal importance as a tool to distinguish between formation scenarios. For example, if ejections are frequent and constitute an important formation mechanism of isolated BDs, the multiplicity properties of proto-BDs should differ from those of protostars. In particular, in the ejection scenario it would be expected that a smaller number of binary systems survive the ejection, being close (a few au) BD-BD binaries the most successful outcomes (Stamatellos and Whitworth, 2009; Basu and Vorobyov, 2012). On the other hand, in the star-like scenario BD-BD binaries with mass ratios close to unity are expected, with average separations of several tenths of au, and multiplicity fractions of 10–20% increasing with primary mass (Bate, 2012, 2019). The

star-like scenario is also required to explain the anticorrelation between close binary fraction and metallicity seen in simulations (Bate, 2019). What is more, in the star-like scenario a trend similar to what is seen in protostars would be expected for BDs as well, mainly that multiplicity is more frequent for more embedded protostars (e.g., Chen et al., 2013; Tobin et al., 2016b). All these features constitute excellent tests to elucidate among the different BD formation scenarios.

Furthermore, crowded star-forming regions could favor dynamical interactions and influence the formation of binary systems in very low-mass objects. A recent study carried out in the Orion Nebula Cluster in the substellar regime reveals an excess of very low mass binaries in this region compared to the Galactic field (De Furio et al., 2022), consistent with Pearson and McCaughrean (2023), and revealing that the primordial multiplicity properties might be different from those of the field, and that subsequent dynamical interactions are required to obtain the multiplicity properties of the observed field BDs.

Regarding the most embedded stages, there are a few works that focused on multiplicity including VeLLOs and/or proto-BD candidates. Chen et al. (2013) present SMA observations at 0.85–1.3 mm for a sample of 33 Class 0 protostars in nearby clouds including 1 VeLLO (L1521F) and 2 proto-BD candidates (IC348-MMS and IRAM04191, Table 3). In this work, 64% of the sample have signatures of multiplicity (multiplicity fraction), with separations in the range 50–5000 au, and circumstellar mass ratios below 0.5. One of the most relevant results of this study is that the multiplicity fraction is two times larger in Class 0 sources than in Class I sources, suggesting that multiplicity properties evolve along with protostars. In the Chen et al. (2013) work, one of the two proto-BD candidates was found to split up into two sources. In a more recent work, Maury et al. (2019) undergo a multiplicity study with the PdBI for a sample of 16 Class 0 protostars, including one VeLLO (L1521F) and one proto-BD candidate (IRAM04191, Table 3). This study explores multiplicity at scales similar to the work of Chen et al. (2013), 100–5000 au, and reports multiplicity fractions  $\lesssim 57\%$ , consistent with Chen et al. (2013). Important results regarding multiplicity have been reported also from the large-project VLA/ALMA Nascent disc and Multiplicity survey (VANDAM). Tobin et al. (2016b, 2018) study multiplicity of all known protostars in Perseus (94 objects in total) using the Very Large Array (VLA) at 0.8, 1, 4 and 6.6 cm and ALMA, including several VeLLOs and FHCs, and find a multiplicity fraction of  $(57 \pm 9)\%$  for Class 0 protostars and  $(23 \pm 8)\%$  for Class I, again consistent with previous works. A similar work in 328 protostars of the Orion cloud is presented in Tobin et al. (2022), measuring a multiplicity fraction of 30% for separations of 20–10 000 au.

Overall, specific studies focusing on the particular multiplicity properties of proto-BD candidates are still lacking, and the aforementioned studies will be an excellent base to compare multiplicity between proto-BDs and higher mass protostars.

#### 5.4. Comparison of proto-BD candidate properties with the well-known correlations of protostars

A number of works have explored the behavior of the known protostellar correlations in the low-mass end, mainly using single-dish telescopes. We present here four correlations well established for protostellar sources, and overplot the most recent measurements of the corresponding properties for VeLLOs/proto-BDs, in order to explore if they follow the same behavior as their higher mass counterparts.

##### 5.4.1. The $\dot{M}_{\text{inf}}$ vs $L_{\text{bol}}$ correlation

Regarding the infall and accretion process, Kim et al. (2021) measured the mass infall rate  $\dot{M}_{\text{inf}}$  in the VeLLOs sample of Kim et al. (2016) and find a relation of  $\dot{M}_{\text{inf}}$  with  $L_{\text{int}}$ . In order to explore if the relation of Kim et al. (2021) is an extension of a possible relation for higher mass protostars, in Fig. 5a we include the Kim et al. (2021) measurements along with other measurements reported in the literature (Belloche et al., 2002; Furuya et al., 2009; Wyrowski et al., 2016; Keown et al., 2016; Yue et al., 2021; Pillai et al., 2023; Xu et al., 2023, the entire compilation is listed in Table B.7), allowing us to explore a range in  $L_{\text{bol}}$  from 0.01 to  $10^6 L_{\odot}$ <sup>17</sup>. It is important to stress that Fig. 5a includes only measurements with single-dish telescopes. In the figure, the objects of our compilation that were classified in Sec. 5.2 as proto-BD candidates (Table 3) are indicated as red squares. Although there is a significant dispersion in the intermediate/high-mass regime, the figure shows a clear trend of smaller values of  $\dot{M}_{\text{inf}}$  for smaller  $L_{\text{bol}}$ . A linear fit to these data was performed, excluding the proto-BD candidates and using the ODR package (weighting by errors in both axes):

$$\log(\dot{M}_{\text{inf}}) = (-4.72 \pm 0.17) + (0.63 \pm 0.04)\log(L_{\text{bol}}), \quad (16)$$

where  $\dot{M}_{\text{inf}}$  is given in  $M_{\odot} \text{ yr}^{-1}$  and  $L_{\text{bol}}$  is given in  $L_{\odot}$ . In all panels of Fig. 5, shaded areas correspond to two times (dark) and five times (light) the uncertainty of the fit. As can be seen from Fig. 5a, the values measured for the proto-BD candidates (red squares) lie within the shaded area, indicating that the least massive objects of the sample, reaching  $0.004 L_{\odot}$ , might share a common process of accretion with more massive protostars.

Assuming that  $\dot{M}_{\text{inf}}$  is related to the mass accretion rate, these results are consistent with previous works reporting evidence that the relation of mass accretion rate vs stellar mass extends down to  $\sim 0.015 M_{\odot}$  (Muzerolle et al., 2005; Alcalá et al., 2014; Almendros-Abad et al., 2024), with these works being focused on Class II objects. Using a large compilation of sub-stellar accretion diagnostics, Betti et al. (2023) has confirmed these results but have also suggested that the BD and stellar populations are better described separately, taking into account both mass and evolutionary effects. This could partially explain

<sup>17</sup>In panels ‘a’, ‘b’, and ‘c’ of Fig. 5,  $L_{\text{bol}}$  for the VeLLOs and proto-BD candidates is taken as  $L_{\text{int}}$  because the least luminous objects are most affected by the ISRF (as explained in Sec. 2) and the accretion/ejection processes are expected to be driven by the mass of the central object, more closely related to  $L_{\text{int}}$  than to  $L_{\text{bol}}$  (see also AMI Consortium et al., 2011).



the results found by [Riaz and Bally \(2021\)](#) in a sample of 6 proto-BD candidates, where accretion luminosity and accretion rates are within the range measured for low-mass protostars, and higher than Class II brown dwarfs. It remains to be explored whether this excess is due to the different methodologies used in each work or it is related to the evolutionary stage.

#### 5.4.2. The $L_{\text{cm}}$ vs $L_{\text{bol}}$ correlation

Regarding the outflow phenomena, the centimeter luminosity,  $L_{\text{cm}}$ , tracing thermal radiojets, is known to be well correlated with  $L_{\text{bol}}$ . This was recently reviewed by [Anglada et al. \(2018\)](#) and, in Fig. 5b, the relation of  $L_{\text{cm}}$  vs  $L_{\text{bol}}$  compiled in [Anglada et al. \(2018\)](#) is presented, indicating in red squares the objects that are classified in Sec. 5.2 (Table 3) as proto-BD candidates (the entire compilation is listed in Table B.8). A linear fit was performed to the data of Fig. 5b, excluding the proto-BD candidates and following the same method used for Fig. 5a:

$$\log(L_{\text{cm}}) = (-2.05 \pm 0.08) + (0.66 \pm 0.03)\log(L_{\text{bol}}), \quad (17)$$

where  $L_{\text{cm}}$  is given in  $\text{mJy kpc}^2$  and  $L_{\text{bol}}$  is given in  $L_{\odot}$ . In this case, the least massive proto-BD candidates, of  $0.002$ – $0.006 L_{\odot}$ , lie slightly above the shaded area. This could be related to the finding of [Ellerbroek et al. \(2013\)](#), who report an excess of mass outflow rate vs mass accretion rate for the lowest-mass objects of the sample. In line with the findings of [Riaz and Bally \(2021\)](#), see previous paragraph) and [Betti et al. \(2023\)](#), the deviation from the protostellar correlation could be related with an evolutionary effect and/or variability. Further studies improving the sampling in the lower end of these diagrams need to be carried out to better establish whether these excesses in the BD regime are significant or not.

#### 5.4.3. The $F_{\text{out}}$ vs $L_{\text{bol}}$ correlation

Another well-known protostellar correlation concerns the momentum rate or outflow force of the outflowing gas,  $F_{\text{out}}$  and  $L_{\text{bol}}$  and  $M_{\text{env}}$  for Class 0 and I protostars (e.g., [Bontemps et al., 1996](#)). [Schwarz et al. \(2012\)](#) study a sample of 39 low-luminosity objects using a single-dish telescope with a beam of  $30''$ , and obtained a surprisingly low detection rate, suggesting that beam dilution could be important for the low-luminosity objects. In a more recent study, [Kim et al. \(2019\)](#) explore the CO emission in the VeLLOs sample of [Kim et al. \(2016\)](#) using also single-dish telescopes, and compare the outflow force vs  $L_{\text{bol}}$  and  $M_{\text{env}}$  as in [Bontemps et al. \(1996\)](#). They find that most of the objects follow the trend reported for protostellar objects (observed also with single-dish), down to  $\sim 0.05 L_{\odot}$ , but a number of VeLLOs present much lower outflow forces than expected for this relation. These cases could be related to a group of particularly compact outflows, whose CO emission might have been significantly diluted within the single-dish beam. [van der Marel et al. \(2013\)](#) also performed a similar study in Ophiuchus using the JCMT and again find a few objects with a deficit of outflow force, more clearly seen in the relation of [Towner et al. \(2024\)](#). Instead, when outflow emission from VeLLOs is studied with interferometers, their  $F_{\text{out}}$

seems to better follow the trend of protostars, as shown by, e.g., [Takahashi and Ho \(2012\)](#) and [Takahashi et al. \(2013\)](#). However, these works compare the results from interferometric observations for VeLLOs with the results from single-dish observations for higher-mass protostars.

In order to perform a more uniform comparison between VeLLOs and protostars and to avoid beam dilution problems, [Palau et al. \(2014\)](#) compiled a sample of protostellar objects whose outflow parameters were studied using only interferometers, reaching  $L_{\text{bol}} \sim 5000 L_{\odot}$ . In Fig. 5c, the relation of  $F_{\text{out}}$  vs  $L_{\text{bol}}$  of [Palau et al. \(2014\)](#) is updated with subsequent works of the literature ([Tobin et al., 2016c](#); [Lee et al., 2018b](#); [Busch et al., 2020](#); [Furuya et al., 2019](#); [Podio et al., 2021](#); [Vazzano et al., 2021](#); [Dutta et al., 2024](#)), all based on interferometric observations, spanning a range of  $L_{\text{bol}}$  from  $0.002$  to  $10^4 L_{\odot}$ . This compilation is provided in Table B.9. As in Figs. 5a-b, we have marked with red squares the proto-BD candidates of Sec. 5.2 (Table 3), and have included two additional, tentative, proto-BD candidates not reported in SUCANES (i.e., in Table 3) that have  $F_{\text{out}}$  measured with interferometers (e.g., [Phan-Bao 2022](#), [Palau et al. 2022](#)). Following the same method as in previous panels, a linear fit was performed to the data excluding the proto-BD candidates, and a shaded area corresponding to two and five times the uncertainty of the fit is indicated in the figure. The linear fit is:

$$\log(F_{\text{out}}) = (-5.59 \pm 0.14) + (0.99 \pm 0.08)\log(L_{\text{bol}}), \quad (18)$$

where  $F_{\text{out}}$  is given in  $M_{\odot} \text{ km s}^{-1} \text{ yr}^{-1}$  and  $L_{\text{bol}}$  is given in  $L_{\odot}$ . This panel shows that  $F_{\text{out}}$  of the least massive proto-BD candidates, of  $\lesssim 0.006 L_{\odot}$ , falls within the shaded area of the fit uncertainty in the protostellar relation.

#### 5.4.4. The $F_{\text{out}}$ vs $M_{\text{env}}$ correlation

Finally, Fig. 5d presents the  $F_{\text{out}}$  vs  $M_{\text{env}}$  relation for the same sample of the previous panel. In this case,  $M_{\text{env}}$  has been taken from the same interferometric studies used to estimate  $F_{\text{out}}$ , thus the filtering of the interferometer affects equally both parameters. The linear fit and shaded areas are performed as in the previous panel, excluding the proto-BD candidates:

$$\log(F_{\text{out}}) = (-4.73 \pm 0.15) + (1.07 \pm 0.14)\log(M_{\text{env}}), \quad (19)$$

where  $F_{\text{out}}$  is given in  $M_{\odot} \text{ km s}^{-1} \text{ yr}^{-1}$  and  $M_{\text{env}}$  is given in  $M_{\odot}$ . As can be seen in Fig. 5d,  $F_{\text{out}}$  of the least massive proto-BD candidates also lies within the shaded area of the  $F_{\text{out}}$  vs  $M_{\text{env}}$  protostellar relation. This is consistent with the pioneering work of [Greaves et al. \(2003\)](#), and provides a larger statistical sample.

To sum up, although more proto-BD candidates should be added in the future to properly populate the low-luminosity end of each panel of Fig. 5, the four protostellar relations preliminary studied here seem to extend down to  $L_{\text{int}} \sim 0.006 L_{\odot}$ , corresponding to masses of  $M_{\text{acc}} \sim 0.024 \pm 0.007 M_{\odot}$  according to the fit of Fig. 2.

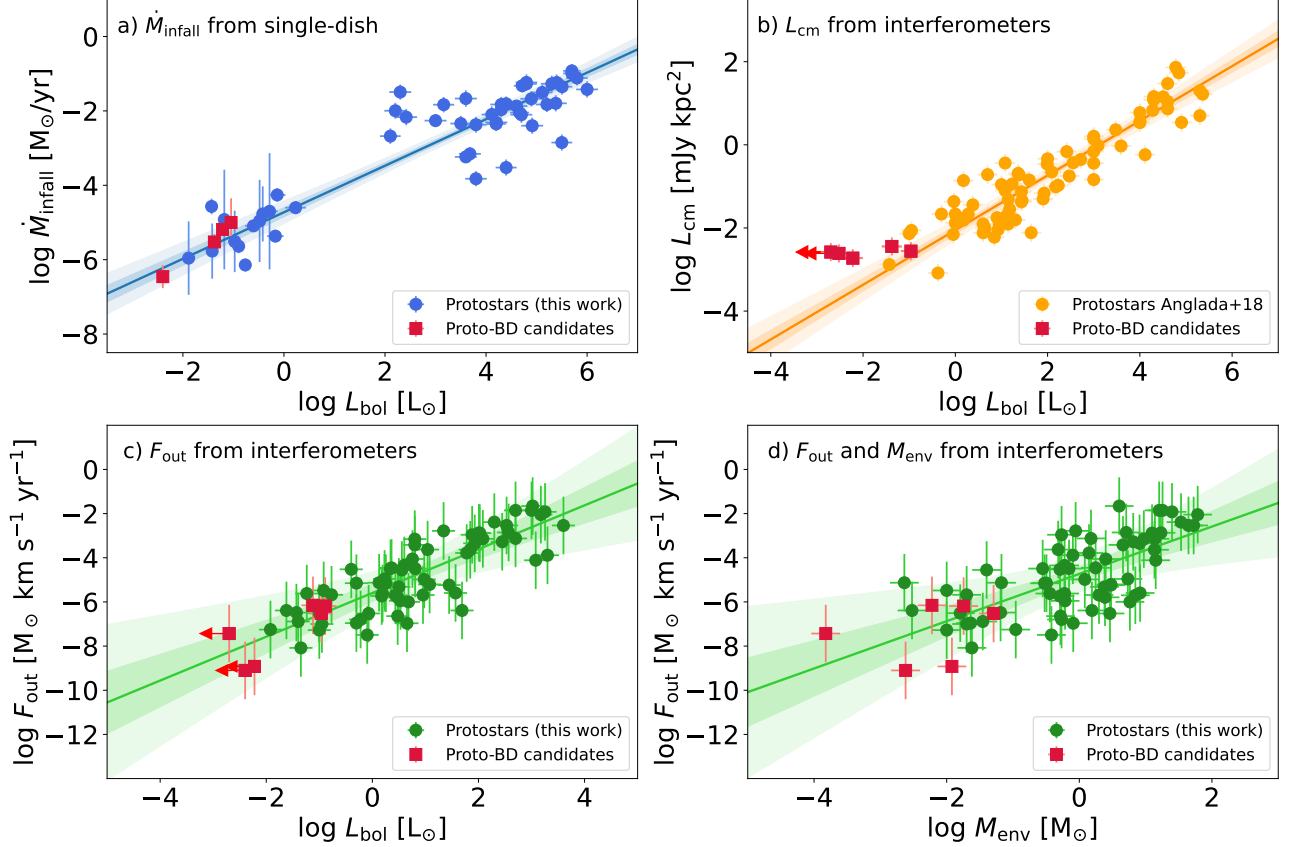


Figure 5: Well-known relations for protostars with the proto-BD candidates of Table 3 marked as red squares (also indicated in the last rows of Tables B.7, B.8 and B.9). The fits have been performed excluding the proto-BD candidates and using the ODR package of Python weighting by both x and y errors. Shaded areas correspond to two times (dark) and 5 times (light) the uncertainty of the fit. a) Mass infall rate  $\dot{M}_{\text{inf}}$  vs  $L_{\text{bol}}$  compiled in this work (Sec. 5.4). All the measurements of  $\dot{M}_{\text{inf}}$  have been obtained using single-dish telescopes and are listed in Table B.7. The linear fit is:  $\log(\dot{M}_{\text{inf}}) = (-4.72 \pm 0.17) + (0.63 \pm 0.04)\log(L_{\text{bol}})$ . b) Centimeter luminosity  $L_{\text{cm}}$  vs  $L_{\text{bol}}$  from Anglada et al. (2018). All the measurements of  $L_{\text{cm}}$  have been obtained using interferometers and are listed in Table B.8. The linear fit is:  $\log(L_{\text{cm}}) = (-2.05 \pm 0.08) + (0.66 \pm 0.03)\log(L_{\text{bol}})$ . c) Outflow force  $F_{\text{out}}$  vs  $L_{\text{bol}}$  compiled in this work (Sec. 5.4). All the measurements of  $F_{\text{out}}$  have been obtained using interferometers to avoid beam dilution problems for the most compact outflows, and are listed in Table B.9. The linear fit is:  $\log(F_{\text{out}}) = (-5.59 \pm 0.14) + (0.99 \pm 0.08)\log(L_{\text{bol}})$ . d) Outflow force  $F_{\text{out}}$  vs  $M_{\text{env}}$  compiled in this work (Sec. 5.4). All the measurements of  $F_{\text{out}}$  and  $M_{\text{env}}$  have been obtained using interferometers as in the previous panel, and are listed in Table B.9. The linear fit is:  $\log(F_{\text{out}}) = (-4.73 \pm 0.15) + (1.07 \pm 0.14)\log(L_{\text{bol}})$ .

## 6. Main properties of pre-BDs

The study and the census of pre-BDs could also potentially shed critical light on the formation mechanism of BDs, because if the planet-like scenario had a dominant role, the number of pre-BDs should be very small. However, given the difficulties to identify true pre-BDs, reliable statistics for these kind of objects are still lacking.

As shown in Sec. 3.1.2, most of the detections of pre-BD candidates are based on millimetre/sub-millimetre observations of objects that do not show counterparts at any other wavelength (e.g. André et al. 2012; Palau et al. 2012; Huélamo et al. 2017; Santamaría-Miranda et al. 2020). In general, they are identified as dusty cores with masses (dust+gas) around the substellar limit ( $\lesssim 0.1 M_{\odot}$ ) in single-dish data. Then, continuum interferometric observations can help confirm the presence of a compact source inside the core, while molecular gas observations allow to assess the stability of the core, by comparing  $M_{\text{env}}$  with  $M_{\text{vir}}$  or  $M_{\text{grav}}$  (Sec. 2). One of the first pre-BD candidates reported in the literature is Oph B-11 (André et al., 2012), in which interferometric dust and gas observations reveal a 3.2 mm continuum source with substellar mass.  $\text{N}_2\text{H}^+$  was found associated with the compact millimetre source, and a virial analysis indicates that the object is gravitationally unstable (André et al., 2012). From these pioneering works, the main requirements for an object to be a promising pre-BD candidate can be identified as:

**No evidence of (sub)stellar activity:** Similar to the case of pre-stellar cores, which are cores on the verge to collapse but with no hydrostatic core yet (e.g., Caselli, 2011), pre-BDs do not have a hydrostatic core either, implying that should not have any infrared/optical counterpart, or signs of ejection activity such as a molecular outflows or jets.

**Gravitationally bound core,  $M_{\text{env}} > M_{\text{grav}}$ :** In order to assure that the object will form a compact object in the future, the object should be gravitationally bound and preferentially gravitationally unstable. This can be assessed by measuring different quantities. First, the Jeans mass could be estimated and compared to the observed mass of the core, which should be larger than the Jeans mass if gravitationally unstable. However, the Jeans criterion assumes linear density perturbations, while this is not expected if the cores are assembled by turbulent flows, which naturally yield non-linear density perturbations bounded by the shock ram pressure (Padoan and Nordlund, 2004). Thus, an estimate more consistent with the Padoan and Nordlund (2004) scenario is to compare the observed mass with the Bonnor-Ebert mass,  $M_{\text{BE}}$  (see eq. 12). If the observed mass is larger than  $M_{\text{BE}}$ , then the object is gravitationally unstable. The stability study can also be performed with the virial analysis. In this case, the observed mass should be larger than  $M_{\text{vir}}$  as given in eq. 10 (e.g., André et al., 2012; Tokuda et al., 2019). Alternatively,  $M_{\text{grav}}$  could be used instead of  $M_{\text{vir}}$ , following eq. 11, which is a less strict constraint and was used by the first pioneering works and subsequent works (e.g., Pound and Blitz, 1993, 1995; Palau et al., 2012). It is important to note that the

assessment of gravitational instability based on the aforementioned simplified criteria (comparing  $M_{\text{env}}$  vs a critical mass) might not be fully accurate, as it might depend on the scale over which the measurements are performed (e.g., Gómez et al., 2021). Thus, the association of the single-dish core with a compact source detected with interferometers can be considered an evidence of on-going gravitational contraction as well (Huélamo et al., 2017; Santamaría-Miranda et al., 2021), as explained below.

**Envelope mass low enough,  $M_{\text{env}} < 0.15 M_{\odot}$ :** In principle, if we assumed a 10% of SFE as in Sec. 5.1,  $M_{\text{env}}$  for pre-BDs could be as high as  $0.7 M_{\odot}$ , given that the hydrostatic core is not formed yet or it still has a negligible mass. However, this criterion has been used in the literature much more strictly to assure that the object will remain substellar, and is typically adopted around  $0.1 M_{\odot}$  (e.g., Pound and Blitz, 1993, 1995; André et al., 2012; Palau et al., 2012; de Gregorio-Monsalvo et al., 2016; Barrado et al., 2018; Huélamo et al., 2017; Tokuda et al., 2019; Santamaría-Miranda et al., 2021). We propose here the conservative case that  $M_{\text{env}} \leq 0.15 M_{\odot}$ , to consider a CFE of 50%. The mass limit of  $M_{\text{env}} \leq 0.15 M_{\odot}$  is also of the order of the mass of the core that Machida et al. (2009) used as initial condition for their simulation of a BD in a star-like scenario, of  $\sim 0.2 M_{\odot}$ . By adopting this criterion, and assuming that the object is gravitationally unstable, the probability of ending with a substellar object is very high.

These main properties of pre-BDs relative to other stages of the star/BD formation process are summarized in Fig. 8. In Table 4 we present all the pre-BD candidates compiled in SUCANES, which amount to 26 candidates. We note that SUCANES just lists the pre-BD candidates reported in the literature, and that in many cases the criteria outlined above could not be applied because of molecular gas detection is missing. Thus, further more dedicated and sensitive interferometric studies need to be carried out to confirm the nature of the objects in Table 4 as pre-BDs. In particular, the second criteria is one of the most difficult to assess. According to SUCANES, there are  $\sim 28$  pre-BD candidates mainly identified in surveys in Lupus I, III clouds (Santamaría-Miranda et al., 2021), Chamaeleon II (de Gregorio-Monsalvo et al., 2016), and Barnard 30 region (Huélamo et al., 2017; Barrado et al., 2018), Ophiuchus (Pound and Blitz, 1995), and Taurus (Palau et al., 2012; Tokuda et al., 2019). All these objects have been detected in single-dish observations, and part of them have been further confirmed with interferometers.

In the cases in which both single-dish and interferometric observations are available, this comparison has resulted in ‘contradictory’ results, since many of the cores with compact sources at their centers, indicative of on-going collapse, were classified as gravitationally stable. Gómez et al. (2021) propose an alternative scenario to explain this contradiction, and consists on assuming that the cores with compact sources at their centers are already the result of gravitational contraction, constituting the

‘tip of the iceberg’ of a larger-scale collapse. As explained in Huélamo et al. (2017), in this scenario, the collapse is expected to occur from the outside-in and it develops self-consistently a near  $r^{-2}$  density profile. Hence, a comparison between the dust masses at different core radii can help test the validity of this prediction, along with the search of infall signatures in molecular tracers at large scales.

Overall, since the identifications of the first pre-BDs by several authors (André et al., 2012; Nakamura et al., 2012; Palau et al., 2012), a number of candidates, although not confirmed, have been added to the list, making their search more difficult than previously thought. This suggests that their presence is either very difficult to identify or that they are rarer than expected for the star-like scenario. Further efforts, both from the numerical and observational side, need to be carried out to elucidate how common are pre-BDs in molecular clouds.

## 7. Proto-BD candidates in different clouds of the Solar Neighborhood

A study of the spatial distribution or the number of proto-BD candidates in the nearby clouds could also give important hints on the formation mechanisms of BDs. In Figures C.1–C.7, the candidates listed in Table 3 are overplotted on the corresponding *Herschel* image at 250  $\mu\text{m}$ , and in the further subsections we analyse the potential relations between the number of proto-BD candidates and the cloud properties.

### 7.1. Are proto-BD candidates following the well-known relations of star formation in molecular clouds?

A well-known property of molecular clouds is that there is a tight relation between the number of protostars and the dense gas mass (defined as the mass above  $A_V=7$  mag, equivalent to  $A_K=0.8$  mag), reported by Lada et al. (2010), and later confirmed by many further investigations (e.g., Hacar et al., 2024), some of which suggest that the relation is a proof of molecular cloud collapse (e.g., Ballesteros-Paredes et al., 2024; Zamora-Aviles et al., 2024).

In order to study these kind of relations, in Table 5 we list, for a number of molecular clouds, their distance, the cloud area (taken from Heiderman et al. 2010 and Carpenter 2000), the total number of young stellar objects or  $N_{\text{YSO}}$  (taken from Heiderman et al. 2010 and Kim et al. 2016, and typically including young stellar objects in all evolutionary stages, from Class 0 to Class III, e.g., Rygl et al. 2013), the total mass of the cloud, the mass of dense gas, the Star Formation Rate (SFR, estimated using equation (1) of Lada et al. 2010), the surface density of young stellar objects (calculated using  $N_{\text{YSO}}$  and the area given in the table), the logarithm of the FUV flux (taken from Gupta et al. 2024 and Xia et al. 2022), and the assigned evolutionary or dynamical age of each cloud according to the model of Vázquez-Semadeni et al. (2018) (which essentially adopts the ratio of dense gas vs total mass as a proxy for evolutionary stage of the cloud, see details in Table 5).

Table 6 summarizes the number of protostars and proto-BD candidates for each cloud computed in a number of ways. The

table first lists  $N_{\text{protostar}}$  (corresponding to the number of young stellar objects for which  $T_{\text{bol}} \leq 650$  K, thus including both Class 0 and Class I), and  $N_{\text{proto-Lrestrict}}$ , which corresponds to the subset of  $N_{\text{protostar}}$  whose  $L_{\text{int}}$  is in the range  $0.13\text{--}1 L_{\odot}$  (this will allow to compare our data to Mužić et al. 2019). The table also lists  $N_{\text{proBD}}$ , the total number of proto-BD candidates listed in Table 3 that belong to the catalog of Kim et al. (2016). This requirement is necessary because Kim et al. (2016) searched for proto-BDs uniformly across all these clouds, making the comparison among clouds feasible and sound.

In order to take into account possible incompleteness effects, especially in the regions that are further away, we re-calculated  $N_{\text{proBD}}$  including only the objects down to the same  $L_{\text{int}}$  threshold for all the clouds. The  $L_{\text{int}}$  threshold was adopted from Fig. 6 of Dunham et al. (2008) for which the average  $3\sigma$  sensitivity from the c2d *Spitzer* program can be estimated as  $L_{\text{int}} = 4 \times 10^{-3} (D/140 \text{ pc})^2 L_{\odot}$ . The  $L_{\text{int}}$  threshold in our case will be given by the region with largest distance (Serpens-Aquila at 436 pc), corresponding to a completeness limit of  $0.04 L_{\odot}$  for  $L_{\text{int}}$ . The number of proto-BD candidates in Table 3 that belong to Kim et al. (2016) and whose  $L_{\text{int}} \geq 0.04 L_{\odot}$  is designated as  $N_{\text{proBD-c004}}$ . According to the correlation between  $L_{\text{int}}$  and  $M_{\text{dyn}}$  of Fig. 2,  $L_{\text{int}} = 0.04 L_{\odot}$  corresponds to  $M_{\text{dyn}} = 77 \pm 20 M_{\text{Jup}}$ . This is about a factor of 2 larger than the threshold used by Mužić et al. (2019) and Almendros-Abad et al. (2023) to estimate the star-to-BD ratio in more advanced (Class II/III) evolutionary stages (of  $\sim 30 M_{\text{Jup}}$ ). When applying this completeness criterion, the most affected clouds are Taurus and Lupus I (and III), while, as expected, Serpens-Aquila and Orion A-B remain almost with the same number of objects. We will further discuss this in Secs. 7.3 and 7.4.

In the left panels of Fig. 6, the relation between  $N_{\text{protostar}}$  vs dense gas mass, SFR and dynamical age for all the clouds of Table 5 are shown. For each plot, the Spearman’s rank correlation coefficient  $\rho$  and the  $p$  value, are indicated in the top-right corner. From the left panels of the figure, the well-known correlations of  $N_{\text{protostar}}$  with cloud properties are recovered, as expected (e.g., Lada et al., 2010; Hacar et al., 2024). Although the three relations are well-known and very strong, the  $p$  values indicate that the strongest relation is  $N_{\text{protostar}}$  vs SFR ( $p$  value 0.001), followed by  $N_{\text{protostar}}$  vs dense gas mass ( $p$  value 0.005), and followed by  $N_{\text{protostar}}$  vs cloud dynamical age ( $p$  value 0.006).

The panels on the right of Fig. 6 present the behavior of  $N_{\text{proBD}}$  vs the same cloud properties of the left panels. In the panels on the right, the pink dots correspond directly to  $N_{\text{proBD}}$ , the total number of proto-BD candidates reported in Table 3 that belong to Kim et al. (2016). As can be seen from the figure, the pink dots do not present any correlation with cloud properties. However, once  $N_{\text{proBD}}$  is corrected for completeness, i.e., when  $N_{\text{proBD-c004}}$  is plotted (purple dots), strong correlations are found of  $N_{\text{proBD-c004}}$  with cloud properties, as for the case of  $N_{\text{protostar}}$ , again being the relation of  $N_{\text{proBD-c004}}$  vs SFR the strongest ( $p$  value 0.001), followed by the relation with dense gas mass ( $p$  value 0.012), and followed by the relation with cloud dynamical age ( $p$  value 0.015), being the same behaviour as protostars. Although the values of  $N_{\text{proBD-c004}}$  are very small



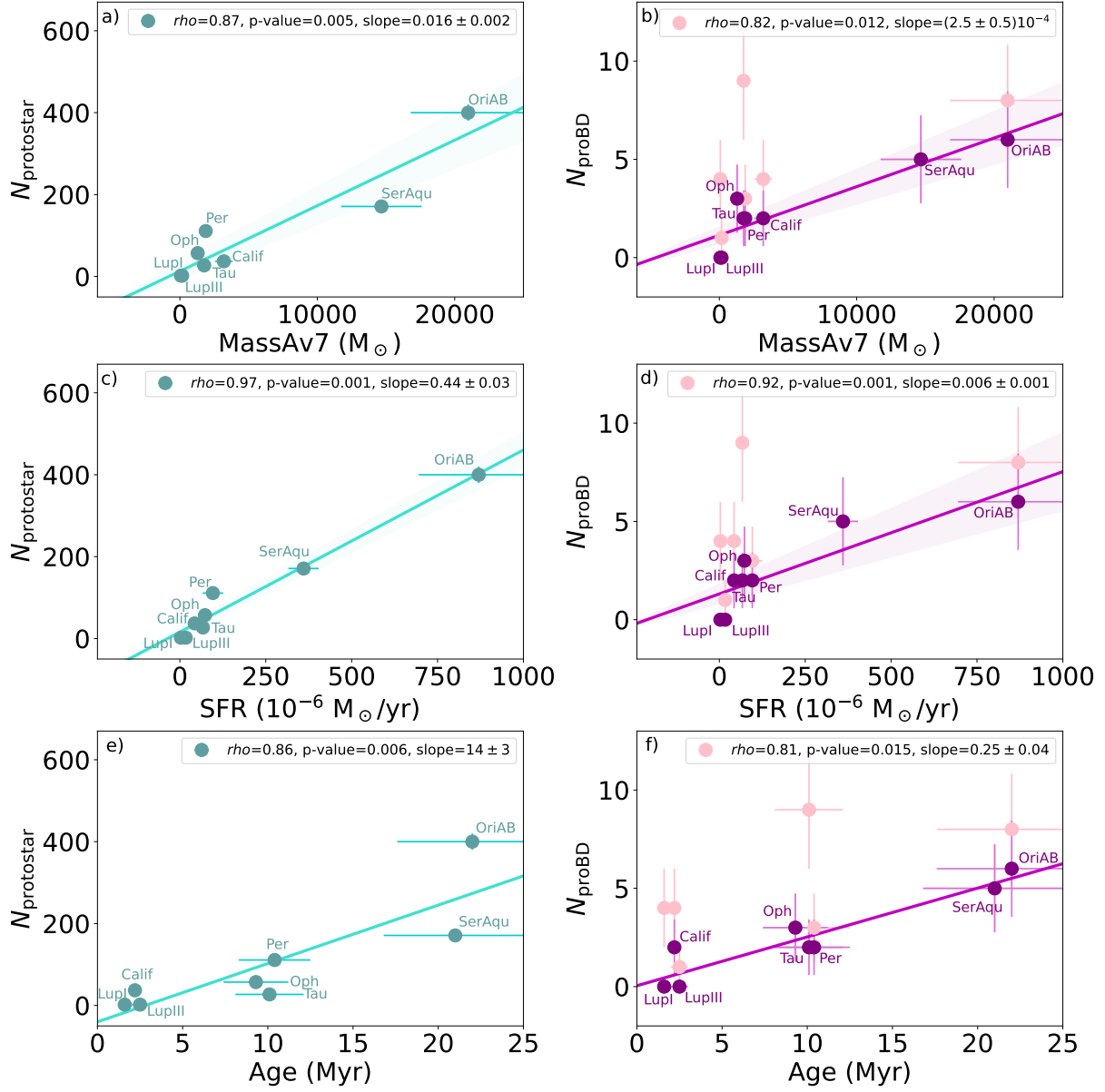


Figure 6: Relation between number of protostellar sources  $N_{\text{protostar}}$  (left) or  $N_{\text{proBD}}$  (right) vs several cloud properties. In all panels on the right, the y-axis shows  $N_{\text{proBD}}$  calculated in two ways. The pink dots correspond to all  $N_{\text{proBD}}$  of Table 3 for each region that belong to Kim et al. (2016) catalog. The purple dots correspond to the same  $N_{\text{proBD}}$  but computed down to the same completeness threshold for all regions, of  $L_{\text{int}} = 0.04 L_{\odot}$  ( $N_{\text{proBD-c004}}$ ). (a)  $N_{\text{protostar}}$  vs. dense gas mass. (b)  $N_{\text{proBD}}$  (pink) or  $N_{\text{proBD-c004}}$  (purple) vs. dens gas mass. (c)  $N_{\text{protostar}}$  vs. SFR. (d)  $N_{\text{proBD}}$  (pink) or  $N_{\text{proBD-c004}}$  (purple) vs. SFR. (e)  $N_{\text{protostar}}$  vs. cloud dynamical age. (f)  $N_{\text{proBD}}$  (pink) or  $N_{\text{proBD-c004}}$  (purple) vs. cloud dynamical age. In all panels, the solid line corresponds to the linear fit (done with curvefit in python), and the shaded areas correspond to the  $1\sigma$  uncertainty of the fit. The uncertainty in the mass, dynamical age, and SFR of the cloud are assumed to be of 20%. The uncertainty in the number counts of protostars or proto-BD candidates are adopted as the square root of the corresponding number.

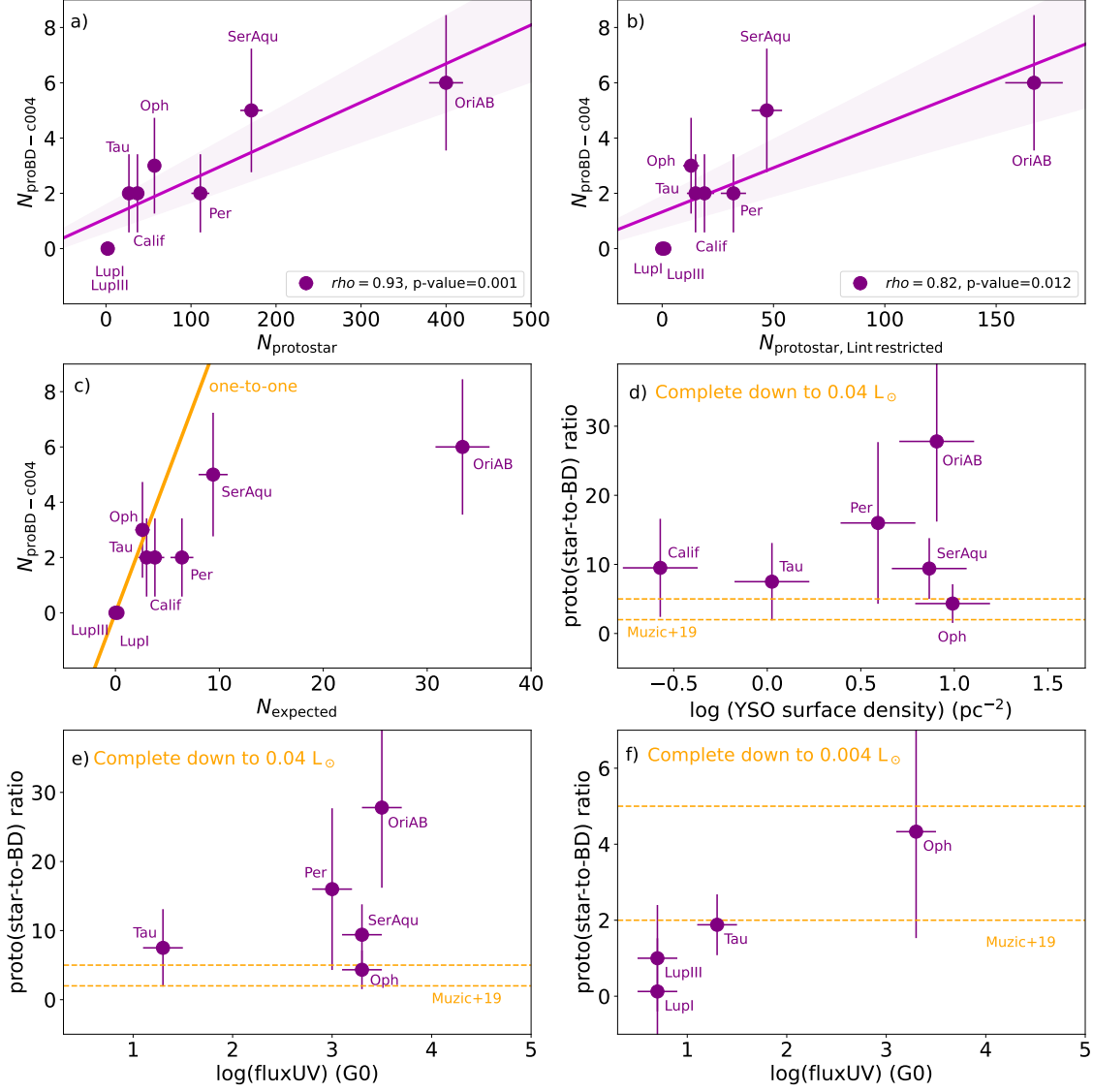


Figure 7: (a)  $N_{\text{proBD-c004}}$  (complete down to  $0.04 L_{\odot}$ ) vs  $N_{\text{protostar}}$ . (b)  $N_{\text{proBD-c004}}$  (complete down to  $0.04 L_{\odot}$ ) vs  $N_{\text{protostar-Lrestricted}}$  ( $N_{\text{protostar}}$  within the luminosity range  $0.13-1 L_{\odot}$ ). (c)  $N_{\text{proBD-c004}}$  (complete down to  $0.04 L_{\odot}$ ) vs  $N_{\text{expected}}$  (where  $N_{\text{expected}} = N_{\text{protostar-Lrestricted}}/5$ , see Sec. 7.2). The orange solid line corresponds to the one-to-one relation. (d) Proto(star-to-BD) ratio vs  $\log$  of protostar surface density. This plot is comparable to Fig. 15 of Mužić et al. (2019) or Fig. 11 of Almendros-Abad et al. (2023). (e) Proto(star-to-BD) ratio vs  $\log$  of FUV flux. (f) Proto(star-to-BD) ratio vs  $\log$  of FUV flux, with the proto(star-to-BD) ratio estimated for the most nearby clouds and therefore down to  $0.004 L_{\odot}$ , near the planetary boundary (see Sec. 7.3).

and more dedicated studies should be carried out to enlarge the samples, this preliminary result suggests that the formation of objects down to  $L_{\text{int}} \sim 0.04 L_{\odot}$  seems to take place similarly to the star formation process.

### 7.2. Proto(star-to-BD) ratio down to $L_{\text{int}} \sim 0.04 L_{\odot}$ among the different nearby clouds

In this subsection we consider the possibility that the number of proto-BD candidates depends on the cloud environment. Variations in the luminosity function in the sub-stellar regime of different clouds were explored by several authors (Sec. 1), but no clear conclusions can be inferred yet from these works. To further explore this, Table 6 additionally provides  $N_{\text{expected}}$ , the number of expected proto-BDs, calculated as  $N_{\text{expected}} = N_{\text{proto-Lrestrict}}/5$ , where  $N_{\text{proto-Lrestrict}}$  is the number of protostars in each region with  $L_{\text{int}}$  between 0.13 and  $1 L_{\odot}$ . In this expression, using  $N_{\text{proto-Lrestrict}}$  is required to make our analysis comparable to the analysis of Mužić et al. (2019) and Almendros-Abad et al. (2023), who calculate the star-to-BD ratio by restricting the stars to the range of  $0.075\text{--}1 M_{\odot}$ . The factor of 5 applied is taken also from Mužić et al. (2019) and Almendros-Abad et al. (2023), and corresponds to the upper-end of the star-to-BD ranges found in these works. The table also provides the proto(star-to-BD) ratio for each cloud, which is the equivalent to the star-to-BD ratio (used in Mužić et al. 2019; Almendros-Abad et al. 2023) but in the deeply embedded phase, and is estimated as  $N_{\text{proto-Lrestrict}}/N_{\text{proBD-c004}}$ .

In Fig. 7-a we present the relation between  $N_{\text{proBD-c004}}$  and  $N_{\text{protostar}}$ , which is found to be highly correlated ( $\rho = 0.93$ ,  $p$  value 0.001). Such a strong correlation is the reason why in Fig. 6 (previous section) the behavior of  $N_{\text{proBD-c004}}$  with cloud properties is the same as the behavior of  $N_{\text{protostar}}$ . The fact that  $N_{\text{proBD-c004}}$  correlates so strongly with  $N_{\text{protostar}}$  suggests that the formation of objects down to  $L_{\text{int}} \sim 0.04 L_{\odot}$  ( $M_{\text{acc}} \sim 77 \pm 20 M_{\text{Jup}}$ ) is intimately linked to the star formation process.

Fig. 7-b presents the same relation but with  $N_{\text{proto-Lrestrict}}$  instead of  $N_{\text{protostar}}$ , which is slightly worse than in the previous case because of the restriction in luminosity. Fig. 7-c shows  $N_{\text{proBD-c004}}$  vs  $N_{\text{expected}}$ , with the one-to-one relation indicated as an orange solid line. While there are a number of clouds that lie close to the one-to-one relation, there are also a few clouds, such as Perseus, Serpens-Aquila, and most extremely Orion A-B, for which  $N_{\text{proBD-c004}} \ll N_{\text{expected}}$ . This can be further seen in Figs. 7-d-e, where the proto(star-to-BD) ratio is shown vs protostar surface density and the FUV flux. Fig. 7-d is comparable to Fig. 15 of Mužić et al. (2019) or Fig. 11 of Almendros-Abad et al. (2023). In Figs. 7-d-e, the range of 2–5, measured for the star-to-BD ratio in Mužić et al. (2019) and Almendros-Abad et al. (2023), is marked with dashed orange lines. While these two panels show no trend of the proto(star-to-BD) ratio with protostar surface density or FUV flux, they clearly show that in the embedded (Class 0/I) phase the ratio calculated here is generally much larger than in the more evolved phase studied by Mužić et al. (2019) and Almendros-Abad et al. (2023). This is related to the fact that we are sensitive to more massive proto-BD candidates (mass  $\gtrsim 0.077 \pm 20 M_{\odot}$ ) than in the aforementioned works (mass  $\gtrsim 0.03 M_{\odot}$ ), and/or that we are still

missing an important fraction of Class 0 proto-BDs due to the current identification strategies.

### 7.3. Proto(star-to-BD) ratio down to $L_{\text{int}} \sim 0.004 L_{\odot}$

As a last attempt to study a possible relation of the number of proto-BD candidates with their environment, we focused on the least massive objects of our compilation. These could only be detected in the most nearby clouds: Taurus, Lupus I, Lupus III and Ophiuchus, for which we are sensitive down to  $L_{\text{int}} = 0.004 L_{\odot}$  (following the same argument as in Sec. 7.1). Table 6 lists  $N_{\text{proBD-c0004}}$ , the number of proto-BD candidates included in Kim et al. (2016) which are complete down to  $0.004 L_{\odot}$ . Here a very different behavior for these clouds can be appreciated: while for Ophiuchus  $N_{\text{proBD-c0004}} = N_{\text{proBD-c004}}$ , meaning that all the proto-BD candidates in Ophiuchus have  $L_{\text{int}} \geq 0.04 L_{\odot}$ , for Taurus and Lupus I,  $N_{\text{proBD-c0004}} \gg N_{\text{proBD-c004}}$ , meaning that most of the proto-BD candidates in these two clouds have  $L_{\text{int}} < 0.04 L_{\odot}$ . Actually, the median  $L_{\text{int}}$  of Taurus and Lupus I is very low, of  $0.0075$  and  $0.010 L_{\odot}$ , respectively. This is also shown in Fig. 7-f, where the proto(star-to-BD) ratio down to  $0.004 L_{\odot}$  is estimated as  $N_{\text{proto-Lrestrict}}/N_{\text{proBD-c0004}}$ . Again following the fit of Fig. 2,  $L_{\text{int}} = 0.004 L_{\odot}$  corresponds to  $M_{\text{acc}} = 18 \pm 5 M_{\text{Jup}}$ . This corresponds to low-mass BDs and is close to the planetary boundary of  $\sim 10 M_{\text{Jup}}$ .

Consequently, Fig. 7-f indicates that there is a deficit of low-mass proto-BD candidates in Ophiuchus compared to Taurus and Lupus (or conversely, an excess in Taurus and Lupus). A deficit of BDs in Ophiuchus was also suggested by Rieke et al. (1989), Erickson et al. (2011), and measured by Alves de Oliveira et al. (2012). In particular, Alves de Oliveira et al. (2012) report a BD-to-star ratio of  $0.09^{+0.04}_{-0.02}$  for Ophiuchus and of 0.18 for Taurus, i.e., Ophiuchus seems to have a number of BDs relative to stars that is a factor of 2 lower than the same number for Taurus. Although Alves de Oliveira et al. (2012) warn that this measurements should be regarded with caution due to poor accuracy of spectral classification of substellar objects, the fact that we find here a significant result showing the same trend suggests that the early findings by Rieke et al. (1989), Erickson et al. (2011), and Alves de Oliveira et al. (2012) could be real.

### 7.4. Possible explanations for the deficit of planetary-mass proto-BD candidates in Ophiuchus relative to Taurus and Lupus

There are several scenarios that could explain the deficit of proto-BD candidates in Ophiuchus relative to Taurus/Lupus. First, it is interesting to note that a very recent episode of star formation, consistent with the short cloud dynamical age estimated from the model of Vázquez-Semadeni et al. (2018) (see Fig. 6-f), has been proposed for Lupus I (Rygl et al., 2013; Benedettini et al., 2018), because it has a large number of prestellar objects with respect to more evolved objects, compared to other clouds. This would suggest that the two phenomena, a recent star formation episode and an excess of low-mass proto-BD candidates, could be related. If this was the case, the

excess of proto-BD candidates in clouds with shortest dynamical ages would be indicative that the proto-BD phase is shorter than the protostellar phase, in line with the simulations of Bate (2019), where BDs accrete from the cloud for a period of time shorter than protostars do, making the typical ‘lifetime’ of a proto-BD much shorter than the typical ‘lifetime’ of a protostar (e.g., Vorobyov, 2010). While this idea (proto-BD lifetimes shorter than protostars lifetimes) is worth exploring in future studies, this is not fully consistent with the fact that we also do see an excess of low-mass proto-BD candidates in Taurus, compared to Ophiuchus, and no recent star formation episode has been identified in Taurus (actually, Taurus and Ophiuchus share the same cloud dynamical age, Fig. 6-f). This might suggest that the important stellar feedback associated with Ophiuchus could be related to the deficit of low-mass proto-BD candidates in this cloud.

Therefore, a second scenario to explain the result of Fig. 7-f is that the feedback from nearby OB stars shortens the proto-BD phase in Ophiuchus compared to this phase in Taurus and Lupus clouds. This would be consistent with a star-like scenario, followed by a very short timescale of the proto-BD phase due to the photo-erosion mechanism, that is expected to quickly deprive a contracting core from their associated envelope of gas and dust (e.g., Whitworth and Zinnecker, 2004; Whitworth, 2018). In this case, regions with strong stellar feedback should present high proto(star-to-BD) ratios (because of the short embedded phase, as Ophiuchus in Fig. 7-f) but very low (evolved) star-to-BD ratios, since the lifetime of later stages would be longer and BD formation would be favored by photo-erosion. Actually, the recent findings of an excess of BDs (i.e., a very low star-to-BD ratio) in NGC 2264, a region with a high number of OB stars, and for which BDs are preferentially distributed closer to the OB stars in the cluster than stars (see Sec. 4.3 of Almendros-Abad et al., 2023), support the photo-erosion scenario in this region. However, it is not likely that photo-erosion is at work in Ophiuchus. The photo-erosion mechanism has been found to be very inefficient, as it requires a massive core, of about  $\sim 75 M_{\odot}$  to form one single BD of  $75 M_{\text{Jup}}$  at a distance of 0.1 pc of the ionizing star (following eq. 60 of Whitworth, 2018). In addition, the typical distance of BDs to OB stars in NGC 2264 is only 0.3–0.5 pc, while the distance of the massive OB stars (earlier than B1) of the Sco OB2 association to the border of the Ophiuchus cloud facing them (comprising OphA, C, E and F) is more than 5 pc (the stars closer to Ophiuchus are all of B-type:  $\sigma$ -Sco at  $\sim 4$  pc is a B1, and both HD 147889 at  $\sim 0.5$  pc, and  $\rho$ -Oph at  $\sim 2$  pc are B2). Thus, NGC 2264 and Ophiuchus are very different cases and does not seem likely that photo-erosion could strongly affect the BD content in the Ophiuchus cloud.

Finally, a third possibility is that the OB stars in the surroundings of the Ophiuchus cloud efficiently heat the cloud, increasing the average temperature of the gas and dust of the cloud. Such an effect has already been reported in previous works (e.g., Sánchez-Monge et al., 2013; Rumble et al., 2021; Kahle et al., 2024). If the Ophiuchus cloud was on average warmer than Taurus and Lupus, the Jeans mass in Ophiuchus would be larger, naturally suppressing the formation of the least massive

objects, as proposed by Bate (2009) and consistent with Bate (2023). In order to test this hypothesis, we performed preliminary estimates of the average dust temperatures in these clouds. Dust temperature images for Gould Belt clouds are provided by the *Herschel* Gould Belt survey key project (André et al., 2010). To estimate average dust temperatures, we selected regions in each cloud above a column density of  $4 \times 10^{21} \text{ cm}^{-2}$ , which is around the star formation threshold reported by Heiderman et al. (2010) and Whitworth (2016). For the Ophiuchus cloud, the average and standard deviation dust temperature measured in the map of Ladjelate et al. (2020) above the aforementioned threshold is  $17 \pm 2$  K, while for Taurus this is  $12.9 \pm 0.7$  K (using the dust temperature map of André et al. 2010; Könyves et al. 2015; Marsh et al. 2016) and for Lupus I this is  $13.6 \pm 0.7$  K (using the dust temperature map of Rygl et al. 2013; Benedettini et al. 2018). The fact that the Ophiuchus cloud seems to be slightly warmer than other clouds and heated by the nearby massive stars has also been recognized by other authors (e.g., Friesen et al., 2009; Kirk et al., 2007; Rumble et al., 2021). Assuming a density fluctuation of  $10^9 \text{ cm}^{-3}$  and a temperature of  $\sim 13$  K, the corresponding Jeans mass is of  $9 M_{\text{Jup}}$  (following eq. 14). But if the temperature increases up to 19 K due to feedback, then the Jeans mass increases up to  $17 M_{\text{Jup}}$ , suppressing the formation of low-mass BDs in the warmest regions, as suggested by other authors (e.g., Rumble et al., 2021). This is consistent with the result of Benedettini et al. (2018), who show that, in the Lupus (and Taurus) clouds, the star formation activity is associated with lower column densities compared to other clouds. This can be explained in terms of Jeans fragmentation: if a cloud is colder on average, then the minimum density required to form stars of a given mass is also smaller because the Jeans mass goes with the inverse square root of the density. Given that Jeans fragmentation is known to regulate the star formation process in the dense parts of molecular clouds (e.g., Motte et al., 1998; Gutermuth et al., 2011; Palau et al., 2015, 2021; Kainulainen et al., 2016; Beuther et al., 2018; Saha et al., 2022; Morii et al., 2024), the results outlined here are consistent with the same formation mechanism for BDs and stars, not only for high-mass BDs but also for the low-mass BDs near the planetary boundary, of  $\sim 10 M_{\text{Jup}}$ . This possibility is consistent also with the recent findings of Panwar et al. (2024) in Berkeley 59.

In addition, a particularly strong magnetic field permeating the Ophiuchus cloud could also contribute to increasing the critical mass required for an object to undergo collapse. Actually, Lê et al. (2024) have recently reported that Ophiuchus seems to be a magnetically dominated cloud. It would be important to further explore this possibility (low-mass BDs are suppressed in regions with higher dust temperatures and/or higher magnetic field strengths) in other clouds with different average dust temperatures or magnetic field strengths and to explore a potential relation between spatial distribution and these quantities in the cloud.



## 8. Putting everything together: constraints on the BD formation theories from the current observations

In the paragraphs below, we list the main results presented in this work:

- A correlation between  $L_{\text{int}}$  and  $M_{\text{dyn}}$  has been found, which is consistent with the [D’Antona and Mazzitelli \(1994\)](#) and [Vorobyov et al. \(2017b\)](#) models at  $5 \times 10^5$  yr, a typical lifetime for the Class 0/I phase. In the following, this relation has been used to estimate the accreted mass given  $L_{\text{int}}$ .
- As a preliminary result, the well-known correlations associated with infall and outflow phenomena in protostars extend reasonably well in general down to  $L_{\text{bol}} \sim 0.006 L_{\odot}$ , corresponding to low-mass BDs of  $M_{\text{dyn}} \sim 0.024 \pm 0.007 M_{\odot}$  (Sec. 5.4). When using single-dishes, a deficit of outflow force has been reported in some cases, probably related to beam dilution effects.
- The systematic searches performed so far to identify pre-BDs have provided candidates that need to be confirmed (Sec. 6) in most of the cases. The scarcity of robust pre-BD candidates is probably due to the challenging nature of these observational projects, requiring very deep interferometric observations to obtain conclusive results.
- The number of proto-BD candidates with  $L_{\text{int}} \gtrsim 0.04 L_{\odot}$  present the same correlations with molecular cloud properties as the number of protostars (Sec. 7.1). This arises from the fact that these two numbers are highly correlated (Sec. 7.2). Although larger samples of proto-BDs are mandatory to confirm it, this preliminary result suggests that the formation of low-mass objects down to  $0.04 L_{\odot}$  (corresponding to very low-mass stars and massive BDs,  $M_{\text{acc}} \sim 0.077 \pm 0.020 M_{\odot}$ ) seems to take place in a star-like manner. Improving the sensitivity to detect less massive BDs would allow to be complete down to lower masses. However, this does not warrant that the correlation of  $N_{\text{protostar}}$  vs  $N_{\text{proBD}}$  would improve, because for low-mass BDs the environmental effects could become important, as shown in Sec. 7.4 and next paragraphs. This constitutes an excellent test for the future.
- The proto(star-to-BD ratio) computed for  $L_{\text{int}} \gtrsim 0.04 L_{\odot}$  in general yields values larger than the star-to-BD ratio measured in more evolved objects (Sec. 7.2), due to the fact that we are sensitive only to the most massive proto-BD candidates.
- The proto(star-to-BD ratio) including low-mass BDs ( $L_{\text{int}} \gtrsim 0.004 L_{\odot}$  or  $M_{\text{acc}} \sim 0.018 \pm 0.005 M_{\odot}$ ), which could be determined only for Taurus, Lupus and Ophiuchus clouds, is significantly lower for Taurus and Lupus than for Ophiuchus. This suggests that there is a deficit of low-mass BDs in Ophiuchus (compared to Taurus and Lupus), which could be related to the measured higher average dust temperature in Ophiuchus, suppressing fragmentation near this mass range ( $\sim 0.018 M_{\odot}$ ) because of the

higher Jeans mass. This indicates a possible star-like scenario down to the planetary boundary regime (Secs. 7.3 and 7.4).

There are at least two caveats in the results presented above. First, each one of these evidences should be further studied in future projects focused at confirming the current proto- and pre-BD candidates and enlarging their statistics, so that the results are settled on a more robust base. Second, it is important to keep in mind that in Sec. 5.1, a requirement for a robust proto-BD candidate was that its SED must be similar to Class 0 or Class I SEDs of protostars. However, if proto-BDs are formed from disc fragmentation and subsequently ejected, such a SED shape could change, with the object being equally young. Thus, up to a certain point, it is natural that, given our requirements, we have picked up only the objects that form like stars<sup>18</sup>. Further theoretical work about the expected SEDs for ejected objects from discs would be very helpful to deal with those possible biases.

In spite of these caveats, the compiled, in some cases preliminary results presented in this work seem to consistently point towards a star-like scenario for BDs down to the planetary boundary,  $\sim 0.01 M_{\odot}$ . This is consistent with reported properties of the least massive BDs, like e.g. the finding that BDs with masses down to  $10 M_{\text{Jup}}$  show discs as those detected around stars, reinforcing the idea that they are a scaled-down version of stellar objects (see [Scholz et al., 2023](#), and references therein). Given the increasing evidence that BDs seem to form like stars at least down to the planetary-boundary mass regime, the next question is what happens below this boundary (i.e.,  $\leq 0.01 M_{\odot}$ ).

Although the data gathered in the present work are not well suited to answer which is the main formation mechanism below  $\sim 0.01 M_{\odot}$ , there are recent works shedding light on this question. In Sec. 1, a number of works focused on the study of the low-mass end of the IMF were mentioned. Most of the 20 IMF works cited in Sec. 1 cover masses  $> 0.01 M_{\odot}$ , and only three of them include the planetary regime down to  $\sim 0.005 M_{\odot}$ : [Miret-Roig et al. \(2022\)](#), [Parker and Alves de Oliveira \(2023\)](#), and [Chabrier and Lenoble \(2023\)](#). On one hand, both [Parker and Alves de Oliveira \(2023\)](#) and [Chabrier and Lenoble \(2023\)](#) find that for the galactic bulge and NGC 1333, the mass distribution, spatial distribution and kinematics of FFPs are consistent with a star-like scenario. On the other hand, [Miret-Roig et al. \(2022\)](#) report a rich population of FFPs down to  $5 M_{\text{Jup}}$  in Upper Scorpius and Ophiuchus clouds, which seems to exceed the predictions from numerical simulations of the star-like scenario by [Haugbølle et al. \(2018\)](#) and [Bate \(2019\)](#). This is interpreted as an evidence that other mechanisms have to be at work in this regime, such as disc fragmentation and subsequent ejection, although the numerical simulations of the star-like scenario should be further explored to really assure that

<sup>18</sup>However, the fact that proto-BD candidates with  $L_{\text{int}} > 0.04 L_{\odot}$  follow the same behavior as protostars in several molecular clouds (Sec. 7.1) suggests that at least for the massive proto-BDs, the contribution from ejection might not be highly significant.

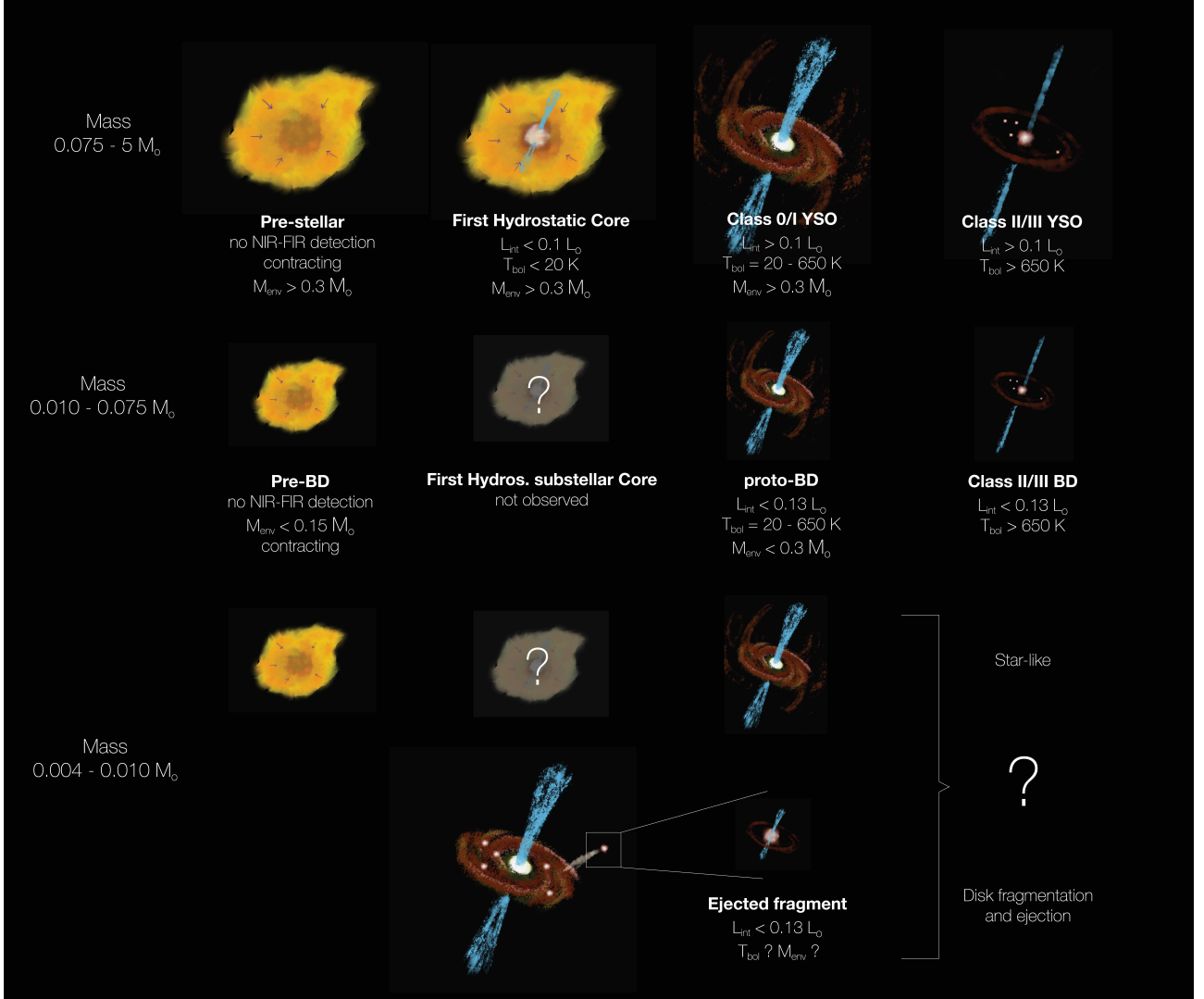


Figure 8: Sketch of the probable/dominant formation process in the different mass regimes. The top row corresponds to the process of low-mass star formation, covering masses from  $0.075$  to  $\sim 5 M_{\odot}$ , and undergoing the pre-stellar, FHC, Class 0/I and Class II/III phases. The second row corresponds to the process of BD formation, including masses from  $\sim 0.010$  to  $0.075 M_{\odot}$ , and most likely undergoing the pre-BD, proto-BD and Class II/III phases (see Sec. 8). The FHC phase of a substellar object should exist if they form as low-mass stars, but has not been observed yet. The third and fourth rows correspond to the process of FFP formation, including masses from  $0.004$  to  $0.010 M_{\odot}$ . The third row corresponds to a star-like scenario, while the forth row corresponds to the disc fragmentation + ejection scenario. The question mark indicates the current debate about the role of each scenario in this mass range.

cannot reproduce these observations, as indicated by Chabrier and Lenoble (2023).

In conclusion, a combined scenario for BD formation, where objects above the planetary regime ( $> 0.01 M_{\odot}$ ) form mainly like stars, while objects below this regime ( $0.004\text{--}0.010 M_{\odot}$ ) form through a combination of both star-like and planet-like scenarios, seems feasible and consistent with the data presented in this work and previous recent findings. Fig. 8 summarizes this combined scenario. The top row of the figure describes the main observational stages that lead to the formation of a low-mass star, starting with the pre-stellar core, passing through the FHC, Class 0/I and Class II/III stages. The second row describes the formation of BDs that range from  $0.010$  to  $0.075 M_{\odot}$  approximately. For BDs, it seems that the formation process is a scaled-down version of low-mass stars (with the only exception that the FHC has not been observed yet). Finally, for objects below the planetary-boundary of  $0.01 M_{\odot}$ , the dominant process could be different in different environments, suggesting that both star-like and planet-like scenarios could be at work, being this an open question.

In this sense, one of the main results found in this work might be worth exploring in the future: the role of the environment in shaping the low-mass end of the IMF. Although this is usually considered to be negligible, in Sec. 7.3 and 7.4 it was shown that Ophiuchus seems to under-produce low-mass BDs, and that one possibility to explain this deficit is the heating of the cloud by the nearby OB stars of the Sco OB2 association, naturally increasing the Jeans mass and thus suppressing fragmentation below a certain mass. This opens the possibility that the environment plays a subtle role in shaping the IMF, most apparent in the planetary-boundary and below, precisely the mass range that has been typically uncovered by most of the studies of the IMF, both observational and theoretical. An excellent test to further explore this hypothesis would be to apply the same methodology of Miret-Roig et al. (2022) to Taurus and Lupus: we would expect a lower star-to-BD ratio in the planetary boundary in these two clouds compared to Ophiuchus, something which was marginally found by Alves de Oliveira et al. (2012) but needs to be confirmed with deeper studies in a large number of clouds. If confirmed, this would favor the fact that the environment where a cloud is embedded can affect the very low-mass end of the IMF by suppressing/allowing the formation of the lowest-mass BDs in a Jeans-like, therefore star-like, manner.

To sum up, taking into account all these considerations and the observational evidence presented in this work, it would be very useful for observers that the following aspects were taken into account from the theoretical and numerical side: i) predictions of number of pre-BD cores in molecular clouds; ii) differences between expected SEDs for star-like proto-BDs and proto-BDs ejected from discs; iii) simulations that fully sample the planetary-mass regime<sup>19</sup>; iv) simulations that take into account heating of molecular clouds by external feedback from

OB stars in realistic conditions. These studies would allow to contrast on a more robust base the observations and the theories in the decisive regime where planets and BDs overlap.

## 9. What can we learn from the current observations to design future strategies

In this section we discuss how we could use *Spitzer*, *Herschel* (archival), ALMA, JWST, *Euclid*, the ngVLA, SKA and future facilities to efficiently search, identify and characterize proto-BDs.

ALMA will be upgraded to a much higher sensitivity, and the ngVLA is planned to start operations in 2032 and its observing bands range from 1.3 GHz to 116 GHz. Thus, it will be feasible to search for faint dusty envelopes associated with proto-BDs with these new generation of interferometers.

In Sec. 3.2, a number of proto-BD candidates were reported to be found serendipitously in the surroundings ( $\lesssim 5000$  au) of other protostars or proto-BDs, suggesting that a promising strategy to search for proto-BDs would be to carry out deep interferometric observations in the immediate surroundings of Class 0 protostars. In this sense, the ngVLA will be a great instrument, since it will be able to reach sensitivities at 3 mm of  $\sim 1 \mu\text{Jy beam}^{-1}$  in only 1 hour, allowing to observe envelope masses as low as  $0.3 M_{\text{Jup}}$ , or about 6 times the mass of Neptune, at the distance of Orion. In addition, one single pointing at 3 mm will provide a field of view of  $\sim 34$  arcsec, corresponding to  $\sim 5000$  au at the distance of Taurus, making the searches of proto-BDs near protostars very efficient because no mosaicing would be needed. What is more, these deep observations around Class 0 protostars would also allow to explore the possibility that proto-BDs are triggered by the jets from their nearby protostars, which would compress the surrounding dense gas, favoring the fragmentation of very low-mass objects. If this scenario is at work, the deep millimetre and centimetre observations from next-generation interferometers would allow to gather statistically significant numbers of proto-BDs near protostars, and robustly test whether they are preferentially formed along the outflow directions.

Another important test that could be performed with the next-generation millimetre interferometers is studying the role of ambipolar diffusion in the formation process of BDs. Ambipolar diffusion could play an important role if BDs form as a scaled-down version of stars, because it would allow to build the dense gravitationally bound condensations that will end up as proto-BDs. This could be observationally tested by observing molecular lines from both ionized and neutral species because, if ambipolar diffusion is important, a significant velocity drift between ionized and neutral species is expected (e.g., Yen et al., 2018; Tritsis et al., 2023). This cannot be easily studied nowadays because detecting molecular gas around proto-BDs is challenging, but with the orders-of-magnitude increase in sensitivity of the next-generation interferometers, this will be a feasible test.

Deep interferometric studies will also be essential to elucidate the nature of the current pre-BD candidates (such as those

<sup>19</sup>The simulations from Haugbølle et al. (2018) sample masses down to  $\sim 0.02 M_{\odot}$ , while the simulations from Bate (2019) sample masses down to  $\sim 0.01 M_{\odot}$ , and do not reach statistically the lowest masses observed by Miret-Roig et al. (2022), of  $0.005 M_{\odot}$ .

listed in Table 4) and to search for new candidates in the solar neighborhood clouds. Most of the candidates of Table 4 still lack very deep interferometric observations to: look for potential compact sources associated, detect the gas and assess gravitational instability, study the density profile and study possible infall motions associated with the objects. Since pre-BD candidates are so faint, very deep observations are required and next-generation interferometers will be decisive in this sense.

In addition, the ngVLA and SKA will allow to search for extremely faint thermal radiojets such as the one found in IC348-SMM2E or the candidates identified in Taurus (Forbrich et al., 2015; Morata et al., 2015; Rodríguez et al., 2017). Taking the flux density measured in IC348-SMM2E at 3.3 cm, of  $23 \mu\text{Jy beam}^{-1}$ , which was detected at the  $3\sigma$  level, the ngVLA in the Main array could detect it in one hour with a signal-to-noise ratio of 90, a factor of 30 larger than the current marginal detection (the sensitivity of the Main array at 3.6 cm or 8 GHz in 1 hour is of  $0.25 \mu\text{Jy beam}^{-1}$ ). This also means that we could detect these proto-BD radiojets up to 1.5 kpc (at  $4\sigma$ ), opening a window to search them well outside the solar neighborhood. Furthermore, these new-generation interferometers, along with ALMA in its most extended configurations, will also allow to study multiplicity, including very compact companions, in large samples of proto-BDs, a crucial piece to understand their formation process. For example, the ngVLA at 3 mm will reach an angular resolution of 0.08 mas, corresponding to  $\sim 0.01$  au at the distance of Taurus.

Moving to shorter wavelengths, the *Euclid* mission, whose goal is to establish the nature of dark matter and dark energy, will also play a role in the search and characterizations of BDs. Several deep observations have been already taken in the  $\sigma$ ,  $\lambda$  Orionis, and Taurus star-forming regions, among others, during its first operational months (see Martín et al., 2024). These data should extend the IMFs down to the mass of Jupiter, and should confirm whether there is a cut-off and its relation with the proposed formation mechanism. In particular, these observations would be very useful to test if the population of BDs in the planetary-boundary presents a deficit in Ophiuchus compared to Taurus and Lupus, as expected from the results of Sec. 7.3 and 7.4. In addition, these *Euclid* observations will be important to validate previously identified proto-BD candidates and, as a wide-field survey, will provide the opportunity of many serendipitous discoveries in several star-forming regions. However, since the longest wavelengths of *Euclid* lie in the near-infrared, it will probably still miss the most embedded and least massive proto-BDs, whose SED peak lies near 70–100  $\mu\text{m}$ . For the extreme most embedded cases, the *Herschel* or James Webb Space telescopes, observing at longer wavelengths, would be required.

JWST, launched in December 2022, is providing an extraordinary wealth of information in multiple fields. We have already mentioned the recent works by Pearson and McCaughrean (2023) and McCaughrean and Pearson (2023), who have found hundreds of BD and FFP candidates in the Trapezium cluster using deep near- and mid-IR imaging. A detailed follow-up is expected, using its spectroscopic capabilities. Thus, detailed properties will be derived, such as kine-

matics, including the outflows (following the steps of Ray et al. 2023 in the case of the well-known outflow HH 211) or atmospheric compositions. Thus, the JWST is revealing an otherwise hidden population of BDs in the planetary-mass regime, opening the opportunity to test the different formation scenarios. In particular, the star-like formation scenario can be tested through the study of chemical signatures of BD atmospheres (Zhang et al., 2021b,a). As an example, Barrado et al. (2023) have recently presented JWST observations of a cool BD-BD binary with  $15 M_{\text{Jup}}$  components, and conclude that it has most probably formed in a star-like manner by using the  $^{15}\text{NH}_3$  as a diagnostic tool to distinguish among formation scenarios. However, some caveats should be taken into account, since very high quality data and further improvements in the modelling are needed. The extent of these chemical studies to larger samples will definitely help to confirm the star-like formation scenario for these objects.

The deep observations of the JWST, along with *Euclid*, and further exploitation of *Spitzer* and *Herschel* data are required to build samples of much less luminous objects compared to the current samples. Our requirement that  $L_{\text{int}} < 0.13 L_{\odot}$  necessarily includes a fraction of ‘contaminant’ protostars, because  $L_{\text{int}} < 0.13 L_{\odot}$  corresponds to  $M_{\text{dyn}} < 0.12 M_{\odot}$  according to Fig. 2. The  $L_{\text{int}} < 0.13 L_{\odot}$  requirement was used in Sec. 5.1 as a first best-effort basis to take into account the typical uncertainties in  $M_{\text{dyn}}$  of about 50%, but strictly speaking and following the relation of Fig. 2, one should be using the requirement of  $L_{\text{int}} < 0.04 L_{\odot}$  to select  $M_{\text{dyn}} < 0.075 M_{\odot}$  and, to do this, new techniques, strategies and observatories are required to efficiently identify candidates that are much less luminous than what has been explored so far.

Finally, as mentioned in Sec. 7.4, a promising research line could be the study of molecular cloud properties, such as dust temperature or magnetic fields, with the spatial distribution of low-mass BDs, because if they form in a star-like manner it would be expected some kind of relation based on Jeans fragmentation. To do this, the combined observations of *Herschel* and JWST will be pivotal, because the JWST will allow to detect embedded objects with masses of the order of the Jupiter mass in clouds such as Orion, about one order of magnitude lower than the mass sensitivity achieved in this work using *Spitzer* data. However, the JWST longest wavelengths reach 28  $\mu\text{m}$ , and the most embedded objects are expected to lie in extended and colder regions emitting at the *Herschel*/PACS frequencies. Thus, a selection strategy combining criteria using both JWST and *Herschel* bands stands as very promising to have complete counts of the most embedded objects down to a few Jupiter masses. This in turn might shed important clues on how the low-mass end of the IMF is shaped.

## Acknowledgements

The authors are grateful to the referee for his valuable and detailed comments that helped complete and clarify the paper. The authors are grateful to Hervé Bouy, Núria Miret-Roig, Koraljka Muzic, Matthew Bate, Enrique Vázquez-Semadeni, Javier Ballesteros-Paredes, Melodie Kao, and Òscar Morata for



insightful and stimulating discussions. The authors are grateful to Kazi Rygl and Milena Benedettini for kindly sharing the column density and dust temperature maps of the Lupus I cloud from *Herschel* data, and to Eduard Vorobyov for kindly sharing their models published in 2017. The authors are grateful to Ana María Pérez-García for her invaluable help on the SUCANES database, to Sundar Srinivasan and Pedro Mas-Buitrago for support on data analysis methods, and to Miguel Agustín Sánchez Valdés for support on the graphical design of Figs. 1 and 8. AP acknowledges financial support from the UNAM-PAPIIT IN111421 and IG100223 grants, the Sistema Nacional de Investigadores of CONAHCyT, México. DB and NH have been funded by grants No. MDM-2017-0737 Unidad de Excelencia “María de Maeztu”- Centro de Astrobiología (CSIC/INTA) and by the Spanish grants MCIN/AEI/10.13039/501100011033 PID2019-107061GB-C61 and PID2023-150468NB-I00. CWL acknowledges support from the Basic Science Research Program through the NRF funded by the Ministry of Education, Science and Technology (NRF- 2019R1A2C1010851) and by the Korea Astronomy and Space Science Institute grant funded by the Korea government (MSIT; project No. 2024-1-841-00). This work has made use of the SUCANES database, a joint project funded by ESA Faculty under contract No. 4000129603/19/ES/CM, ISDEFE and CSIC, and has made use of data from the Herschel Gould Belt survey (HGBS) project (<http://gouldbelt-herschel.cea.fr>). The HGBS is a Herschel Key Programme jointly carried out by SPIRE Specialist Astronomy Group 3 (SAG 3), scientists of several institutes in the PACS Consortium (CEA Saclay, INAF-IFSI Rome and INAF-Arcetri, KU Leuven, MPIA Heidelberg), and scientists of the Herschel Science Center (HSC). This paper makes use of the following ALMA data: ADS/JAO ALMA#2013.1.00157.S, 2013.1.00220.S, 2013.1.00465.S, 2013.1.00474.S, 2015.1.00041.S, 2015.1.00186.S, 2015.1.00223.S, 2015.1.00310.S, 2015.1.00741.S, 2015.1.01510.S, 2016.1.00039.S, 2016.1.00085.S, 2016.1.00460.S, 2017.1.01462.S, 2017.1.01693.S, 2018.1.00126.S, 2018.1.00756.S, 2019.1.00218.S, 2019.1.00847.S, 2019.1.01813.S, and 2022.1.01270.S. ALMA is a partnership of ESO (representing its member states), NSF (USA) and NINS (Japan), together with NRC (Canada), NSTC and ASIAA (Taiwan), and KASI (Republic of Korea), in cooperation with the Republic of Chile. The Joint ALMA Observatory is operated by ESO, AUI/NRAO and NAOJ.

Table 1: Compilation of Fig. 2 of  $L_{\text{int}}$  and  $M_{\text{dyn}}$  for proto-BD candidates, VeLLOs and protostars with  $L_{\text{int}} < 10 L_{\odot}$ , and for which a velocity gradient has been observed

Source	$M_{\text{dyn}}^{\text{a}}$ ( $M_{\odot}$ )	$L_{\text{int}}^{\text{a}}$ ( $L_{\odot}$ )	$T_{\text{bol}}^{\text{a}}$ (K)	Excluded from fit <sup>b</sup>	Refs. <sup>c</sup>
L328-IRS	$0.27 \pm 0.15$	$0.121 \pm 0.020$	67	–	L18
I04158+2805	$0.30 \pm 0.15$	$0.065 \pm 0.010$	337	–	A08,Ra21
I16253–2429	$0.14 \pm 0.03$	$0.129 \pm 0.030$	37	–	H19,A23
Mayrit1701117	$0.35 \pm 0.17$	$0.27 \pm 0.06$	100	–	R19
ISO-Oph200	$0.23 \pm 0.12$	$0.090 \pm 0.018$	329	–	Ri21
I15398–3359	$0.05 \pm 0.04$	1.34	122	outbursting	O14,Y17, O18
L1451-mm	$0.06 \pm 0.03$	$0.020 \pm 0.004$	19	$T_{\text{bol}} < 20$ K	Mau20
Cha-MMS1	$0.03 \pm 0.01$	$0.024 \pm 0.004$	20	–	Mau20
IC348-SMM2E	$0.07 \pm 0.04$	$0.109 \pm 0.020$	23	–	P14
IRAM04191	$0.05 \pm 0.03$	$0.042 \pm 0.008$	59	–	H24
I04191+1523A	$0.14 \pm 0.07$	$0.18 \pm 0.03$	–	–	L17
I04191+1523B	$0.12 \pm 0.06$	$0.18 \pm 0.03$	–	–	L17
L1448-C	$1.5 \pm 0.7$	$7.5 \pm 2.5$	–	–	Mar20,H10
L1527-IRS	$0.55 \pm 0.15$	$0.9 \pm 0.1$	–	–	T12,Mar20
L1448-IRS3B	$1.0 \pm 0.5$	$2.4 \pm 0.5$	–	–	T16
Per-Bolo58	$0.12 \pm 0.06$	$0.019 \pm 0.002$	20	–	Mau20
Lupus3-MMS	$0.23 \pm 0.11$	$0.41 \pm 0.20$	39	–	Y17
TMC-1A	$0.64 \pm 0.32$	$2.7 \pm 1.3$	–	–	Y17
RCrA-IRS7B	$2.3 \pm 1.1$	$4.6 \pm 2.3$	–	–	Y17
IRS43	$1.9 \pm 1.0$	$6 \pm 3$	–	–	Y17
L1489-IRS	$1.6 \pm 0.8$	$3.7 \pm 1.8$	–	–	Y17
L1551NE	$0.8 \pm 0.4$	$4.2 \pm 2.1$	–	–	Y17
IRS63	$0.8 \pm 0.4$	$1.0 \pm 0.5$	–	–	Y17
TMC1	$0.54 \pm 0.27$	$0.9 \pm 0.4$	–	–	Y17
B335	$0.15 \pm 0.1$	1.4	–	outbursting	Y17,E23
VLA1623	$0.2 \pm 0.1$	$1.1 \pm 0.6$	–	multiple	Y17
N1333-IRAS4A2	$0.08 \pm 0.04$	$1.9 \pm 0.9$	–	multiple	Y17
HH211	$0.05 \pm 0.02$	1.0	–	shocks at $70 \mu\text{m}$	Y17,P21
L1521F-IRS	$0.18 \pm 0.09$	$0.037 \pm 0.003$	16	$T_{\text{bol}} < 20$ K	T17

<sup>a</sup>  $L_{\text{int}}$  is taken from SUCANES database when available or from the references listed in the table. Its uncertainty is taken as 20%. For  $M_{\text{dyn}}$ , a typical uncertainty of 50% is adopted.  $M_{\text{dyn}}$  for ISO-Oph200 is re-calculated in this work using Fig. 5 of [Riaz and Machida \(2021\)](#). For IC348-SMM2E, both  $M_{\text{dyn}}$  and  $L_{\text{int}}$  are re-calculated to the new distance of 320 pc ([Ortiz-León et al., 2018](#)). In addition, since IC348-SMM2E presents emission at  $4.5 \mu\text{m}$  associated with the blueshifted lobe [Palau et al. \(2014\)](#), suggesting that the outflow is inclined with respect to the plane of sky, a range of inclinations  $30\text{--}60^\circ$  were adopted, corresponding to  $36\text{--}110 M_{\text{Jup}}$ . For I16253–2429, the results of [Yen et al. \(2017\)](#) were also taken into account, but we finally adopted the  $M_{\text{dyn}}$  from [Hsieh et al. \(2019a\)](#) because these authors include the [Yen et al. \(2017\)](#) work in their analysis and in addition obtain results consistent with the more recent work by [Aso et al. \(2023\)](#). For Mayrit1701117, ISO-Oph200, and I04191+1523A,B,  $L_{\text{int}}$  is recalculated from the flux at  $70 \mu\text{m}$  from the SED of the reference paper, and following eq. 6.  $L_{\text{int}}$  for IRAS15398 is  $1.34 L_{\odot}$  using the measured flux at  $70 \mu\text{m}$  ( $24 \text{ Jy}$ ) from [Benedettini et al. \(2018\)](#), consistent with the IRAS fluxes. However, [Jørgensen et al. \(2013\)](#) argue that this object is outbursting and that its true  $L_{\text{int}}$  is two orders of magnitude smaller. Given these extreme characteristics, I15398–3359 has been excluded from the fit of Fig. 2.  $T_{\text{bol}}$  is taken from SUCANES if the source is included in this database.

<sup>b</sup> Reason why the object has been excluded from the fit of Fig. 2. Wherever ‘multiple’ is indicated, it refers to the fact that  $L_{\text{int}}$  includes all components of the multiple system while the velocity gradient has been identified in only one of the components, yielding an evident mismatch between  $L_{\text{int}}$  and  $M_{\text{dyn}}$ . Objects with  $T_{\text{bol}} < 20$  K have been excluded from the  $L_{\text{int}}$  vs  $M_{\text{dyn}}$  relation because very low  $T_{\text{bol}}$  can be associated also with pre-stellar cores (e.g., [Young and Evans, 2005](#)).

<sup>c</sup> References: A08: [Andrews et al. \(2008\)](#); A23: [Aso et al. \(2023\)](#); E23: [Evans et al. \(2023\)](#); H10: [Hirano et al. \(2010\)](#); H19: [Hsieh et al. \(2019a\)](#); H24: [Huelamo et al. \(2024\)](#); L17: [Lee et al. \(2017\)](#); L18: [Lee et al. \(2018b\)](#); Mar20: [Maret et al. \(2020\)](#); Mau20: [Maureira et al. \(2020\)](#); O14: [Oya et al. \(2014\)](#); O18: [Okoda et al. \(2018\)](#); P14: [Palau et al. \(2014\)](#); P21: [Pezzuto et al. \(2021\)](#); R19: [Riaz et al. \(2019a\)](#); Ra21: [Ragusa et al. \(2021\)](#); Ri21: [Riaz and Machida \(2021\)](#); T12: [Tobin et al. \(2012\)](#); T16: [Tobin et al. \(2016a\)](#); T17: [Tokuda et al. \(2017\)](#); Y17: [Yen et al. \(2017\)](#).

Table 2: Objects from SUCANES with  $L_{\text{int}} \leq 0.13 L_{\odot}$  that do not fulfill the  $T_{\text{bol}}$  and/or  $M_{\text{env}}$  criteria of Sec. 5.1

Source	Region	Dist. (pc)	R.A.	Dec.	$L_{\text{int}}$ ( $L_{\odot}$ )	$T_{\text{bol}}$ (K)	$M_{\text{env}}^{\text{a}}$ ( $M_{\odot}$ )	$L_{\text{bol}}$ ( $L_{\odot}$ )	Class	Type <sup>b</sup>	Refs. <sup>c</sup>
L1451-mm	Perseus	293	03:25:09.5	+30:23:51	$< 0.020$	19	0.48	0.099	0	VeLLO/FHC	E06,Mau20,P11
L1448-IRS2E	Perseus	293	03:25:22.4	+30:45:13	$< 0.033$	–	0.047	–	0	VeLLO/FHC	C10,Mau20
Per-Bolo58	Perseus	293	03:29:25.5	+31:28:15	$0.019 \pm 0.002$	20	1.64	0.174	0	FHC	E10
B1b-N	Perseus	293	03:33:21.2	+31:07:44	$< 0.014$	15	1.20	0.433	0	VeLLO/FHC	H14,G17,H99
B1b-S	Perseus	293	03:33:21.4	+31:07:26	$0.058 \pm 0.038$	18	1.20	0.757	0	VeLLO/FHC	H14,G17,H99
J041726	Taurus	137	04:17:26.4	+27:39:20	$< 0.001$	–	0.005	–	I	protoBD	P12,M15
J041913	Taurus	137	04:19:13.1	+27:47:26	$< 0.001$	–	0.0007	–	I	protoBD	P12,M15
L1521F-IRS	Taurus	137	04:28:38.9	+26:51:36	$0.037 \pm 0.001$	16	0.40	0.479	0	protoBD	D08,K16
G192-S-B30	$\lambda$ -Ori	380	05:29:54.4	+12:16:30	$0.080 \pm 0.005$	113	0.66	0.339	I	protoBD	L16
Cha-MMS1	Cha I	192	11:06:31.7	–77:23:33	$0.041 \pm 0.005$	20	2.36	0.246	0	FHC	Mau20,B20
ALMA-J153914	Lupus I	153	15:39:15.0	–33:29:08	$< 0.002$	–	0.017	–	I	protoBD	S21
J160115	Lupus IV	150	16:01:15.5	–41:52:35	$0.099 \pm 0.002$	129	0.40	0.131	I	protoBD	D08,K16
Source-X	Ophiuchus	137	16:26:27.4	–24:24:18	$< 0.082$	–	0.04	–	0	protoBD	K17,K18,J00
SM1-A	Ophiuchus	137	16:26:27.8	–24:23:59	$< 0.082$	21	4.6	0.214	0	protoBD	K17,K18,J00
L328-IRS	Ophiuchus	217	18:16:59.5	–18:02:30	$0.121 \pm 0.005$	67	0.90	0.126	0	protoBD	L09,L13,K16,L18
J182912	Aqu-Ser	436	18:29:12.1	–01:48:45	$0.025 \pm 0.003$	310	–	0.038	I	VeLLO	K16
J182958	Aqu-Ser	436	18:29:58.3	–01:57:40	$0.101 \pm 0.009$	112	–	0.070	I	VeLLO	K16
J190418	CrAus	150	19:04:18.6	–37:35:56	$0.014 \pm 0.001$	672	0.0002	0.016	II	VeLLO	K16
L1148-IRS	Cepheus	330	20:40:56.7	+67:23:05	$0.112 \pm 0.004$	122	0.58	0.164	I	protoBD	K05,D08,K16
J222933	Cepheus	339	22:29:33.3	+75:13:16	$0.036 \pm 0.003$	324	1.02	0.104	I	VeLLO	K16
L1014-IRS	Cygnus	258	21:24:07.5	+49:59:09	$0.100 \pm 0.037$	65	0.70	0.451	0	protoBD	K08,D08,K16,H06
J214457	IC 5146	600	21:44:57.0	+47:41:52	$0.085 \pm 0.031$	211	0.74	0.632	I	VeLLO	K16

<sup>a</sup> Envelope masses taken from Kim et al. (2016). For objects not included in the compilation of Kim et al. (2016) the envelope masses are those measured with single-dish as reported in the literature, except for the Morata et al. (2015) sources, for which  $M_{\text{env}}$  was estimated from the emission at 250  $\mu\text{m}$ , following Sec. 4.2 of Kim et al. (2016). For J222933, we calculated  $M_{\text{env}}$  from the flux at 1.2 mm given by Dunham et al. (2015), of  $\sim 0.35$  Jy, and assuming a dust temperature of 15 K and a dust opacity per mass of gas and dust of 0.01  $\text{cm}^2 \text{g}^{-1}$  (Ossenkopf and Henning, 1994).

<sup>b</sup> The type corresponds to the classification assigned in previous works.

<sup>c</sup> References: B20: Busch et al. (2020); C10: Chen et al. (2010); D08: Dunham et al. (2008); E06: Enoch et al. (2006); E10: Enoch et al. (2010); G17: Gerin et al. (2017); H99: Hirano et al. (1999) H06: Huard et al. (2006); H14: Hirano and Liu (2014); J00: Johnstone et al. (2000); K05: Kauffmann et al. (2005); K08: Kauffmann et al. (2008); K16: Kim et al. (2016); K17: Kirk et al. (2017); K18: Kawabe et al. (2018) L09: Lee et al. (2009); L13: Lee et al. (2013); L16: Liu et al. (2016); L18: Lee et al. (2018b); M15: Morata et al. (2015); Mau20: Maureira et al. (2020); P11: Pineda et al. (2011); P12: Palau et al. (2012); S21: Santamaría-Miranda et al. (2021).

Table 3: 68 proto-BD candidates that fulfill criteria of Sec. 5.1

Source <sup>a</sup>	Region	Dist. (pc)	R.A.	Dec.	$L_{\text{int}}$ ( $L_{\odot}$ )	$T_{\text{bol}}$ (K)	$M_{\text{env}}^{\text{b}}$ ( $M_{\odot}$ )	$L_{\text{bol}}$ ( $L_{\odot}$ )	Class	Type	Refs. <sup>c</sup>	ALMA Data <sup>c</sup>
Per-Bolo25	Perseus	293	03:28:32.5	+31:11:05	$0.061 \pm 0.009$	113	0.122	0.224	I	protoBD	D08,K16,C16	2017.1.01693, H19
Per-Bolo30	Perseus	293	03:28:39.1	+31:06:01	$0.022 \pm 0.004$	31	0.154	0.136	0	protoBD	D08,K16,C16	2017.1.01693, H19
IC348-SMM2E	Perseus	320	03:43:57.7	+32:03:10	$0.109 \pm 0.015$	23	0.051	0.287	0	protoBD	P14,K16	2017.1.01462, Y21
I04111+2800G	Taurus	137	04:14:12.3	+28:08:37	$0.061 \pm 0.014$	74	0.020	0.095	0/I	protoBD	K16	2018.1.00756, Tok20
J041740	Taurus	140	04:17:40.3	+28:24:15	$0.0014 \pm 0.0003$	397	0.0006	0.003	I	protoBD	P12,M15	–
J041757	Taurus	140	04:17:57.7	+27:41:06	$< 0.002$	158	0.0024	0.003	I	protoBD	B09,P12,PB14,M15	2013.1.00465, P22
J041828	Taurus	140	04:18:28.1	+27:49:11	$0.0015 \pm 0.0004$	125 <sup>d</sup>	0.0014	0.003 <sup>d</sup>	I	protoBD	P12,M15	–
J041836	Taurus	140	04:18:36.3	+27:14:43	$< 0.003$	281 <sup>d</sup>	0.0012	0.005 <sup>d</sup>	I	protoBD	P12,M15	2013.1.00465
J041840	Taurus	137	04:18:40.2	+28:29:25	$0.0041 \pm 0.0007$	86 <sup>d</sup>	0.002	0.002 <sup>d</sup>	I	VeLLO	K16	–
I04158+2805	Taurus	140	04:18:58.1	+28:12:24	$0.065 \pm 0.009$	337	0.030	0.210	I	protoBD	W04,A08	2016.1.00460, Rag21, V20
J041938	Taurus	140	04:19:38.8	+28:23:41	$0.006 \pm 0.002$	170	0.0012	0.005	I	protoBD	P12,M15	2013.1.00465
[GKH94]41	Taurus	140	04:19:46.6	+27:12:55	$0.017 \pm 0.002$	292	0.0044	0.081	I	protoBD	D16, this work	–
J042019	Taurus	140	04:20:19.2	+28:06:10	$< 0.002$	322 <sup>d</sup>	0.0009	0.003 <sup>d</sup>	I	protoBD	P12,M15	–
J042118	Taurus	140	04:21:18.4	+28:06:41	$< 0.002$	173	0.0007	0.002	I	protoBD	P12,M15	–
IRAM04191	Taurus	140	04:21:56.9	+15:29:46	$0.042 \pm 0.001$	59	0.050	0.065	0	protoBD	A99,D08,K16	2015.1.00186
J042513	Taurus	137	04:25:13.2	+26:31:45	$0.008 \pm 0.002$	54 <sup>d</sup>	0.001	0.006 <sup>d</sup>	0	VeLLO	K16	–
J043202	Taurus	137	04:32:02.0	+25:16:41	$0.006 \pm 0.001$	90 <sup>d</sup>	0.001	0.004 <sup>d</sup>	I	VeLLO	K16	–
J043411	Taurus	137	04:34:11.5	+24:03:41	$0.013 \pm 0.002$	96 <sup>d</sup>	0.100	0.008 <sup>d</sup>	I	VeLLO	K16	–
J043909	Taurus	137	04:39:09.0	+26:14:49	$0.011 \pm 0.002$	87 <sup>d</sup>	0.004	0.006 <sup>d</sup>	0/I	VeLLO	K16	–
J044022	Taurus	137	04:40:22.4	+25:58:32	$0.002 \pm 0.001$	102 <sup>d</sup>	0.001	0.005 <sup>d</sup>	I	VeLLO	K16	–
J044209	Taurus	137	04:42:09.4	+25:16:35	$0.007 \pm 0.001$	89 <sup>d</sup>	0.0001	0.005 <sup>d</sup>	I	VeLLO	K16	–
I04489+3042	Taurus	140	04:52:06.7	+30:47:17	$0.123 \pm 0.016$	304	0.003	0.418	I	protoBD	W04	2019.1.00847
J040129	Califor	450	04:01:29.0	+41:21:28	$0.032 \pm 0.003$	74 <sup>d</sup>	0.010	0.027 <sup>d</sup>	0/I	VeLLO	K16	–
J042815	Califor	450	04:28:15.1	+36:30:28	$0.048 \pm 0.010$	399	0.100	0.314	I	VeLLO	K16	–
J042818	Califor	450	04:28:18.6	+36:54:35	$0.014 \pm 0.004$	122 <sup>d</sup>	0.003	0.027 <sup>d</sup>	I	VeLLO	K16	–
J043014	Califor	450	04:30:14.9	+36:00:08	$0.079 \pm 0.010$	79	0.300	0.260	0/I	VeLLO	K16	–



Table 3: (cont.) 68 proto-BD candidates that fulfill criteria of Sec. 5.1

Source <sup>a</sup>	Region	Dist. (pc)	R.A.	Dec.	$L_{\text{int}}$ ( $L_{\odot}$ )	$T_{\text{bol}}$ (K)	$M_{\text{env}}^b$ ( $M_{\odot}$ )	$L_{\text{bol}}$ ( $L_{\odot}$ )	Class	Type	Refs. <sup>c</sup>	ALMA Data <sup>c</sup>
J053504	Orion	420	05:35:04.7	−05:37:12	$0.100 \pm 0.020$	30 <sup>d</sup>	0.300	1.78 <sup>d</sup>	0	VeLLO	K16	2015.1.00041, Tob20
J053534	Orion	420	05:35:34.2	−04:59:52	$0.049 \pm 0.011$	50 <sup>d</sup>	0.100	0.590 <sup>d</sup>	0	VeLLO	K16	2015.1.00041, Tob20
J053612	Orion	420	05:36:12.9	−06:23:30	$0.104 \pm 0.025$	241 <sup>d</sup>	0.003	0.212 <sup>d</sup>	I	VeLLO	K16	2019.1.01813, vT22
J053630	Orion	420	05:36:30.3	−04:32:16	$0.148 \pm 0.028$	306	0.200	1.03	I	VeLLO	K16	–
J054020	Orion	420	05:40:20.3	−07:51:14	$0.129 \pm 0.025$	69	0.020	0.327	0	VeLLO	K16	2015.1.00041, Tob20
J054128	Orion	420	05:41:28.9	−02:23:19	$0.167 \pm 0.032$	74	0.030	0.377	0	VeLLO	K16	2015.1.00041, Tob20
J054239	Orion	420	05:42:39.2	−10:01:47	$0.006 \pm 0.002$	128 <sup>d</sup>	0.002	0.037 <sup>d</sup>	I	VeLLO	K16	–
J055418	Orion	420	05:54:18.4	+01:49:03	$0.018 \pm 0.004$	127 <sup>d</sup>	0.050	0.049 <sup>d</sup>	I	VeLLO	K16	2015.1.00041, Tob20
J080533	BHR16	440	08:05:33.0	−39:09:24	$0.079 \pm 0.009$	264	0.001	0.104	I	VeLLO	K16	2022.1.01270
J105959	Cha I	192	10:59:59.7	−77:11:18	$0.019 \pm 0.002$	583	0.0013	0.016	Flat	VeLLO	K16	–
J121406	Cha III	193	12:14:06.5	−80:26:25	$0.043 \pm 0.005$	59 <sup>d</sup>	0.0042	0.028 <sup>d</sup>	0	VeLLO	K16	–
Cha-APEX-L	Cha II	198	12:52:55.8	−77:07:35	< 0.014	30 <sup>d</sup>	0.059	0.071 <sup>d</sup>	0	protoBD	dG16	–
J125701	Cha II	198	12:57:01.5	−76:48:34	$0.081 \pm 0.005$	119 <sup>d</sup>	0.0002	0.076 <sup>d</sup>	I	VeLLO	K16	–
J154216	DC3272	250	15:42:16.9	−52:48:02	$0.043 \pm 0.017$	42	0.040	0.180	0	protoBD	D08,K16	2016.1.00085
J153834	Lupus I	150	15:38:34.6	−34:48:19	$0.006 \pm 0.002$	184 <sup>d</sup>	0.0001	0.005 <sup>d</sup>	I	VeLLO	K16	2015.1.01510, V21
J154051	Lupus I	150	15:40:51.6	−34:21:04	$0.029 \pm 0.007$	52 <sup>d</sup>	0.0001	0.019 <sup>d</sup>	0/I	protoBD	D08,K16	2015.1.01510, V21
L1YSO 5	Lupus I	153	15:42:14.6	−34:10:25	$0.050 \pm 0.006$	161	0.0074	0.052	I	VeLLO	M17, this work	2013.1.00474
ALMA-J154229	Lupus I	153	15:42:29.8	−33:42:42	< 0.002	52 <sup>d</sup>	0.010	0.002 <sup>d</sup>	0/I	protoBD	S21	2018.1.00126, S21
J154339	Lupus I	150	15:43:39.9	−33:35:54	$0.005 \pm 0.001$	574	0.0003	0.005	I	VeLLO	K16	–
J154548	Lupus I	150	15:45:48.2	−34:05:10	$0.014 \pm 0.003$	262	0.0001	0.011	I	VeLLO	K16	2015.1.01510, V21
J160754	Lupus III	200	16:07:54.7	−39:15:44	$0.013 \pm 0.003$	432	0.0002	0.020	I	VeLLO	K16	2013.1.00220, A16

Table 3: (cont.) 68 proto-BD candidates that fulfill criteria of Sec. 5.1

Source <sup>a</sup>	Region	Dist. (pc)	R.A.	Dec.	$L_{\text{int}}$ ( $L_{\odot}$ )	$T_{\text{bol}}$ (K)	$M_{\text{env}}^{\text{b}}$ ( $M_{\odot}$ )	$L_{\text{bol}}$ ( $L_{\odot}$ )	Class	Type	Refs. <sup>c</sup>	ALMA data <sup>c</sup>
J162145	Ophiuchus	138	16:21:45.1	−23:42:31	$0.095 \pm 0.004$	138	0.0015	0.105	I	VeLLO	K16	2013.1.00157, C17
J162648	Ophiuchus	138	16:26:48.4	−24:28:38	$0.047 \pm 0.002$	587	0.013	0.212	Flat	VeLLO	A94,K16	2015.1.00741, E21
I16253−2429	Ophiuchus	138	16:28:21.6	−24:36:23	$0.129 \pm 0.005$	37	0.076	0.237	0	protoBD	D08,K16,H16	2015.1.00741, H19b, E21
J163136	Ophiuchus	144	16:31:36.8	−24:04:20	$0.057 \pm 0.006$	32	0.053	0.656	0/I	protoBD	RB21	2015.1.00741, E21
ISO-Oph200	Ophiuchus	144	16:31:43.8	−24:55:24	$0.076 \pm 0.007$	329	0.059	0.600	I	protoBD	RM21	2015.1.00741, RM21, E21
J163152	Ophiuchus	144	16:31:52.3	−24:55:36	$0.060 \pm 0.007$	122	0.100	0.352	0/I	protoBD	RB21,E09	2015.1.00741, E21
J171941	Pipe Nebula	130	17:19:41.2	−26:55:31	$0.018 \pm 0.015$	175	0.0037	0.033	I	VeLLO	F09, this work	–
J180439	Aqu-Rift	436	18:04:39.9	−04:01:22	$0.028 \pm 0.005$	69 <sup>d</sup>	0.0007	0.021 <sup>d</sup>	0/I	VeLLO	K16	–
J180449	Aqu-Rift	436	18:04:49.3	−04:36:39	$0.128 \pm 0.010$	474 <sup>d</sup>	0.007	0.493 <sup>d</sup>	I	VeLLO	K16	2019.1.00218, A22
J180941	Aqu-Rift	436	18:09:41.9	−03:31:26	$0.048 \pm 0.009$	121 <sup>d</sup>	0.0007	0.116 <sup>d</sup>	I	VeLLO	K16	–
MHO3257	Aqu-Serp	436	18:29:40.2	+00:15:13	$0.075 \pm 0.009$	372	0.027	0.212	I	Proto-BD	R18	–
J182854	Aqu-Serp	436	18:28:54.9	+00:18:32	$0.116 \pm 0.010$	49	0.046	0.431	I	Proto-BD	R18	2015.1.00310, F19
J182925	Aqu-Serp	436	18:29:25.1	−01:47:37	$0.107 \pm 0.008$	391	0.012	0.250	Flat	VeLLO	K16	–
J182933	Aqu-Serp	436	18:29:33.6	−01:45:10	$0.069 \pm 0.008$	648	0.150	0.282	Flat	VeLLO	K16	–
J182952	Aqu-Serp	436	18:29:52.9	−01:58:05	$0.122 \pm 0.007$	33	0.034	0.200	0	VeLLO	K16	2015.1.00223
J183047	Aqu-Serp	436	18:30:47.6	−02:43:56	$0.085 \pm 0.014$	82 <sup>d</sup>	0.0017	0.059 <sup>d</sup>	0/I	VeLLO	K16	–
J183245	Aqu-Serp	436	18:32:45.6	−02:46:57	$0.069 \pm 0.009$	186 <sup>d</sup>	0.022	0.098 <sup>d</sup>	I	VeLLO	K16	–
L673-7-IRS	L673	300	19:21:34.8	+11:21:23	$0.043 \pm 0.027$	26	0.100	0.097	0	VeLLO	K08,D10,K19	2016.1.00039
J210227	Cepheus	300	21:02:27.3	+67:54:18	$0.090 \pm 0.005$	100	0.010	0.161	I	VeLLO	K16	–
J210340	Cepheus	300	21:03:40.4	+68:26:31	$0.064 \pm 0.005$	181 <sup>d</sup>	0.010	0.129 <sup>d</sup>	I	VeLLO	K16	–
J215607	Cepheus	300	21:56:07.3	+76:42:29	$0.023 \pm 0.002$	458	0.010	0.053	Flat	VeLLO	K16	–

<sup>a</sup> Detailed information about specific candidates (some of them controversial) can be found in Pérez-García et al. (2025). Here we only list the sub-sample of SUCANES that fulfill the criteria given in Sec. 5.1.

<sup>b</sup> Envelope masses are taken from different papers of the literature as reported in Pérez-García et al. (2025). In the case of updated distances to the sources, these masses have also been updated (see Pérez-García et al., 2025). For those objects that do not have  $M_{\text{env}}$  estimated in the literature but do have a submillimetre flux, we calculated  $M_{\text{env}}$  in this work, assuming a dust temperature of 15 K, and a dust opacity per mass of dust and gas of  $0.19 \text{ cm}^2 \text{ g}^{-1}$  at  $250 \mu\text{m}$  as in Kim et al. (2016), or  $0.0175 \text{ cm}^2 \text{ g}^{-1}$  at  $850 \mu\text{m}$ . These objects are: J041740, J041828, J041836, J041938, J042019 (flux density at  $250 \mu\text{m}$  from Morata et al. 2015), [GKH94]41 and L1YSO5 (flux density at  $250 \mu\text{m}$  measured in this work within an aperture of about  $23 \times 23 \text{ arcsec}^2$ , using the *Herschel* images; the fluxes are  $\sim 0.5 \text{ Jy}$ , and  $\sim 0.7 \text{ Jy}$ , respectively), J171941 (flux density at  $250 \mu\text{m}$  is  $0.49 \pm 0.08 \text{ Jy}$ , obtained from the *Herschel*/SPIRE Point Source Catalog: <https://www.cosmos.esa.int/web/herschel/spire-point-source-catalogue>), and J162648, which has no  $250 \mu\text{m}$  data. For this last object,  $M_{\text{env}}$  was estimated from SCUBA-2 data at  $850 \mu\text{m}$ , assuming a dust temperature of 10 K according to Kim et al. (2016).

<sup>b</sup> References and ALMA project number used in Fig. 4 and Fig. A.9: A08: Andrews et al. (2008); A16: Ansdell et al. (2016); A94: Andre and Montmerle (1994); A99: André et al. (1999); A22: Anderson et al. (2022); B09: Barrado et al. (2009); C16: Carney et al. (2016); C17: Cox et al. (2017); D16: Dang-Duc et al. (2016); D08: Dunham et al. (2008); D10: Dunham et al. (2010); dG16: de Gregorio-Monsalvo et al. (2016); E09: Enoch et al. (2009); E21: Encalada et al. (2021); F09: Forbrich et al. (2009); F19: Francis et al. (2019); H16: Hsieh et al. (2016); H19: Hsieh et al. (2019b); H19b: Hsieh et al. (2019a); K08: Kauffmann et al. (2008); K16: Kim et al. (2016); K19: Kim et al. (2019); M15: Morata et al. (2015); M17: Mowat et al. (2017); P12: Palau et al. (2012); P14: Palau et al. (2014); P22: Palau et al. (2022); PB14: Phan-Bao et al. (2014); R18: Riaz et al. (2018); Rag21: Ragusa et al. (2021); RB21: Riaz and Bally (2021); RM21: Riaz and Machida (2021); S21: Santamaría-Miranda et al. (2021); Tob20: Tobin et al. (2020); Tok20: Tokuda et al. (2020); vT22: van Terwisga et al. (2022); V20: Villenave et al. (2020); V21: Vazzano et al. (2021); W04: White and Hillenbrand (2004); Y21: Yang et al. (2021).

<sup>d</sup> For these objects,  $T_{\text{bol}}$  and  $L_{\text{bol}}$  have been obtained using detections in two photometric tables only, instead of three as required in SUCANES (Pérez-García et al., 2025).

Table 4: 26 pre-BD candidates from SUCANES database

Source	Region	Dist. (pc)	RA (h m s)	DEC (d m s)	$L_{\text{int}}^{\text{a}}$ ( $L_{\odot}$ )	$M_{\text{env}}$ ( $M_{\odot}$ )	Type	Refs. <sup>b</sup>
J041757-NE	Taurus	140	04:18:00.30	+27:41:36.3	–	0.020	Pre-BD	P12
B30-LB10	Barnard30	400	05:31:09.29	+12:11:08.8	–	0.044	Pre-BD	H17
B30-LB31	Barnard30	400	05:31:15.32	+12:03:38.2	–	0.078	Pre-BD	H17
B30-LB08	Barnard30	400	05:31:22.97	+12:11:34.7	< 0.1	0.101	VeLLO/Pre-BD	H17
ChaII-APEX-N	Cha II	198	12:51:55.8	–77:08:43	–	0.023	Pre-BD	dG16
ChaII-APEX-A	Cha II	198	12:53:30.5	–77:11:07	–	0.020	Pre-BD	dG16
ChaII-APEX-J	Cha II	198	12:53:44.8	–77:04:43	–	0.029	Pre-BD	dG16
ChaII-APEX-G	Cha II	198	12:54:12.3	–77:06:47	–	0.098	Pre-BD	dG16
ChaII-APEX-B	Cha II	198	12:54:17.3	–77:10:23	–	0.020	Pre-BD	dG16
ChaII-APEX-F	Cha II	198	12:54:21.9	–77:06:59	–	0.026	Pre-BD	dG16
ChaII-APEX-I	Cha II	198	12:54:27.7	–77:04:27	–	0.023	Pre-BD	dG16
ChaII-APEX-H	Cha II	198	12:54:40.8	–77:04:35	–	0.034	Pre-BD	dG16
ChaII-APEX-C	Cha II	198	12:56:03.3	–77:11:43	–	0.027	Pre-BD	dG16
ALMA-J153702	Lupus I	94	15:37:02.65	–33:19:24.9	< 0.00075	0.00085	Pre-BD	S21
ALMA-J154228	Lupus I	153	15:42:28.67	–33:42:30.2	< 0.002	0.039	Pre-BD	S21
ALMA-J154456	Lupus I	153	15:44:56.52	–34:25:33.0	< 0.003	0.029	Pre-BD	S21
ALMA-J154458	Lupus I	153	15:44:58.06	–34:25:28.5	< 0.002	0.017	Pre-BD	S21
ALMA-J154506	Lupus I	153	15:45:06.52	–34:43:26.2	< 0.002	0.0485	Pre-BD	S21
ALMA-J154634	Lupus I	153	15:46:34.17	–34:33:01.9	< 0.002	0.171	Pre-BD	S21
ALMA-J160658	Lupus III	155	16:06:58.60	–39:04:07.9	< 0.002	0.00095	Pre-BD	S21
ALMA-J160804	Lupus III	155	16:08:04.17	–39:04:52.8	< 0.002	0.002	Pre-BD	S21
ALMA-J160920	Lupus III	155	16:09:20.09	–38:45:15.9	< 0.002	0.002	Pre-BD	S21
ALMA-J160920	Lupus III	155	16:09:20.17	–38:44:56.4	< 0.002	0.002	Pre-BD	S21
ALMA-J160932	Lupus III	155	16:09:32.17	–39:08:32.3	< 0.003	0.087	Pre-BD	S21
ALMA-J161030	Lupus III	155	16:10:30.27	–38:31:54.5	< 0.003	0.001	Pre-BD	S21
OphB-11	Ophiuchus	138	16:27:13.96	–24:28:29.3	< 0.006	0.009	Pre-BD	A12

<sup>a</sup> ‘–’ corresponds to no data or no measurement of the flux at 70  $\mu\text{m}$  provided in the reference.

<sup>b</sup> Refs: A12: [André et al. \(2012\)](#); dG16: [de Gregorio-Monsalvo et al. \(2016\)](#); H17: [Huélamo et al. \(2017\)](#); P12: [Palau et al. \(2012\)](#); S21: [Santamaría-Miranda et al. \(2021\)](#).

Table 5: Properties of nearby molecular clouds used in this work

Source	Project	Distance <sup>a</sup> (pc)	Area <sup>b</sup> (pc <sup>2</sup> )	$N_{\text{YSO}}^b$	Mass <sup>c</sup> ( $M_{\odot}$ )	Mass <sub>Av7</sub> <sup>c</sup> ( $M_{\odot}$ )	SFR <sup>d</sup> ( $10^{-6} M_{\odot} \text{ yr}^{-1}$ )	YSO surf dens <sup>e</sup> (pc <sup>-2</sup> )	$\log F_{\text{FUV}}^e$ (G <sub>0</sub> )	Age <sup>f</sup> (Myr)	Refs. <sup>f</sup>
Lupus I	c2d	150 ± 20	8.9 ± 2.4	13	787	75	3	1.47	0.7	1.6	E09
Ophiucus	c2d	125 ± 25	30 ± 12	290	14165	1296	73	9.80	3.3	9.3	E09
Perseus	c2d	293 ± 22	98 ± 29	385	18438	1880	96	3.91	3.0	10.4	E09
Ser-Aquila	GBS	436 ± 00	196 ± 15	1440	67500	14700	360	7.35	3.3	21.	P23
Taurus	c2d	137 ± 10	252 ± 50	267	14964	1766	67	1.06	1.3	10.1	R10
OrionA-B	–	420 ± 42	432 ± 86	3479	139542	20982	870	8.05	3.5	22.	M12
Lupus III	c2d	200 ± 20	15.4 ± 3.1	68	2157	163	17	4.41	0.7	2.5	E09
California	GBS	450 ± 23	646 ± 13	173	99930	3199	43	0.27	–	2.2	B14

<sup>a</sup> The distance to California is taken as  $450 \pm 23$  pc as this is the average distance found by [Zucker et al. \(2020\)](#). We note that [Álvarez-Gutiérrez et al. \(2021\)](#) report a distance of  $511 \pm 17$  pc, but this is mainly towards the L1482 cloud, which lies at the eastern side of the entire cloud, while [Zucker et al. \(2019\)](#) report a distance gradient from the east (further away) to the west (closer), and the proto-BD candidates studied lie outside L1482.

<sup>b</sup> Areas were adopted from [Heiderman et al. \(2010\)](#) or estimated from [Carpenter \(2000\)](#) and assuming 20% of uncertainty.  $N_{\text{YSO}}$  includes young stellar objects of all evolutionary stages, from Class 0 to Class III. For most of the clouds, this number corresponds to  $N_{\text{YSO,tot}}$  reported by [Heiderman et al. \(2010\)](#). For Taurus, OrionA-B, and California,  $N_{\text{YSO}}$  is taken from [Rebull et al. \(2010\)](#), [Megeath et al. \(2012\)](#) and [Kim et al. \(2016\)](#), respectively. For the particular case of Taurus,  $N_{\text{YSO}}$  is obtained by summing the number of previously identified young stellar objects by [Rebull et al. \(2010\)](#), see their Table 3), 215, plus the number of new candidate young stellar objects including only the confirmed, probable and possible, 52, reported in Table 8 of the same paper.

<sup>c</sup> Masses are taken from [Lada et al. \(2010\)](#), with the exception of Serpens-Aquila. In this case, the mass above the  $A_V=7$  mag threshold (which corresponds to  $N(\text{H}_2)=6.9 \times 10^{21} \text{ cm}^{-2}$  according to the relation of [Bohlin et al. 1978](#) and [Könyves et al. 2015](#)) was estimated using the *Herschel* column density map provided by [André et al. \(2010\)](#) and [Könyves et al. \(2015\)](#), and following [Könyves et al. \(2015\)](#) and [Shimoikura et al. \(2020\)](#), assuming a distance of 436 pc. Our mass is consistent with the mass from [Schneider et al. \(2022\)](#). The total mass for this cloud was taken from [Könyves et al. \(2015\)](#), of  $24000 M_{\odot}$ , corrected to our adopted distance.

<sup>d</sup> SFRs are calculated following equation (1) of [Lada et al. \(2010\)](#),  $\text{SFR} = 0.25 N_{\text{YSO}} \times 10^{-6} M_{\odot} \text{ yr}^{-1}$ , and using  $N_{\text{YSO}}$  given in this table.

<sup>e</sup> The YSO surface density is calculated using  $N_{\text{YSO}}$  and the area given in this table. The logarithm of the FUV flux is taken from [Gupta et al. \(2024\)](#) and [Xia et al. \(2022\)](#).

<sup>f</sup> The cloud age is estimated following [Vázquez-Semadeni et al. \(2018\)](#), who model the evolution of molecular clouds undergoing global and hierarchical collapse. The model inputs are the total mass of the cloud and the mass fraction in dense gas (taken as the mass above  $A_V=7$  mag as in [Lada et al. 2010](#), over the total mass). Since Serpens-Aquila is not included in the work of [Vázquez-Semadeni et al. \(2018\)](#), we estimated the age using our measured values for the mass and mass above a threshold.

<sup>g</sup> E09: [Evans et al. \(2009\)](#); R10: [Rebull et al. \(2010\)](#); M12: [Megeath et al. \(2012\)](#); B14: [Broekhoven-Fiene et al. \(2014\)](#); P23: [Pokhrel et al. \(2023\)](#).



Table 6: Numbers of protostars and proto-BD candidates in nearby molecular clouds

Source	$N_{\text{protostar}}^{\text{a}}$	$N_{\text{proto-Lrestrict}}^{\text{a}}$	$N_{\text{proBD}}^{\text{b}}$	$N_{\text{proBD-c004}}^{\text{b}}$	$N_{\text{expected}}^{\text{c}}$	Proto- star-to-BD <sup>c</sup>	$N_{\text{proBD-c0004}}^{\text{b}}$	Proto- star-to-BD0004 <sup>c</sup>	Refs. <sup>d</sup>
Lupus I	2	0	4	0	0	–	4	0.25	E09
Ophiucus	57	13	3	3	2.6	4.3	3	4.3	E09
Perseus	111	32	3	2	6.4	16	–	–	E09
Ser-Aquila	171	47	5	5	9.4	9.4	–	–	P23
Taurus	27	15	9	2	3.0	7.5	8	1.9	R10
OrionA-B	400	167	8	6	33	27.8	–	–	M12
Lupus III	2	1	1	0	0.2	–	1	1.0	E09
California	37	19	4	2	3.8	9.5	–	–	B14

<sup>a</sup>  $N_{\text{protostar}}$  corresponds to the number of YSOs for which  $T_{\text{bol}} \leq 650$  K, thus including both Class 0 and Class I. For the catalogs where  $T_{\text{bol}}$  is not given, we included those objects classified as Class I.  $N_{\text{proto-Lrestrict}}$  is obtained by restricting  $N_{\text{protostar}}$  to those objects whose  $L_{\text{int}}$  is in the range  $0.13\text{--}1 L_{\odot}$ . When no  $L_{\text{int}}$  is given, we estimated  $L_{\text{int}}$  from the flux at  $70 \mu\text{m}$  and following eq. 6.

<sup>b</sup>  $N_{\text{proBD}}$  corresponds to the number of proto-BD listed in Table 3 that belong to the catalog of Kim et al. (2016).  $N_{\text{proBD-c004}}$  corresponds to  $N_{\text{proBD}}$  restricted only to those objects with  $L_{\text{int}} \geq 0.04 L_{\odot}$ , which is the minimum  $L_{\text{int}}$  detectable at the distance of the most distant cloud. Thus,  $N_{\text{proBD-c004}}$  is complete down to  $0.04 L_{\odot}$ .  $N_{\text{proBD-c0004}}$  corresponds to  $N_{\text{proBD}}$  complete down to  $0.004 L_{\odot}$ , which is only possible to obtain for the most nearby clouds Ophiucus, Taurus, Lupus I and Lupus III.

<sup>c</sup>  $N_{\text{expected}}$  is the number of expected proto-BDs, given  $N_{\text{protostar}}$ , and is calculated as  $N_{\text{expected}} = N_{\text{proto-Lrestrict}}/5$ . In this expression, we have used  $N_{\text{proto-Lrestrict}}$  to make it comparable to the analysis of Mužić et al. (2019) and Almendros-Abad et al. (2023), who calculate the star-to-BD ratio by restricting the stars to the range of  $0.075\text{--}1 M_{\odot}$ . Similarly, the factor of 5 applied is taken from Mužić et al. (2019) and Almendros-Abad et al. (2023), which corresponds to the upper-end of star-to-BD ranges found in these works for more evolved objects. Proto(star-to-BD) is estimated as  $N_{\text{proto-Lrestrict}}/N_{\text{proBD-c004}}$ , and is comparable to the star-to-BD ratio measured by Mužić et al. (2019) and Almendros-Abad et al. (2023). Proto(star-to-BD0004) is estimated as  $N_{\text{proto-Lrestrict}}/N_{\text{proBD-c0004}}$ , and is presumably sensitive to the planetary-mass regime.

<sup>d</sup> References:  $N_{\text{protostar}}$  has been obtained from E09: Evans et al. (2009); R10: Rebull et al. (2010); M12: Megeath et al. (2012); B14: Broekhoven-Fiene et al. (2014); P23: Pokhrel et al. (2023).

## Appendix A. ALMA archive images of the proto-BD candidates of Table 3 that have not been detected with ALMA

In Sec. 5.2, a sample of 68 proto-BD candidates was presented, and the ALMA archive was searched to explore the properties of the millimetre continuum emission in each case. Out of the 68 candidates, 33 were found to have ALMA data available in the archive, and only four out of the 34 are non-detections. We present in this Appendix these four ALMA non-detections.

## Appendix B. Data used for Fig. 5

In Sec. 5.4 the well-known correlations that hold for proto-stellar objects were explored in the substellar regime. In this Appendix we provide the tables with the data used to make this comparison.

## Appendix C. Images of spatial distribution of VeLLOs/proto-BD candidates within their molecular clouds

In this Appendix, the *Herschel*/SPIRE images at  $250\ \mu\text{m}$  for different molecular clouds are presented, with black open circles indicating the positions of the SUCANES candidates (Pérez-García et al., 2025), white open circles indicating the positions of the Kim et al. (2016) candidates, and red filled circles indicating the positions of the proto-BD candidates selected in this work and listed in Table 3.

## References

- Adams, F.C., Lada, C.J., Shu, F.H., 1987. Spectral Evolution of Young Stellar Objects. *Astrophys. Journal* 312, 788. doi:[10.1086/164924](https://doi.org/10.1086/164924).
- Alcalá, J.M., Natta, A., Manara, C.F., Spezzi, L., Stelzer, B., Frasca, A., Biazio, K., Covino, E., Randich, S., Rigliaco, E., Testi, L., Comerón, F., Cupani, G., D'Elia, V., 2014. X-shooter spectroscopy of young stellar objects. IV. Accretion in low-mass stars and substellar objects in Lupus. *Astronomy & Astrophysics* 561, A2. doi:[10.1051/0004-6361/201322254](https://doi.org/10.1051/0004-6361/201322254), [arXiv:1310.2069](https://arxiv.org/abs/1310.2069).
- Almendros-Abad, V., Manara, C.F., Testi, L., Natta, A., Claes, R.A.B., Mužić, K., Sanchis, E., Alcalá, J.M., Bayo, A., Scholz, A., 2024. Evolution of the relation between the mass accretion rate and the stellar and disk mass from brown dwarfs to stars. *Astronomy & Astrophysics* 685, A118. doi:[10.1051/0004-6361/202348649](https://doi.org/10.1051/0004-6361/202348649), [arXiv:2402.10523](https://arxiv.org/abs/2402.10523).
- Almendros-Abad, V., Mužić, K., Bouy, H., Bayo, A., Scholz, A., Peña Ramírez, K., Moitinho, A., Kubiak, K., Schöedel, R., Barač, R., Brčić, P., Ascenso, J., Jayawardhana, R., 2023. Spectroscopic substellar initial mass function of NGC 2244. *Astronomy & Astrophysics* 677, A26. doi:[10.1051/0004-6361/202346237](https://doi.org/10.1051/0004-6361/202346237), [arXiv:2305.07158](https://arxiv.org/abs/2305.07158).
- Álvarez-Gutiérrez, R.H., Stutz, A.M., Law, C.Y., Reissl, S., Klessen, R.S., Leigh, N.W.C., Liu, H.L., Reeves, R.A., 2021. Filament Rotation in the California L1482 Cloud. *Astrophys. Journal* 908, 86. doi:[10.3847/1538-4357/abd47c](https://doi.org/10.3847/1538-4357/abd47c), [arXiv:2010.11211](https://arxiv.org/abs/2010.11211).
- Alves, J., Lombardi, M., Lada, C.J., 2007. The mass function of dense molecular cores and the origin of the IMF. *Astronomy & Astrophysics* 462, L17–L21. doi:[10.1051/0004-6361:20066389](https://doi.org/10.1051/0004-6361:20066389), [arXiv:astro-ph/0612126](https://arxiv.org/abs/astro-ph/0612126).
- Alves de Oliveira, C., Moraux, E., Bouvier, J., Bouy, H., 2012. Spectroscopy of new brown dwarf members of  $\rho$  Ophiuchi and an updated initial mass function. *Astronomy & Astrophysics* 539, A151. doi:[10.1051/0004-6361/201118230](https://doi.org/10.1051/0004-6361/201118230), [arXiv:1201.1912](https://arxiv.org/abs/1201.1912).

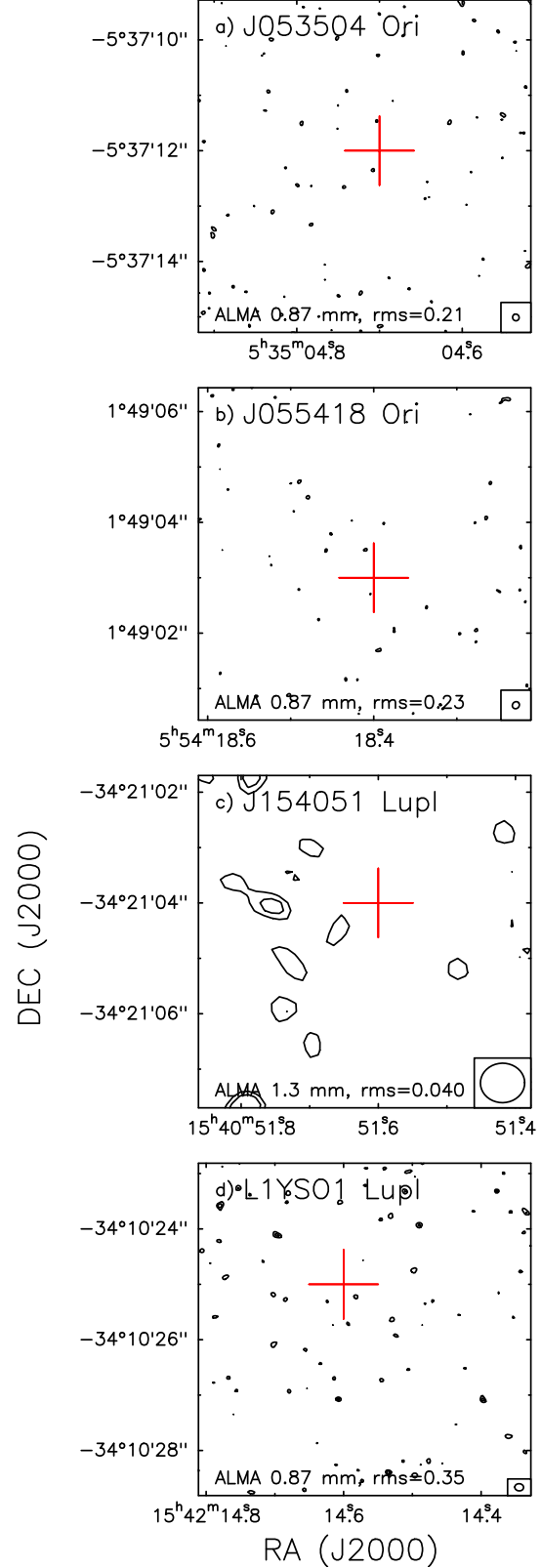


Figure A.9: Archive ALMA emission of the four proto-BD candidates of Table 3 that are non-detections. In all the panels, the field of view is  $6'' \times 6''$ , the beam is shown in the bottom-right corner, and the contours correspond to the 1.3 mm or 0.87 mm continuum emission (3, and 4  $\times$  the rms noise). The rms noise of each image is indicated at the bottom of each panel and is given in  $\text{mJy beam}^{-1}$ . In all the panels, the red plus sign corresponds to the coordinates of the proto-BD candidate as provided in the SUCANES database (Pérez-García et al., 2025). The ALMA project codes along with the corresponding

Table B.7: Data used for the  $\dot{M}_{\text{inf}}$  vs  $L_{\text{bol}}$  relation of Fig. 5a

Source	$L_{\text{bol}}^{\text{a}}$ ( $L_{\odot}$ )	error ( $L_{\odot}$ )	$\dot{M}_{\text{inf}}$ ( $M_{\odot} \text{ yr}^{-1}$ )	error ( $M_{\odot} \text{ yr}^{-1}$ )	Refs.
J033032	0.106	0.014	3.1E-6	5.9E-6	Kim et al. (2021, Tables 1 and 3)
L1521F-IRS	0.038	0.004	1.7E-6	2.9E-6	Kim et al. (2021, Tables 1 and 3)
J0430149	0.013	0.002	1.1E-6	2.5E-6	Kim et al. (2021, Tables 1 and 3)
L328-IRS	0.172	0.046	7.2E-7	2.9E-7	Kim et al. (2021, Tables 1 and 3)
J1830144	0.25	0.095	8.1E-6	2.7E-6	Kim et al. (2021, Tables 1 and 3)
J1830156	0.735	0.278	5.5E-5	2.3E-5	Kim et al. (2021, Tables 1 and 3)
J1830162	0.519	0.194	2.0E-5	7.2E-5	Kim et al. (2021, Tables 1 and 3)
J1832424	0.677	0.253	4.3E-6	1.7E-6	Kim et al. (2021, Tables 1 and 3)
L1148-IRS	0.127	0.014	2.3E-6	1.0E-6	Kim et al. (2021, Tables 1 and 3)
J2102212	0.381	0.037	1.7E-5	2.9E-5	Kim et al. (2021, Tables 1 and 3)
J2144570	0.066	0.015	1.2E-5	3.7E-5	Kim et al. (2021, Tables 1 and 3)
J2229594	0.33	0.032	1.1E-5	2.8E-5	Kim et al. (2021, Tables 1 and 3)
GF9-2	1.7	0.8	2.5E-5	1.0E-5	Furuya et al. (2009)
G34.26+0.2	46000.0	20000.0	0.009	0.004	Wyrowski et al. (2016, Tables 1 and 5)
G327.29−0.6	82000.0	41000.0	0.004	0.002	Wyrowski et al. (2016, Tables 1 and 5)
G351.58−0.4	240000.0	120000.0	0.016	0.008	Wyrowski et al. (2016, Tables 1 and 5)
G23.21−0.3	13000.0	6000.0	0.008	0.004	Wyrowski et al. (2016, Tables 1 and 5)
G35.20−0.7	25000.0	12000.0	3.0E-4	1.5E-4	Wyrowski et al. (2016, Tables 1 and 5)
G34.41+0.2	4800.0	2400.0	7.0E-4	3.0E-4	Wyrowski et al. (2016, Tables 1 and 5)
L1521F	0.037	0.001	2.7E-5	1.3E-5	Keown et al. (2016)
I09018	52000.0	20000.0	0.0475	0.02	Yue et al. (2021, Table 1)
I13134	40000.0	20000.0	0.0135	0.005	Yue et al. (2021, Table 1)
I14382	160000.0	80000.0	0.0149	0.007	Yue et al. (2021, Table 1)
I14498	25000.0	12000.0	0.0156	0.007	Yue et al. (2021, Table 1)
I15520	130000.0	60000.0	0.0314	0.015	Yue et al. (2021, Table 1)
I15596	320000.0	150000.0	0.0448	0.022	Yue et al. (2021, Table 1)
I16060	630000.0	310000.0	0.0767	0.035	Yue et al. (2021, Table 1)
I16071	63000.0	31000.0	0.0583	0.029	Yue et al. (2021, Table 1)
I16076	200000.0	100000.0	0.0537	0.027	Yue et al. (2021, Table 1)
I16272	20000.0	10000.0	0.0149	0.007	Yue et al. (2021, Table 1)
I16348	250000.0	120000.0	0.0581	0.029	Yue et al. (2021, Table 1)
I16351	79000.0	40000.0	0.0212	0.01	Yue et al. (2021, Table 1)
I17160	1000000.0	500000.0	0.0379	0.019	Yue et al. (2021, Table 1)
I17204	16000.0	8000.0	0.0049	0.002	Yue et al. (2021, Table 1)
I17220	500000.0	200000.0	0.1194	0.05	Yue et al. (2021, Table 1)
I18056	500000.0	200000.0	0.1022	0.05	Yue et al. (2021, Table 1)
I18182	20000.0	10000.0	0.0108	0.005	Yue et al. (2021, Table 1)
I18507	63000.0	30000.0	0.0533	0.02	Yue et al. (2021, Table 1)
AGAL008.206+00.191	127.6	60.0	0.0021	0.001	Pillai et al. (2023, Table 3), Urquhart et al. (2018, Table 5)
AGAL008.706−00.414	1452.0	700.0	0.0147	0.007	Pillai et al. (2023, Table 3), Urquhart et al. (2018, Table 5)
AGAL022.376+00.447	263.0	130.0	0.0068	0.0034	Pillai et al. (2023, Table 3), Urquhart et al. (2018, Table 5)
AGAL024.373−00.159	160.0	80.0	0.0101	0.005	Pillai et al. (2023, Table 3), Urquhart et al. (2018, Table 5)
BG009.212	3981.0	2000.0	5.8E-4	2.0E-4	Xu et al. (2023, Tables 1 and 5)
BG012.889	15849.0	7000.0	0.00447	0.002	Xu et al. (2023, Tables 1 and 5)
BG014.606	6310.0	3100.0	1.5E-4	7.0E-5	Xu et al. (2023, Tables 1 and 5)
BG025.400	316228.0	150000.0	0.00141	7.0E-4	Xu et al. (2023, Tables 1 and 5)
BG028.565	200.0	100.0	0.0321	0.015	Xu et al. (2023, Tables 1 and 5)
BG030.719	50119.0	25000.0	0.00791	0.004	Xu et al. (2023, Tables 1 and 5)
BG033.740	3162.0	1500.0	0.00458	0.0022	Xu et al. (2023, Tables 1 and 5)
BG081.721	3981.0	2000.0	0.0215	0.011	Xu et al. (2023, Tables 1 and 5)
BG133.748	6310.0	3100.0	0.00426	0.0021	Xu et al. (2023, Tables 1 and 5)
BG133.949	1000.0	500.0	0.00548	0.0022	Xu et al. (2023, Tables 1 and 5)
J032832/Per-Bolo25 <sup>b</sup>	0.061	0.008	6.5E-6	1.4E-6	Kim et al. (2021, Table 3), this work (Table 3)
J041840 <sup>b</sup>	0.004	0.001	3.5E-7	2.5E-7	Kim et al. (2021, Table 3), this work (Table 3)
J210227 <sup>b</sup>	0.090	0.017	1.0E-5	1.5E-5	Kim et al. (2021, Table 3), this work (Table 3)
IRAM 04191 <sup>b</sup>	0.042	0.001	3.0E-6	1.5E-6	Belloche et al. (2002), this work (Table 3)

<sup>a</sup>  $L_{\text{bol}}$  for the proto-BD candidates is taken as  $L_{\text{int}}$  because the least luminous objects are most affected by the ISRF and the accretion/ejection processes must be driven by the mass of the central object, more closely related to  $L_{\text{int}}$  than to  $L_{\text{bol}}$ .

<sup>b</sup> Proto-BD candidate included in Table 3. This object is not included to perform the fit shown in Fig. 5a.

Table B.8: Data used for the  $L_{\text{cm}}$  vs  $L_{\text{bol}}$  relation of Fig. 5b

Source	D (kpc)	$L_{\text{bol}}^{\text{a}}$ ( $L_{\odot}$ )	$F_{3.6\text{cm}}^{\text{b}}$ (mJy)	Refs.
L1014IRS	0.258	0.1	0.11	<a href="#">Anglada et al. (2018, Table 2)</a> , <a href="#">Pérez-García et al. (2025)</a>
L1148-IRS	0.33	0.112	0.08	<a href="#">Anglada et al. (2018, Table 2)</a> , <a href="#">Pérez-García et al. (2025)</a>
L1521F-IRS	0.137	0.037	0.07	<a href="#">Anglada et al. (2018, Table 2)</a> , <a href="#">Pérez-García et al. (2025)</a>
HH30	0.14	0.42	0.042	<a href="#">Anglada et al. (2018, Table 2)</a>
L1262	0.2	1.0	0.33	<a href="#">Anglada et al. (2018, Table 2)</a>
VLA1623	0.16	1.5	0.6	<a href="#">Anglada et al. (2018, Table 2)</a>
L723	0.3	2.4	0.4	<a href="#">Anglada et al. (2018, Table 2)</a>
L1489	0.14	4.4	0.5	<a href="#">Anglada et al. (2018, Table 2)</a>
B335	0.25	4.0	0.2	<a href="#">Anglada et al. (2018, Table 2)</a>
NGC2264G	0.8	5.0	0.3	<a href="#">Anglada et al. (2018, Table 2)</a>
AS353A	0.3	8.4	0.1	<a href="#">Anglada et al. (2018, Table 2)</a>
L1448C	0.35	9.0	0.1	<a href="#">Anglada et al. (2018, Table 2)</a>
L1448N(A)	0.35	10.0	0.9	<a href="#">Anglada et al. (2018, Table 2)</a>
RNO43	0.4	12.0	0.5	<a href="#">Anglada et al. (2018, Table 2)</a>
L483	0.2	14.0	0.31	<a href="#">Anglada et al. (2018, Table 2)</a>
L1251B	0.2	14.0	1.2	<a href="#">Anglada et al. (2018, Table 2)</a>
TTAU	0.14	17.0	5.8	<a href="#">Anglada et al. (2018, Table 2)</a>
HH111	0.46	24.0	0.9	<a href="#">Anglada et al. (2018, Table 2)</a>
IRAS16293	0.16	27.0	2.9	<a href="#">Anglada et al. (2018, Table 2)</a>
L1251A	0.3	27.0	0.47	<a href="#">Anglada et al. (2018, Table 2)</a>
HAR04-255FIR	0.48	28.0	0.2	<a href="#">Anglada et al. (2018, Table 2)</a>
L1551-IRS5	0.14	20.0	0.8	<a href="#">Anglada et al. (2018, Table 2)</a>
HLTAU	0.16	44.0	0.3	<a href="#">Anglada et al. (2018, Table 2)</a>
L1228	0.2	7.0	0.15	<a href="#">Anglada et al. (2018, Table 2)</a>
PVCEP	0.5	80.0	0.2	<a href="#">Anglada et al. (2018, Table 2)</a>
L1641N	0.42	170.0	0.6	<a href="#">Anglada et al. (2018, Table 2)</a>
FIRSSE101	0.45	123.0	1.1	<a href="#">Anglada et al. (2018, Table 2)</a>
HH7-11VLA3	0.35	150.0	0.8	<a href="#">Anglada et al. (2018, Table 2)</a>
RE50	0.46	295.0	0.84	<a href="#">Anglada et al. (2018, Table 2)</a>
SERPENS	0.415	98.0	2.0	<a href="#">Anglada et al. (2018, Table 2)</a>
IRAS22198	1.3	1240.0	0.57	<a href="#">Anglada et al. (2018, Table 2)</a>
NGC2071-IRS3	0.39	520.0	2.9	<a href="#">Anglada et al. (2018, Table 2)</a>
HH34	0.42	15.0	0.16	<a href="#">Anglada et al. (2018, Table 2)</a>
AF5142CM1	2.14	10000.0	1.3	<a href="#">Anglada et al. (2018, Table 2)</a>
AF5142CM2	2.14	1000.0	0.35	<a href="#">Anglada et al. (2018, Table 2)</a>
CepAHW2	0.725	10000.0	6.9	<a href="#">Anglada et al. (2018, Table 2)</a>
IRAS20126	1.7	13000.0	0.2	<a href="#">Anglada et al. (2018, Table 2)</a>
HH80-81	1.7	20000.0	5.0	<a href="#">Anglada et al. (2018, Table 2)</a>
V645Cyg	3.5	40000.0	0.6	<a href="#">Anglada et al. (2018, Table 2)</a>
IRAS16547	2.9	60000.0	8.7	<a href="#">Anglada et al. (2018, Table 2)</a>
IRAS18566B	6.7	80000.0	0.077	<a href="#">Anglada et al. (2018, Table 2)</a>
IRAS04579	2.5	3910.0	0.15	<a href="#">Anglada et al. (2018, Table 2)</a>
GGD14-VLA7	0.9	1000.0	0.18	<a href="#">Anglada et al. (2018, Table 2)</a>
IRAS23139	4.8	20000.0	0.53	<a href="#">Anglada et al. (2018, Table 2)</a>
N7538-IRS9	2.8	40000.0	3.8	<a href="#">Anglada et al. (2018, Table 2)</a>
N7538-IRS9A1	2.8	40000.0	1.4	<a href="#">Anglada et al. (2018, Table 2)</a>
IRAS16562	1.6	70000.0	21.1	<a href="#">Anglada et al. (2018, Table 2)</a>
I18264-1152F	3.5	10000.0	0.28	<a href="#">Anglada et al. (2018, Table 2)</a>
G31.41	7.9	200000.0	0.32	<a href="#">Anglada et al. (2018, Table 2)</a>
AF2591-VLA3	3.3	230000.0	1.52	<a href="#">Anglada et al. (2018, Table 2)</a>
I18182-1433b	4.5	20000.0	0.6	<a href="#">Anglada et al. (2018, Table 2)</a>
I18089-1732(1)a	3.6	32000.0	1.1	<a href="#">Anglada et al. (2018, Table 2)</a>



Table B.8: (cont.) Data used for the  $L_{\text{cm}}$  vs  $L_{\text{bol}}$  relation of Fig. 5b

Source	D (kpc)	$L_{\text{bol}}^{\text{a}}$ ( $L_{\odot}$ )	$F_{3.6\text{cm}}^{\text{b}}$ (mJy)	Refs.
G28S-JVLA1	4.8	100.0	0.02	Anglada et al. (2018, Table 2)
G28N-JVLA2N	4.8	1000.0	0.06	Anglada et al. (2018, Table 2)
G28N-JVLA2S	4.8	1000.0	0.03	Anglada et al. (2018, Table 2)
L1287	0.85	1000.0	0.5	Anglada et al. (2018, Table 2)
DGTauB	0.15	0.9	0.31	Anglada et al. (2018, Table 2)
ZCMa	1.15	3000.0	1.74	Anglada et al. (2018, Table 2)
W3IRS5(d)	1.83	200000.0	1.5	Anglada et al. (2018, Table 2)
YLW16A	0.16	13.0	0.78	Anglada et al. (2018, Table 2)
YLW15-VLA1	0.12	1.0	1.5	Anglada et al. (2018, Table 2)
L778	0.25	0.93	0.69	Anglada et al. (2018, Table 2)
W75N(B)VLA1	1.3	19000.0	4.0	Anglada et al. (2018, Table 2)
NGC1333-VLA2	0.235	1.5	2.5	Anglada et al. (2018, Table 2)
NGC1333-IRAS4A1	0.235	8.0	0.32	Anglada et al. (2018, Table 2)
NGC1333-IRAS4B	0.235	1.1	0.33	Anglada et al. (2018, Table 2)
L1551NE-A	0.14	4.0	0.39	Anglada et al. (2018, Table 2)
Haro6-10-VLA1	0.14	0.5	1.1	Anglada et al. (2018, Table 2)
L1527-VLA1	0.14	1.9	1.1	Anglada et al. (2018, Table 2)
OMC2/3-VLA4	0.414	40.0	0.83	Anglada et al. (2018, Table 2)
HH1-2-VLA1	0.414	23.0	1.2	Anglada et al. (2018, Table 2)
HH1-2-VLA3	0.414	84.0	0.4	Anglada et al. (2018, Table 2)
OMC2-VLA11	0.414	360.0	2.16	Anglada et al. (2018, Table 2)
HH46/47	0.45	12.0	1.8	Anglada et al. (2018, Table 2)
IRAS20050	0.7	260.0	1.4	Anglada et al. (2018, Table 2)
J041757 <sup>c</sup>	0.137	< 0.002	0.14	Anglada et al. (2018, Table 2), Pérez-García et al. (2025)
J041836 <sup>c</sup>	0.137	< 0.003	0.13	Anglada et al. (2018, Table 2), Pérez-García et al. (2025)
J041938 <sup>c</sup>	0.137	0.006	0.10	Anglada et al. (2018, Table 2), Pérez-García et al. (2025)
IRAM04191 <sup>c</sup>	0.160	0.042	0.14	Anglada et al. (2018, Table 2), Pérez-García et al. (2025)
IC348-SMM2E <sup>c</sup>	0.320	0.109	0.027	Anglada et al. (2018, Table 2), Pérez-García et al. (2025)

<sup>a</sup>  $L_{\text{bol}}$  for the proto-BD candidates is taken as  $L_{\text{int}}$  because the least luminous objects are most affected by the ISRF and the accretion/ejection processes must be driven by the mass of the central object, more closely related to  $L_{\text{int}}$  than to  $L_{\text{bol}}$  (AMI Consortium et al., 2011).

<sup>b</sup> Flux density at 3.6 cm.

<sup>c</sup> Proto-BD candidate included in Table 3. This object is not included to perform the fit shown in Fig. 5b.

Table B.9: Interferometric data used for the  $F_{\text{out}}$  vs  $L_{\text{bol}}$  and  $F_{\text{out}}$  vs  $M_{\text{env}}$  relations of Fig. 5c,d

Source	$L_{\text{bol}}^{\text{a}}$ ( $L_{\odot}$ )	$F_{\text{out}}^{\text{b}}$ ( $M_{\odot} \text{ km s}^{-1} \text{ yr}^{-1}$ )	$M_{\text{env}}^{\text{b}}$ ( $M_{\odot}$ )	Refs.
IRAS 20343+4129 IRS1	2000.0	1.3E-4	0.8	Beltrán et al. (2008, Table 5)
L1206	1200.0	7.7E-5	14.2	Beltrán et al. (2008, Table 5)
Cepheus E	70.0	2.3E-4	13.6	Beltrán et al. (2008, Table 5)
IRAS 21391+5802	370.0	0.0014	5.1	Beltrán et al. (2008, Table 5)
IRAS 20050+2720 A	280.0	5.3E-4	6.5	Beltrán et al. (2008, Table 5)
OMC-2/3 MM7	76.0	0.0011	0.54	Beltrán et al. (2008, Table 5)
IRAS 20293+3952 A	1050.0	0.022	4.0	Beltrán et al. (2008, Table 5)
IRAS 22171+5549	1800.0	0.012	25.0	Beltrán et al. (2008, Table 5)
IRAS 21307+5049	4000.0	0.0029	53.0	Beltrán et al. (2008, Table 5)
S235 NE-SW	1000.0	0.014	16.0	Beltrán et al. (2008, Table 5)
IRAS 23385+6053	1500.0	0.009	61.0	Beltrán et al. (2008, Table 5)
HH 288	500.0	0.014	18.0	Beltrán et al. (2008, Table 5)
IRAS 00117 MM1	500.0	7.5E-4	1.5	Palau et al. (2010, Tables 3 and 6)
HH 211	3.6	2.8E-5	0.04	Palau et al. (2006, Table 1)
CB17-IRS	0.5	1.1E-7	0.023	Chen et al. (2012b, Tables 3 and 5)
CygX-N3 MM1	106.0	0.00131	12.5	Duarte-Cabral et al. (2013, Table 2)
CygX-N3 MM2	121.0	7.2E-4	13.8	Duarte-Cabral et al. (2013, Table 2)
CygX-N48 MM1	102.0	0.00135	17.0	Duarte-Cabral et al. (2013, Table 2)
CygX-N48 MM2	85.0	4.5E-4	8.1	Duarte-Cabral et al. (2013, Table 2)
CygX-N53 MM1	199.0	0.00412	34.2	Duarte-Cabral et al. (2013, Table 2)
CygX-N63 MM1	339.0	0.00291	44.3	Duarte-Cabral et al. (2013, Table 2)
Per-Bolo58	0.012	5.6E-8	0.11	Dunham et al. (2011, Tables 2, 3 and 4)
L1451mm	0.045	8.3E-9	0.024	Pineda et al. (2011, Tables 11 and 12)
B1b-S	0.058	2.4E-6	0.36	Hirano and Liu (2014, Tables 6 and 7), this work (Table 2)
L1521F-IRS	0.037	3.3E-7	0.065	Takahashi et al. (2013, Sec. 3.1, Table 2), this work (Table 2)
L1148-IRS	0.112	1.0E-7	0.02 <sup>c</sup>	Kauffmann et al. (2011, Sec. 3.3, Table 1), this work (Table 2)
L1014-IRS	0.100	5.3E-8	0.010	Bourke et al. (2005b, Secs. 3, 4.1), this work (Table 2)
082012	6.3	7.0E-4	9.4	Tobin et al. (2016c, Tables 4 and 5), Tobin et al. (2015, Table 2)
093005	1.7	1.1E-5	5.4	Tobin et al. (2016c, Tables 4 and 5)
090003	2.71	2.0E-6	7.0	Tobin et al. (2016c, Tables 4 and 5)
135003	12.0	6.2E-6	3.0	Tobin et al. (2016c, Tables 4 and 5)
119019	1.56	2.4E-6	0.6	Tobin et al. (2016c, Tables 4 and 5)
302002	0.85	3.0E-7	2.9	Tobin et al. (2016c, Tables 4 and 5)
019003A	3.16	4.8E-6	2.4	Tobin et al. (2016c, Tables 4 and 5)
HOPS68	5.7	8.8E-5	2.5	Tobin et al. (2016c, Tables 4 and 5), Tobin et al. (2015, Table 2)
HOPS223	28.0	5.8E-6	3.0	Tobin et al. (2016c, Tables 4 and 5), Tobin et al. (2015, Table 2)
L328-IRS	0.121	3.3E-6 <sup>d</sup>	0.01	Lee et al. (2018b), this work (Table 2)
GF9-2 <sup>e</sup>	1.7	7.4E-6	0.067	Busch et al. (2020, Table 5), Furuya et al. (2019, Table 2)
Cha-MMS1	0.041	4.1E-7	0.003	Busch et al. (2020, Sec. 3.1 and Table 5), this work (Table 2)
SerpM-S68Nb	1.8	7.0E-6	0.30 <sup>f</sup>	Podio et al. (2021, Table 5), Maury et al. (2019, Table 4)
IRAS4B1	2.3	3.5E-5	1.76 <sup>f</sup>	Podio et al. (2021, Table 5), Maury et al. (2019, Table 4)
L1157	4.0	4.5E-5	0.60 <sup>f</sup>	Podio et al. (2021, Table 5), Maury et al. (2019, Table 4)
L1448C	11.0	2.35E-4	0.48 <sup>f</sup>	Podio et al. (2021, Table 5), Maury et al. (2019, Table 4)
IRAS15398-3359	1.34	7.4E-6	0.0023	Vazzano et al. (2021, Tables 6 and 8), this work (footnote a of Table 1)
IRAS16059-3857	0.17	2.1E-6	0.02	Vazzano et al. (2021, Tables 6, 8 and 11)
J160115-4152	0.099	3.1E-7	0.016	Vazzano et al. (2021, Tables 6 and 8), this work (Table 2)
G191.9S	0.4	2.992E-5	0.51	Dutta et al. (2024, Tables 2 and 3)
G203.2W2	0.5	7.07E-6	0.32	Dutta et al. (2024, Tables 2 and 3)
G205.4M1B	4.8	1.0E-6	5.8	Dutta et al. (2024, Tables 2 and 3)
G205.4S1A	22.0	0.00165	0.88	Dutta et al. (2024, Tables 2 and 3)
G209.5S2	3.4	1.12E-6	0.61	Dutta et al. (2024, Tables 2 and 3)
G205.4S3	6.4	3.25E-5	0.7	Dutta et al. (2024, Tables 2 and 3)
G206.1	3.0	1.62E-6	2.44	Dutta et al. (2024, Tables 2 and 3)

Table B.9: (cont.) Interferometric data used for the  $F_{\text{out}}$  vs  $L_{\text{bol}}$  and  $F_{\text{out}}$  vs  $M_{\text{env}}$  relations of Fig. 5c,d

Source	$L_{\text{bol}}^{\text{a}}$ ( $L_{\odot}$ )	$F_{\text{out}}^{\text{b}}$ ( $M_{\odot} \text{ km s}^{-1} \text{ yr}^{-1}$ )	$M_{\text{env}}^{\text{b}}$ ( $M_{\odot}$ )	Refs.
G206.9W2	6.3	3.83E-4	4.56	Dutta et al. (2024, Tables 2 and 3)
G208.6N1	37.0	2.54E-6	8.26	Dutta et al. (2024, Tables 2 and 3)
G208.8E	2.2	3.24E-5	0.28	Dutta et al. (2024, Tables 2 and 3)
G208.8Walma	0.8	3.2E-8	0.38	Dutta et al. (2024, Tables 2 and 3)
G210.3S	0.6	1.6E-7	0.54	Dutta et al. (2024, Tables 2 and 3)
G210.4W	60.0	1.64E-4	1.4	Dutta et al. (2024, Tables 2 and 3)
G200.3N	1.5	1.85E-6	0.51	Dutta et al. (2024, Tables 2 and 3)
G192.1	9.5	1.04E-5	1.21	Dutta et al. (2024, Tables 2 and 3)
G209.5N1	9.0	2.05E-6	1.98	Dutta et al. (2024, Tables 2 and 3)
G208.6S	49.0	4.1E-7	1.55	Dutta et al. (2024, Tables 2 and 3)
G211.0N	4.5	1.08E-7	0.81	Dutta et al. (2024, Tables 2 and 3)
G212.8N	3.0	2.28E-7	0.52	Dutta et al. (2024, Tables 2 and 3)
I16253–2429 <sup>g</sup>	0.129	6.5E-7	0.018	Hsieh et al. (2016, Sec. 4.2.1 and Table 3), this work (Table 3)
ISO-Oph200 <sup>g</sup>	0.076	7E-7	0.006	Riaz and Machida (2021, Sec. 5.2 and Table 1), this work (Table 3)
IC348-SMM2E <sup>g</sup>	0.109	2.7E-7	0.051	Palau et al. (2014, Table 4), this work (Table 3)
J041757B <sup>g</sup>	< 0.002	3.7E-8	0.00015	Palau et al. (2022), this work (Table 3)
SMA1627-2441 <sup>h</sup>	< 0.004	7.9E-10	0.0024	Phan-Bao (2022)
J041757NE-MM1 <sup>h</sup>	< 0.006	1.2E-9	0.012	Palau et al. (2022)

<sup>a</sup>  $L_{\text{bol}}$  for the proto-BD candidates is taken as  $L_{\text{int}}$  because the least luminous objects are most affected by the ISRF and the accretion/ejection processes must be driven by the mass of the central object, more closely related to  $L_{\text{int}}$  than to  $L_{\text{bol}}$  (AMI Consortium et al., 2011).

<sup>b</sup>  $F_{\text{out}}$  corresponds to the outflow momentum rate or outflow force (uncorrected for inclination/opacity in most of the cases), while  $M_{\text{env}}$  corresponds to the envelope mass of the driving source, all of them observed with interferometers.  $M_{\text{env}}$  is obtained from the same work that estimate  $F_{\text{out}}$ . Thus the interferometric configuration was the same in both measurements, being both equally affected by missing flux.

<sup>c</sup> Upper limit for  $M_{\text{env}}$  from Kauffmann et al. (2011, Sec. 3.3).

<sup>d</sup>  $F_{\text{out}}$  for L328-IRS has been estimated from equation (2) of Lee et al. (2018b),  $F_{\text{out}} = 0.025 \dot{M}_{\text{acc}} V_{\text{W}}$ , and adopting a mass accretion rate of  $8.9 \times 10^{-7} M_{\odot} \text{ yr}^{-1}$  and  $V_{\text{W}} \sim 150 \text{ km s}^{-1}$  (Lee et al., 2018b).

<sup>e</sup> For GF9-2, Busch et al. (2020) adopted the most recent distance of 474 pc (instead of 200 pc as previously used), and  $F_{\text{out}}$  is given for this new distance. For  $M_{\text{env}}$ , we have taken the value from Table 2 of Furuya et al. (2019) for the frequency of the SMA data used to estimate the outflow parameters (345 GHz), and re-scaled it to the new distance.  $L_{\text{bol}}$  is taken from Furuya et al. (2006) and has also been re-scaled to the new distance.

<sup>f</sup>  $M_{\text{env}}$  has been estimated using the flux density reported by Maury et al. (2019, Table 4), assuming 20 K and the dust opacity from Ossenkopf and Henning (1994, thin ice mantles at  $10^6 \text{ cm}^{-3}$ ) and the distance given in Table 1 of Podio et al. (2021). For SerpM-S68Nb, the peak intensity at 94 GHz reported in Table 3 of Maury et al. (2019) was used because this source is not included in their Table 4.

<sup>g</sup> Proto-BD candidate included in Table 3. This object is not included to perform the fits shown in Fig. 5c and d. For the case of IC348-SMM2E, all the values have been updated to the new distance of 320 pc, and an inclination with respect to the plane-of-sky of  $40^\circ$  has been assumed.

<sup>h</sup> Tentative proto-BD candidate for which signs of outflow have been reported but there are no infrared counterparts. This object is not included to perform the fits shown in Fig. 5c and d.

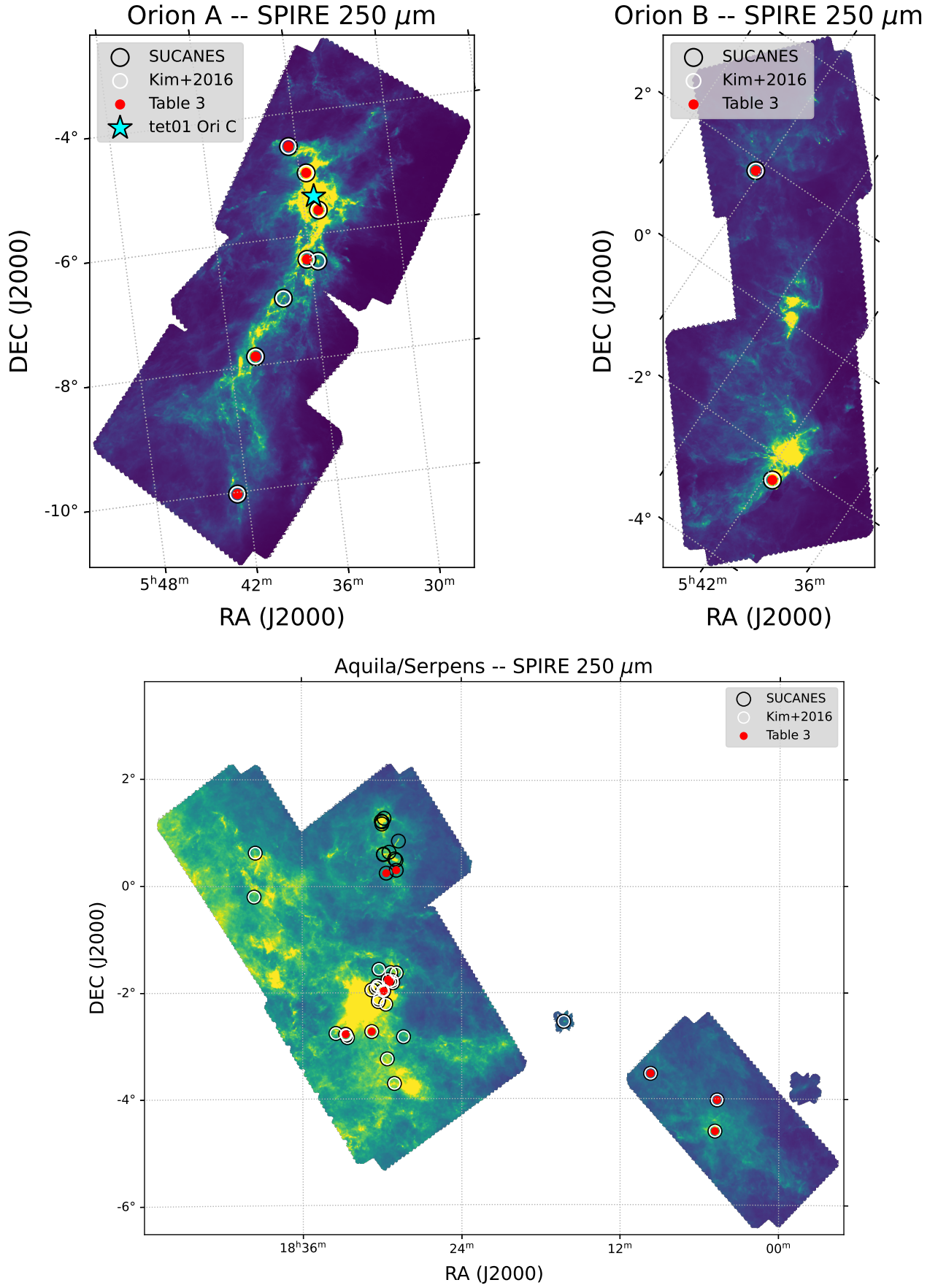


Figure C.1: RGB Herschel/SPIRE image of Orion (top) and Aquila/Serpens (bottom) molecular clouds, with the open black circles indicating the SUCANES objects, the white open circles indicating the subsample of SUCANES that belong to Kim et al. (2016) groups A+B, and the red circles corresponding to the subsample of SUCANES that include the proto-BD candidates of Table 3 selected in this work.



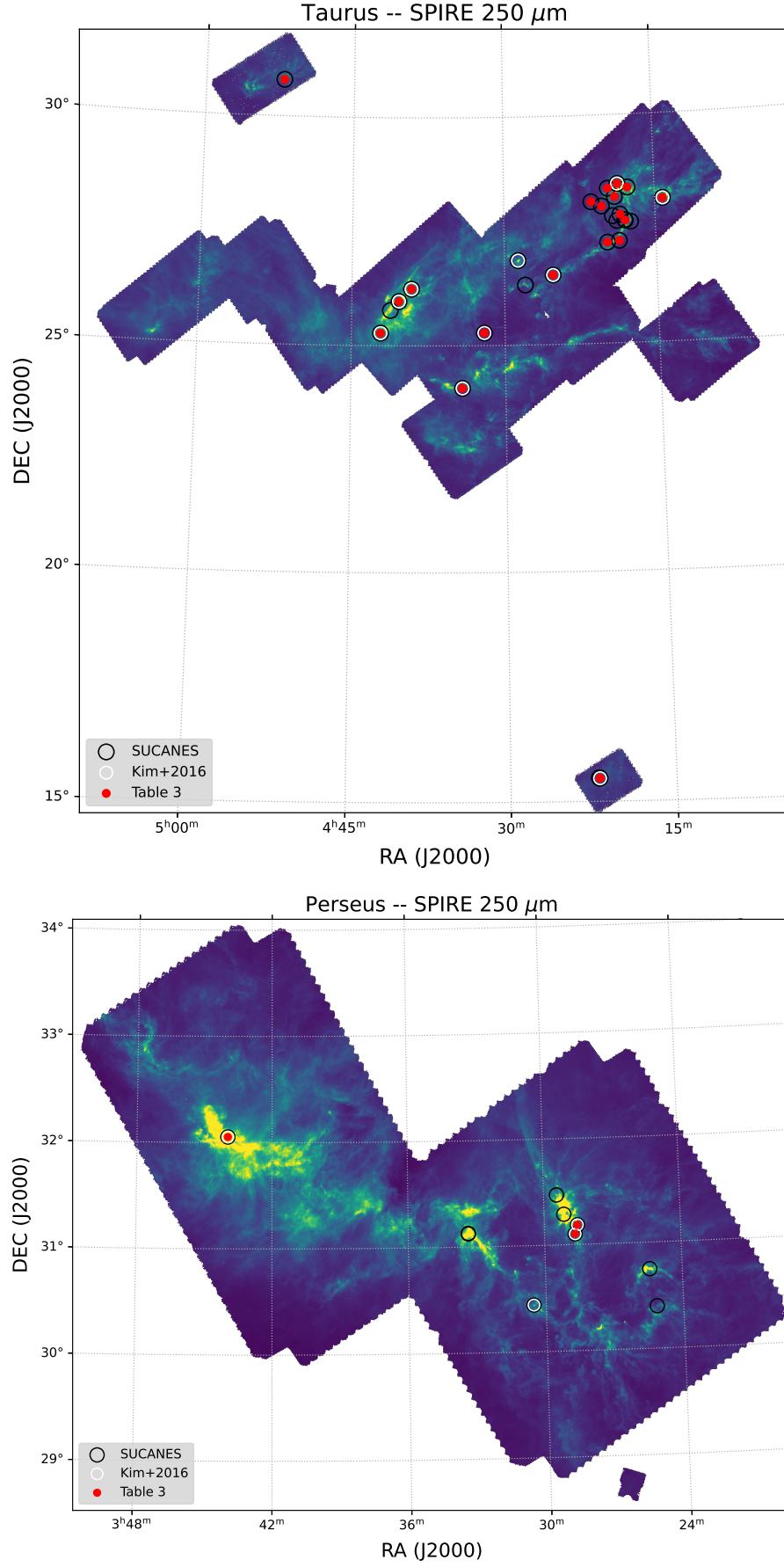


Figure C.2: RGB Herschel/SPIRE image of Taurus (top) and Perseus (bottom) molecular clouds, with the open black circles indicating the SUCANES objects, the white open circles indicating the subsample of SUCANES that belong to Kim et al. (2016) groups A+B, and the red circles corresponding to the subsample of SUCANES that include the proto-BD candidates of Table 3 selected in this work.

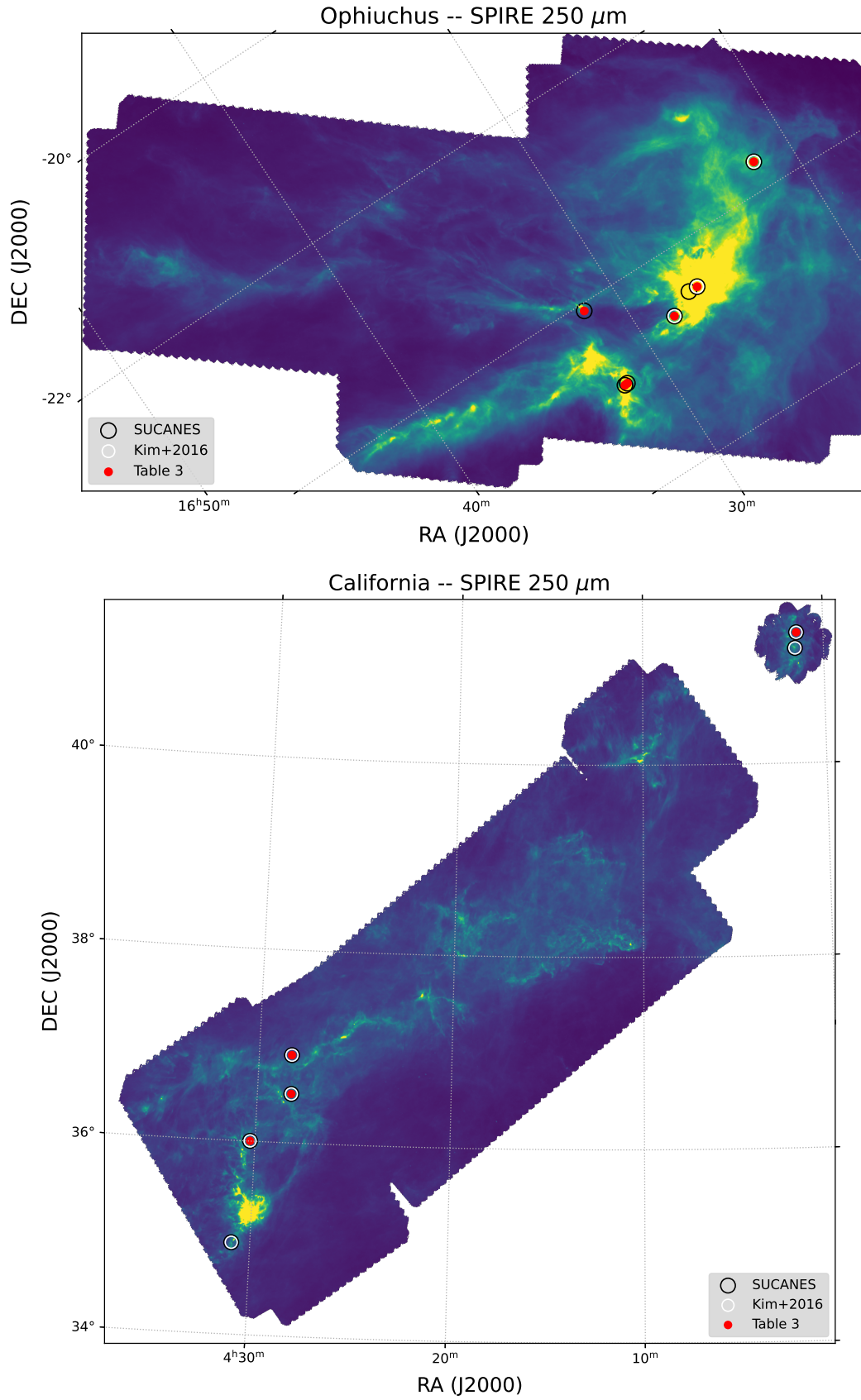


Figure C.3: RGB Herschel/SPIRE image of Ophiuchus (top) and California (bottom) molecular clouds, with the open black circles indicating the SUCANES objects, the white open circles indicating the subsample of SUCANES that belong to Kim et al. (2016) groups A+B, and the red circles corresponding to the subsample of SUCANES that include the proto-BD candidates of Table 3 selected in this work.

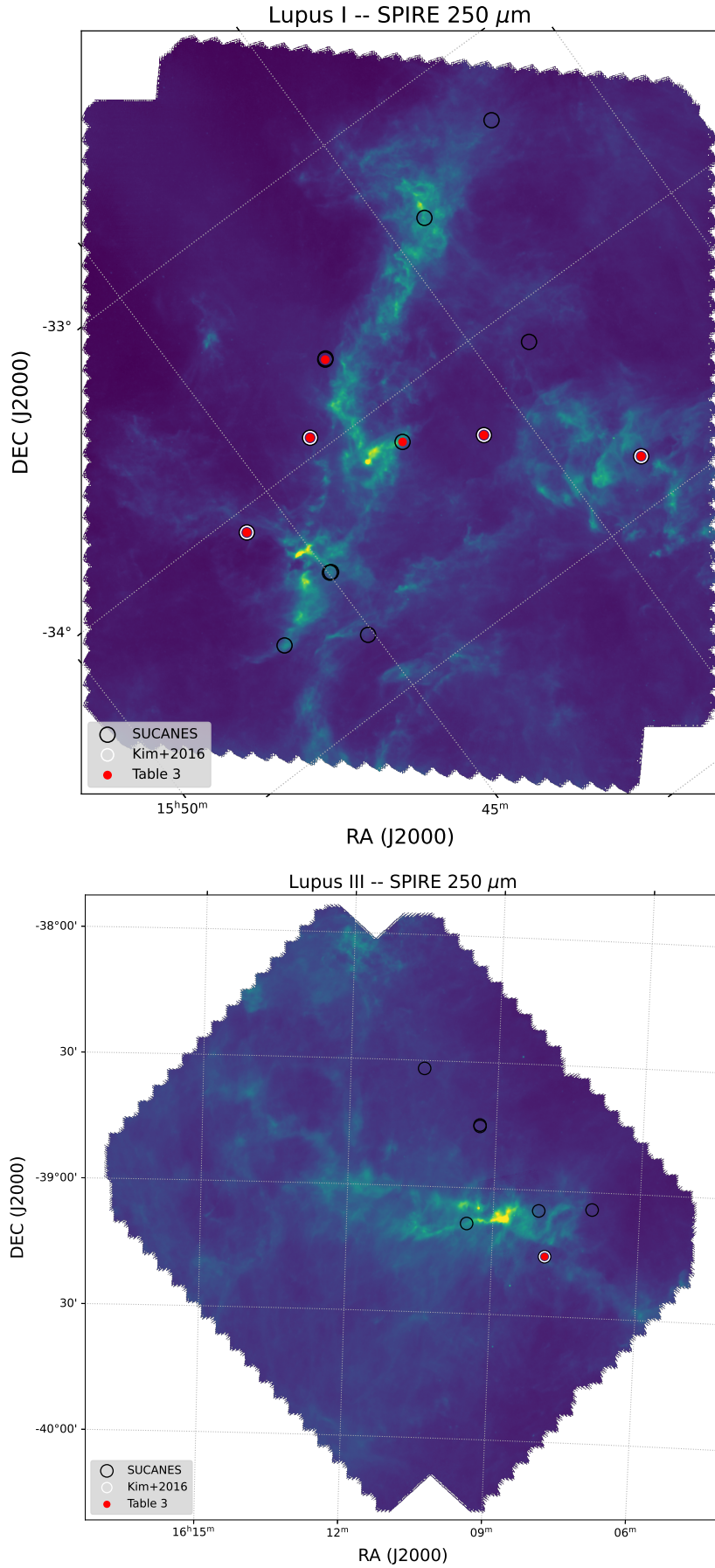


Figure C.4: RGB Herschel/SPIRE image of Lupus I (top) and Lupus III (bottom) molecular clouds, with the open black circles indicating the SUCANES objects, the white open circles indicating the subsample of SUCANES that belong to Kim et al. (2016) groups A+B, and the red circles corresponding to the subsample of SUCANES that include the proto-BD candidates of Table 3 selected in this work.

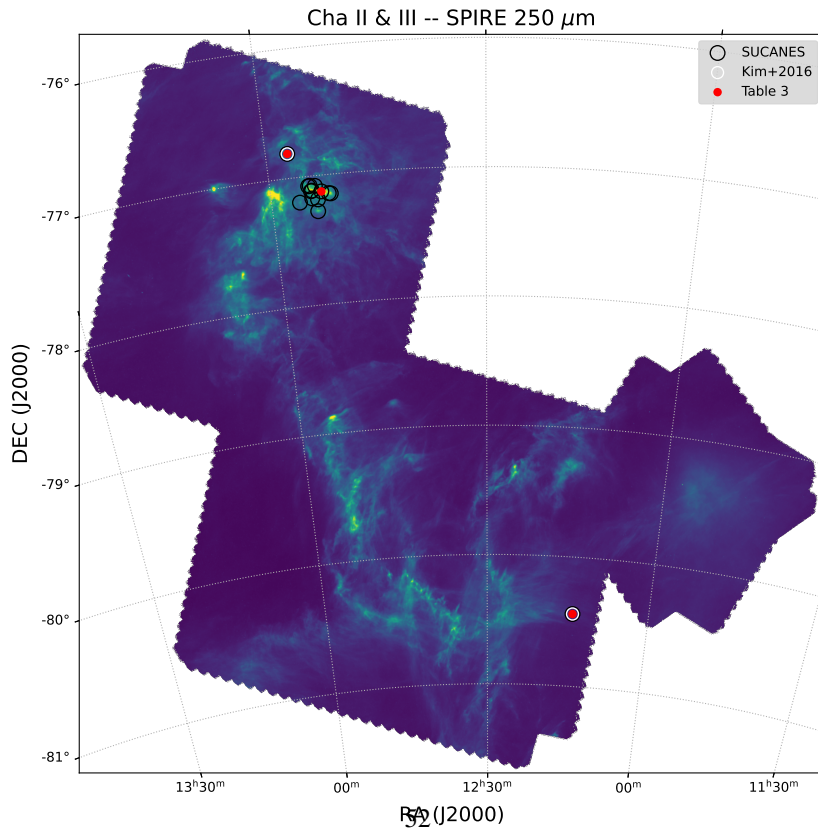
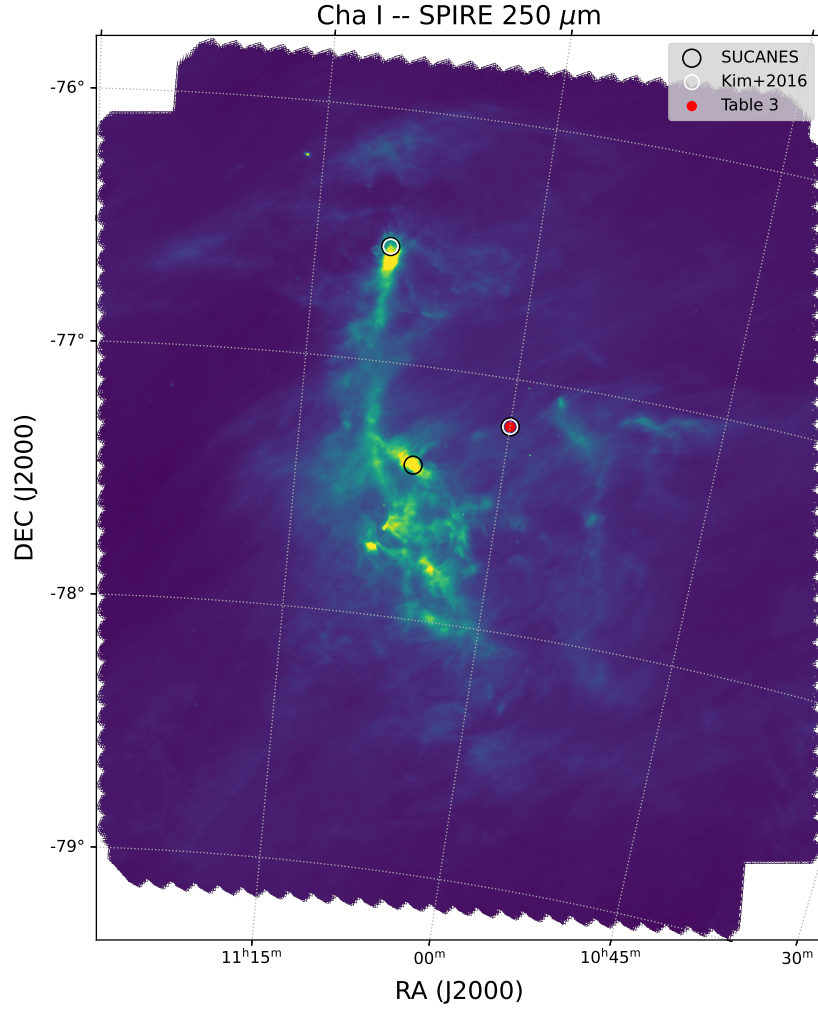


Figure C.5: RGB Herschel/SPIRE image of Chamaleon I (top) and Chamaleon II/III (bottom) molecular clouds, with the open black circles indicating the SUCANES objects, the white open circles indicating the subsample of SUCANES that belong to Kim et al. (2016) groups A+B, and the red circles corresponding to the subsample of SUCANES that include the proto-BD candidates of Table 3 selected in this work.



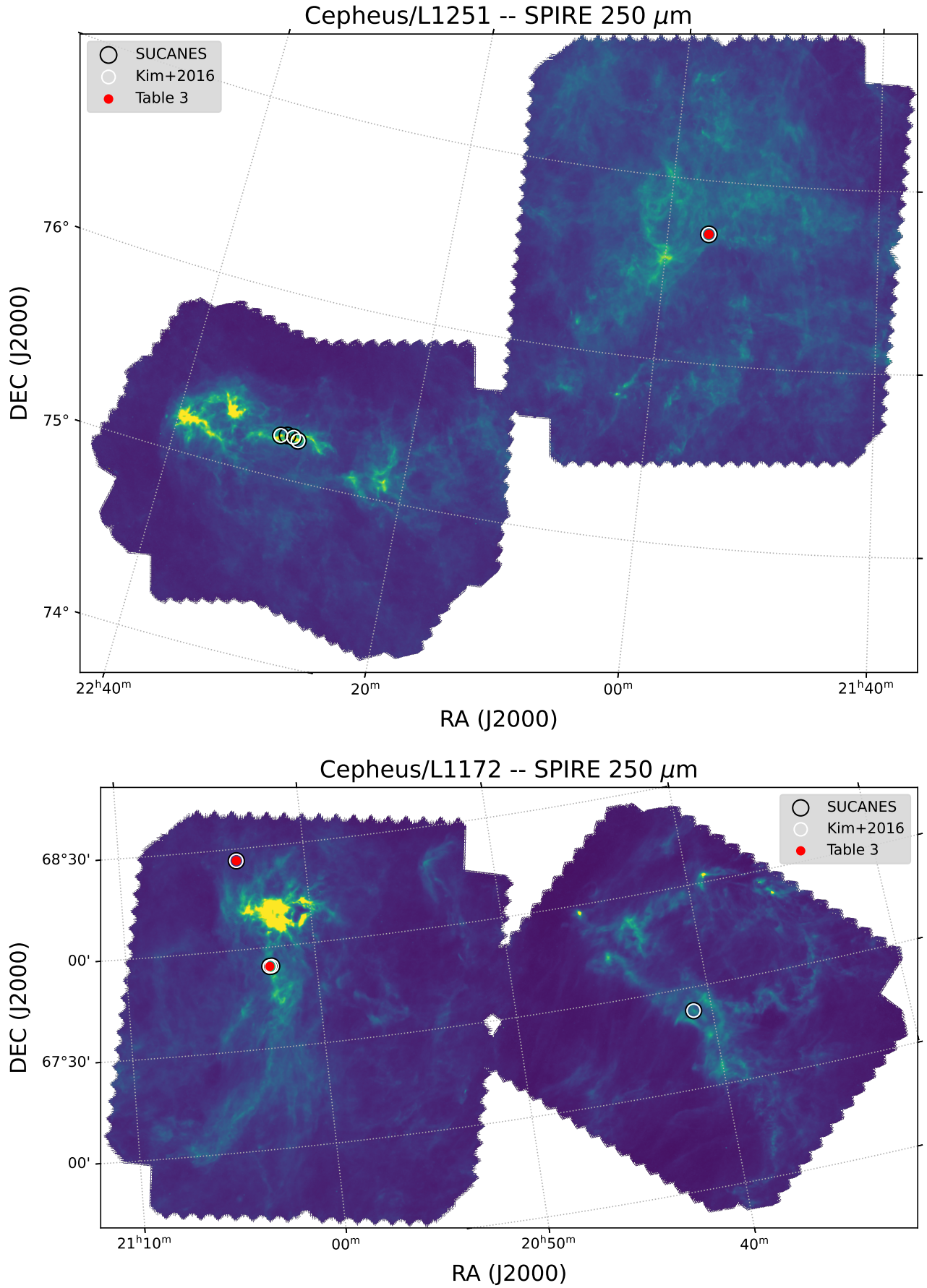


Figure C.6: RGB Herschel/SPIRE image of L1251 (top) and L1172 (bottom) Cepheus molecular clouds, with the open black circles indicating the SUCANES objects, the white open circles indicating the subsample of SUCANES that belong to Kim et al. (2016) groups A+B, and the red circles corresponding to the subsample of SUCANES that include the proto-BD candidates of Table 3 selected in this work.

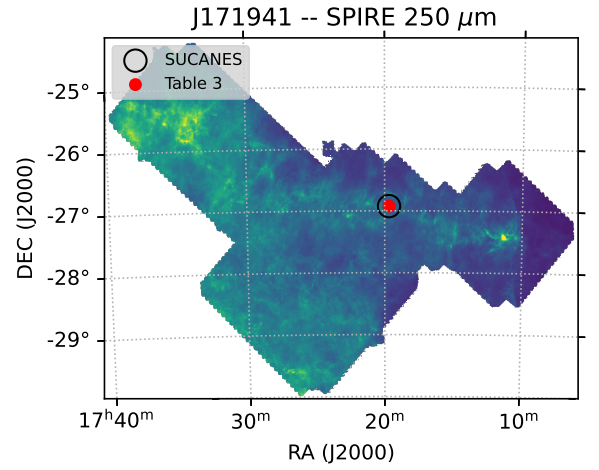
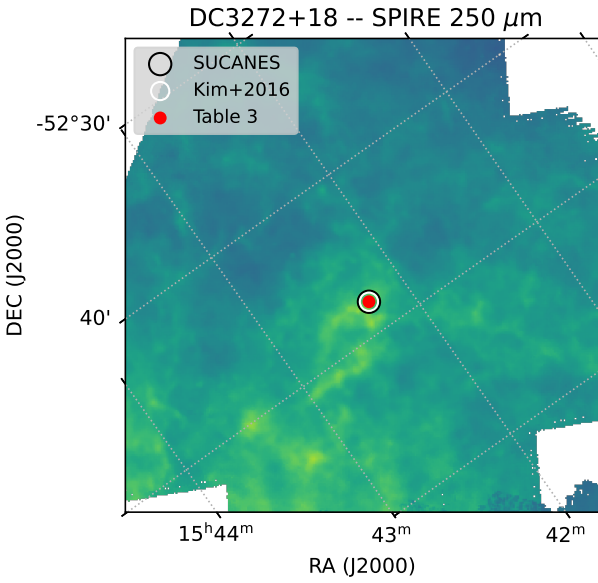
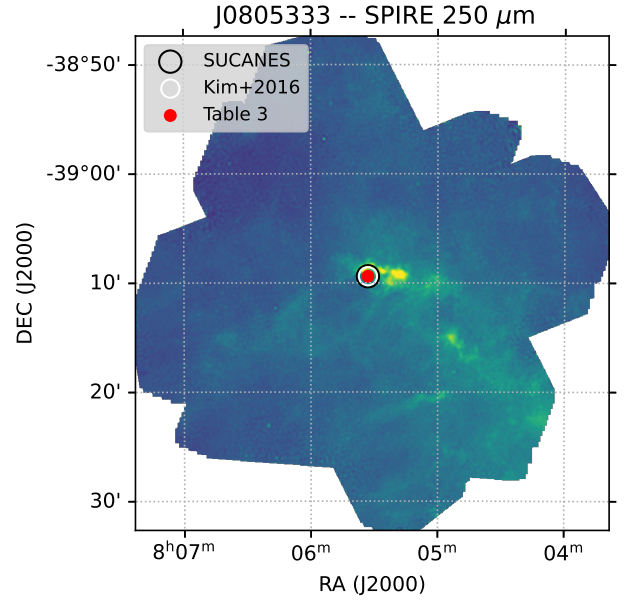
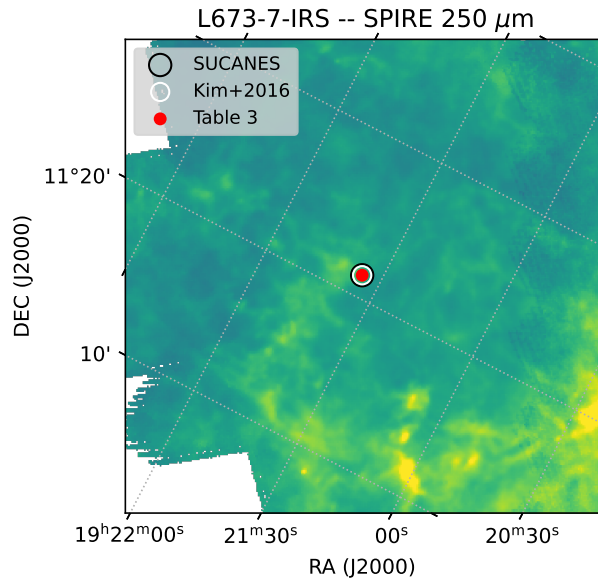


Figure C.7: RGB Herschel/SPIRE image of L673-7 (top-left), J080533 (top-right), DC3272 (bottom-left) and J171941 (bottom-right) isolated molecular clouds, with the open black circles indicating the SUCANES objects, the white open circles indicating the subsample of SUCANES that belong to Kim et al. (2016) groups A+B, and the red circles corresponding to the subsample of SUCANES that include the proto-BD candidates of Table 3 selected in this work.

- AMI Consortium, Scaife, A.M.M., Curtis, E.I., Davies, M., Franzen, T.M.O., Grainge, K.J.B., Hobson, M.P., Hurley-Walker, N., Lasenby, A.N., Olamaie, M., Pooley, G.G., Rodríguez-González, C., Saunders, R.D.E., Schammel, M., Scott, P.F., Shimwell, T., Titterton, D., Waldram, E., Zwart, J.T.L., 2011. AMI Large Array radio continuum observations of Spitzer c2d small clouds and cores. *Monthly Notice of the Royal Astronomical Society* 410, 2662–2678. doi:[10.1111/j.1365-2966.2010.17644.x](#), [arXiv:1009.0348](#).
- Anderl, S., Maret, S., Cabrit, S., Maury, A.J., Belloche, A., André, P., Bacmann, A., Codella, C., Podio, L., Gueth, F., 2020. Probing episodic accretion with chemistry: CALYPSO observations of the very-low-luminosity Class 0 protostar IRAM 04191+1522. Results from the CALYPSO IRAM-PdBI survey. *Astronomy & Astrophysics* 643, A123. doi:[10.1051/0004-6361/201936926](#), [arXiv:2011.05979](#).
- Anderson, A.R., Williams, J.P., van der Marel, N., Law, C.J., Ricci, L., Tobin, J.J., Tong, S., 2022. Protostellar and Protoplanetary Disk Masses in the Serpens Region. *Astrophys. Journal* 938, 55. doi:[10.3847/1538-4357/ac8ff0](#), [arXiv:2204.08731](#).
- André, P., Men'shchikov, A., Bontemps, S., Könyves, V., Motte, F., Schneider, N., Didelon, P., Minier, V., Saraceno, P., Ward-Thompson, D., di Francesco, J., White, G., Molinari, S., Testi, L., Abergel, A., Griffin, M., Henning, T., Royer, P., Merín, B., Vavrek, R., Attard, M., Arzoumanian, D., Wilson, C.D., Ade, P., Aussel, H., Baluteau, J.P., Benedettini, M., Bernard, J.P., Blommaert, J.A.D.L., Cambrésy, L., Cox, P., di Giorgio, A., Hargrave, P., Hennemann, M., Huang, M., Kirk, J., Krause, O., Launhardt, R., Leeks, S., Le Penne, J., Li, J.Z., Martin, P.G., Maury, A., Olofsson, G., Omont, A., Peretto, N., Pezzuto, S., Prusti, T., Roussel, H., Russeil, D., Sauvage, M., Sibthorpe, B., Sicilia-Aguilar, A., Spinoglio, L., Waelkens, C., Woodcraft, A., Zavagno, A., 2010. From filamentary clouds to prestellar cores to the stellar IMF: Initial highlights from the Herschel Gould Belt Survey. *Astronomy & Astrophysics* 518, L102. doi:[10.1051/0004-6361/201014666](#), [arXiv:1005.2618](#).
- Andre, P., Montmerle, T., 1994. From T Tauri Stars to Protostars: Circumstellar Material and Young Stellar Objects in the rho Ophiuchi Cloud. *Astrophys. Journal* 420, 837. doi:[10.1086/173608](#).
- André, P., Motte, F., Bacmann, A., 1999. Discovery of an Extremely Young Accreting Protostar in Taurus. *Astrophys. Journal Letters* 513, L57–L60. doi:[10.1086/311908](#).
- Andre, P., Ward-Thompson, D., Barsony, M., 1993. Submillimeter Continuum Observations of rho Ophiuchi A: The Candidate Protostar VLA 1623 and Prestellar Clumps. *Astrophys. Journal* 406, 122. doi:[10.1086/172425](#).
- André, P., Ward-Thompson, D., Greaves, J., 2012. Interferometric Identification of a Pre-Brown Dwarf. *Science* 337, 69. doi:[10.1126/science.1222602](#), [arXiv:1207.1220](#).
- Andrews, S.M., Liu, M.C., Williams, J.P., Allers, K.N., 2008. Submillimeter Observations of the Young Low-Mass Object IRAS 04158+2805. *Astrophys. Journal* 685, 1039–1045. doi:[10.1086/591417](#), [arXiv:0806.4163](#).
- Anglada, G., Rodríguez, L.F., Carrasco-González, C., 2018. Radio jets from young stellar objects. *Astronomy and Astrophysics Reviews* 26, 3. doi:[10.1007/s00159-018-0107-z](#), [arXiv:1806.06444](#).
- Ansdell, M., Williams, J.P., van der Marel, N., Carpenter, J.M., Guidi, G., Hogerheijde, M., Mathews, G.S., Manara, C.F., Miotello, A., Natta, A., Oliveira, I., Tazzari, M., Testi, L., van Dishoeck, E.F., van Terwisga, S.E., 2016. ALMA Survey of Lupus Protoplanetary Disks. I. Dust and Gas Masses. *Astrophys. Journal* 828, 46. doi:[10.3847/0004-637X/828/1/46](#), [arXiv:1604.05719](#).
- Apai, D., Tóth, L.V., Henning, T., Vavrek, R., Kovács, Z., Lemke, D., 2005. HST/NICMOS observations of a proto-brown dwarf candidate. *Astronomy & Astrophysics* 433, L33–L36. doi:[10.1051/0004-6361/200500098](#), [arXiv:astro-ph/0502484](#).
- Aso, Y., Kwon, W., Ohashi, N., Jørgensen, J.K., Tobin, J.J., Aikawa, Y., de Gregorio-Monsalvo, I., Han, I., Kido, M., Koch, P.M., Lai, S.P., Lee, C.W., Lee, J.E., Li, Z.Y., Lin, Z.Y.D., Looney, L.W., Narayanan, S., Phuong, N.T., Sai, J.I.C., Saigo, K., Santamaría-Miranda, A., Sharma, R., Takakuwa, S., Thieme, T.J., Tomida, K., Williams, J.P., Yen, H.W., 2023. Early Planet Formation in Embedded Disks (eDisk). VI. Kinematic Structures around the Very-low-mass Protostar IRAS 16253-2429. *Astrophys. Journal* 954, 101. doi:[10.3847/1538-4357/ace624](#), [arXiv:2309.01891](#).
- Ballesteros-Paredes, J., Zamora-Avilés, M., Román-Zúñiga, C., Palau, A., Cervantes-Sodi, B., Gutiérrez-Dávila, K., Camacho, V., Jiménez-Andrade, E., Gazol, A., 2024. Gravity or turbulence? - VI. The physics behind the Kennicutt-Schmidt relation. *Monthly Notice of the Royal Astronomical Society* 534, 1043–1059. doi:[10.1093/mnras/stae2036](#), [arXiv:2408.13636](#).
- Baraffe, I., Chabrier, G., Allard, F., Hauschildt, P., 2003. Evolutionary models for low mass stars and brown dwarfs at young ages, in: Martín, E. (Ed.), *Brown Dwarfs*, p. 41.
- Baraffe, I., Elbakyan, V.G., Vorobyov, E.I., Chabrier, G., 2017. Self-consistent evolution of accreting low-mass stars and brown dwarfs. *Astronomy & Astrophysics* 597, A19. doi:[10.1051/0004-6361/201629303](#), [arXiv:1608.07428](#).
- Barrado, D., de Gregorio Monsalvo, I., Huélamo, N., Morales-Calderón, M., Bayo, A., Palau, A., Ruiz, M.T., Rivière-Marichalar, P., Bouy, H., Morata, Ó., Stauffer, J.R., Eiroa, C., Noriega-Crespo, A., 2018. Early phases in the stellar and substellar formation and evolution. Infrared and submillimeter data in the Barnard 30 dark cloud. *Astronomy & Astrophysics* 612, A79. doi:[10.1051/0004-6361/201527938](#), [arXiv:1712.06399](#).
- Barrado, D., Mollière, P., Patapis, P., Min, M., Tremblin, P., Ardevol Martínez, F., Whiteford, N., Vasisht, M., Argyriou, I., Samland, M., Lagage, P.O., Decin, L., Waters, R., Henning, T., Morales-Calderón, M., Guedel, M., Vandenbussche, B., Absil, O., Baudoz, P., Boccaletti, A., Bouwman, J., Cossou, C., Coulais, A., Crouzet, N., Gastaal, R., Glasse, A., Glauser, A.M., Kamp, I., Kendrew, S., Krause, O., Lahuis, F., Mueller, M., Olofsson, G., Pye, J., Rouan, D., Royer, P., Scheithauer, S., Waldmann, I., Colina, L., van Dishoeck, E.F., Ray, T., Östlin, G., Wright, G., 2023.  $^{15}\text{NH}_3$  in the atmosphere of a cool brown dwarf. *Nature* 624, 263–266. doi:[10.1038/s41586-023-06813-y](#), [arXiv:2311.08054](#).
- Barrado, D., Morales-Calderón, M., Palau, A., Bayo, A., de Gregorio-Monsalvo, I., Eiroa, C., Huélamo, N., Bouy, H., Morata, O., Schmidtobreick, L., 2009. A proto brown dwarf candidate in Taurus. *Astronomy & Astrophysics* 508, 859–867. doi:[10.1051/0004-6361/200912276](#).
- Barrado y Navascués, D., Bouvier, J., Stauffer, J.R., Lodieu, N., McCaughrean, M.J., 2002. A substellar mass function for Alpha Persei. *Astronomy & Astrophysics* 395, 813–821. doi:[10.1051/0004-6361:20021262](#), [arXiv:astro-ph/0209032](#).
- Barrado y Navascués, D., Stauffer, J.R., Bouvier, J., Jayawardhana, R., Cuillandre, J.C., 2004. The Substellar Population of the Young Cluster  $\lambda$  Orionis. *Astrophys. Journal* 610, 1064–1078. doi:[10.1086/421762](#), [arXiv:astro-ph/0404072](#).
- Barrado y Navascués, D., Stauffer, J.R., Bouvier, J., Martín, E.L., 2001. From the Top to the Bottom of the Main Sequence: A Complete Mass Function of the Young Open Cluster M35. *Astrophys. Journal* 546, 1006–1018. doi:[10.1086/318283](#), [arXiv:astro-ph/0011136](#).
- Basu, S., Vorobyov, E.I., 2012. A Hybrid Scenario for the Formation of Brown Dwarfs and Very Low Mass Stars. *Astrophys. Journal* 750, 30. doi:[10.1088/0004-637X/750/1/30](#), [arXiv:1203.0274](#).
- Bate, M.R., 2009. The importance of radiative feedback for the stellar initial mass function. *Monthly Notice of the Royal Astronomical Society* 392, 1363–1380. doi:[10.1111/j.1365-2966.2008.14165.x](#), [arXiv:0811.1035](#).
- Bate, M.R., 2012. Stellar, brown dwarf and multiple star properties from a radiation hydrodynamical simulation of star cluster formation. *Monthly Notice of the Royal Astronomical Society* 419, 3115–3146. doi:[10.1111/j.1365-2966.2011.19955.x](#), [arXiv:1110.1092](#).
- Bate, M.R., 2019. The statistical properties of stars and their dependence on metallicity. *Monthly Notice of the Royal Astronomical Society* 484, 2341–2361. doi:[10.1093/mnras/stz103](#), [arXiv:1901.03713](#).
- Bate, M.R., 2023. The statistical properties of stars at redshift,  $z = 5$ , compared with the present epoch. *Monthly Notice of the Royal Astronomical Society* 519, 688–708. doi:[10.1093/mnras/stac3481](#), [arXiv:2211.15727](#).
- Bate, M.R., Bonnell, I.A., Bromm, V., 2002. The formation mechanism of brown dwarfs. *Monthly Notice of the Royal Astronomical Society* 332, L65–L68. doi:[10.1046/j.1365-8711.2002.05539.x](#), [arXiv:astro-ph/0206365](#).
- Bate, M.R., Tricco, T.S., Price, D.J., 2014. Collapse of a molecular cloud core to stellar densities: stellar-core and outflow formation in radiation magnetohydrodynamic simulations. *Monthly Notice of the Royal Astronomical Society* 437, 77–95. doi:[10.1093/mnras/stt1865](#), [arXiv:1310.1092](#).
- Bayo, A., Barrado, D., Stauffer, J., Morales-Calderón, M., Melo, C., Huélamo, N., Bouy, H., Stelzer, B., Tamara, M., Jayawardhana, R., 2011. Spectroscopy of very low mass stars and brown dwarfs in the Lambda Orionis star forming region. I. Enlarging the census down to the planetary



- mass domain in Collinder 69. *Astronomy & Astrophysics* 536, A63. doi:[10.1051/0004-6361/201116617](https://doi.org/10.1051/0004-6361/201116617), [arXiv:1109.4917](https://arxiv.org/abs/1109.4917).
- Belloche, A., André, P., Despois, D., Blinder, S., 2002. Molecular line study of the very young protostar IRAM 04191 in Taurus: infall, rotation, and outflow. *Astronomy & Astrophysics* 393, 927–947. doi:[10.1051/0004-6361:20021054](https://doi.org/10.1051/0004-6361:20021054), [arXiv:astro-ph/0207287](https://arxiv.org/abs/astro-ph/0207287).
- Beltrán, M.T., Estalella, R., Girart, J.M., Ho, P.T.P., Anglada, G., 2008. On the nature of outflows in intermediate-mass protostars: a case study of IRAS 20050+2720. *Astronomy & Astrophysics* 481, 93–105. doi:[10.1051/0004-6361:20078045](https://doi.org/10.1051/0004-6361:20078045), [arXiv:0712.1757](https://arxiv.org/abs/0712.1757).
- Benedettini, M., Pezzuto, S., Schisano, E., André, P., Könyves, V., Men'shchikov, A., Ladjelate, B., Di Francesco, J., Elia, D., Arzoumanian, D., Louvet, F., Palmeirim, P., Rygl, K.L.J., Schneider, N., Spinoglio, L., Ward-Thompson, D., 2018. A catalogue of dense cores and young stellar objects in the Lupus complex based on Herschel. Gould Belt Survey observations. *Astronomy & Astrophysics* 619, A52. doi:[10.1051/0004-6361/201833364](https://doi.org/10.1051/0004-6361/201833364), [arXiv:1809.04463](https://arxiv.org/abs/1809.04463).
- Berger, E., Ball, S., Becker, K.M., Clarke, M., Frail, D.A., Fukuda, T.A., Hoffman, I.M., Mellon, R., Momjian, E., Murphy, N.W., Teng, S.H., Woodruff, T., Zauderer, B.A., Zavala, R.T., 2001. Discovery of radio emission from the brown dwarf LP944-20. *Nature* 410, 338–340. doi:[10.48550/arXiv.astro-ph/0102301](https://doi.org/10.48550/arXiv.astro-ph/0102301), [arXiv:astro-ph/0102301](https://arxiv.org/abs/astro-ph/0102301).
- Betti, S.K., Follette, K.B., Ward-Duong, K., Peck, A.E., Aoyama, Y., Bary, J., Dacus, B., Edwards, S., Marleau, G.D., Mohamed, K., Palmo, J., Plunkett, C., Robinson, C., Wang, H., 2023. The Comprehensive Archive of Substellar and Planetary Accretion Rates. *Astron. Journal* 166, 262. doi:[10.3847/1538-3881/ad06b8](https://doi.org/10.3847/1538-3881/ad06b8), [arXiv:2310.00072](https://arxiv.org/abs/2310.00072).
- Beuther, H., Mottram, J.C., Ahmadi, A., Bosco, F., Linz, H., Henning, T., Klaassen, P., Winters, J.M., Maud, L.T., Kuiper, R., Semenov, D., Gieser, C., Peters, T., Urquhart, J.S., Pudritz, R., Ragan, S.E., Feng, S., Keto, E., Leurini, S., Cesaroni, R., Beltrán, M., Palau, A., Sánchez-Monge, Á., Galvan-Madrid, R., Zhang, Q., Schilke, P., Wyrowski, F., Johnston, K.G., Longmore, S.N., Lumsden, S., Hoare, M., Menten, K.M., Csengeri, T., 2018. Fragmentation and disk formation during high-mass star formation. IRAM NOEMA (Northern Extended Millimeter Array) large program CORE. *Astronomy & Astrophysics* 617, A100. doi:[10.1051/0004-6361/201833021](https://doi.org/10.1051/0004-6361/201833021), [arXiv:1805.01191](https://arxiv.org/abs/1805.01191).
- Bohlin, R.C., Savage, B.D., Drake, J.F., 1978. A survey of interstellar H I from  $\Lambda$  absorption measurements. II. *Astrophys. Journal* 224, 132–142. doi:[10.1086/156357](https://doi.org/10.1086/156357).
- Bonnell, I.A., Bate, M.R., 2006. Star formation through gravitational collapse and competitive accretion. *Monthly Notice of the Royal Astronomical Society* 370, 488–494. doi:[10.1111/j.1365-2966.2006.10495.x](https://doi.org/10.1111/j.1365-2966.2006.10495.x), [arXiv:astro-ph/0604615](https://arxiv.org/abs/astro-ph/0604615).
- Bonnell, I.A., Clark, P., Bate, M.R., 2008. Gravitational fragmentation and the formation of brown dwarfs in stellar clusters. *Monthly Notice of the Royal Astronomical Society* 389, 1556–1562. doi:[10.1111/j.1365-2966.2008.13679.x](https://doi.org/10.1111/j.1365-2966.2008.13679.x), [arXiv:0807.0460](https://arxiv.org/abs/0807.0460).
- Bonnor, W.B., 1956. Boyle's Law and gravitational instability. *Monthly Notice of the Royal Astronomical Society* 116, 351. doi:[10.1093/mnras/116.3.351](https://doi.org/10.1093/mnras/116.3.351).
- Bontemps, S., André, P., Terebey, S., Cabrit, S., 1996. Evolution of outflow activity around low-mass embedded young stellar objects. *Astronomy & Astrophysics* 311, 858–872.
- Bontemps, S., Motte, F., Csengeri, T., Schneider, N., 2010. Fragmentation and mass segregation in the massive dense cores of Cygnus X. *Astronomy & Astrophysics* 524, A18. doi:[10.1051/0004-6361/200913286](https://doi.org/10.1051/0004-6361/200913286), [arXiv:0909.2315](https://arxiv.org/abs/0909.2315).
- Bourke, T.L., Crapsi, A., Myers, P.C., Evans, Neal J., I., Wilner, D.J., Huard, T.L., Jørgensen, J.K., Young, C.H., 2005a. Discovery of a Low-Mass Bipolar Molecular Outflow from L1014-IRS with the Submillimeter Array. *Astrophys. Journal Letters* 633, L129–L132. doi:[10.1086/498449](https://doi.org/10.1086/498449), [arXiv:astro-ph/0509865](https://arxiv.org/abs/astro-ph/0509865).
- Bourke, T.L., Hyland, A.R., Robinson, G., 2005b. On the Identification of High-Mass Star Forming Regions Using IRAS: Contamination by Low-Mass Protostars. *Astrophys. Journal* 625, 883–890. doi:[10.1086/429818](https://doi.org/10.1086/429818), [arXiv:astro-ph/0504500](https://arxiv.org/abs/astro-ph/0504500).
- Bouy, H., Bertin, E., Sarro, L.M., Barrado, D., Moraux, E., Bouvier, J., Cuillandre, J.C., Berihuete, A., Olivares, J., Beletsky, Y., 2015. The Seven Sisters DANCE. I. Empirical isochrones, luminosity, and mass functions of the Pleiades cluster. *Astronomy & Astrophysics* 577, A148. doi:[10.1051/0004-6361/201425019](https://doi.org/10.1051/0004-6361/201425019), [arXiv:1502.03728](https://arxiv.org/abs/1502.03728).
- Bouy, H., Brandner, W., Martín, E.L., Delfosse, X., Allard, F., Basri, G., 2003. Multiplicity of Nearby Free-Floating Ultracool Dwarfs: A Hubble Space Telescope WFC2 Search for Companions. *Astron. Journal* 126, 1526–1554. doi:[10.1086/377343](https://doi.org/10.1086/377343), [arXiv:astro-ph/0305484](https://arxiv.org/abs/astro-ph/0305484).
- Bouy, H., Huélamo, N., Barrado Y Navascués, D., Martín, E.L., Petr-Gotzens, M.G., Kolb, J., Marchetti, E., Morales-Calderón, M., Bayo, A., Artigau, E., Hartung, M., Marchis, F., Tamura, M., Sterzik, M., Köhler, R., Ivanov, V.D., Nürnberger, D., 2009. A deep look into the core of young clusters. II.  $\lambda$ -Orionis. *Astronomy & Astrophysics* 504, 199–209. doi:[10.1051/0004-6361/200912569](https://doi.org/10.1051/0004-6361/200912569), [arXiv:0907.0322](https://arxiv.org/abs/0907.0322).
- Broekhoven-Fiene, H., Matthews, B.C., Harvey, P.M., Gutermuth, R.A., Huard, T.L., Tothill, N.F.H., Nutter, D., Bourke, T.L., DiFrancesco, J., Jørgensen, J.K., Allen, L.E., Chapman, N.L., Dunham, M.M., Merín, B., Miller, J.F., Terebey, S., Peterson, D.E., Stapelfeldt, K.R., 2014. The Spitzer Survey of Interstellar Clouds in the Gould Belt. VI. The Auriga-California Molecular Cloud Observed with IRAC and MIPS. *Astrophys. Journal* 786, 37. doi:[10.1088/0004-637X/786/1/37](https://doi.org/10.1088/0004-637X/786/1/37), [arXiv:1402.6329](https://arxiv.org/abs/1402.6329).
- Bulger, J., Patience, J., Ward-Duong, K., Pinte, C., Bouy, H., Ménard, F., Monin, J.L., 2014. The Taurus Boundary of Stellar/Substellar (TBOSS) Survey. I. Far-IR disk emission measured with Herschel. *Astronomy & Astrophysics* 570, A29. doi:[10.1051/0004-6361/201323088](https://doi.org/10.1051/0004-6361/201323088), [arXiv:1407.4802](https://arxiv.org/abs/1407.4802).
- Burgasser, A.J., Kirkpatrick, J.D., Reid, I.N., Brown, M.E., Miskey, C.L., Gizis, J.E., 2003. Binarity in Brown Dwarfs: T Dwarf Binaries Discovered with the Hubble Space Telescope Wide Field Planetary Camera 2. *Astrophys. Journal* 586, 512–526. doi:[10.1086/346263](https://doi.org/10.1086/346263), [arXiv:astro-ph/0211470](https://arxiv.org/abs/astro-ph/0211470).
- Burrows, A., Hubbard, W.B., Lunine, J.I., Liebert, J., 2001. The theory of brown dwarfs and extrasolar giant planets. *Reviews of Modern Physics* 73, 719–765. doi:[10.1103/RevModPhys.73.719](https://doi.org/10.1103/RevModPhys.73.719), [arXiv:astro-ph/0103383](https://arxiv.org/abs/astro-ph/0103383).
- Busch, L.A., Belloche, A., Cabrit, S., Hennebelle, P., Commerçon, B., 2020. The dynamically young outflow of the Class 0 protostar Chamaeleon 1. *Astronomy & Astrophysics* 633, A126. doi:[10.1051/0004-6361/201936432](https://doi.org/10.1051/0004-6361/201936432), [arXiv:1911.11194](https://arxiv.org/abs/1911.11194).
- Camacho, V., Vázquez-Semadeni, E., Palau, A., Zamora-Avilés, M., 2023. The kinetic and magnetic energy budget of hub-filament systems during the gravitational fragmentation of molecular clouds. *Monthly Notice of the Royal Astronomical Society* 523, 3376–3392. doi:[10.1093/mnras/stad1581](https://doi.org/10.1093/mnras/stad1581), [arXiv:2212.10610](https://arxiv.org/abs/2212.10610).
- Carney, M.T., Yıldız, U.A., Mottram, J.C., van Dishoeck, E.F., Ramchandani, J., Jørgensen, J.K., 2016. Classifying the embedded young stellar population in Perseus and Taurus and the LOMASS database. *Astronomy & Astrophysics* 586, A44. doi:[10.1051/0004-6361/201526308](https://doi.org/10.1051/0004-6361/201526308), [arXiv:1511.03136](https://arxiv.org/abs/1511.03136).
- Carpenter, J.M., 2000. 2MASS Observations of the Perseus, Orion A, Orion B, and Monoceros R2 Molecular Clouds. *Astron. Journal* 120, 3139–3161. doi:[10.1086/316845](https://doi.org/10.1086/316845), [arXiv:astro-ph/0009118](https://arxiv.org/abs/astro-ph/0009118).
- Caselli, P., 2011. Observational Studies of Pre-Stellar Cores and Infrared Dark Clouds, in: Cernicharo, J., Bachiller, R. (Eds.), *The Molecular Universe*, pp. 19–32. doi:[10.1017/S1743921311024835](https://doi.org/10.1017/S1743921311024835), [arXiv:1107.4707](https://arxiv.org/abs/1107.4707).
- Chabrier, G., 2005. The Initial Mass Function: From Salpeter 1955 to 2005, in: Corbelli, E., Palla, F., Zinnecker, H. (Eds.), *The Initial Mass Function 50 Years Later*, p. 41. doi:[10.1007/978-1-4020-3407-7\\_5](https://doi.org/10.1007/978-1-4020-3407-7_5), [arXiv:astro-ph/0409465](https://arxiv.org/abs/astro-ph/0409465).
- Chabrier, G., Baraffe, I., Allard, F., Hauschildt, P., 2000. Evolutionary Models for Very Low-Mass Stars and Brown Dwarfs with Dusty Atmospheres. *Astrophys. Journal* 542, 464–472. doi:[10.1086/309513](https://doi.org/10.1086/309513), [arXiv:astro-ph/0005557](https://arxiv.org/abs/astro-ph/0005557).
- Chabrier, G., Baraffe, I., Phillips, M., Debras, F., 2023. Impact of a new H/He equation of state on the evolution of massive brown dwarfs. New determination of the hydrogen burning limit. *Astronomy & Astrophysics* 671, A119. doi:[10.1051/0004-6361/202243832](https://doi.org/10.1051/0004-6361/202243832), [arXiv:2212.07153](https://arxiv.org/abs/2212.07153).
- Chabrier, G., Hennebelle, P., 2010. Star Formation: Statistical Measure of the Correlation between the Prestellar Core Mass Function and the Stellar Initial Mass Function. *Astrophys. Journal Letters* 725, L79–L83. doi:[10.1088/2041-8205/725/1/L79](https://doi.org/10.1088/2041-8205/725/1/L79), [arXiv:1011.1185](https://arxiv.org/abs/1011.1185).
- Chabrier, G., Johansen, A., Janson, M., Rafikov, R., 2014. Giant Planet and Brown Dwarf Formation, in: Beuther, H., Klessen, R.S., Dullemond, C.P., Henning, T. (Eds.), *Protostars and Planets VI*, pp. 619–642. doi:[10.2458/0004-6361/201425019](https://doi.org/10.2458/0004-6361/201425019), [arXiv:1502.03728](https://arxiv.org/abs/1502.03728).

- azu\_uapress\_9780816531240-ch027, arXiv:1401.7559.
- Chabrier, G., Lenoble, R., 2023. Probing the Milky Way stellar and brown dwarf initial mass function with modern microlensing observations. arXiv e-prints, arXiv:2301.05139 arXiv:2301.05139.
- Chen, C., Martin, R.G., Lubow, S.H., Nixon, C.J., 2023. Tilted circumbinary planetary systems as efficient progenitors of free-floating planets. arXiv e-prints, arXiv:2310.15603 arXiv:2310.15603.
- Chen, H., Myers, P.C., Ladd, E.F., Wood, D.O.S., 1995. Bolometric Temperature and Young Stars in the Taurus and Ophiuchus Complexes. *Astrophys. Journal* 445, 377. doi:10.1086/175703.
- Chen, X., Arce, H.G., Dunham, M.M., Zhang, Q., 2012a. Discovery of a Binary System in IRAM 04191+1522. *Astrophys. Journal Letters* 747, L43. doi:10.1088/2041-8205/747/2/L43, arXiv:1202.2807.
- Chen, X., Arce, H.G., Dunham, M.M., Zhang, Q., Bourke, T.L., Launhardt, R., Schmalzl, M., Henning, T., 2012b. Submillimeter Array and Spitzer Observations of Bok Globule CB 17: A Candidate First Hydrostatic Core? *Astrophys. Journal* 751, 89. doi:10.1088/0004-637X/751/2/89, arXiv:1203.5252.
- Chen, X., Arce, H.G., Zhang, Q., Bourke, T.L., Launhardt, R., Jørgensen, J.K., Lee, C.F., Foster, J.B., Dunham, M.M., Pineda, J.E., Henning, T., 2013. SMA Observations of Class 0 Protostars: A High Angular Resolution Survey of Protostellar Binary Systems. *Astrophys. Journal* 768, 110. doi:10.1088/0004-637X/768/2/110, arXiv:1304.0436.
- Chen, X., Arce, H.G., Zhang, Q., Bourke, T.L., Launhardt, R., Schmalzl, M., Henning, T., 2010. L1448 IRS2E: A Candidate First Hydrostatic Core. *Astrophys. Journal* 715, 1344–1351. doi:10.1088/0004-637X/715/2/1344, arXiv:1004.2443.
- Close, L.M., Siegler, N., Freed, M., Biller, B., 2003. Detection of Nine M8.0-L0.5 Binaries: The Very Low Mass Binary Population and Its Implications for Brown Dwarf and Very Low Mass Star Formation. *Astrophys. Journal* 587, 407–422. doi:10.1086/368177, arXiv:astro-ph/0301095.
- Coleman, G.A.L., DeRocco, W., 2024. Predicting the Galactic population of free-floating planets from realistic initial conditions. arXiv e-prints, arXiv:2407.05992 doi:10.48550/arXiv.2407.05992, arXiv:2407.05992.
- Commerçon, B., Launhardt, R., Dullemond, C., Henning, T., 2012. Synthetic observations of first hydrostatic cores in collapsing low-mass dense cores. I. Spectral energy distributions and evolutionary sequence. *Astronomy & Astrophysics* 545, A98. doi:10.1051/0004-6361/201118706, arXiv:1207.0656.
- Cox, E.G., Harris, R.J., Looney, L.W., Chiang, H.F., Chandler, C., Kratter, K., Li, Z.Y., Perez, L., Tobin, J.J., 2017. Protoplanetary Disks in  $\rho$  Ophiuchus as Seen from ALMA. *Astrophys. Journal* 851, 83. doi:10.3847/1538-4357/aa97e2, arXiv:1711.03974.
- Damian, B., Jose, J., Biller, B., Herczeg, G.J., Albert, L., Allers, K., Zhang, Z., Liu, M.C., Dubber, S., Paul, K., Chen, W.P., Lalchand, B., Sharma, T., Oasa, Y., 2023. A novel survey for young substellar objects with the W-band filter VI: Spectroscopic census of sub-stellar members and the IMF of  $\sigma$  Orionis cluster. arXiv e-prints, arXiv:2303.17424 arXiv:2303.17424.
- Dang-Duc, C., Phan-Bao, N., Dao-Van, D.T., 2016. Two confirmed class I very low-mass objects in Taurus. *Astronomy & Astrophysics* 588, L2. doi:10.1051/0004-6361/201527942, arXiv:1602.06357.
- D’Antona, F., Mazzitelli, I., 1994. New Pre-Main-Sequence Tracks for M  $\approx$  2.5  $M_{\odot}$  as Tests of Opacities and Convection Model. *Astrophysical Journal Supplement Series* 90, 467. doi:10.1086/191867.
- De Furio, M., Meyer, M.R., Reiter, M., Monnier, J., Kraus, A., Dupuy, T., 2022. Binary Formation in the Orion Nebula Cluster: Exploring the Substellar Limit. *Astrophys. Journal* 925, 112. doi:10.3847/1538-4357/ac36d4, arXiv:2111.02914.
- de Gregorio-Monsalvo, I., Barrado, D., Bouy, H., Bayo, A., Palau, A., Morales-Calderón, M., Huélamo, N., Morata, O., Merín, B., Eiroa, C., 2016. A submillimetre search for pre- and proto-brown dwarfs in Chamaeleon II. *Astronomy & Astrophysics* 590, A79. doi:10.1051/0004-6361/201424149, arXiv:1512.00418.
- DeRocco, W., Smyth, N., Profumo, S., 2024. Constraints on sub-terrestrial free-floating planets from Subaru microlensing observations. *Monthly Notice of the Royal Astronomical Society* 527, 8921–8930. doi:10.1093/mnras/stad3824, arXiv:2308.13593.
- Dhandha, J., Faes, Z., Smith, R.J., 2023. Decaying turbulence in molecular clouds: how does it affect filament networks and star formation? arXiv e-prints, arXiv:2307.12428 doi:10.48550/arXiv.2307.12428, arXiv:2307.12428.
- Di Francesco, J., André, P., Myers, P.C., 2004. Quiescent Dense Gas in Protostellar Clusters: The Ophiuchus A Core. *Astrophys. Journal* 617, 425–438. doi:10.1086/425264, arXiv:astro-ph/0408411.
- di Francesco, J., Evans, N. J., I., Caselli, P., Myers, P.C., Shirley, Y., Aikawa, Y., Tafalla, M., 2007. An Observational Perspective of Low-Mass Dense Cores I: Internal Physical and Chemical Properties, in: Reipurth, B., Jewitt, D., Keil, K. (Eds.), *Protostars and Planets V*, p. 17. doi:10.48550/arXiv.astro-ph/0602379, arXiv:astro-ph/0602379.
- Di Francesco, J., Johnstone, D., Kirk, H., MacKenzie, T., Ledwosinska, E., 2008. The SCUBA Legacy Catalogues: Submillimeter-Continuum Objects Detected by SCUBA. *Astrophysical Journal Supplement Series* 175, 277–295. doi:10.1086/523645, arXiv:0801.2595.
- Draine, B.T., 2011. *Physics of the Interstellar and Intergalactic Medium*.
- Drass, H., Haas, M., Chini, R., Bayo, A., Hackstein, M., Hoffmeister, V., Godoy, N., Vogt, N., 2016. The bimodal initial mass function in the Orion nebula cloud. *Monthly Notice of the Royal Astronomical Society* 461, 1734–1744. doi:10.1093/mnras/stw1094, arXiv:1605.03600.
- Duarte-Cabral, A., Bontemps, S., Motte, F., Hennemann, M., Schneider, N., André, P., 2013. CO outflows from high-mass Class 0 protostars in Cygnus-X. *Astronomy & Astrophysics* 558, A125. doi:10.1051/0004-6361/201321393, arXiv:1308.6490.
- Dunham, M.M., Allen, L.E., Evans, Neal J., I., Broekhoven-Fiene, H., Cieza, L.A., Di Francesco, J., Gutermuth, R.A., Harvey, P.M., Hatchell, J., Heiderman, A., Huard, T.L., Johnstone, D., Kirk, J.M., Matthews, B.C., Miller, J.F., Peterson, D.E., Young, K.E., 2015. Young Stellar Objects in the Gould Belt. *Astrophysical Journal Supplement Series* 220, 11. doi:10.1088/0067-0049/220/1/11, arXiv:1508.03199.
- Dunham, M.M., Chen, X., Arce, H.G., Bourke, T.L., Schnee, S., Enoch, M.L., 2011. Detection of a Bipolar Molecular Outflow Driven by a Candidate First Hydrostatic Core. *Astrophys. Journal* 742, 1. doi:10.1088/0004-637X/742/1/1, arXiv:1108.1342.
- Dunham, M.M., Crapsi, A., Evans, Neal J., I., Bourke, T.L., Huard, T.L., Myers, P.C., Kauffmann, J., 2008. Identifying the Low-Luminosity Population of Embedded Protostars in the c2d Observations of Clouds and Cores. *Astrophysical Journal Supplement Series* 179, 249–282. doi:10.1086/591085, arXiv:0806.1754.
- Dunham, M.M., Evans, N.J., Bourke, T.L., Myers, P.C., Huard, T.L., Stutz, A.M., 2010. The Spitzer c2d Survey of Nearby Dense Cores. IX. Discovery of a Very Low Luminosity Object Driving a Molecular Outflow in the Dense Core L673-7. *Astrophys. Journal* 721, 995–1013. doi:10.1088/0004-637X/721/2/995, arXiv:1008.1049.
- Dunham, M.M., Vorobyov, E.I., 2012. Resolving the Luminosity Problem in Low-mass Star Formation. *Astrophys. Journal* 747, 52. doi:10.1088/0004-637X/747/1/52, arXiv:1112.4789.
- Dutta, S., Lee, C.F., Johnstone, D., Lee, J.E., Hirano, N., Di Francesco, J., Moraghan, A., Liu, T., Sahu, D., Liu, S.Y., Tatematsu, K., Goldsmith, P.F., Lee, C.W., Li, S., Eden, D., Juvela, M., Bronfman, L., Hsu, S.Y., Kim, K.T., Kwon, W., Sanhueza, P., Liu, X., López-Vázquez, J.A., Luo, Q., Yi, H.W., 2024. ALMA Survey of Orion Planck Galactic Cold Clumps (ALMASOP): Molecular Jets and Episodic Accretion in Protostars. *Astron. Journal* 167, 72. doi:10.3847/1538-3881/ad152b, arXiv:2306.15346.
- Ebert, R., 1957. Zur Instabilität kugelsymmetrischer Gasverteilungen. Mit 2 Textabbildungen. *Zeitschrift fuer Astrophysik* 42, 263.
- Ellerbroek, L.E., Podio, L., Kaper, L., Sana, H., Huppenkothen, D., de Koter, A., Monaco, L., 2013. The outflow history of two Herbig-Haro jets in RCW 36: HH 1042 and HH 1043. *Astronomy & Astrophysics* 551, A5. doi:10.1051/0004-6361/201220635, arXiv:1212.4144.
- Encalada, F.J., Looney, L.W., Tobin, J.J., Sadavoy, S.I., Segura-Cox, D., Cox, E., Li, Z.Y., Novak, G., 2021. 870  $\mu$ m Dust Continuum of the Youngest Protostars in Ophiuchus. *Astrophys. Journal* 913, 149. doi:10.3847/1538-4357/abf4fd, arXiv:2105.00514.
- Enoch, M.L., Evans, Neal J., I., Sargent, A.I., Glenn, J., 2009. Properties of the Youngest Protostars in Perseus, Serpens, and Ophiuchus. *Astrophys. Journal* 692, 973–997. doi:10.1088/0004-637X/692/2/973, arXiv:0809.4012.
- Enoch, M.L., Evans, Neal J., I., Sargent, A.I., Glenn, J., Rosolowsky, E., Myers, P., 2008. The Mass Distribution and Lifetime of Prestellar Cores in Perseus, Serpens, and Ophiuchus. *Astrophys. Journal* 684, 1240–1259. doi:10.1086/589963, arXiv:0805.1075.
- Enoch, M.L., Glenn, J., Evans, Neal J., I., Sargent, A.I., Young, K.E., Huard,



- T.L., 2007. Comparing Star Formation on Large Scales in the c2d Legacy Clouds: Bolocam 1.1 mm Dust Continuum Surveys of Serpens, Perseus, and Ophiuchus. *Astrophys. Journal* 666, 982–1001. doi:[10.1086/520321](#), [arXiv:0705.3984](#).
- Enoch, M.L., Lee, J.E., Harvey, P., Dunham, M.M., Schnee, S., 2010. A Candidate Detection of the First Hydrostatic Core. *Astrophys. Journal Letters* 722, L33–L38. doi:[10.1088/2041-8205/722/1/L33](#), [arXiv:1009.0536](#).
- Enoch, M.L., Young, K.E., Glenn, J., Evans, Neal J., I., Golwala, S., Sargent, A.I., Harvey, P., Aguirre, J., Goldin, A., Haig, D., Huard, T.L., Lange, A., Laurent, G., Maloney, P., Maukopf, P., Rossinot, P., Sayers, J., 2006. Bolocam Survey for 1.1 mm Dust Continuum Emission in the c2d Legacy Clouds. I. Perseus. *Astrophys. Journal* 638, 293–313. doi:[10.1086/498678](#), [arXiv:astro-ph/0510202](#).
- Erickson, K.L., Wilking, B.A., Meyer, M.R., Robinson, J.G., Stephenson, L.N., 2011. The Initial Mass Function and Disk Frequency of the  $\rho$  Ophiuchi Cloud: An Extinction-limited Sample. *Astron. Journal* 142, 140. doi:[10.1088/0004-6256/142/4/140](#), [arXiv:1109.0561](#).
- Evans, Neal J., I., Dunham, M.M., Jørgensen, J.K., Enoch, M.L., Merín, B., van Dishoeck, E.F., Alcalá, J.M., Myers, P.C., Stapelfeldt, K.R., Huard, T.L., Allen, L.E., Harvey, P.M., van Kempen, T., Blake, G.A., Koerner, D.W., Mundy, L.G., Padgett, D.L., Sargent, A.I., 2009. The Spitzer c2d Legacy Results: Star-Formation Rates and Efficiencies; Evolution and Lifetimes. *Astrophysical Journal Supplement Series* 181, 321–350. doi:[10.1088/0067-0049/181/2/321](#), [arXiv:0811.1059](#).
- Evans, Neal J., I., Yang, Y.L., Green, J.D., Zhao, B., Di Francesco, J., Lee, J.E., Jørgensen, J.K., Choi, M., Myers, P.C., Mardones, D., 2023. Models of Rotating Infall for the B335 Protostar. *Astrophys. Journal* 943, 90. doi:[10.3847/1538-4357/acaa38](#), [arXiv:2212.03746](#).
- Favre, C., Vastel, C., Jimenez-Serra, I., Quénard, D., Caselli, P., Ceccarelli, C., Chacón-Tanarro, A., Fontani, F., Holdship, J., Oya, Y., Punanova, A., Sakai, N., Spezzano, S., Yamamoto, S., Neri, R., López-Sepulcre, A., Alves, F., Bachiller, R., Balucani, N., Bianchi, E., Bizzocchi, L., Codella, C., Caux, E., De Simone, M., Enrique Romero, J., Dulieu, F., Feng, S., Jaber Al-Edhari, A., Lefloch, B., Ospina-Zamudio, J., Pineda, J., Podio, L., Rimola, A., Segura-Cox, D., Sims, I.R., Taquet, V., Testi, L., Theulé, P., Ugliengo, P., Vasyunin, A.I., Vazart, F., Viti, S., Witzel, A., 2020. Seeds of Life in Space (SOLIS). VII. Discovery of a cold dense methanol blob toward the L1521F VeLLO system. *Astronomy & Astrophysics* 635, A189. doi:[10.1051/0004-6361/201937297](#), [arXiv:2002.07004](#).
- Forbrich, J., Lada, C.J., Muench, A.A., Alves, J., Lombardi, M., 2009. A Spitzer Census of Star Formation Activity in the Pipe Nebula. *Astrophys. Journal* 704, 292–305. doi:[10.1088/0004-637X/704/1/292](#), [arXiv:0908.4086](#).
- Forbrich, J., Rodríguez, L.F., Palau, A., Zapata, L.A., Muzerolle, J., Gutermuth, R.A., 2015. Radio Monitoring of the Periodically Variable IR Source LRL 54361: No Direct Correlation between the Radio and IR Emissions. *Astrophys. Journal* 814, 15. doi:[10.1088/0004-637X/814/1/15](#), [arXiv:1510.01233](#).
- Francis, L., Johnstone, D., Dunham, M.M., Hunter, T.R., Mairs, S., 2019. Identifying Variability in Deeply Embedded Protostars with ALMA and CARMA. *Astrophys. Journal* 871, 149. doi:[10.3847/1538-4357/aaf972](#), [arXiv:1902.00588](#).
- Friesen, R.K., Di Francesco, J., Shirley, Y.L., Myers, P.C., 2009. The Initial Conditions of Clustered Star Formation. I. NH<sub>3</sub> Observations of Dense Cores in Ophiuchus. *Astrophys. Journal* 697, 1457–1480. doi:[10.1088/0004-637X/697/2/1457](#), [arXiv:0903.0690](#).
- Furuya, R.S., Kitamura, Y., Shinnaga, H., 2006. The Initial Conditions for Gravitational Collapse of a Core: An Extremely Young Low-Mass Class 0 Protostar GF 9-2. *Astrophys. Journal* 653, 1369–1390. doi:[10.1086/508405](#), [arXiv:astro-ph/0608357](#).
- Furuya, R.S., Kitamura, Y., Shinnaga, H., 2009. Spectroscopic Evidence for Gas Infall in GF 9-2. *Astrophys. Journal Letters* 692, L96–L99. doi:[10.1088/0004-637X/692/2/L96](#), [arXiv:0901.0730](#).
- Furuya, R.S., Kitamura, Y., Shinnaga, H., 2019. A 1000 au Scale Molecular Outflow Driven by a Protostar with an Age of  $\lesssim 4000$  yr. *Astrophys. Journal* 871, 137. doi:[10.3847/1538-4357/aaf85c](#), [arXiv:1812.07806](#).
- Furuya, R.S., Kitamura, Y., Wootten, A., Claussen, M.J., Kawabe, R., 2003. Water Maser Survey toward Low-Mass Young Stellar Objects in the Northern Sky with the Nobeyama 45 Meter Telescope and the Very Large Array. *Astrophysical Journal Supplement Series* 144, 71–134. doi:[10.1086/342749](#).
- Gahm, G.F., Persson, C.M., Mäkelä, M.M., Haikala, L.K., 2013. Mass and motion of globulets in the Rosette Nebula. *Astronomy & Astrophysics* 555, A57. doi:[10.1051/0004-6361/201321547](#), [arXiv:1305.2485](#).
- Gerin, M., Pety, J., Commerçon, B., Fuente, A., Cernicharo, J., Marcelino, N., Ciardi, A., Lis, D.C., Roueff, E., Wootten, H.A., Chapillon, E., 2017. Evidence for disks at an early stage in class 0 protostars? *Astronomy & Astrophysics* 606, A35. doi:[10.1051/0004-6361/201630187](#), [arXiv:1709.07702](#).
- Gómez, G.C., Vázquez-Semadeni, E., Palau, A., 2021. Density profile evolution during prestellar core collapse: collapse starts at the large scale. *Monthly Notice of the Royal Astronomical Society* 502, 4963–4971. doi:[10.1093/mnras/stab394](#), [arXiv:2009.14151](#).
- Gómez, J.F., Palau, A., Uscanga, L., Manjarrez, G., Barrado, D., 2017. A Search for Water Maser Emission from Brown Dwarfs and Low-luminosity Young Stellar Objects. *Astron. Journal* 153, 221. doi:[10.3847/1538-3881/aa6622](#), [arXiv:1703.04323](#).
- González Picos, D., Snellen, I.A.G., de Regt, S., Landman, R., Zhang, Y., Gandhi, S., Ginski, C., Kesseli, A.Y., Mollière, P., Stolker, T., 2024. The ESO SupJup Survey: II. The <sup>12</sup>C/<sup>13</sup>C isotope ratios of three young brown dwarfs with CRILES<sup>+</sup>. *Astronomy & Astrophysics* 689, A212. doi:[10.1051/0004-6361/202450028](#), [arXiv:2407.07678](#).
- Greaves, J.S., Holland, W.S., Pound, M.W., 2003. Star-like activity from a very young ‘isolated planet’. *Monthly Notice of the Royal Astronomical Society* 346, 441–446. doi:[10.1046/j.1365-2966.2003.07100.x](#).
- Greene, T.P., Young, E.T., 1992. Near-Infrared Observations of Young Stellar Objects in the rho Ophiuchi Dark Cloud. *Astrophys. Journal* 395, 516. doi:[10.1086/171672](#).
- Guilloteau, S., Simon, M., Piétu, V., Di Folco, E., Dutrey, A., Prato, L., Chapillon, E., 2014. The masses of young stars: CN as a probe of dynamical masses. *Astronomy & Astrophysics* 567, A117. doi:[10.1051/0004-6361/201423765](#), [arXiv:1406.3805](#).
- Gupta, S., Jose, J., Ranjan Das, S., Guo, Z., Damian, B., Prakash, P., Ranjan Samal, M., 2024. Search for Brown Dwarfs in IC 1396 with Subaru HSC: Interpreting the Impact of Environmental Factors on Sub-stellar Population. *arXiv e-prints*, [arXiv:2402.05207](#) [arXiv:2402.05207](#).
- Gutermuth, R.A., Pipher, J.L., Megeath, S.T., Myers, P.C., Allen, L.E., Allen, T.S., 2011. A Correlation between Surface Densities of Young Stellar Objects and Gas in Eight Nearby Molecular Clouds. *Astrophys. Journal* 739, 84. doi:[10.1088/0004-637X/739/2/84](#), [arXiv:1107.0966](#).
- Guzmán Ccolque, E., Fernández López, M., Vazzano, M.M., de Gregorio, I., Plunkett, A., Santamaría-Miranda, A., 2024. Episodicity in accretion-ejection processes associated with IRAS 15398-3359. *arXiv e-prints*, [arXiv:2403.12841](#) doi:[10.48550/arXiv.2403.12841](#), [arXiv:2403.12841](#).
- Hacar, A., Socci, A., Bonanomi, F., Petry, D., Tafalla, M., Harsono, D., Forbrich, J., Alves, J., Grossschedl, J., Goicoechea, J.R., Pety, J., Burkert, A., Li, G.X., 2024. Emergence of high-mass stars in complex fiber networks (EMERGE). I. Early ALMA Survey: observations and massive data reduction. *arXiv e-prints*, [arXiv:2403.08091](#) doi:[10.48550/arXiv.2403.08091](#), [arXiv:2403.08091](#).
- Hallinan, G., Bourke, S., Lane, C., Antonova, A., Zavala, R.T., Briskin, W.F., Boyle, R.P., Vrba, F.J., Doyle, J.G., Golden, A., 2007. Periodic Bursts of Coherent Radio Emission from an Ultracool Dwarf. *Astrophys. Journal Letters* 663, L25–L28. doi:[10.1086/519790](#), [arXiv:0705.2054](#).
- Hartmann, L., 1998. Accretion Processes in Star Formation.
- Harvey, P., Merín, B., Huard, T.L., Rebull, L.M., Chapman, N., Evans, Neal J., I., Myers, P.C., 2007. The Spitzer c2d Survey of Large, Nearby, Interstellar Clouds. IX. The Serpens YSO Population as Observed with IRAC and MIPS. *Astrophys. Journal* 663, 1149–1173. doi:[10.1086/518646](#), [arXiv:0704.0009](#).
- Harvey, P.M., Fallscheer, C., Ginsburg, A., Terebey, S., André, P., Bourke, T.L., Di Francesco, J., Könyves, V., Matthews, B.C., Peterson, D.E., 2013. A First Look at the Auriga-California Giant Molecular Cloud with Herschel and the CSO: Census of the Young Stellar Objects and the Dense Gas. *Astrophys. Journal* 764, 133. doi:[10.1088/0004-637X/764/2/133](#), [arXiv:1212.6966](#).
- Harvey, P.M., Henning, T., Liu, Y., Ménard, F., Pinte, C., Wolf, S., Cieza, L.A., Evans, Neal J., I., Pascucci, I., 2012a. A Herschel Survey of Cold Dust in Disks around Brown Dwarfs and Low-mass Stars. *Astrophys. Journal* 755, 67. doi:[10.1088/0004-637X/755/1/67](#), [arXiv:1206.1161](#).
- Harvey, P.M., Henning, T., Ménard, F., Wolf, S., Liu, Y., Cieza, L.A., Evans,

- N.J., Pascucci, I., Merín, B., Pinte, C., 2012b. A Herschel Search for Cold Dust in Brown Dwarf Disks: First Results. *Astrophys. Journal Letters* 744, L1. doi:[10.1088/2041-8205/744/L1/L1](#), [arXiv:1110.4586](#).
- Hatchell, J., Fuller, G.A., Richer, J.S., Harries, T.J., Ladd, E.F., 2007. Star formation in Perseus. II. SEDs, classification, and lifetimes. *Astronomy & Astrophysics* 468, 1009–1024. doi:[10.1051/0004-6361:20066466](#), [arXiv:astro-ph/0612601](#).
- Haugbølle, T., Padoan, P., Nordlund, Å., 2018. The Stellar IMF from Isothermal MHD Turbulence. *Astrophys. Journal* 854, 35. doi:[10.3847/1538-4357/aaa432](#), [arXiv:1709.01078](#).
- Hayashi, C., Nakano, T., 1963. Evolution of Stars of Small Masses in the Pre-Main-Sequence Stages. *Progress of Theoretical Physics* 30, 460–474. doi:[10.1143/PTP.30.460](#).
- Heiderman, A., Evans, Neal J., I., 2015. The Gould Belt 'MISFITS' Survey: The Real Solar Neighborhood Protostars. *Astrophys. Journal* 806, 231. doi:[10.1088/0004-637X/806/2/231](#), [arXiv:1503.06810](#).
- Heiderman, A., Evans, Neal J., I., Allen, L.E., Huard, T., Heyer, M., 2010. The Star Formation Rate and Gas Surface Density Relation in the Milky Way: Implications for Extragalactic Studies. *Astrophys. Journal* 723, 1019–1037. doi:[10.1088/0004-637X/723/2/1019](#), [arXiv:1009.1621](#).
- Hennebelle, P., Chabrier, G., 2008. Analytical Theory for the Initial Mass Function: CO Clumps and Prestellar Cores. *Astrophys. Journal* 684, 395–410. doi:[10.1086/589916](#), [arXiv:0805.0691](#).
- Hirano, N., Ho, P.P.T., Liu, S.Y., Shang, H., Lee, C.F., Bourke, T.L., 2010. Extreme Active Molecular Jets in L1448C. *Astrophys. Journal* 717, 58–73. doi:[10.1088/0004-637X/717/1/58](#), [arXiv:1005.0703](#).
- Hirano, N., Kamazaki, T., Mikami, H., Ohashi, N., Umemoto, T., 1999. Discovery of Two Extreme Young Protostars in Barnard 1, in: Nakamoto, T. (Ed.), *Star Formation 1999*, pp. 181–182.
- Hirano, N., Liu, F., 2014. Two Extreme Young Objects in Barnard 1-b. *Astrophys. Journal* 789, 50. doi:[10.1088/0004-637X/789/1/50](#), [arXiv:1406.0068](#).
- Hsieh, T.H., Hirano, N., Belloche, A., Lee, C.F., Aso, Y., Lai, S.P., 2019a. ALMA Observations of the Protostellar Disk around the VeLLO IRAS 16253-2429. *Astrophys. Journal* 871, 100. doi:[10.3847/1538-4357/aaf4fe](#), [arXiv:1811.11651](#).
- Hsieh, T.H., Lai, S.P., 2013. Populations of Young Stellar Objects in Nearby Molecular Clouds. *Astrophysical Journal Supplement Series* 205, 5. doi:[10.1088/0067-0049/205/1/5](#), [arXiv:1301.5426](#).
- Hsieh, T.H., Lai, S.P., Belloche, A., Wyrowski, F., 2016. IRAS 16253-2429: The First Proto-brown Dwarf Binary Candidate Identified through the Dynamics of Jets. *Astrophys. Journal* 826, 68. doi:[10.3847/0004-637X/826/1/68](#), [arXiv:1605.03055](#).
- Hsieh, T.H., Murillo, N.M., Belloche, A., Hirano, N., Walsh, C., van Dishoeck, E.F., Jørgensen, J.K., Lai, S.P., 2019b. Chronology of Episodic Accretion in Protostars—An ALMA Survey of the CO and H<sub>2</sub>O Snowlines. *Astrophys. Journal* 884, 149. doi:[10.3847/1538-4357/ab425a](#), [arXiv:1909.02706](#).
- Hsieh, T.H., Murillo, N.M., Belloche, A., Hirano, N., Walsh, C., van Dishoeck, E.F., Lai, S.P., 2018. Probing Episodic Accretion in Very Low Luminosity Objects. *Astrophys. Journal* 854, 15. doi:[10.3847/1538-4357/aaa7f6](#), [arXiv:1801.04524](#).
- Huard, T.L., Myers, P.C., Murphy, D.C., Crews, L.J., Lada, C.J., Bourke, T.L., Crapsi, A., Evans, Neal J., I., McCarthy, Donald W., J., Kulesa, C., 2006. Deep Near-Infrared Observations of L1014: Revealing the Nature of the Core and Its Embedded Source. *Astrophys. Journal* 640, 391–401. doi:[10.1086/498742](#), [arXiv:astro-ph/0509302](#).
- Huélamo, N., de Gregorio-Monsalvo, I., Palau, A., Barrado, D., Bayo, A., Ruiz, M.T., Zapata, L., Bouy, H., Morata, O., Morales-Calderón, M., Eiroa, C., Ménard, F., 2017. A search for pre- and proto-brown dwarfs in the dark cloud Barnard 30 with ALMA. *Astronomy & Astrophysics* 597, A17. doi:[10.1051/0004-6361/201628510](#), [arXiv:1712.06400](#).
- Huston, M.J., Luhman, K.L., 2021. The Initial Mass Function of Low-mass Stars and Brown Dwarfs in the W3 Complex. *Astron. Journal* 161, 138. doi:[10.3847/1538-3881/abe044](#), [arXiv:2101.11497](#).
- Jeans, J.H., 1928. *Astronomy and cosmogony*.
- Johnstone, D., Wilson, C.D., Moriarty-Schieven, G., Joncas, G., Smith, G., Gregersen, E., Fich, M., 2000. Large-Area Mapping at 850 Microns. II. Analysis of the Clump Distribution in the  $\rho$  Ophiuchi Molecular Cloud. *Astrophys. Journal* 545, 327–339. doi:[10.1086/317790](#).
- Jørgensen, J.K., Bourke, T.L., Myers, P.C., Di Francesco, J., van Dishoeck, E.F., Lee, C.F., Ohashi, N., Schöier, F.L., Takakuwa, S., Wilner, D.J., Zhang, Q., 2007. PROSAC: A Submillimeter Array Survey of Low-Mass Protostars. I. Overview of Program: Envelopes, Disks, Outflows, and Hot Cores. *Astrophys. Journal* 659, 479–498. doi:[10.1086/512230](#), [arXiv:astro-ph/0701115](#).
- Jørgensen, J.K., Johnstone, D., Kirk, H., Myers, P.C., Allen, L.E., Shirley, Y.L., 2008. Current Star Formation in the Ophiuchus and Perseus Molecular Clouds: Constraints and Comparisons from Unbiased Submillimeter and Mid-Infrared Surveys. II. *Astrophys. Journal* 683, 822–843. doi:[10.1086/589956](#), [arXiv:0805.0599](#).
- Jørgensen, J.K., Visser, R., Sakai, N., Bergin, E.A., Brinch, C., Harsono, D., Lindberg, J.E., van Dishoeck, E.F., Yamamoto, S., Bisschop, S.E., Persson, M.V., 2013. A Recent Accretion Burst in the Low-mass Protostar IRAS 15398-3359: ALMA Imaging of Its Related Chemistry. *Astrophys. Journal Letters* 779, L22. doi:[10.1088/2041-8205/779/2/L22](#), [arXiv:1312.0724](#).
- Kahle, K.A., Wyrowski, F., König, C., Christensen, I.B., Tiwari, M., Menten, K.M., 2024. The effects of stellar feedback on molecular clumps in the Lagoon Nebula (M8). *Astronomy & Astrophysics* 687, A162. doi:[10.1051/0004-6361/202349009](#), [arXiv:2404.07920](#).
- Kainulainen, J., Hacar, A., Alves, J., Beuther, H., Bouy, H., Tafalla, M., 2016. Gravitational fragmentation caught in the act: the filamentary Musca molecular cloud. *Astronomy & Astrophysics* 586, A27. doi:[10.1051/0004-6361/201526017](#), [arXiv:1507.03742](#).
- Kao, M.M., Hallinan, G., Pineda, J.S., 2019. Constraints on magnetospheric radio emission from Y dwarfs. *Monthly Notice of the Royal Astronomical Society* 487, 1994–2004. doi:[10.1093/mnras/stz1372](#).
- Kao, M.M., Hallinan, G., Pineda, J.S., Escala, I., Burgasser, A., Bourke, S., Stevenson, D., 2016. Auroral Radio Emission from Late L and T Dwarfs: A New Constraint on Dynamo Theory in the Substellar Regime. *Astrophys. Journal* 818, 24. doi:[10.3847/0004-637X/818/1/24](#), [arXiv:1511.03661](#).
- Kao, M.M., Hallinan, G., Pineda, J.S., Stevenson, D., Burgasser, A., 2018. The Strongest Magnetic Fields on the Coolest Brown Dwarfs. *Astrophysical Journal Supplement Series* 237, 25. doi:[10.3847/1538-4365/aac2d5](#), [arXiv:1808.02485](#).
- Kao, M.M., Mioduszewski, A.J., Villadsen, J., Shkolnik, E.L., 2023. Resolved imaging confirms a radiation belt around an ultracool dwarf. *Nature* 619, 272–275. doi:[10.1038/s41586-023-06138-w](#), [arXiv:2302.12841](#).
- Kauffmann, J., Bertoldi, F., Bourke, T.L., Evans, N. J., I., Lee, C.W., 2008. MAMBO mapping of Spitzer c2d small clouds and cores. *Astronomy & Astrophysics* 487, 993–1017. doi:[10.1051/0004-6361:200809481](#), [arXiv:0805.4205](#).
- Kauffmann, J., Bertoldi, F., Bourke, T.L., Myers, P.C., Lee, C.W., Huard, T.L., 2011. Confirmation of the VeLLO L1148-IRS: star formation at very low (column) density. *Monthly Notice of the Royal Astronomical Society* 416, 2341–2358. doi:[10.1111/j.1365-2966.2011.19205.x](#), [arXiv:1106.2545](#).
- Kauffmann, J., Bertoldi, F., Evans, N. J., I., C2D Collaboration, 2005. Spitzer discovery of very low luminosity objects. *Astronomische Nachrichten* 326, 878–881. doi:[10.1002/asna.200310446](#), [arXiv:astro-ph/0510501](#).
- Kawabe, R., Hara, C., Nakamura, F., Saigo, K., Kamazaki, T., Shimajiri, Y., Tomida, K., Takakuwa, S., Tsuboi, Y., Machida, M.N., Di Francesco, J., Friesen, R., Hirano, N., Oasa, Y., Tamura, M., Tamura, Y., Tsukagoshi, T., Wilner, D., 2018. Extremely Dense Cores Associated with Chandra Sources in Ophiuchus A: Forming Brown Dwarfs Unveiled? *Astrophys. Journal* 866, 141. doi:[10.3847/1538-4357/aae153](#), [arXiv:1810.00573](#).
- Keown, J., Schnee, S., Bourke, T.L., Di Francesco, J., Friesen, R., Caselli, P., Myers, P., Williger, G., Tafalla, M., 2016. Infall/Expansion Velocities in the Low-mass Dense Cores L492, L694-2, and L1521F: Dependence on Position and Molecular Tracer. *Astrophys. Journal* 833, 97. doi:[10.3847/1538-4357/833/1/97](#), [arXiv:1610.01233](#).
- Kim, G., Lee, C.W., Maheswar, G., Kim, M.R., Soam, A., Saito, M., Kiyokane, K., Kim, S., 2019. CO Outflow Survey of 68 Very Low Luminosity Objects: A Search for Proto-brown-dwarf Candidates. *Astrophysical Journal Supplement Series* 240, 18. doi:[10.3847/1538-4365/aaf889](#), [arXiv:1812.08275](#).
- Kim, M.R., Lee, C.W., Dunham, M.M., Evans, Neal J., I., Kim, G., Allen, L.E., 2016. A Search for Very Low-luminosity Objects in Gould Belt Clouds. *Astrophysical Journal Supplement Series* 225, 26. doi:[10.3847/0067-0049/225/2/26](#).

- Kim, M.R., Lee, C.W., Maheswar, G., Myers, P.C., Kim, G., 2021. Gas Infalling Motions in the Envelopes of Very Low Luminosity Objects. *Astrophys. Journal* 910, 112. doi:[10.3847/1538-4357/abe4d3](https://doi.org/10.3847/1538-4357/abe4d3), [arXiv:2102.10896](https://arxiv.org/abs/2102.10896).
- Kirk, H., Dunham, M.M., Di Francesco, J., Johnstone, D., Offner, S.S.R., Sadavoy, S.I., Tobin, J.J., Arce, H.G., Bourke, T.L., Mairs, S., Myers, P.C., Pineda, J.E., Schnee, S., Shirley, Y.L., 2017. ALMA Observations of Starless Core Substructure in Ophiuchus. *Astrophys. Journal* 838, 114. doi:[10.3847/1538-4357/aa63f8](https://doi.org/10.3847/1538-4357/aa63f8), [arXiv:1703.00506](https://arxiv.org/abs/1703.00506).
- Kirk, H., Johnstone, D., Tafalla, M., 2007. Dynamics of Dense Cores in the Perseus Molecular Cloud. *Astrophys. Journal* 668, 1042–1063. doi:[10.1086/521395](https://doi.org/10.1086/521395), [arXiv:0707.2769](https://arxiv.org/abs/0707.2769).
- Kirkpatrick, J.D., Marocco, F., Gelino, C.R., Raghu, Y., Faherty, J.K., Bardalez Gagliuffi, D.C., Schurr, S.D., Apps, K., Schneider, A.C., Meisner, A.M., Kuchner, M.J., Caselden, D., Smart, R.L., Casewell, S.L., Raddi, R., Kesseli, A., Andersen, N.S., Antonini, E., Beaulieu, P., Bickle, T.P., Bilsing, M., Chieng, R., Colin, G., Deen, S., Dereveanco, A., Doll, K., Durantini Luca, H.A., Frazer, A., Gantier, J.M., Gramaize, L., Grant, K., Hamlet, L.K., Higashimura, H., Hyogo, M., Jałowiczor, P.A., Jonkeren, A., Kabatnik, M., Kiy, F., Martin, D.W., Michaels, M.N., Pendrill, W., Machado, C.P., Pumphrey, B., Rothermich, A., Russwurm, R., Sainio, A., Sanchez, J., Sapelkin-Tambling, F.T., Schümann, J., Selg-Mann, K., Singh, H., Stenner, A., Sun, G., Tanner, C., Thévenot, M., Ventura, M., Voloshin, N.V., Walla, J., Wedracki, Z., Adorno, J.I., Aganze, C., Allers, K.N., Brooks, H., Burgasser, A.J., Calamari, E., Connor, T., Costa, E., Eisenhardt, P.R., Gagné, J., Gerasimov, R., Gonzales, E.C., Hsu, C.C., Kiman, R., Li, G., Low, R., Mamajek, E., Pantoja, B.M., Popinchalk, M., Rees, J.M., Stern, D., Suárez, G., Theissen, C., Tsai, C.W., Vos, J.M., Zurek, D., Backyard Worlds: Planet 9 Collaboration, 2024. The Initial Mass Function Based on the Full-sky 20 pc Census of ~3600 Stars and Brown Dwarfs. *Astrophysical Journal Supplement Series* 271, 55. doi:[10.3847/1538-4365/ad24e2](https://doi.org/10.3847/1538-4365/ad24e2), [arXiv:2312.03639](https://arxiv.org/abs/2312.03639).
- Kirkpatrick, J.D., Martin, E.C., Smart, R.L., Cayago, A.J., Beichman, C.A., Marocco, F., Gelino, C.R., Faherty, J.K., Cushing, M.C., Schneider, A.C., Mace, G.N., Tinney, C.G., Wright, E.L., Lowrance, P.J., Ingalls, J.G., Vrba, F.J., Munn, J.A., Dahm, S.E., McLean, I.S., 2019. Preliminary Trigonometric Parallaxes of 184 Late-T and Y Dwarfs and an Analysis of the Field Substellar Mass Function into the “Planetary” Mass Regime. *Astrophysical Journal Supplement Series* 240, 19. doi:[10.3847/1538-4365/aaf6af](https://doi.org/10.3847/1538-4365/aaf6af), [arXiv:1812.01208](https://arxiv.org/abs/1812.01208).
- Klein, R., Apai, D., Pascucci, I., Henning, T., Waters, L.B.F.M., 2003. First Detection of Millimeter Dust Emission from Brown Dwarf Disks. *Astrophys. Journal Letters* 593, L57–L60. doi:[10.1086/377729](https://doi.org/10.1086/377729), [arXiv:astro-ph/0307076](https://arxiv.org/abs/astro-ph/0307076).
- Könyves, V., André, P., Men'shchikov, A., Palmeirim, P., Arzoumanian, D., Schneider, N., Roy, A., Didelon, P., Maury, A., Shimajiri, Y., Di Francesco, J., Bontemps, S., Peretto, N., Benedettini, M., Bernard, J.P., Elia, D., Grifin, M.J., Hill, T., Kirk, J., Ladjelate, B., Marsh, K., Martin, P.G., Motte, F., Nguyễn Luong, Q., Pezzuto, S., Roussel, H., Rygl, K.L.J., Sadavoy, S.I., Schisano, E., Spinoglio, L., Ward-Thompson, D., White, G.J., 2015. A census of dense cores in the Aquila cloud complex: SPIRE/PACS observations from the Herschel Gould Belt survey. *Astronomy & Astrophysics* 584, A91. doi:[10.1051/0004-6361/201525861](https://doi.org/10.1051/0004-6361/201525861), [arXiv:1507.05926](https://arxiv.org/abs/1507.05926).
- Kratter, K., Lodato, G., 2016. Gravitational Instabilities in Circumstellar Disks. *Annual Review of Astron and Astrophys* 54, 271–311. doi:[10.1146/annurev-astro-081915-023307](https://doi.org/10.1146/annurev-astro-081915-023307), [arXiv:1603.01280](https://arxiv.org/abs/1603.01280).
- Kulterer, B.M., Wampfler, S.F., Ligterink, N.F.W., Murillo, N., Hsieh, T.H., McClure, M.K., Boogert, A., Kipfer, K., Bjerkeli, P., Drozdovskaya, M.N., 2024. Post-Outburst Chemistry in a Very Low-Luminosity Object: Peculiar High Abundance of Nitric Oxide. *arXiv e-prints*, [arXiv:2409.04575](https://arxiv.org/abs/2409.04575)doi:[10.48550/arXiv.2409.04575](https://doi.org/10.48550/arXiv.2409.04575).
- Kumar, S.S., 1963. The Structure of Stars of Very Low Mass. *Astrophys. Journal* 137, 1121. doi:[10.1086/147589](https://doi.org/10.1086/147589).
- Kuruwita, R., Tychoniec, Ł., Federrath, C., 2024. Star Formation. *arXiv e-prints*, [arXiv:2409.03371](https://arxiv.org/abs/2409.03371)doi:[10.48550/arXiv.2409.03371](https://doi.org/10.48550/arXiv.2409.03371), [arXiv:2409.03371](https://arxiv.org/abs/2409.03371).
- Lada, C.J., 1987. Star formation: from OB associations to protostars., in: Peimbert, M., Jugaku, J. (Eds.), *Star Forming Regions*, p. 1.
- Lada, C.J., Lombardi, M., Alves, J.F., 2010. On the Star Formation Rates in Molecular Clouds. *Astrophys. Journal* 724, 687–693. doi:[10.1088/0004-637X/724/1/687](https://doi.org/10.1088/0004-637X/724/1/687), [arXiv:1009.2985](https://arxiv.org/abs/1009.2985).
- Ladjelate, B., André, P., Könyves, V., Ward-Thompson, D., Men'shchikov, A., Bracco, A., Palmeirim, P., Roy, A., Shimajiri, Y., Kirk, J.M., Arzoumanian, D., Benedettini, M., Di Francesco, J., Fiorellino, E., Schneider, N., Pezzuto, S., Motte, F., Herschel Gould Belt Survey Team, 2020. The Herschel view of the dense core population in the Ophiuchus molecular cloud. *Astronomy & Astrophysics* 638, A74. doi:[10.1051/0004-6361/201936442](https://doi.org/10.1051/0004-6361/201936442), [arXiv:2001.11036](https://arxiv.org/abs/2001.11036).
- Langeveld, A.B., Scholz, A., Mužić, K., Jayawardhana, R., Capela, D., Albert, L., Doyon, R., Flagg, L., de Furio, M., Johnstone, D., Lafrèniere, D., Meyer, M., 2024. The JWST/NIRISS Deep Spectroscopic Survey for Young Brown Dwarfs and Free-floating Planets. *Astron. Journal* 168, 179. doi:[10.3847/1538-3881/ad6f0c](https://doi.org/10.3847/1538-3881/ad6f0c), [arXiv:2408.12639](https://arxiv.org/abs/2408.12639).
- Larson, R.B., 1969. Numerical calculations of the dynamics of collapsing proto-star. *Monthly Notice of the Royal Astronomical Society* 145, 271. doi:[10.1093/mnras/145.3.271](https://doi.org/10.1093/mnras/145.3.271).
- Lê, N., Tram, L.N., Karska, A., Hoang, T., Diep, P.N., Hanasz, M., Ngoc, N.B., Phuong, N.T., Menten, K.M., Wyrowski, F., Nguyen, D.D., Hoang, T.D., Khang, N.M., 2024. Mapping and characterizing magnetic fields in the Rho Ophiuchus-A molecular cloud with SOFIA/HAWC+. *Astronomy & Astrophysics* 690, A191. doi:[10.1051/0004-6361/202348008](https://doi.org/10.1051/0004-6361/202348008), [arXiv:2408.17122](https://arxiv.org/abs/2408.17122).
- Lecavelier des Etangs, A., Lissauer, J.J., 2022. The IAU working definition of an exoplanet. *New Astronomy Review* 94, 101641. doi:[10.1016/j.newar.2022.101641](https://doi.org/10.1016/j.newar.2022.101641), [arXiv:2203.09520](https://arxiv.org/abs/2203.09520).
- Lee, C.F., Li, Z.Y., Hirano, N., Shang, H., Ho, P.T.P., Zhang, Q., 2018a. ALMA Observations of the Very Young Class 0 Protostellar System HH211-mm: A 30 au Dusty Disk with a Disk Wind Traced by SO? *Astrophys. Journal* 863, 94. doi:[10.3847/1538-4357/aad2da](https://doi.org/10.3847/1538-4357/aad2da), [arXiv:1807.05336](https://arxiv.org/abs/1807.05336).
- Lee, C.W., Bourke, T.L., Myers, P.C., Dunham, M., Evans, N., Lee, Y., Huard, T., Wu, J., Gutermuth, R., Kim, M.R., Kang, H.W., 2009. The Spitzer c2d Survey of Nearby Dense Cores. V. Discovery of a VeLLO in the “Starless” Dense Core L328. *Astrophys. Journal* 693, 1290–1299. doi:[10.1088/0004-637X/693/2/1290](https://doi.org/10.1088/0004-637X/693/2/1290), [arXiv:0812.2012](https://arxiv.org/abs/0812.2012).
- Lee, C.W., Kim, G., Myers, P.C., Saito, M., Kim, S., Kwon, W., Lyo, A.R., Soam, A., Kim, M.R., 2018b. High-resolution ALMA Study of the Proto-brown-dwarf Candidate L328-IRS. *Astrophys. Journal* 865, 131. doi:[10.3847/1538-4357/aadcf6](https://doi.org/10.3847/1538-4357/aadcf6), [arXiv:1809.10466](https://arxiv.org/abs/1809.10466).
- Lee, C.W., Kim, M.R., Kim, G., Saito, M., Myers, P.C., Kuroono, Y., 2013. Early Star-forming Processes in Dense Molecular Cloud L328; Identification of L328-IRS as a Proto-brown Dwarf. *Astrophys. Journal* 777, 50. doi:[10.1088/0004-637X/777/1/50](https://doi.org/10.1088/0004-637X/777/1/50).
- Lee, J.E., 2007. Chemical Evolution in VeLLOs. *Journal of Korean Astronomical Society* 40, 83–89. doi:[10.5303/JKAS.2007.40.4.083](https://doi.org/10.5303/JKAS.2007.40.4.083), [arXiv:0712.1866](https://arxiv.org/abs/0712.1866).
- Lee, J.E., Lee, S., Dunham, M.M., Tatematsu, K., Choi, M., Bergin, E.A., Evans, N.J., 2017. Formation of wide binaries by turbulent fragmentation. *Nature Astronomy* 1, 0172. doi:[10.1038/s41550-017-0172](https://doi.org/10.1038/s41550-017-0172), [arXiv:1707.00233](https://arxiv.org/abs/1707.00233).
- Li, J., Jiang, B., Zhao, H., Chen, X., Yang, Y., 2024. Spatial Variations of Dust Opacity and Grain Growth in Dark Clouds: L1689, L1709 and L1712. *arXiv e-prints*, [arXiv:2402.10431](https://arxiv.org/abs/2402.10431)[arXiv:2402.10431](https://arxiv.org/abs/2402.10431).
- Lin, Z.Y.D., Lee, C.F., Li, Z.Y., Tobin, J.J., Turner, N.J., 2021. Inferring (sub)millimetre dust opacities and temperature structure in edge-on protostellar discs from resolved multiwavelength continuum observations: the case of the HH 212 disc. *Monthly Notice of the Royal Astronomical Society* 501, 1316–1335. doi:[10.1093/mnras/staa3685](https://doi.org/10.1093/mnras/staa3685), [arXiv:2008.08627](https://arxiv.org/abs/2008.08627).
- Liu, T., Zhang, Q., Kim, K.T., Wu, Y., Lee, C.W., Lee, J.E., Tatematsu, K., Choi, M., Juvela, M., Thompson, M., Goldsmith, P.F., Liu, S.Y., Naomi, H., Koch, P., Henkel, C., Sanhueza, P., He, J., Rivera-Ingraham, A., Wang, K., Cunningham, M.R., Tang, Y.W., Lai, S.P., Yuan, J., Li, D., Fuller, G., Kang, M., Nguyen Luong, Q., Liu, H.B., Ristorcelli, I., Yang, J., Xu, Y., Hirota, T., Mardones, D., Qin, S.L., Chen, H.R., Kwon, W., Meng, F., Zhang, H., Kim, M.R., Yi, H.W., 2016. Planck Cold Clumps in the  $\lambda$  Orionis Complex. I. Discovery of an Extremely Young Class 0 Protostellar Object and a Proto-brown Dwarf Candidate in the Bright-rimmed Clump PGCC G192.32-11.88. *Astrophysical Journal Supplement Series* 222, 7. doi:[10.3847/0067-0049/222/1/7](https://doi.org/10.3847/0067-0049/222/1/7), [arXiv:1511.09121](https://arxiv.org/abs/1511.09121).
- Lodieu, N., Hambly, N.C., Jameson, R.F., Hodgkin, S.T., Carraro, G., Kendall, T.R., 2007. New brown dwarfs in Upper Sco using UKIDSS Galactic Cluster Survey science verification data. *Monthly Notice of the Royal Astronomical Society* 374, 372–384. doi:[10.1111/j.1365-2966.2006.11151.x](https://doi.org/10.1111/j.1365-2966.2006.11151.x).



[arXiv:astro-ph/0610140](https://arxiv.org/abs/astro-ph/0610140).

- Lomax, O., Whitworth, A.P., Hubber, D.A., 2016. Forming isolated brown dwarfs by turbulent fragmentation. *Monthly Notice of the Royal Astronomical Society* 458, 1242–1252. doi:[10.1093/mnras/stw406](https://doi.org/10.1093/mnras/stw406), [arXiv:1602.05789](https://arxiv.org/abs/1602.05789).
- Luhman, K.L., Allen, P.R., Espaillat, C., Hartmann, L., Calvet, N., 2010. The Disk Population of the Taurus Star-Forming Region. *Astrophysical Journal Supplement Series* 186, 111–174. doi:[10.1088/0067-0049/186/1/111](https://doi.org/10.1088/0067-0049/186/1/111), [arXiv:0911.5457](https://arxiv.org/abs/0911.5457).
- Machida, M.N., Inutsuka, S.i., Matsumoto, T., 2009. First Direct Simulation of Brown Dwarf Formation in a Compact Cloud Core. *Astrophys. Journal Letters* 699, L157–L160. doi:[10.1088/0004-637X/699/2/L157](https://doi.org/10.1088/0004-637X/699/2/L157), [arXiv:0907.3255](https://arxiv.org/abs/0907.3255).
- Magnani, L., Blitz, L., Mundy, L., 1985. Molecular gas at high galactic latitudes. *Astrophys. Journal* 295, 402–421. doi:[10.1086/163385](https://doi.org/10.1086/163385).
- Maret, S., Bergin, E.A., Tafalla, M., 2013. Chemical modeling of the L1498 and L1517B prestellar cores: CO and HCO<sup>+</sup> depletion. *Astronomy & Astrophysics* 559, A53. doi:[10.1051/0004-6361/201322089](https://doi.org/10.1051/0004-6361/201322089), [arXiv:1309.4988](https://arxiv.org/abs/1309.4988).
- Maret, S., Maury, A.J., Belloche, A., Gaudel, M., André, P., Cabrit, S., Codella, C., Lefèvre, C., Podio, L., Anderl, S., Gueth, F., Hennebelle, P., 2020. Searching for kinematic evidence of Keplerian disks around Class 0 protostars with CALYPSO. *Astronomy & Astrophysics* 635, A15. doi:[10.1051/0004-6361/201936798](https://doi.org/10.1051/0004-6361/201936798), [arXiv:2001.06355](https://arxiv.org/abs/2001.06355).
- Marsh, K.A., Kirk, J.M., André, P., Griffin, M.J., Könyves, V., Palmeirim, P., Men'shchikov, A., Ward-Thompson, D., Benedettini, M., Bresnahan, D.W., di Francesco, J., Elia, D., Motte, F., Peretto, N., Pezzuto, S., Roy, A., Sadavoy, S., Schneider, N., Spinoglio, L., White, G.J., 2016. A census of dense cores in the Taurus L1495 cloud from the Herschel. *Monthly Notice of the Royal Astronomical Society* 459, 342–356. doi:[10.1093/mnras/stw301](https://doi.org/10.1093/mnras/stw301), [arXiv:1602.03143](https://arxiv.org/abs/1602.03143).
- Martín, E.L., Barrado y Navascués, D., Baraffe, I., Bouy, H., Dahm, S., 2003. A Hubble Space Telescope Wide Field Planetary Camera 2 Survey for Brown Dwarf Binaries in the  $\alpha$  Persei and Pleiades Open Clusters. *Astrophys. Journal* 594, 525–532. doi:[10.1086/376938](https://doi.org/10.1086/376938), [arXiv:astro-ph/0305316](https://arxiv.org/abs/astro-ph/0305316).
- Martín, E.L., Žerjal, M., Bouy, H., Martín-González, D., Muñiz Torres, S., Barrado, D., Olivares, J., Pérez-Garrido, A., Mas-Buitrago, P., Cruz, P., Solano, E., Zapatero Osorio, M.R., Lodieu, N., Béjar, V.J.S., Zhang, J.Y., del Burgo, C., Huélamo, N., Laureijs, R., Mora, A., Saifollahi, T., Cuillandre, J.C., Schirmer, M., Tata, R., Points, S., Phan-Bao, N., Goldman, B., Casewell, S.L., Reylé, C., Smart, R.L., Aghanim, N., Altieri, B., Andreon, S., Auricchio, N., Baldi, M., Balestra, A., Bardelli, S., Basset, A., Bender, R., Bonino, D., Branchini, E., Brescia, M., Brinchmann, J., Camera, S., Capobianco, V., Carbone, C., Carretero, J., Casas, S., Castellano, M., Cavuoti, S., Cimatti, A., Congedo, G., Conselice, C.J., Conversi, L., Copin, Y., Corcione, L., Courbin, F., Courtois, H.M., Cropper, M., Da Silva, A., Degaudenzi, H., Di Giorgio, A.M., Dinis, J., Dubath, F., Dupac, X., Dusini, S., Ealet, A., Farina, M., Farrens, S., Ferriol, S., Fosalba, P., Frailis, M., Franceschi, E., Fumana, M., Galeotta, S., Garilli, B., Gillard, W., Gillis, B., Giocoli, C., Gómez-Alvarez, P., Grazian, A., Grupp, F., Guzzo, L., Haugan, S.V.H., Hoar, J., Hoekstra, H., Holmes, W., Hook, I., Hormuth, F., Hornstrup, A., Hu, D., Hudelot, P., Jahnke, K., Jhabvala, M., Keihänen, E., Kermiche, S., Kiessling, A., Kilbinger, M., Kitching, T., Kohley, R., Kubik, B., Kümmel, M., Kunz, M., Kurki-Suonio, H., Le Mignant, D., Ligi, S., Lilje, P.B., Lindholm, V., Lloro, I., Maino, D., Maiorano, E., Mansutti, O., Marggraf, O., Martinet, N., Marulli, F., Massey, R., Medinaceli, E., Mei, S., Melchior, M., Mellier, Y., Meneghetti, M., Meylan, G., Mohr, J.J., Moresco, M., Moscardini, L., Niemi, S.M., Padilla, C., Paltani, S., Pasian, F., Pedersen, K., Percival, W.J., Pettorino, V., Pires, S., Polenta, G., Poncet, M., Popa, L.A., Pozzetti, L., Racca, G.D., Raison, F., Rebolo, R., Renzi, A., Rhodes, J., Riccio, G., Rix, H.W., Romelli, E., Roncarelli, M., Rossetti, E., Saglia, R., Sapone, D., Sartoris, B., Sauvage, M., Scaramella, R., Schneider, P., Secroun, A., Seidel, G., Seiffert, M., Serrano, S., Sirignano, C., Sirri, G., Stanco, L., Tallada-Crespí, P., Taylor, A.N., Tepitz, H.I., Tereno, I., Toledo-Moreo, R., Tsygarnov, A., Tutusaus, I., Valenziano, L., Vassallo, T., Verdoes Kleijn, G., Wang, Y., Weller, J., Williams, O.R., Zucca, E., Baccigalupi, C., Willis, G., Simon, P., Martín-Fleitas, J., Scott, D., 2024. Euclid: Early Release Observations – A glance at free-floating new-born planets in the sigma Orionis cluster. *arXiv e-prints*, [arXiv:2405.13497](https://arxiv.org/abs/2405.13497)doi:[10.48550/arXiv.2405.13497](https://doi.org/10.48550/arXiv.2405.13497), [arXiv:2405.13497](https://arxiv.org/abs/2405.13497).
- Maureira, M.J., Arce, H.G., Dunham, M.M., Mardones, D., Guzmán, A.E., Pineda, J.E., Bourke, T.L., 2020. ALMA observations of envelopes around first hydrostatic core candidates. *Monthly Notice of the Royal Astronomical Society* 499, 4394–4417. doi:[10.1093/mnras/staa2894](https://doi.org/10.1093/mnras/staa2894), [arXiv:2009.08740](https://arxiv.org/abs/2009.08740).
- Maury, A.J., André, P., Testi, L., Maret, S., Belloche, A., Hennebelle, P., Cabrit, S., Codella, C., Gueth, F., Podio, L., Anderl, S., Bacmann, A., Bontemps, S., Gaudel, M., Ladjelate, B., Lefèvre, C., Tabone, B., Lefloch, B., 2019. Characterizing young protostellar disks with the CALYPSO IRAM-PdBI survey: large Class 0 disks are rare. *Astronomy & Astrophysics* 621, A76. doi:[10.1051/0004-6361/201833537](https://doi.org/10.1051/0004-6361/201833537), [arXiv:1810.11221](https://arxiv.org/abs/1810.11221).
- McCaughrean, M.J., Pearson, S.G., 2023. A JWST survey of the Trapezium Cluster & inner Orion Nebula. I. Observations & overview. *arXiv e-prints*, [arXiv:2310.03552](https://arxiv.org/abs/2310.03552)doi:[10.48550/arXiv.2310.03552](https://doi.org/10.48550/arXiv.2310.03552), [arXiv:2310.03552](https://arxiv.org/abs/2310.03552).
- Megeath, S.T., Gutermuth, R., Muzerolle, J., Kryukova, E., Flaherty, K., Hora, J.L., Allen, L.E., Hartmann, L., Myers, P.C., Pipher, J.L., Stauffer, J., Young, E.T., Fazio, G.G., 2012. The Spitzer Space Telescope Survey of the Orion A and B Molecular Clouds. I. A Census of Dusty Young Stellar Objects and a Study of Their Mid-infrared Variability. *Astron. Journal* 144, 192. doi:[10.1088/0004-6256/144/6/192](https://doi.org/10.1088/0004-6256/144/6/192), [arXiv:1209.3826](https://arxiv.org/abs/1209.3826).
- Miret-Roig, N., 2023. The origin of free-floating planets. *arXiv e-prints*, [arXiv:2303.05522](https://arxiv.org/abs/2303.05522)arXiv:2303.05522.
- Miret-Roig, N., Bouy, H., Raymond, S.N., Tamura, M., Bertin, E., Barrado, D., Olivares, J., Galli, P.A.B., Cuillandre, J.C., Sarro, L.M., Berihuete, A., Huélamo, N., 2022. A rich population of free-floating planets in the Upper Scorpius young stellar association. *Nature Astronomy* 6, 89–97. doi:[10.1038/s41550-021-01513-x](https://doi.org/10.1038/s41550-021-01513-x), [arXiv:2112.11999](https://arxiv.org/abs/2112.11999).
- Morata, O., Palau, A., González, R.F., de Gregorio-Monsalvo, I., Ribas, Á., Perger, M., Bouy, H., Barrado, D., Eiroa, C., Bayo, A., Huélamo, N., Morales-Calderón, M., Rodríguez, L.F., 2015. First Detection of Thermal Radiojets in a Sample of Proto-brown Dwarf Candidates. *Astrophys. Journal* 807, 55. doi:[10.1088/0004-637X/807/1/55](https://doi.org/10.1088/0004-637X/807/1/55), [arXiv:1505.07586](https://arxiv.org/abs/1505.07586).
- Moraux, E., Bouvier, J., Stauffer, J.R., Barrado y Navascués, D., Cuillandre, J.C., 2007. The lower mass function of the young open cluster Blanco 1: from 30  $M_{Jup}$  to 3  $M_{\odot}$ . *Astronomy & Astrophysics* 471, 499–513. doi:[10.1051/0004-6361/20066308](https://doi.org/10.1051/0004-6361/20066308), [arXiv:0706.2102](https://arxiv.org/abs/0706.2102).
- Moraux, E., Bouvier, J., Stauffer, J.R., Cuillandre, J.C., 2003. Brown dwarfs in the Pleiades cluster: Clues to the substellar mass function. *Astronomy & Astrophysics* 400, 891–902. doi:[10.1051/0004-6361:20021903](https://doi.org/10.1051/0004-6361:20021903), [arXiv:astro-ph/0212571](https://arxiv.org/abs/astro-ph/0212571).
- Morii, K., Sanhueza, P., Zhang, Q., Nakamura, F., Li, S., Sabatini, G., Olguin, F.A., Beuther, H., Tafuya, D., Izumi, N., Tatematsu, K., Sakai, T., 2024. The ALMA Survey of 70  $\mu$ m Dark High-mass Clumps in Early Stages (ASHES). XI. Statistical Study of Early Fragmentation. *arXiv e-prints*, [arXiv:2403.07058](https://arxiv.org/abs/2403.07058)doi:[10.48550/arXiv.2403.07058](https://doi.org/10.48550/arXiv.2403.07058), [arXiv:2403.07058](https://arxiv.org/abs/2403.07058).
- Motte, F., André, P., 2001. The circumstellar environment of low-mass protostars: A millimeter continuum mapping survey. *Astronomy & Astrophysics* 365, 440–464. doi:[10.1051/0004-6361:20000072](https://doi.org/10.1051/0004-6361:20000072).
- Motte, F., André, P., Neri, R., 1998. The initial conditions of star formation in the rho Ophiuchi main cloud: wide-field millimeter continuum mapping. *Astronomy & Astrophysics* 336, 150–172.
- Mowat, C., Hatchell, J., Rumble, D., Kirk, H., Buckle, J., Berry, D.S., Broekhoven-Fiene, H., Currie, M.J., Jenness, T., Johnstone, D., Mottram, J.C., Pattle, K., Tisi, S., Di Francesco, J., Hogerheijde, M.R., Ward-Thompson, D., Bastien, P., Bresnahan, D., Butner, H., Chen, M., Chrysostomou, A., Coudé, S., Davis, C.J., Drabek-Mauder, E., Duarte-Cabral, A., Fich, M., Fiege, J., Friberg, P., Friesen, R., Fuller, G.A., Graves, S., Greaves, J., Holland, W., Joncas, G., Kirk, J.M., Knee, L.B.G., Mairs, S., Marsh, K., Matthews, B.C., Moriarty-Schieven, G., Rawlings, J., Retter, B., Richer, J., Robertson, D., Rosolowsky, E., Sadavoy, S., Thomas, H., Tothill, N., Viti, S., White, G.J., Wouterloot, J., Yates, J., Zhu, M., 2017. The JCMT Gould Belt Survey: A First Look at SCUBA-2 Observations of the Lupus I Molecular Cloud. *Monthly Notice of the Royal Astronomical Society* 467, 812–835. doi:[10.1093/mnras/stx042](https://doi.org/10.1093/mnras/stx042).
- Mužić, K., Scholz, A., Peña Ramírez, K., Jayawardhana, R., Schödel, R., Geers, V.C., Cieza, L.A., Bayo, A., 2019. Looking Deep into the Rosette Nebula's Heart: The (Sub)stellar Content of the Massive Young Cluster NGC 2244. *Astrophys. Journal* 881, 79. doi:[10.3847/1538-4357/ab2da4](https://doi.org/10.3847/1538-4357/ab2da4), [arXiv:1907.00617](https://arxiv.org/abs/1907.00617).



- Muzerolle, J., Luhman, K.L., Briceño, C., Hartmann, L., Calvet, N., 2005. Measuring Accretion in Young Substellar Objects: Approaching the Planetary Mass Regime. *Astrophys. Journal* 625, 906–912. doi:[10.1086/429483](#), [arXiv:astro-ph/0502023](#).
- Myers, P.C., Fuller, G.A., Mathieu, R.D., Beichman, C.A., Benson, P.J., Schild, R.E., Emerson, J.P., 1987. Near-Infrared and Optical Observations of IRAS Sources in and near Dense Cores. *Astrophys. Journal* 319, 340. doi:[10.1086/165458](#).
- Myers, P.C., Ladd, E.F., 1993. Bolometric Temperatures of Young Stellar Objects. *Astrophys. Journal Letters* 413, L47. doi:[10.1086/186956](#).
- Nakajima, T., Oppenheimer, B.R., Kulkarni, S.R., Golimowski, D.A., Matthews, K., Durrance, S.T., 1995. Discovery of a cool brown dwarf. *Nature* 378, 463–465. doi:[10.1038/378463a0](#).
- Nakamura, F., Takakuwa, S., Kawabe, R., 2012. Substellar-mass Condensations in Prestellar Cores. *Astrophys. Journal Letters* 758, L25. doi:[10.1088/2041-8205/758/2/L25](#), [arXiv:1209.3801](#).
- Natta, A., Testi, L., Comerón, F., Oliva, E., D’Antona, F., Baffa, C., Comoretto, G., Gennari, S., 2002. Exploring brown dwarf disks in rho Ophiuchi. *Astronomy & Astrophysics* 393, 597–609. doi:[10.1051/0004-6361:20021065](#), [arXiv:astro-ph/0207463](#).
- Oasa, Y., Tamura, M., Sunada, K., Sugitani, K., 2008. Luminosity and Mass Functions at the Very Low Mass Side in NGC 1333. *Astron. Journal* 136, 1372–1387. doi:[10.1088/0004-6256/136/3/1372](#).
- Offner, S.S.R., Moe, M., Kratter, K.M., Sadavoy, S.I., Jensen, E.L.N., Tobin, J.J., 2023. The Origin and Evolution of Multiple Star Systems, in: Inutsuka, S., Aikawa, Y., Muto, T., Tomida, K., Tamura, M. (Eds.), *Protostars and Planets VII*, p. 275. doi:[10.48550/arXiv.2203.10066](#), [arXiv:2203.10066](#).
- Okoda, Y., Oya, Y., Francis, L., Johnstone, D., Ceccarelli, C., Codella, C., Chandler, C.J., Sakai, N., Aikawa, Y., Alves, F.O., Herbst, E., Maureira, M.J., Bouvier, M., Caselli, P., Choudhury, S., De Simone, M., Jiménez-Serra, I., Pineda, J., Yamamoto, S., 2023. FAUST. VII. Detection of a Hot Corino in the Prototypical Warm Carbon-chain Chemistry Source IRAS 15398-3359. *Astrophys. Journal* 948, 127. doi:[10.3847/1538-4357/acc1e5](#), [arXiv:2303.03564](#).
- Okoda, Y., Oya, Y., Francis, L., Johnstone, D., Inutsuka, S.I., Ceccarelli, C., Codella, C., Chandler, C., Sakai, N., Aikawa, Y., Alves, F.O., Balucani, N., Bianchi, E., Bouvier, M., Caselli, P., Caux, E., Charnley, S., Choudhury, S., De Simone, M., Dulieu, F., Durán, A., Evans, L., Favre, C., Fedele, D., Feng, S., Fontani, F., Hama, T., Hanawa, T., Herbst, E., Hirota, T., Imai, M., Isella, A., Jiménez-Serra, I., Kahane, B., Lefloch, B., Loinard, L., López-Sepulcre, A., Maud, L.T., Maureira, M.J., Menard, F., Mercimek, S., Miotello, A., Moellenbrock, G., Mori, S., Murillo, N.M., Nakatani, R., Nomura, H., Oba, Y., O’Donoghue, R., Ohashi, S., Ospina-Zamudio, J., Pineda, J.E., Podio, L., Rimola, A., Sakai, T., Segura-Cox, D., Shirley, Y., Svoboda, B., Taquet, V., Testi, L., Vastel, C., Viti, S., Watanabe, N., Watanabe, Y., Witzel, A., Xue, C., Zhang, Y., Zhao, B., Yamamoto, S., 2021. FAUST. II. Discovery of a Secondary Outflow in IRAS 15398-3359: Variability in Outflow Direction during the Earliest Stage of Star Formation? *Astrophys. Journal* 910, 11. doi:[10.3847/1538-4357/abddb1](#), [arXiv:2101.07404](#).
- Okoda, Y., Oya, Y., Sakai, N., Watanabe, Y., Jørgensen, J.K., Van Dishoeck, E.F., Yamamoto, S., 2018. The Co-evolution of Disks and Stars in Embedded Stages: The Case of the Very-low-mass Protostar IRAS 15398-3359. *Astrophys. Journal Letters* 864, L25. doi:[10.3847/2041-8213/aad8ba](#), [arXiv:1809.00500](#).
- Oppenheimer, B.R., Kulkarni, S.R., Matthews, K., Nakajima, T., 1995. Infrared Spectrum of the Cool Brown Dwarf Gl 229B. *Science* 270, 1478–1479. doi:[10.1126/science.270.5241.1478](#).
- Ortiz-León, G.N., Dzib, S.A., Loinard, L., Gong, Y., Pillai, T., Plunkett, A., 2023. The distance to the Serpens South cluster from H<sub>2</sub>O masers. *Astronomy & Astrophysics* 673, L1. doi:[10.1051/0004-6361/202346369](#), [arXiv:2304.07270](#).
- Ortiz-León, G.N., Loinard, L., Dzib, S.A., Galli, P.A.B., Kounkel, M., Mioduszewski, A.J., Rodríguez, L.F., Torres, R.M., Hartmann, L., Boden, A.F., Evans, Neal J., I., Briceño, C., Tobin, J.J., 2018. The Gould’s Belt Distances Survey (GOBELINS). V. Distances and Kinematics of the Perseus Molecular Cloud. *Astrophys. Journal* 865, 73. doi:[10.3847/1538-4357/aada49](#), [arXiv:1808.03499](#).
- Ossenkopf, V., Henning, T., 1994. Dust opacities for protostellar cores. *Astronomy & Astrophysics* 291, 943–959.
- Oya, Y., Sakai, N., Sakai, T., Watanabe, Y., Hirota, T., Lindberg, J.E., Bisschop, S.E., Jørgensen, J.K., van Dishoeck, E.F., Yamamoto, S., 2014. A Substellar-mass Protostar and its Outflow of IRAS 15398-3359 Revealed by Subarcsecond-resolution Observations of H<sub>2</sub>CO and CCH. *Astrophys. Journal* 795, 152. doi:[10.1088/0004-637X/795/2/152](#), [arXiv:1410.5945](#).
- Padoan, P., Nordlund, Å., 2002. The Stellar Initial Mass Function from Turbulent Fragmentation. *Astrophys. Journal* 576, 870–879. doi:[10.1086/341790](#), [arXiv:astro-ph/0011465](#).
- Padoan, P., Nordlund, Å., 2004. The “Mysterious” Origin of Brown Dwarfs. *Astrophys. Journal* 617, 559–564. doi:[10.1086/345413](#), [arXiv:astro-ph/0205019](#).
- Pagani, L., Ristorcelli, I., Boudet, N., Giard, M., Abergel, A., Bernard, J.P., 2010. L1506: a prestellar core in the making. *Astronomy & Astrophysics* 512, A3. doi:[10.1051/0004-6361/200912859](#), [arXiv:0912.1193](#).
- Palau, A., Ballesteros-Paredes, J., Vázquez-Semadeni, E., Sánchez-Monge, Á., Estalella, R., Fall, S.M., Zapata, L.A., Camacho, V., Gómez, L., Naranjo-Romero, R., Busquet, G., Fontani, F., 2015. Gravity or turbulence? - III. Evidence of pure thermal Jeans fragmentation at ~0.1 pc scale. *Monthly Notice of the Royal Astronomical Society* 453, 3785–3797. doi:[10.1093/mnras/stv1834](#), [arXiv:1504.07644](#).
- Palau, A., de Gregorio-Monsalvo, I., Morata, Ò., Stamatellos, D., Huélamo, N., Eiroa, C., Bayo, A., Morales-Calderón, M., Bouy, H., Ribas, Á., Asmus, D., Barrado, D., 2012. A search for pre-substellar cores and proto-brown dwarf candidates in Taurus: multiwavelength analysis in the B213-L1495 clouds. *Monthly Notice of the Royal Astronomical Society* 424, 2778–2791. doi:[10.1111/j.1365-2966.2012.21390.x](#), [arXiv:1205.5722](#).
- Palau, A., Durán-García, M., Fernández-López, M., Zapata, L.A., Morata, O., de Gregorio-Monsalvo, I., Barrado, D., Huélamo, N., Bayo, A., Ruiz, M.T., Bouy, H., Ribas, A., Morales-Calderon, M., Rodríguez, L.F., 2022. Confirmation of the proto-brown dwarf SSB213-J041757B and discovery of a nearby new candidate with ALMA and CARMA, in: *The 21st Cambridge Workshop on Cool Stars, Stellar Systems, and the Sun*, p. 204. doi:[10.5281/zenodo.7593206](#).
- Palau, A., Fuente, A., Girart, J.M., Estalella, R., Ho, P.T.P., Sánchez-Monge, Á., Fontani, F., Busquet, G., Commerçon, B., Hennebelle, P., Boissier, J., Zhang, Q., Cesaroni, R., Zapata, L.A., 2013. Early Stages of Cluster Formation: Fragmentation of Massive Dense Cores down to ~1000 AU. *Astrophys. Journal* 762, 120. doi:[10.1088/0004-637X/762/2/120](#), [arXiv:1211.2666](#).
- Palau, A., Ho, P.T.P., Zhang, Q., Estalella, R., Hirano, N., Shang, H., Lee, C.F., Bourke, T.L., Beuther, H., Kuan, Y.J., 2006. Submillimeter Emission from the Hot Molecular Jet HH 211. *Astrophys. Journal Letters* 636, L137–L140. doi:[10.1086/500242](#), [arXiv:astro-ph/0512306](#).
- Palau, A., Sánchez-Monge, Á., Busquet, G., Estalella, R., Zhang, Q., Ho, P.T.P., Beltrán, M.T., Beuther, H., 2010. Three intermediate-mass young stellar objects with different properties emerging from the same natal cloud in IRAS 00117+6412. *Astronomy & Astrophysics* 510, A5. doi:[10.1051/0004-6361/200913215](#), [arXiv:0911.4072](#).
- Palau, A., Zapata, L.A., Rodríguez, L.F., Bouy, H., Barrado, D., Morales-Calderón, M., Myers, P.C., Chapman, N., Juárez, C., Li, D., 2014. IC 348-SMM2E: a Class 0 proto-brown dwarf candidate forming as a scaled-down version of low-mass stars. *Monthly Notice of the Royal Astronomical Society* 444, 833–845. doi:[10.1093/mnras/stu1461](#), [arXiv:1407.7764](#).
- Palau, A., Zhang, Q., Girart, J.M., Liu, J., Rao, R., Koch, P.M., Estalella, R., Chen, H.T.V., Liu, H.B., Qiu, K., Li, Z.Y., Zapata, L.A., Bontemps, S., Ho, P.T.P., Beuther, H., King, T.C., Shinnaga, H., Ahmadi, A., 2021. Does the Magnetic Field Suppress Fragmentation in Massive Dense Cores? *Astrophys. Journal* 912, 159. doi:[10.3847/1538-4357/abee1e](#), [arXiv:2010.12099](#).
- Pandian, J.D., Chatterjee, R., Csengeri, T., Williams, J.P., Wyrowski, F., Menten, K.M., 2024. Mass assembly in massive star formation: a fragmentation study of ATLASGAL clumps. *arXiv e-prints*, [arXiv:2403.02725](#)doi:[10.48550/arXiv.2403.02725](#), [arXiv:2403.02725](#).
- Panwar, N., Rishi, C., Sharma, S., Ojha, D.K., Samal, M.R., Singh, H.P., Yadav, R.K., 2024. Low-mass Stellar and Substellar Content of the Young Cluster Berkeley 59. *Astron. Journal* 168, 89. doi:[10.3847/1538-3881/ad5552](#), [arXiv:2406.08261](#).
- Parker, R.J., Alves de Oliveira, C., 2023. On the origin of planetary-mass objects in NGC 1333. *Monthly Notice of the Royal Astronomical Society* 525, 1677–1686. doi:[10.1093/mnras/stad2378](#), [arXiv:2308.01335](#).
- Pearson, S.G., McCaughrean, M.J., 2023. Jupiter Mass Binary Objects in the

- Trapezium Cluster. arXiv e-prints, arXiv:2310.01231 [arXiv:2310.01231](#).
- Pérez-García, A.M., Huélamo, N., García-López, A., Pérez-Martínez, R., Verdugo, E., Palau, A., de Gregorio-Monsalvo, I., Morata, O., Barrado, D., Morales-Calderón, M., Mas-Hesse, M., Bayo, A., Maucó, K., Bouy, H., 2025. Substellar candidates at the earliest stages: the SUCANES database. *Astronomy & Astrophysics*, submitted.
- Pezzuto, S., Benedettini, M., Di Francesco, J., Palmeirim, P., Sadavoy, S., Schisano, E., Li Causi, G., André, P., Arzoumanian, D., Bernard, J.P., Bon-temps, S., Elia, D., Fiorellino, E., Kirk, J.M., Könyves, V., Ladjelate, B., Men'shchikov, A., Motte, F., Piccotti, L., Schneider, N., Spinoglio, L., Ward-Thompson, D., Wilson, C.D., 2021. Physical properties of the ambient medium and of dense cores in the Perseus star-forming region derived from Herschel Gould Belt Survey observations. *Astronomy & Astrophysics* 645, A55. doi:[10.1051/0004-6361/201936534](#), [arXiv:2010.00006](#).
- Phan-Bao, N., 2022. A proto-brown dwarf candidate in  $\rho$ -Ophiucus. *Communications in Physics* 32, 95. doi:[https://doi.org/10.15625/0868-3166/16258](#).
- Phan-Bao, N., Lee, C.F., Ho, P.T.P., Martín, E.L., 2014. Submillimeter Array observations of the proto brown dwarf candidate SSTB213 J041757. *Astronomy & Astrophysics* 564, A32. doi:[10.1051/0004-6361/201323055](#), [arXiv:1403.1926](#).
- Phan-Bao, N., Riaz, B., Lee, C.F., Tang, Y.W., Ho, P.T.P., Martín, E.L., Lim, J., Ohashi, N., Shang, H., 2008. First Confirmed Detection of a Bipolar Molecular Outflow from a Young Brown Dwarf. *Astrophys. Journal Letters* 689, L141. doi:[10.1086/595961](#), [arXiv:0810.2588](#).
- Pillai, T.G.S., Urquhart, J.S., Leurini, S., Zhang, Q., Traficante, A., Colombo, D., Wang, K., Gomez, L., Wyrowski, F., 2023. Infall and outflow towards high-mass starless clump candidates. *Monthly Notice of the Royal Astronomical Society* 522, 3357–3366. doi:[10.1093/mnras/stad1073](#), [arXiv:2305.04256](#).
- Pineda, J.E., Arce, H.G., Schnee, S., Goodman, A.A., Bourke, T., Foster, J.B., Robitaille, T., Tanner, J., Kauffmann, J., Tafalla, M., Caselli, P., Anglada, G., 2011. The Enigmatic Core L1451-mm: A First Hydrostatic Core? Or a Hidden VeLLO? *Astrophys. Journal* 743, 201. doi:[10.1088/0004-637X/743/2/201](#), [arXiv:1109.1207](#).
- Pineda, J.S., Hallinan, G., Kao, M.M., 2017. A Panchromatic View of Brown Dwarf Aurorae. *Astrophys. Journal* 846, 75. doi:[10.3847/1538-4357/aa8596](#), [arXiv:1708.02942](#).
- Podio, L., Tabone, B., Codella, C., Gueth, F., Maury, A., Cabrit, S., Lefloch, B., Maret, S., Belloche, A., André, P., Anderl, S., Gaudel, M., Testi, L., 2021. The CALYPSO IRAM-PdBI survey of jets from Class 0 protostars. Exploring whether jets are ubiquitous in young stars. *Astronomy & Astrophysics* 648, A45. doi:[10.1051/0004-6361/202038429](#), [arXiv:2012.15379](#).
- Pokhrel, R., Megeath, S.T., Gutermuth, R.A., Furlan, E., Fischer, W.J., Federman, S., Tobin, J.J., Stutz, A.M., Hartmann, L., Osorio, M., Watson, D.M., Stanke, T., Manoj, P., Narang, M., Atagulov, P., Habel, N., Zakri, W., 2023. Extension of HOPS out to 500 pc (eHOPS). I. Identification and Modeling of Protostars in the Aquila Molecular Clouds. *Astrophysical Journal Supplement Series* 266, 32. doi:[10.3847/1538-4365/acbfac](#), [arXiv:2209.12090](#).
- Pound, M.W., Blitz, L., 1993. Proto-Brown Dwarfs. I. Methods and Results for High-Latitude Clouds. *Astrophys. Journal* 418, 328. doi:[10.1086/173394](#).
- Pound, M.W., Blitz, L., 1995. Proto-Brown Dwarfs. II. Results in the Ophiuchus and Taurus Molecular Clouds. *Astrophys. Journal* 444, 270. doi:[10.1086/175602](#).
- Ragusa, E., Fasano, D., Toci, C., Duchêne, G., Cuello, N., Villenave, M., van der Plas, G., Lodato, G., Ménard, F., Price, D.J., Pinte, C., Stapelfeldt, K., Wolff, S., 2021. Circumbinary and circumstellar discs around the eccentric binary IRAS 04158+2805 - a testbed for binary-disc interaction. *Monthly Notice of the Royal Astronomical Society* 507, 1157–1174. doi:[10.1093/mnras/stab2179](#), [arXiv:2107.13566](#).
- Ray, T.P., McCaughrean, M.J., Caratti o Garatti, A., Kavanagh, P.J., Justtanont, K., van Dishoeck, E.F., Reitsma, M., Beuther, H., Francis, L., Gieser, C., Klaassen, P., Perotti, G., Tychoniec, L., van Gelder, M., Colina, L., Greve, T.R., Güdel, M., Henning, T., Lagage, P.O., Östlin, G., Vandenbussche, B., Waelkens, C., Wright, G., 2023. Outflows from the youngest stars are mostly molecular. *Nature* 622, 48–52. doi:[10.1038/s41586-023-06551-1](#).
- Rebolo, R., Zapatero Osorio, M.R., Martín, E.L., 1995. Discovery of a brown dwarf in the Pleiades star cluster. *Nature* 377, 129–131. doi:[10.1038/377129a0](#).
- Rebull, L.M., Padgett, D.L., McCabe, C.E., Hillenbrand, L.A., Stapelfeldt, K.R., Noriega-Crespo, A., Carey, S.J., Brooke, T., Huard, T., Terebey, S., Audard, M., Monin, J.L., Fukagawa, M., Güdel, M., Knapp, G.R., Menard, F., Allen, L.E., Angione, J.R., Baldwin-Saavedra, C., Bouvier, J., Briggs, K., Dougados, C., Evans, N.J., Flagey, N., Guieu, S., Grosso, N., Glauser, A.M., Harvey, P., Hines, D., Latter, W.B., Skinner, S.L., Strom, S., Tromp, J., Wolf, S., 2010. The Taurus Spitzer Survey: New Candidate Taurus Members Selected Using Sensitive Mid-Infrared Photometry. *Astrophysical Journal Supplement Series* 186, 259–307. doi:[10.1088/0067-0049/186/2/259](#), [arXiv:0911.3176](#).
- Reipurth, B., Bally, J., Yen, H.W., Arce, H.G., Rodríguez, L.F., Raga, A.C., Geballe, T.R., Rao, R., Comerón, F., Mikkola, S., Aspin, C.A., Walawender, J., 2023. The HH 24 Complex: Jets, Multiple Star Formation, and Orphaned Protostars. *Astron. Journal* 165, 209. doi:[10.3847/1538-3881/acadd4](#), [arXiv:2301.01813](#).
- Reipurth, B., Clarke, C., 2001. The Formation of Brown Dwarfs as Ejected Stellar Embryos. *Astron. Journal* 122, 432–439. doi:[10.1086/321121](#), [arXiv:astro-ph/0103019](#).
- Reipurth, B., Mikkola, S., 2015. Brown Dwarf Binaries from Disintegrating Triple Systems. *Astron. Journal* 149, 145. doi:[10.1088/0004-6256/149/4/145](#), [arXiv:1501.02008](#).
- Riaz, B., Bally, J., 2021. Accretion and outflow activity in proto-brown dwarfs. *Monthly Notice of the Royal Astronomical Society* 501, 3781–3805. doi:[10.1093/mnras/staa3905](#), [arXiv:2012.08612](#).
- Riaz, B., Briceño, C., Whelan, E.T., Heathcote, S., 2017. First Large-scale Herbig-Haro Jet Driven by a Proto-brown Dwarf. *Astrophys. Journal* 844, 47. doi:[10.3847/1538-4357/aa70e8](#), [arXiv:1705.01170](#).
- Riaz, B., Machida, M.N., 2021. Complex structure of a proto-brown dwarf. *Monthly Notice of the Royal Astronomical Society* 504, 6049–6066. doi:[10.1093/mnras/stab547](#), [arXiv:2102.09640](#).
- Riaz, B., Machida, M.N., Stamatellos, D., 2019a. ALMA reveals a pseudo-disc in a proto-brown dwarf. *Monthly Notice of the Royal Astronomical Society* 486, 4114–4129. doi:[10.1093/mnras/stz1032](#), [arXiv:1904.06418](#).
- Riaz, B., Stamatellos, D., Machida, M.N., 2024a. Observations of spiral and streamer on a candidate proto-brown dwarf. *Monthly Notice of the Royal Astronomical Society* 529, 3601–3609. doi:[10.1093/mnras/stae724](#), [arXiv:2403.07367](#).
- Riaz, B., Thi, W.F., 2022a. A survey of HDCO and D<sub>2</sub>CO towards Class 0/I proto-brown dwarfs. *Monthly Notice of the Royal Astronomical Society* 514, 3604–3611. doi:[10.1093/mnras/stac1573](#), [arXiv:2206.02669](#).
- Riaz, B., Thi, W.F., 2022b. Deuterium chemistry and D/H ratios in Class 0/I proto-brown dwarfs. *Monthly Notice of the Royal Astronomical Society* 511, 6110–6125. doi:[10.1093/mnras/stac156](#), [arXiv:2201.07315](#).
- Riaz, B., Thi, W.F., 2022c. First CH<sub>3</sub>D detection in Class 0/I proto-brown dwarfs: constraints on CH<sub>4</sub> abundances. *Monthly Notice of the Royal Astronomical Society* 511, L50–L54. doi:[10.1093/mnras/lsac007](#), [arXiv:2201.07064](#).
- Riaz, B., Thi, W.F., Caselli, P., 2018. Chemical tracers in proto-brown dwarfs: CN, HCN, and HNC observations. *Monthly Notice of the Royal Astronomical Society* 481, 4662–4679. doi:[10.1093/mnras/sty2583](#), [arXiv:1809.10164](#).
- Riaz, B., Thi, W.F., Caselli, P., 2019b. Chemical tracers in proto-brown dwarfs: CO, ortho-H<sub>2</sub>CO, para-H<sub>2</sub>CO, HCO<sup>+</sup>, CS observations. *Monthly Notice of the Royal Astronomical Society* 483, 1139–1157. doi:[10.1093/mnras/sty3111](#), [arXiv:1811.01722](#).
- Riaz, B., Thi, W.F., Machida, M.N., 2023. First observations of warm and cold methanol in Class 0/I proto-brown dwarfs. *Monthly Notice of the Royal Astronomical Society* 522, 4934–4954. doi:[10.1093/mnras/stad1329](#), [arXiv:2305.04991](#).
- Riaz, B., Thi, W.F., Machida, M.N., 2024b. HCN as a probe of the inner disk in a candidate proto-brown dwarf. arXiv e-prints, arXiv:2405.11321doi:[10.48550/arXiv.2405.11321](#), [arXiv:2405.11321](#).
- Riaz, B., Thompson, M., Whelan, E.T., Lodieu, N., 2015. Very low-luminosity Class I/flat outflow sources in  $\sigma$  Orionis. *Monthly Notice of the Royal Astronomical Society* 446, 2550–2559. doi:[10.1093/mnras/stu2139](#), [arXiv:1410.3377](#).
- Riaz, B., Vorobyov, E., Harsono, D., Caselli, P., Tikare, K., Gonzalez-Martin, O., 2016. A Multiwavelength Characterization of Proto-brown-dwarf Candidates in Serpens. *Astrophys. Journal* 831, 189. doi:[10.3847/0004-637X/831/2/189](#), [arXiv:1610.03093](#).
- Rieke, G.H., Ashok, N.M., Boyle, R.P., 1989. The Initial Mass Function in the Rho Ophiuchi Cluster. *Astrophys. Journal Letters* 339, L71. doi:[10.1086/](#)

185422.

- Rodríguez, L.F., Loinard, L., Zapata, L.A., 2024. A Radio Counterpart to a Jupiter-mass Binary Object in Orion. *Astrophys. Journal Letters* 960, L14. doi:[10.3847/2041-8213/ad18ac](#), [arXiv:2401.04905](#).
- Rodríguez, L.F., Zapata, L.A., Palau, A., 2017. JVLA Observations of Young Brown Dwarfs. *Astron. Journal* 153, 209. doi:[10.3847/1538-3881/aa6681](#), [arXiv:1703.03999](#).
- Rumble, D., Hatchell, J., Kirk, H., Pattle, K., 2021. The JCMT Gould Belt Survey: radiative heating by OB stars. *Monthly Notice of the Royal Astronomical Society* 505, 2103–2110. doi:[10.1093/mnras/stab1354](#), [arXiv:2105.03353](#).
- Rygl, K.L.J., Benedettini, M., Schisano, E., Elia, D., Molinari, S., Pezzuto, S., André, P., Bernard, J.P., White, G.J., Polychroni, D., Bontemps, S., Cox, N.L.J., Di Francesco, J., Facchini, A., Fallscheer, C., di Giorgio, A.M., Hennemann, M., Hill, T., Könyves, V., Minier, V., Motte, F., Nguyen-Luong, Q., Peretto, N., Pestalozzi, M., Sadavoy, S., Schneider, N., Spinoglio, L., Testi, L., Ward-Thompson, D., 2013. Recent star formation in the Lupus clouds as seen by Herschel. *Astronomy & Astrophysics* 549, L1. doi:[10.1051/0004-6361/201219511](#), [arXiv:1211.5232](#).
- Saha, A., Tej, A., Liu, H.L., Liu, T., Issac, N., Lee, C.W., Garay, G., Goldsmith, P.F., Juvela, M., Qin, S.L., Stutz, A., Li, S., Wang, K., Baug, T., Bronfman, L., Xu, F.W., Zhang, Y., Eswaraiah, C., 2022. ATOMS: ALMA three-millimeter observations of massive star-forming regions - XII: Fragmentation and multiscale gas kinematics in protoclusters G12.42+0.50 and G19.88-0.53. *Monthly Notice of the Royal Astronomical Society* 516, 1983–2005. doi:[10.1093/mnras/stac2353](#), [arXiv:2208.09877](#).
- Sánchez-Monge, Á., Palau, A., Fontani, F., Busquet, G., Juárez, C., Estalella, R., Tan, J.C., Sepúlveda, I., Ho, P.T.P., Zhang, Q., Kurtz, S., 2013. Properties of dense cores in clustered massive star-forming regions at high angular resolution. *Monthly Notice of the Royal Astronomical Society* 432, 3288–3319. doi:[10.1093/mnras/stt679](#), [arXiv:1304.5136](#).
- Santamaría-Miranda, A., de Gregorio-Monsalvo, I., Huélamo, N., Plunkett, A.L., Ribas, Á., Comerón, F., Schreiber, M.R., López, C., Mužić, K., Testi, L., 2020. Bipolar molecular outflow of the very low-mass star Par-Lup3-4. Evidence for scaled-down low-mass star formation. *Astronomy & Astrophysics* 640, A13. doi:[10.1051/0004-6361/202038128](#), [arXiv:2006.03063](#).
- Santamaría-Miranda, A., de Gregorio-Monsalvo, I., Plunkett, A.L., Huélamo, N., López, C., Ribas, Á., Schreiber, M.R., Mužić, K., Palau, A., Knee, L.B.G., Bayo, A., Comerón, F., Hales, A., 2021. ALMA observations of the early stages of substellar formation in the Lupus 1 and 3 molecular clouds. *Astronomy & Astrophysics* 646, A10. doi:[10.1051/0004-6361/202039419](#), [arXiv:2012.03985](#).
- Schlaufman, K.C., 2018. Evidence of an Upper Bound on the Masses of Planets and Its Implications for Giant Planet Formation. *Astrophys. Journal* 853, 37. doi:[10.3847/1538-4357/aa961c](#), [arXiv:1801.06185](#).
- Schneider, N., Ossenkopf-Okada, V., Clarke, S., Klessen, R.S., Kabanovic, S., Veltchev, T., Bontemps, S., Dib, S., Csengeri, T., Federrath, C., Di Francesco, J., Motte, F., André, P., Arzoumanian, D., Beattie, J.R., Bonne, L., Didelon, P., Elia, D., Könyves, V., Kritsuk, A., Ladjelate, B., Myers, P., Pezzuto, S., Robitaille, J.F., Roy, A., Seifried, D., Simon, R., Soler, J., Ward-Thompson, D., 2022. Understanding star formation in molecular clouds. IV. Column density PDFs from quiescent to massive molecular clouds. *Astronomy & Astrophysics* 666, A165. doi:[10.1051/0004-6361/202039610](#), [arXiv:2207.14604](#).
- Scholz, A., Jayawardhana, R., Muzic, K., Geers, V., Tamura, M., Tanaka, I., 2012. Substellar Objects in Nearby Young Clusters (SONYC). VI. The Planetary-mass Domain of NGC 1333. *Astrophys. Journal* 756, 24. doi:[10.1088/0004-637X/756/1/24](#), [arXiv:1207.1449](#).
- Scholz, A., Jayawardhana, R., Wood, K., 2006. Exploring Brown Dwarf Disks: A 1.3 mm Survey in Taurus. *Astrophys. Journal* 645, 1498–1508. doi:[10.1086/504464](#), [arXiv:astro-ph/0603619](#).
- Scholz, A., Muzic, K., Jayawardhana, R., Almendros-Abad, V., Wilson, I., 2023. Disks around Young Planetary-mass Objects: Ultradeep Spitzer Imaging of NGC 1333. *Astron. Journal* 165, 196. doi:[10.3847/1538-3881/acc65d](#), [arXiv:2303.12451](#).
- Schwarz, K.R., Shirley, Y.L., Dunham, M.M., 2012. A Systematic Search for Molecular Outflows Toward Candidate Low-luminosity Protostars and Very Low Luminosity Objects. *Astron. Journal* 144, 115. doi:[10.1088/0004-6256/144/4/115](#), [arXiv:1209.2370](#).
- Shimoikura, T., Dobashi, K., Hatano, Y., Nakamura, F., 2020. A Detailed Analysis of the Cloud Structure and Dynamics in Aquila Rift. *Astrophys. Journal* 895, 137. doi:[10.3847/1538-4357/ab8c4f](#).
- Shirley, Y.L., Claussen, M.J., Bourke, T.L., Young, C.H., Blake, G.A., 2007. The Detection and Characterization of Centimeter Radio Continuum Emission from the Low-Mass Protostar L1014-IRS. *Astrophys. Journal* 667, 329–339. doi:[10.1086/520570](#), [arXiv:0705.1747](#).
- Sicilia-Aguilar, A., Henning, T., Juhász, A., Bouwman, J., Garmire, G., Garmire, A., 2008. Very Low Mass Objects in the Coronet Cluster: The Realm of the Transition Disks. *Astrophys. Journal* 687, 1145–1167. doi:[10.1086/591932](#), [arXiv:0807.2504](#).
- Sicilia-Aguilar, A., Henning, T., Kainulainen, J., Roccatagliata, V., 2011. Protostars and Stars in the Coronet Cluster: Age, Evolution, and Cluster Structure. *Astrophys. Journal* 736, 137. doi:[10.1088/0004-637X/736/2/137](#), [arXiv:1105.2702](#).
- Siess, L., Dufour, E., Forestini, M., 2000. An internet server for pre-main sequence tracks of low- and intermediate-mass stars. *Astronomy & Astrophysics* 358, 593–599. doi:[10.48550/arXiv.astro-ph/0003477](#), [arXiv:astro-ph/0003477](#).
- Simpson, R.J., Johnstone, D., Nutter, D., Ward-Thompson, D., Whitworth, A.P., 2011. The initial conditions of isolated star formation - X. A suggested evolutionary diagram for pre-stellar cores. *Monthly Notice of the Royal Astronomical Society* 417, 216–227. doi:[10.1111/j.1365-2966.2011.19163.x](#), [arXiv:1106.1885](#).
- Soam, A., Kwon, J., Maheswar, G., Tamura, M., Lee, C.W., 2015a. First Optical and Near-infrared Polarimetry of a Molecular Cloud Forming a Protobrown Dwarf Candidate. *Astrophys. Journal Letters* 803, L20. doi:[10.1088/2041-8205/803/2/L20](#).
- Soam, A., Lee, C.W., Andersson, B.G., Maheswar, G., Juvela, M., Liu, T., Kim, G., Rao, R., Chung, E.J., Kwon, W., Ekta, S., 2019. First Sub-parsec-scale Mapping of Magnetic Fields in the Vicinity of a Very-low-luminosity Object, L1521F-IRS. *Astrophys. Journal* 883, 9. doi:[10.3847/1538-4357/ab365d](#), [arXiv:1908.01018](#).
- Soam, A., Maheswar, G., Lee, C.W., Dib, S., Bhatt, H.C., Tamura, M., Kim, G., 2015b. Magnetic field structure around cores with very low luminosity objects. *Astronomy & Astrophysics* 573, A34. doi:[10.1051/0004-6361/201322536](#), [arXiv:1411.0785](#).
- Spezzi, L., Cox, N.L.J., Prusti, T., Merín, B., Ribas, Á., Alves de Oliveira, C., Winston, E., Kóspál, Á., Royer, P., Vavrek, R., André, P., Pilbratt, G.L., Testi, L., Bressert, E., Ricci, L., Men'shchikov, A., Könyves, V., 2013. The Herschel Gould Belt Survey in Chamaeleon II. Properties of cold dust in disks around young stellar objects. *Astronomy & Astrophysics* 555, A71. doi:[10.1051/0004-6361/201321444](#), [arXiv:1305.4075](#).
- Staller, R.F.A., de Jong, T., 1981. Theoretical luminosity functions of red and black dwarfs. *Astronomy & Astrophysics* 98, 140–148.
- Stamatellos, D., Hubber, D.A., Whitworth, A.P., 2007. Brown dwarf formation by gravitational fragmentation of massive, extended protostellar discs. *Monthly Notice of the Royal Astronomical Society* 382, L30–L34. doi:[10.1111/j.1745-3933.2007.00383.x](#), [arXiv:0708.2827](#).
- Stamatellos, D., Whitworth, A.P., 2009. The properties of brown dwarfs and low-mass hydrogen-burning stars formed by disc fragmentation. *Monthly Notice of the Royal Astronomical Society* 392, 413–427. doi:[10.1111/j.1365-2966.2008.14069.x](#), [arXiv:0810.1687](#).
- Stevenson, A.T., Haswell, C.A., Barnes, J.R., Barstow, J.K., 2023. Combining the brown dwarf desert with Gaia DR3. *Monthly Notice of the Royal Astronomical Society* 526, 5155–5171. doi:[10.1093/mnras/stad3041](#), [arXiv:2310.02695](#).
- Suárez, G., Downes, J.J., Román-Zúñiga, C., Cerviño, M., Briceño, C., Petrotens, M.G., Vivas, K., 2019. System initial mass function of the 25 Ori group from planetary-mass objects to intermediate/high-mass stars. *Monthly Notice of the Royal Astronomical Society* 486, 1718–1740. doi:[10.1093/mnras/stz756](#), [arXiv:1903.05739](#).
- Tabatabaei, F.S., Redaelli, E., Caselli, P., Alves, F.O., 2023. The kinematics of the magnetized protostellar core IRAS15398-3359. *Astronomy & Astrophysics* 672, A72. doi:[10.1051/0004-6361/202244861](#).
- Tachihara, K., Dobashi, K., Mizuno, A., Ogawa, H., Fukui, Y., 1996. 13CO (J=1–0) Observations of the Lupus Molecular Clouds. *Publications of the ASJ* 48, 489–502. doi:[10.1093/pasj/48.3.489](#).
- Takahashi, S., Ho, P.T.P., 2012. The Discovery of the Youngest Molecular Outflow Associated with an Intermediate-mass Protostellar Core, MMS-6/OMC-3. *Astrophys. Journal Letters* 745, L10. doi:[10.1088/2041-8205/745/1/L10](#), [arXiv:1112.4596](#).



- Takahashi, S., Ohashi, N., Bourke, T.L., 2013. Direct Imaging of a Compact Molecular Outflow from a Very Low Luminosity Object: L1521F-IRS. *Astrophys. Journal* 774, 20. doi:[10.1088/0004-637X/774/1/20](https://doi.org/10.1088/0004-637X/774/1/20), [arXiv:1307.0865](https://arxiv.org/abs/1307.0865).
- Takakuwa, S., Ohashi, N., Aikawa, Y., 2011. Carbon-chain and Organic Molecules Around Very Low Luminosity Protostellar Objects of L1521F-IRS and IRAM 04191+1522. *Astrophys. Journal* 728, 101. doi:[10.1088/0004-637X/728/2/101](https://doi.org/10.1088/0004-637X/728/2/101), [arXiv:1012.1176](https://arxiv.org/abs/1012.1176).
- Thieme, T.J., Lai, S.P., Ohashi, N., Tobin, J.J., Jørgensen, J.K., Sai, J.I.C., Aso, Y., Williams, J.P., Yamato, Y., Aikawa, Y., de Gregorio-Monsalvo, I., Han, I., Kwon, W., Lee, C.W., Lee, J.E., Li, Z.Y., Lin, Z.Y.D., Looney, L.W., Narayanan, S., Phuong, N.T., Plunkett, A.L., Santamaría-Miranda, A., Sharma, R., Takakuwa, S., Yen, H.W., 2023. Early Planet Formation in Embedded Disks (eDisk). VIII. A Small Protostellar Disk around the Extremely Low Mass and Young Class 0 Protostar IRAS 15398-3359. *Astrophys. Journal* 958, 60. doi:[10.3847/1538-4357/ad003a](https://doi.org/10.3847/1538-4357/ad003a), [arXiv:2310.12453](https://arxiv.org/abs/2310.12453).
- Thies, I., Pflamm-Altenburg, J., Kroupa, P., Marks, M., 2015. Characterizing the Brown Dwarf Formation Channels from the Initial Mass Function and Binary-star Dynamics. *Astrophys. Journal* 800, 72. doi:[10.1088/0004-637X/800/1/72](https://doi.org/10.1088/0004-637X/800/1/72), [arXiv:1501.01640](https://arxiv.org/abs/1501.01640).
- Tobin, J.J., Hartmann, L., Chiang, H.F., Wilner, D.J., Looney, L.W., Loinard, L., Calvet, N., D'Alessio, P., 2012. A  $\sim 0.2$ -solar-mass protostar with a Keplerian disk in the very young L1527 IRS system. *Nature* 492, 83–85. doi:[10.1038/nature11610](https://doi.org/10.1038/nature11610), [arXiv:1212.0861](https://arxiv.org/abs/1212.0861).
- Tobin, J.J., Kratter, K.M., Persson, M.V., Looney, L.W., Dunham, M.M., Segura-Cox, D., Li, Z.Y., Chandler, C.J., Sadavoy, S.I., Harris, R.J., Melis, C., Pérez, L.M., 2016a. A triple protostar system formed via fragmentation of a gravitationally unstable disk. *Nature* 538, 483–486. doi:[10.1038/nature20094](https://doi.org/10.1038/nature20094), [arXiv:1610.08524](https://arxiv.org/abs/1610.08524).
- Tobin, J.J., Looney, L.W., Li, Z.Y., Chandler, C.J., Dunham, M.M., Segura-Cox, D., Sadavoy, S.I., Melis, C., Harris, R.J., Kratter, K., Perez, L., 2016b. The VLA Nascent Disk and Multiplicity Survey of Perseus Protostars (VANDAM). II. Multiplicity of Protostars in the Perseus Molecular Cloud. *Astrophys. Journal* 818, 73. doi:[10.3847/0004-637X/818/1/73](https://doi.org/10.3847/0004-637X/818/1/73), [arXiv:1601.00692](https://arxiv.org/abs/1601.00692).
- Tobin, J.J., Looney, L.W., Li, Z.Y., Sadavoy, S.I., Dunham, M.M., Segura-Cox, D., Kratter, K., Chandler, C.J., Melis, C., Harris, R.J., Perez, L., 2018. The VLA/ALMA Nascent Disk and Multiplicity (VANDAM) Survey of Perseus Protostars. VI. Characterizing the Formation Mechanism for Close Multiple Systems. *Astrophys. Journal* 867, 43. doi:[10.3847/1538-4357/aae1f7](https://doi.org/10.3847/1538-4357/aae1f7), [arXiv:1809.06434](https://arxiv.org/abs/1809.06434).
- Tobin, J.J., Offner, S.S.R., Kratter, K.M., Megeath, S.T., Sheehan, P.D., Looney, L.W., Diaz-Rodriguez, A.K., Osorio, M., Anglada, G., Sadavoy, S.I., Furlan, E., Segura-Cox, D., Karnath, N., van't Hoff, M.L.R., van Dishoeck, E.F., Li, Z.Y., Sharma, R., Stutz, A.M., Tychoniec, Ł., 2022. The VLA/ALMA Nascent Disk And Multiplicity (VANDAM) Survey of Orion Protostars. V. A Characterization of Protostellar Multiplicity. *Astrophys. Journal* 925, 39. doi:[10.3847/1538-4357/ac36d2](https://doi.org/10.3847/1538-4357/ac36d2), [arXiv:2111.05801](https://arxiv.org/abs/2111.05801).
- Tobin, J.J., Sheehan, P.D., Megeath, S.T., Díaz-Rodríguez, A.K., Offner, S.S.R., Murillo, N.M., van't Hoff, M.L.R., van Dishoeck, E.F., Osorio, M., Anglada, G., Furlan, E., Stutz, A.M., Reynolds, N., Karnath, N., Fischer, W.J., Persson, M., Looney, L.W., Li, Z.Y., Stephens, I., Chandler, C.J., Cox, E., Dunham, M.M., Tychoniec, Ł., Kama, M., Kratter, K., Kounkel, M., Mazur, B., Maud, L., Patel, L., Perez, L., Sadavoy, S.I., Segura-Cox, D., Sharma, R., Stephenson, B., Watson, D.M., Wyrowski, F., 2020. The VLA/ALMA Nascent Disk and Multiplicity (VANDAM) Survey of Orion Protostars. II. A Statistical Characterization of Class 0 and Class I Protostellar Disks. *Astrophys. Journal* 890, 130. doi:[10.3847/1538-4357/ab6f64](https://doi.org/10.3847/1538-4357/ab6f64), [arXiv:2001.04468](https://arxiv.org/abs/2001.04468).
- Tobin, J.J., Stutz, A.M., Manoj, P., Megeath, S.T., Karska, A., Nagy, Z., Wyrowski, F., Fischer, W.J., Watson, D.M., Stanke, T., 2016c. Characterizing the Youngest Herschel-detected Protostars. II. Molecular Outflows from the Millimeter and the Far-infrared. *Astrophys. Journal* 831, 36. doi:[10.3847/0004-637X/831/1/36](https://doi.org/10.3847/0004-637X/831/1/36), [arXiv:1607.00787](https://arxiv.org/abs/1607.00787).
- Tobin, J.J., Stutz, A.M., Megeath, S.T., Fischer, W.J., Henning, T., Ragan, S.E., Ali, B., Stanke, T., Manoj, P., Calvet, N., Hartmann, L., 2015. Characterizing the Youngest Herschel-detected Protostars. I. Envelope Structure Revealed by CARMA Dust Continuum Observations. *Astrophys. Journal* 798, 128. doi:[10.1088/0004-637X/798/2/128](https://doi.org/10.1088/0004-637X/798/2/128), [arXiv:1411.1026](https://arxiv.org/abs/1411.1026).
- Tokuda, K., Fujishiro, K., Tachihara, K., Takashima, T., Fukui, Y., Zahorecz, S., Saigo, K., Matsumoto, T., Tomida, K., Machida, M.N., Inutsuka, S.I., André, P., Kawamura, A., Onishi, T., 2020. FRAGMENTATION AND EVOLUTION OF DENSE CORES JUDGED BY ALMA (FREJA). I. Overview: Inner  $\sim 1000$  au Structures of Prestellar/Protostellar Cores in Taurus. *Astrophys. Journal* 899, 10. doi:[10.3847/1538-4357/ab9ca7](https://doi.org/10.3847/1538-4357/ab9ca7), [arXiv:2006.06361](https://arxiv.org/abs/2006.06361).
- Tokuda, K., Onishi, T., Saigo, K., Hosokawa, T., Matsumoto, T., Inutsuka, S.I., Machida, M.N., Tomida, K., Kunitomo, M., Kawamura, A., Fukui, Y., Tachihara, K., 2017. A Detached Protostellar Disk around a  $\sim 0.2 M_{\odot}$  Protostar in a Possible Site of a Multiple Star Formation in a Dynamical Environment in Taurus. *Astrophys. Journal* 849, 101. doi:[10.3847/1538-4357/aa8e9e](https://doi.org/10.3847/1538-4357/aa8e9e), [arXiv:1709.07113](https://arxiv.org/abs/1709.07113).
- Tokuda, K., Tachihara, K., Saigo, K., André, P., Miyamoto, Y., Zahorecz, S., Inutsuka, S.I., Matsumoto, T., Takashima, T., Machida, M.N., Tomida, K., Taniguchi, K., Fukui, Y., Kawamura, A., Tatematsu, K., Kandori, R., Onishi, T., 2019. A centrally concentrated sub-solar-mass starless core in the Taurus L1495 filamentary complex. *Publications of the ASJ* 71, 73. doi:[10.1093/pasj/psz051](https://doi.org/10.1093/pasj/psz051), [arXiv:1904.05490](https://arxiv.org/abs/1904.05490).
- Towner, A.P.M., Ginsburg, A., Dell'Ova, P., Gusdorf, A., Bontemps, S., Csengeri, T., Galván-Madrid, R., Louvet, F.K., Motte, F., Sanhueza, P., Stutz, A.M., Bally, J., Baug, T., Chen, H.R.V., Cunningham, N., Fernández-López, M., Liu, H.L., Lu, X., Nony, T., Valeille-Manet, M., Wu, B., Álvarez-Gutiérrez, R.H., Bonfand, M., Di Francesco, J., Nguyen-Luong, Q., Olguin, F., Whitworth, A.P., 2024. ALMA-IMF IX. Catalog and Physical Properties of 315 SiO Outflow Candidates in 15 Massive Protoclusters. *Astrophys. Journal* 960, 48. doi:[10.3847/1538-4357/ad0786](https://doi.org/10.3847/1538-4357/ad0786), [arXiv:2310.13125](https://arxiv.org/abs/2310.13125).
- Treumann, R.A., 2006. The electron-cyclotron maser for astrophysical application. *Astronomy and Astrophysics Reviews* 13, 229–315. doi:[10.1007/s00159-006-0001-y](https://doi.org/10.1007/s00159-006-0001-y).
- Tritsis, A., Basu, S., Federrath, C., 2023. Can we observe the ion-neutral drift velocity in prestellar cores? *Monthly Notice of the Royal Astronomical Society* 521, 5087–5099. doi:[10.1093/mnras/stad829](https://doi.org/10.1093/mnras/stad829), [arXiv:2303.09583](https://arxiv.org/abs/2303.09583).
- Urquhart, J.S., König, C., Giannetti, A., Leurini, S., Moore, T.J.T., Eden, D.J., Pillai, T., Thompson, M.A., Braiding, C., Burton, M.G., Csengeri, T., Dempsey, J.T., Figura, C., Froebrich, D., Menten, K.M., Schuller, F., Smith, M.D., Wyrowski, F., 2018. ATLASGAL - properties of a complete sample of Galactic clumps. *Monthly Notice of the Royal Astronomical Society* 473, 1059–1102. doi:[10.1093/mnras/stx2258](https://doi.org/10.1093/mnras/stx2258), [arXiv:1709.00392](https://arxiv.org/abs/1709.00392).
- Valdivia-Mena, M.T., Pineda, J.E., Segura-Cox, D.M., Caselli, P., Schmiedeke, A., Choudhury, S., Offner, S.S.R., Neri, R., Goodman, A., Fuller, G.A., 2023. Flow of gas detected from beyond the filaments to protostellar scales in Barnard 5. *arXiv e-prints*, arXiv:2307.14337 [arXiv:2307.14337](https://arxiv.org/abs/2307.14337).
- van der Marel, N., Kristensen, L.E., Visser, R., Mottram, J.C., Yıldız, U.A., van Dishoeck, E.F., 2013. Outflow forces of low-mass embedded objects in Ophiuchus: a quantitative comparison of analysis methods. *Astronomy & Astrophysics* 556, A76. doi:[10.1051/0004-6361/201220717](https://doi.org/10.1051/0004-6361/201220717), [arXiv:1305.6453](https://arxiv.org/abs/1305.6453).
- van Terwisga, S.E., Hacar, A., van Dishoeck, E.F., Oonk, R., Portegies Zwart, S., 2022. Survey of Orion Disks with ALMA (SODA). I. Cloud-level demographics of 873 protoplanetary disks. *Astronomy & Astrophysics* 661, A53. doi:[10.1051/0004-6361/202141913](https://doi.org/10.1051/0004-6361/202141913), [arXiv:2202.11057](https://arxiv.org/abs/2202.11057).
- Vázquez-Semadeni, E., Palau, A., Ballesteros-Paredes, J., Gómez, G.C., Zamora-Avilés, M., 2019. Global hierarchical collapse in molecular clouds. Towards a comprehensive scenario. *Monthly Notice of the Royal Astronomical Society* 490, 3061–3097. doi:[10.1093/mnras/stz2736](https://doi.org/10.1093/mnras/stz2736), [arXiv:1903.11247](https://arxiv.org/abs/1903.11247).
- Vázquez-Semadeni, E., Zamora-Avilés, M., Galván-Madrid, R., Forbrich, J., 2018. Molecular cloud evolution - VI. Measuring cloud ages. *Monthly Notice of the Royal Astronomical Society* 479, 3254–3263. doi:[10.1093/mnras/sty1586](https://doi.org/10.1093/mnras/sty1586), [arXiv:1805.07221](https://arxiv.org/abs/1805.07221).
- Vazzano, M.M., Fernández-López, M., Plunkett, A., de Gregorio-Monsalvo, I., Santamaría-Miranda, A., Takahashi, S., Lopez, C., 2021. Outflows, envelopes, and disks as evolutionary indicators in Lupus young stellar objects. *Astronomy & Astrophysics* 648, A41. doi:[10.1051/0004-6361/202039228](https://doi.org/10.1051/0004-6361/202039228), [arXiv:2101.05330](https://arxiv.org/abs/2101.05330).
- Villenave, M., Ménard, F., Dent, W.R.F., Duchêne, G., Stapelfeldt, K.R., Benisty, M., Boehler, Y., van der Plas, G., Pinte, C., Telkamp, Z., Wolff, S., Flores, C., Lesur, G., Louvet, F., Riols, A., Dougados, C., Williams, H., Padgett, D., 2020. Observations of edge-on protoplanetary disks with ALMA. I. Results from continuum data. *Astronomy & Astrophysics* 642, A164. doi:[10.1051/0004-6361/202038087](https://doi.org/10.1051/0004-6361/202038087), [arXiv:2008.06518](https://arxiv.org/abs/2008.06518).
- Vorobyov, E.I., 2010. Lifetime of the Embedded Phase of Low-Mass Star For-

- mation and the Envelope Depletion Rates. *Astrophys. Journal* 713, 1059–1072. doi:[10.1088/0004-637X/713/2/1059](https://doi.org/10.1088/0004-637X/713/2/1059), [arXiv:1003.1400](https://arxiv.org/abs/1003.1400).
- Vorobyov, E.I., Elbakyan, V., Dunham, M.M., Guedel, M., 2017a. The nature of very low luminosity objects (VeLLOs). *Astronomy & Astrophysics* 600, A36. doi:[10.1051/0004-6361/201628922](https://doi.org/10.1051/0004-6361/201628922), [arXiv:1612.03696](https://arxiv.org/abs/1612.03696).
- Vorobyov, E.I., Elbakyan, V., Hosokawa, T., Sakurai, Y., Guedel, M., Yorke, H., 2017b. Effect of accretion on the pre-main-sequence evolution of low-mass stars and brown dwarfs. *Astronomy & Astrophysics* 605, A77. doi:[10.1051/0004-6361/201630356](https://doi.org/10.1051/0004-6361/201630356), [arXiv:1706.00502](https://arxiv.org/abs/1706.00502).
- Vorobyov, E.I., Steinrueck, M.E., Elbakyan, V., Guedel, M., 2017c. Formation of freely floating sub-stellar objects via close encounters. *Astronomy & Astrophysics* 608, A107. doi:[10.1051/0004-6361/201731565](https://doi.org/10.1051/0004-6361/201731565), [arXiv:1708.07166](https://arxiv.org/abs/1708.07166).
- Wang, Y., Perna, R., Zhu, Z., 2023. Floating binary planets from ejections during close stellar encounters. *arXiv e-prints*, [arXiv:2310.06016](https://arxiv.org/abs/2310.06016)doi:[10.48550/arXiv.2310.06016](https://doi.org/10.48550/arXiv.2310.06016), [arXiv:2310.06016](https://arxiv.org/abs/2310.06016).
- Whelan, E.T., Riaz, B., Rouzé, B., 2018. The near-infrared outflow and cavity of the proto-brown dwarf candidate ISO-Oph 200. *Astronomy & Astrophysics* 610, L19. doi:[10.1051/0004-6361/201732291](https://doi.org/10.1051/0004-6361/201732291), [arXiv:1801.08749](https://arxiv.org/abs/1801.08749).
- White, R.J., Hillenbrand, L.A., 2004. On the Evolutionary Status of Class I Stars and Herbig-Haro Energy Sources in Taurus-Auriga. *Astrophys. Journal* 616, 998–1032. doi:[10.1086/425115](https://doi.org/10.1086/425115), [arXiv:astro-ph/0408244](https://arxiv.org/abs/astro-ph/0408244).
- Whitworth, A., Bate, M.R., Nordlund, Å., Reipurth, B., Zinnecker, H., 2007. The Formation of Brown Dwarfs: Theory, in: Reipurth, B., Jewitt, D., Keil, K. (Eds.), *Protostars and Planets V*, p. 459.
- Whitworth, A.P., 2016. A ram-pressure threshold for star formation. *Monthly Notice of the Royal Astronomical Society* 458, 1815–1832. doi:[10.1093/mnras/stw442](https://doi.org/10.1093/mnras/stw442), [arXiv:1605.05728](https://arxiv.org/abs/1605.05728).
- Whitworth, A.P., 2018. Brown Dwarf Formation: Theory, in: Deeg, H.J., Belmonte, J.A. (Eds.), *Handbook of Exoplanets*, p. 95. doi:[10.1007/978-3-319-55333-7\\_95](https://doi.org/10.1007/978-3-319-55333-7_95).
- Whitworth, A.P., Zinnecker, H., 2004. The formation of free-floating brown dwarves and planetary-mass objects by photo-erosion of prestellar cores. *Astronomy & Astrophysics* 427, 299–306. doi:[10.1051/0004-6361:20041131](https://doi.org/10.1051/0004-6361:20041131), [arXiv:astro-ph/0408522](https://arxiv.org/abs/astro-ph/0408522).
- Wyrowski, F., Güsten, R., Menten, K.M., Wiesemeyer, H., Csengeri, T., Heyminck, S., Klein, B., König, C., Urquhart, J.S., 2016. Infall through the evolution of high-mass star-forming clumps. *Astronomy & Astrophysics* 585, A149. doi:[10.1051/0004-6361/201526361](https://doi.org/10.1051/0004-6361/201526361), [arXiv:1510.08374](https://arxiv.org/abs/1510.08374).
- Xia, J., Tang, N., Zhi, Q., Jiao, S., Xie, J., Fuller, G.A., Goldsmith, P.F., Li, D., 2022. The Distribution of UV Radiation Field in the Molecular Clouds of Gould Belt. *Research in Astronomy and Astrophysics* 22, 085017. doi:[10.1088/1674-4527/ac784e](https://doi.org/10.1088/1674-4527/ac784e), [arXiv:2208.05250](https://arxiv.org/abs/2208.05250).
- Xu, F., Wang, K., He, Y., Wu, J., Zhu, L., Mardones, D., 2023. Clump-scale Gas Infall in High-mass Star Formation: A Multitransition View with James Clerk Maxwell Telescope HCN (4-3) Mapping. *Astrophysical Journal Supplement Series* 269, 38. doi:[10.3847/1538-4365/acfee2](https://doi.org/10.3847/1538-4365/acfee2), [arXiv:2309.14686](https://arxiv.org/abs/2309.14686).
- Yang, Y.L., Green, J.D., Pontoppidan, K.M., Bergner, J.B., Cleeves, L.I., Evans, Neal J., I., Garrod, R.T., Jin, M., Kim, C.H., Kim, J., Lee, J.E., Sakai, N., Shingledecker, C.N., Shope, B., Tobin, J.J., van Dishoeck, E.F., 2022. CORINOS. I. JWST/MIRI Spectroscopy and Imaging of a Class 0 Protostar IRAS 15398-3359. *Astrophys. Journal Letters* 941, L13. doi:[10.3847/2041-8213/aca289](https://doi.org/10.3847/2041-8213/aca289), [arXiv:2208.10673](https://arxiv.org/abs/2208.10673).
- Yang, Y.L., Sakai, N., Zhang, Y., Murillo, N.M., Zhang, Z.E., Higuchi, A.E., Zeng, S., López-Sepulcre, A., Yamamoto, S., Lefloch, B., Bouvier, M., Ceccarelli, C., Hirota, T., Imai, M., Oya, Y., Sakai, T., Watanabe, Y., 2021. The Perseus ALMA Chemistry Survey (PEACHES). I. The Complex Organic Molecules in Perseus Embedded Protostars. *Astrophys. Journal* 910, 20. doi:[10.3847/1538-4357/abdf6d](https://doi.org/10.3847/1538-4357/abdf6d), [arXiv:2101.11009](https://arxiv.org/abs/2101.11009).
- Yen, H.W., Koch, P.M., Takakuwa, S., Krasnopolsky, R., Ohashi, N., Aso, Y., 2017. Signs of Early-stage Disk Growth Revealed with ALMA. *Astrophys. Journal* 834, 178. doi:[10.3847/1538-4357/834/2/178](https://doi.org/10.3847/1538-4357/834/2/178), [arXiv:1611.08416](https://arxiv.org/abs/1611.08416).
- Yen, H.W., Zhao, B., Koch, P.M., Krasnopolsky, R., Li, Z.Y., Ohashi, N., Takakuwa, S., 2018. Constraint on ion-neutral drift velocity in the Class 0 protostar B335 from ALMA observations. *Astronomy & Astrophysics* 615, A58. doi:[10.1051/0004-6361/201732195](https://doi.org/10.1051/0004-6361/201732195), [arXiv:1803.09893](https://arxiv.org/abs/1803.09893).
- Young, A.K., 2023. Insights into the first and second hydrostatic core stages from numerical simulations. *Frontiers in Astronomy and Space Sciences* 10, 1288730. doi:[10.3389/fspas.2023.1288730](https://doi.org/10.3389/fspas.2023.1288730), [arXiv:2312.03039](https://arxiv.org/abs/2312.03039).
- Young, C.H., Evans, Neal J., I., 2005. Evolutionary Signatures in the Formation of Low-Mass Protostars. *Astrophys. Journal* 627, 293–309. doi:[10.1086/430436](https://doi.org/10.1086/430436), [arXiv:astro-ph/0503456](https://arxiv.org/abs/astro-ph/0503456).
- Young, C.H., Jørgensen, J.K., Shirley, Y.L., Kauffmann, J., Huard, T., Lai, S.P., Lee, C.W., Crapsi, A., Bourke, T.L., Dullemond, C.P., Brooke, T.Y., Porras, A., Spiesman, W., Allen, L.E., Blake, G.A., Evans, Neal J., I., Harvey, P.M., Koerner, D.W., Mundy, L.G., Myers, P.C., Padgett, D.L., Sargent, A.I., Stapelfeldt, K.R., van Dishoeck, E.F., Bertoldi, F., Chapman, N., Cieza, L., DeVries, C.H., Ridge, N.A., Wahhaj, Z., 2004. A “Starless” Core that Isn’t: Detection of a Source in the L1014 Dense Core with the Spitzer Space Telescope. *Astrophysical Journal Supplement Series* 154, 396–401. doi:[10.1086/422818](https://doi.org/10.1086/422818), [arXiv:astro-ph/0406371](https://arxiv.org/abs/astro-ph/0406371).
- Yu, F., Lai, D., 2024. Free-Floating Planets, Survivor Planets, Captured Planets and Binary Planets from Stellar Flybys. *arXiv e-prints*, [arXiv:2403.07224](https://arxiv.org/abs/2403.07224)doi:[10.48550/arXiv.2403.07224](https://doi.org/10.48550/arXiv.2403.07224), [arXiv:2403.07224](https://arxiv.org/abs/2403.07224).
- Yue, Y.H., Qin, S.L., Liu, T., Tang, M.Y., Wu, Y., Wang, K., Zhang, C., 2021. Infall in massive clumps harboring bright infrared sources. *Research in Astronomy and Astrophysics* 21, 014. doi:[10.1088/1674-4527/21/1/14](https://doi.org/10.1088/1674-4527/21/1/14), [arXiv:2010.10731](https://arxiv.org/abs/2010.10731).
- Zamora-Aviles, M., Camacho, V., Ballesteros-Paredes, J., Vázquez-Semadeni, E., Palau, A., Román-Zúñiga, C., Hernández-Cruz, A., Gómez, G.C., Quesada-Zúñiga, F., Naranjo-Romero, R., 2024. Gravity or turbulence? VII. The Schmidt-Kennicutt law, the star formation efficiency, and the mass density of clusters from gravitational collapse rather than turbulent support. *arXiv e-prints*, [arXiv:2409.11588](https://arxiv.org/abs/2409.11588)doi:[10.48550/arXiv.2409.11588](https://doi.org/10.48550/arXiv.2409.11588), [arXiv:2409.11588](https://arxiv.org/abs/2409.11588).
- Zarka, P., 2007. Plasma interactions of exoplanets with their parent star and associated radio emissions. *Planet. Space Sci* 55, 598–617. doi:[10.1016/j.pss.2006.05.045](https://doi.org/10.1016/j.pss.2006.05.045).
- Zhang, Y., Snellen, I.A.G., Bohn, A.J., Mollière, P., Ginski, C., Hoeijmakers, H.J., Kenworthy, M.A., Mamajek, E.E., Meshkat, T., Reggiani, M., Snik, F., 2021a. The <sup>13</sup>CO-rich atmosphere of a young accreting super-Jupiter. *Nature* 595, 370–372. doi:[10.1038/s41586-021-03616-x](https://doi.org/10.1038/s41586-021-03616-x), [arXiv:2107.06297](https://arxiv.org/abs/2107.06297).
- Zhang, Y., Snellen, I.A.G., Mollière, P., 2021b. The <sup>12</sup>CO/<sup>13</sup>CO isotopologue ratio of a young, isolated brown dwarf. Possibly distinct formation pathways of super-Jupiters and brown dwarfs. *Astronomy & Astrophysics* 656, A76. doi:[10.1051/0004-6361/202141502](https://doi.org/10.1051/0004-6361/202141502), [arXiv:2109.11569](https://arxiv.org/abs/2109.11569).
- Zinnecker, H., 1984. Star formation from hierarchical cloud fragmentation - A statistical theory of the log-normal Initial Mass Function. *Monthly Notice of the Royal Astronomical Society* 210, 43–56. doi:[10.1093/mnras/210.1.43](https://doi.org/10.1093/mnras/210.1.43).
- Zucker, C., Speagle, J.S., Schlafly, E.F., Green, G.M., Finkbeiner, D.P., Goodman, A., Alves, J., 2020. A compendium of distances to molecular clouds in the Star Formation Handbook. *Astronomy & Astrophysics* 633, A51. doi:[10.1051/0004-6361/201936145](https://doi.org/10.1051/0004-6361/201936145), [arXiv:2001.00591](https://arxiv.org/abs/2001.00591).
- Zucker, C., Speagle, J.S., Schlafly, E.F., Green, G.M., Finkbeiner, D.P., Goodman, A.A., Alves, J., 2019. A Large Catalog of Accurate Distances to Local Molecular Clouds: The Gaia DR2 Edition. *Astrophys. Journal* 879, 125. doi:[10.3847/1538-4357/ab2388](https://doi.org/10.3847/1538-4357/ab2388), [arXiv:1902.01425](https://arxiv.org/abs/1902.01425).